COMPARING THE TORANDO ENVIRONMENTS AMONG EAST COAST AND GULF COAST LANDFALLING TROPICAL CYCLONES

by

Matthew J. Toadvine

A thesis submitted to the faculty of
The University of North Carolina at Charlotte
in partial fulfillment of the requirements
for the degree of Master of Science in
Earth Science

Charlotte

2022

Approved by:

_____
Dr. Matthew Eastin

_____
Dr. Casey Davenport

_____
Terry Shirley

ABSTRACT

MATTHEW J. TOADVINE. Comparing the Tornado Environments among East Coast and Gulf Coast Landfalling Tropical Cyclones. (Under the direction of DR. MATTHEW EASTIN)

Tornadoes spawned by the landfalling tropical cyclones (TCs) pose a non-trivial threat to life and property. Previous research efforts have developed TC-tornado climatologies and have noted differences between East coast and Gulf coast landfalls, but a direct climatological comparison between the two affected coastlines has yet to be studied. Moreover, better understanding of significant differences in the mesoscale environments during TC landfalls could improve tornado forecasting techniques. Therefore, this project evaluated similarities and differences between East coast and Gulf coast TC tornadoes with a focus on: (1) the regional TC tornado climatology; and (2) the local environments of TC tornadoes utilizing RUC-RAP 20-km model analysis soundings. The climatological analysis covered a 70-year period (1950-2019), while the environmental analysis covered a 15-year period (2005-2019).

The climatological analysis identified significant differences between East and Gulf coast TCs regarding tornado frequency, seasonality, and spatial distribution. Multiple sounding-based environmental metrics were also identified as being both significantly different between the two coasts and potentially pragmatic for forecasting purposes. In general, among these metrics, the East coast environment exhibited greater low-level moisture and instability, while the Gulf coast environment exhibited greater low-level vertical shear and helicity. An analysis of the synoptic environment identified several patterns that likely contributed to TC tornado development, including close proximity to an upper-level jet, the presence of mid-level dry air intrusions, and the presence of baroclinic boundaries within the onshore front-right quadrant.

ACKNOWLEDGEMENTS

Thank you to my advisor Dr. Matthew Eastin, and other thesis committee members, Dr. Casey Davenport and Terry Shirley, who all provided valuable guidance and support throughout the duration of the project and my academic studies at UNC Charlotte. Another special thanks to my wife, Frankie Toadvine, for her unwavering support, encouragement, and the sacrifices she made as I pursued my undergraduate and graduate studies.

TABLE OF CONTENTS

LIST OF FIGURES

LIST OF TABLES

LIST OF ACRONYMS

AGL - Above Ground Level

BRNSHEAR - BRN Shear

CAPE - Convective Available Potential Energy

CIN - Convective Inhibition

DCAPE - Downdraft CAPE

EFFBOT - Bottom of the Effective Inflow Layer

EFFDEP - Depth of the Effective Inflow Layer

EFFSHEAR - Effective Shear

EFFTOP - Top of the Effective Inflow Layer

EL - Equilibrium Level

LCL - Lifted Condensation Level

LFC - Level of Free Convection

LR - Lapse Rate

LR03 - 0-3 km AGL Lapse Rate

LR700500 - 700-500 mb Lapse Rate

MLCAPE - Mean-Layer CAPE

MLCAPE03 - 0-3 km AGL Mean-Layer CAPE

MLCIN - Mean-Layer CIN

MLRH - Mean-Layer Relative Humidity

MLTHE - Mean-Layer Equivalent Potential Temperature

MUCAPE - Most-Unstable CAPE

MUCIN - Most-Unstable CIN

RH - Relative Humidity

RH02 - 0-2 km AGL Mean Relative Humidity

RH24 - 2-4 km AGL Mean Relative Humidity

RH46 - 4-6 km AGL Mean Relative Humidity

SBCAPE - Surface-Based CAPE

SBCAPE03 - 0-3 km AGL Surface-Based CAPE

SBCIN - Surface-Based CIN

SBTHE - Surface Equivalent Potential Temperature

SCP - Supercell Composite Parameter

SCPEFF - Effective Layer Supercell Composite Parameter

SCPFIX - Fixed Layer Supercell Composite Parameter

SHEAR01 - 0-1 km AGL Vertical Wind Shear

SHEAR03 - 0-6 km AGL Vertical Wind Shear

SHEAR06 - 0-6 km AGL Vertical Wind Shear

SHERBE - Effective Layer Sherburn Parameter

SHERBS3 - 0-3 km AGL Fixed Layer Sherburn Parameter

SRH - Storm-Relative Helicity

SRHEFF - Effective Inflow Layer Storm-Relative Helicity

SRH01 - 0-1 km AGL Storm-Relative Helicity

SRH03 - 0-3 km AGL Storm-Relative Helicity

SRH05 - 0-500 m AGL Storm-Relative Helicity

STMHLF - Half of the Storm Effective Depth

STP - Significant Tornado Parameter

STPEFF - Effective Layer Significant Tornado Parameter

STPFIX - Fixed Layer Significant Tornado Parameter

TC - Tropical Cyclone

TCTOR - Tropical Cyclone Tornado

Chapter 1: Introduction

1.1 Introduction

Tropical cyclones (TCs) are a regular phenomenon in the Atlantic Basin and commonly impact the East and Gulf coasts of the United States. Along with the normal threats associated with TCs (i.e., strong surface winds, coastal storm surge, and inland flooding), TC-induced tornadoes (TCTORs) pose a significant threat to life and property. Hurricane Ivan (2004), which made landfall on the Gulf coast, produced 118 tornadoes that resulted in roughly $86.08 million in damage and 7 deaths. Hurricane Florence (2018) made landfall on the East coast and produced 44 tornadoes which resulted in approximately $2.79 million in damage and one death. Relative to other aspects of TC structure, evolution, and impacts, numerous aspects of TCTORs remain poorly understood. For example, from a synoptic-climatology perspective, regional variations in the spatiotemporal distribution of TCTORs have not been fully studied despite limited evidence that East coast TC landfalls produce less tornadoes than Gulf coast TC landfalls (Gentry 1983; Weiss 1987; McCaul 1991). Schultz and Cecil (2009) compiled the most complete TCTOR climatology to date but did not explore differences between the two coasts. More recently, Moore and Dixon (2011) documented TCTOR activity for Gulf coast landfalls only. A better understanding of tornado activity produced by East-coast TC landfalls is still needed. Do East-coast TC landfalls produce significantly less tornadoes? If so, is the relative dearth related to the angle at which TCs cross the coastline or differences in the local environment?

1.2 Motivation and Goals

It is well-known that the methods for detecting and reporting tornadoes have improved over the years as technology has advanced, coastal populations and storm spotter networks have

grown, and communications have improved. Such advances have led to a steady increase in the annual number of documented TCTORs compared to decades ago. The official TCTOR database began in the year 1950, which was prior to the implementation of operational Doppler radar, so observations were limited to eyewitness reports with varying degrees of reliability (Doswell and Burgess 1988). Even after the Doppler radar was placed in operation, the coverage and quality of those earliest radars were very limited. In the early to mid-1990s, NOAA began to utilize the WSR-88D radars in daily operations which dramatically increased the detection and verification of TCTORs through more advanced detection techniques and vastly improved spatial coverage. As previously mentioned, coastal populations have grown over the past 70 years, and storm spotter training has increased its impact as well. These, along with the rise of social media which has allowed for the sharing of tornado reports and images in near-real-time, have contributed to the growth of the TCTOR database in recent years. With this in mind, and given that the last formal update to the TCTOR climatology record was 12 years ago, another update is needed. Not only will such an update provide the most recent data, but it will also allow for trend analysis within the era of improved detection and reporting. For example, have East coast TCTORs become more or less frequent relative to Gulf coast TCTORs since the introduction of the Doppler radar network?

It has been well documented that TCTORs are notably different from non-TC tornadoes (Edwards 2012). TCTORs are generally less intense than their mid-latitude counterparts with the overwhelming majority rating EF0 or EF1 on the Enhanced Fujita Scale, and no TCTORs rated EF5 have been recorded. TCTORs also have shorter lifespans than non-TC tornadoes; a result of structural differences between their parent supercells. TCTORs are typically produced by what are referred to as “miniature” supercells that are shallower, less intense, and have shorter

lifespans than traditional supercells (Eastin and Link 2009). Miniature supercells typically have weaker radar reflectivities (<50 dBZ) and rotational velocities (<15 m/s), shallower mesocyclones and smaller mesocyclone diameters (~4 km and <7 km, respectively), shallower updrafts (<10 km), and shorter lifespans (<2 hr; Eastin and Link 2009; Schenkel et al. 2020). These differences in structure stem from differences in the local environment in which they develop. TCs are warm-core systems with maximum winds (and maximum vertical wind shear) within the lowest 3 km AGL while exhibiting smaller radius-dependent instability (e.g., CAPE ranges from <500 J/kg near the eyewall to ~2000 J/kg in the outer rainbands). In contrast, mid-latitude cyclones are cold-core systems with maximum winds near the tropopause, strong vertical wind shear throughout the troposphere, and relatively large instability (CAPE often exceeds 2000 J/kg). Currently, TCTOR forecasts are formulated using sounding-derived vertical wind shear, instability, and moisture metrics that have been developed for forecasting mid-latitude supercells. Because of this, TCTOR forecasting is still a significant challenge. Thus, a greater understanding of the local TCTOR environment may help to identify new TCTOR-specific sounding-based metrics that could improve forecasts and explain coastal differences in TCTOR events.

There are four primary goals of this research. The first goal is to update the TCTOR climatology record through 2019. This updated climatology will include the most recent 12 years since the last comprehensive TCTOR database was compiled by Schultz and Cecil (2009). Furthermore, the updated database will be used to identify and assess differences between East coast and Gulf coast landfalling TCs, including their TCTOR production. After the climatologies have been analyzed, RUC-RAP model analyses will be utilized to identify TCTOR proximity soundings and the local TCTOR environment will be analyzed in greater detail. With

regards to the soundings, multiple sounding-based parameters will be evaluated to identify whether significant differences exist between East coast and Gulf coast TCTOR environments. It is anticipated that the results of this study will assist forecasters, emergency managers, and other public officials to recognize the potential for TCTORs prior to, and during, a landfalling TC event. By analyzing the TC environment differently than a traditional mid-latitude system, these organizations and individuals can provide more adequate pre-storm preparedness to at-risk communities, as well as improve real-time warning products and long-term preparedness.

Chapter 2: Background and Literature Review

2.1 Introduction

The following section summarizes the results and findings of previous studies that have been performed with respect to TCTORs. Section 2.2 details the basic TCTOR climatology statistics per TC. Section 2.3 covers the observed TCTOR intensities and how they compare with traditional mid-latitude tornado intensity distributions. Section 2.4 discusses the spatial distributions of TCTORs within a TC-relative framework as well as the distribution within the United States as a function of distance from the coastline. Section 2.5 will focus on the frequency of TCTOR production as a function of the time of day. Section 2.6 discusses the relationship between TC motion and TCTOR production. Section 2.7 looks at the production of TCTORs as a function of TC intensity. Section 2.8 details the distribution of TCTOR production as it relates to the time of TC landfall. Section 2.9 covers the instability parameters that are found within the local TCTOR environment. Section 2.10 focuses on the vertical shear parameters in the local mesoscale environment that influence TCTOR production. Finally, Section 2.11 discusses the critical gaps within the research and how addressing those gaps will be beneficial to the scientific community and public.

2.2 Basic Statistics per Tropical Cyclone

Multiple TCTOR climatologies have been conducted over the past several decades for landfalling TCs impacting the United States. The first was by Novlan and Gray (1974), who focused on TCTORs produced by hurricanes and tropical storms during 1948-1972. In their analysis, a total of 83 TCs made landfall in the United States and only 25% produced tornadoes.

Excluding Hurricane Beulah (which produced 141 TCTORs), the average TC produced 10 tornadoes.

Gentry (1983) also completed a climatology that expanded on the work done by Novlan and Gray (1974). Gentry expanded the climatology to include data from 1948-1982, and then subdivided the years 1948-1980 into three 11-year bins with which he could compare how the number of TCTORs has changed over time. Gentry discovered that there was a 30% increase (from 32% to 62%) in the number of TCs that produced at least one tornado between the first and final 11-year bins. He also found that, beginning in 1959, nearly every TC of hurricane strength that made landfall in the United States had tornadoes reported. Gentry suggested that the increase in TCTORs may have been due to improvement in tornado reporting.

Expanding upon Gentry (1983), McCaul (1991) studied TCTORs that occurred in the years 1948-1986 (adding four years to the TCTOR dataset). A key difference between the studies is that McCaul included tornadoes produced by all TC subgroups present in the HURDAT database (e.g., tropical depression, tropical storm, hurricane, and some subtropical storms) whereas Gentry focused only on those produced by tropical storms and hurricanes. Despite this methodological difference, McCaul found that nearly 59% of all landfalling TCs produced a tornado, which was similar to the findings of Gentry.

Focusing strictly on TCs classified as hurricanes between the years 1954-2004, Verbout et al. (2007) identified 83 hurricanes that made landfall in the United States, and of those, 69 produced at least one reported tornado, or roughly 83%. They noted that of the 14 hurricanes that did not produce tornadoes, only four occurred after 1973, suggesting that most landfalling TCs of at least hurricane strength produce tornadoes that can be readily detected and reported when sufficiently dense observation networks (e.g., Doppler radar networks) are present.

Schultz and Cecil (2009) have produced the most comprehensive TCTOR climatology to date, covering a 58-year period from 1950-2007 and including all TC classifications. While statistics regarding the number of TCTORs per landfalling TC were not explicitly reported, they noted that their findings were "consistent with previous climatologies".

Taking a slightly different approach to building a TCTOR climatology, Moore and Dixon (2011) focused on tornadoes that were produced by hurricanes that made landfall on only the Gulf coast during the years 1950-2005. Their results suggested significant variability in the number of tornadoes produced by each hurricane; some produced no TCTORs while others produced large outbreaks, defined as the number of TCTORs produced by a TC exceeding the 80th percentile. Among the 60 hurricanes included in their analysis, they found that 83% produced tornadoes, consistent with the findings of Verbout et al. (2007) who also focused on only landfalling hurricanes. The average number of TCTORs per hurricane was roughly 12 with a standard deviation of nearly 19, which aligns with the idea that TCTOR counts are highly variable from one TC to the next.

While differences exist between each climatology and how they were compiled, what is easy to see is that there has been an increase in the number of reported TCTORs throughout the years. In more recent studies (Verbout et al. 2007; Schultz and Cecil 2009; Moore and Dixon 2011), the study periods included data after the 1990s when WSR-88D radars were well-incorporated into daily operations. These radars improved observational coverage and the identification of potential convective cells capable of producing tornadoes (i.e., miniature supercells) which may have led to further increases in the number of reported TCTORs (Doswell and Burgess 1988; Verbout et al. 2007; Schultz and Cecil 2009; Edwards 2012). Moreover, most of these studies did not delineate between landfalling coast (i.e., East and Gulf coasts). Only McCaul (1991) briefly provided a comparison of the number and percentage of TC landfalls that

produced tornadoes along each coast, finding that only 40% of East coast TC landfalls produced tornadoes whereas Gulf coast TC landfalls produced tornadoes roughly 70% of the time. Moore and Dixon (2011) focused strictly on Gulf coast hurricane landfalls, and found that 83% produced tornadoes, an apparent increase in comparison to McCaul's findings (that also included tropical storms and depressions). No study has provided a direct detailed comparison between the two coasts, nor has any study focused strictly on an East coast TCTOR climatology.

2.3 Tornado Intensity

Although the variability in the number of tornadoes per TC is high, the distribution of the intensity of TCTORs is more straightforward. Previous research has concluded that the majority of TCTORs are weaker overall than their non-tropical counterparts (Novlan and Gray 1974; McCaul 1991; Schultz and Cecil 2009; Moore and Dixon 2011; Edwards 2012). Schultz and Cecil (2009) report that in their 58-year dataset from 1950-2007, a greater percentage of TCTORs exhibited F0 intensity (49%) when compared to all reported tornadoes across the United States (42%). The difference in percentages between F1 reports is much smaller (32.1% and 32.4%, respectively), but for F2-F5 intensity, the number of TCTORs becomes much less than all other tornadoes. Among the TCTOR reports, those of F2 intensity encompass 11.6%, F3 tornadoes encompass 2.2%, F4 events encompass less than 1%, and no F5 tornadoes have been produced by landfalling TCs.

Presented in a different manner, Edwards (2012) displayed the frequency of TCTOR intensities using a logarithmic scale (Figure 2.1). In Edwards' classification scheme, the majority of TCTORs were classified as "weak" (F0/F1) and encompass ~81% of all TCTORs, while ~14% were classified as "strong" (F2/F3), and less than 1% were classified as "violent" (F4/F5). The remaining 4% were of unknown intensity. Results from Moore and Dixon (2011)

were consistent with these findings along Gulf coast landfalling hurricanes; roughly 81% of such TCTORs were classified as weak (F0/F1), 18% were classified as strong (F2/F3), and the remaining 1% comprised two F4 TCTORs produced by Hurricanes Carla (1961) and Hilda (1964).

TCTORs are generally weaker than traditional mid-latitude tornadoes due to structural and environmental differences between their parent supercells (Novlan and Gray 1974; Schultz and Cecil 2009; Moore and Dixon 2011; Edwards 2012). TC environments are more thermally stable with most of the necessary shear and instability residing near the surface whereas mid-latitude systems have deeper thermal instability and vertical wind shear. Parent supercells of TCTORs are also generally shorter-lived and smaller than those found in the mid-latitudes.

Verbout et al. (2007) identified a trend in which all reported US tornadoes have increased in number while the number of F1+ reports has remained relatively constant over time. However, Schultz and Cecil (2009) suggested that a slight decrease occurred in the number of F1+ TCTOR reports in recent years while the number of F0/all reports increased. With the inclusion of the most recent 12 years of TCTOR data (2008-2019), our study can address whether the trends identified by Schultz and Cecil continue and are robust.

2.4 Spatial Distributions

The spatial distribution of TCTORs within the TC circulation has been analyzed using three different polar grid frameworks: earth-relative, motion-relative, and shear-relative. The earth-relative framework positions each TCTOR relative to the TC circulation center (located at the center of the polar grid) as a simple function of cardinal direction (more specifically, radius and azimuth) relative to the center. The motion-relative framework positions each TCTOR as a function of radius and azimuth relative to the direction of TC motion (whereby the motion vector

always points due north on the polar grid). Similarly, the shear-relative framework positions each TCTOR relative to the direction of the deep-layer environmental vertical shear (often defined between 850-hPa and 200-hPa within 500 km of the TC center and rotated so the shear vector points due north on the polar grid).

The earth- and motion-relative frameworks are two common frameworks that are used to display TCTOR distribution within a TC, but important distinctions must be made between the two in order to understand their significance. The earth-relative framework uses the cardinal directions when locating TCTORs with respect to the TC center. A polar grid is constructed with 0° representing North and increasing in the clockwise direction, and quadrants are referenced using the cardinal nomenclature (i.e., Northeast quadrant). The motion-relative framework; however, uses the TC motion vector as reference with 0° being in-line with the TC motion vector. When referring to specific regions in this framework, regions are named by their location in relation to the TC's motion. For example, the region bounded by -90° to +90°, centered on 0°, is considered to be the "front" or "forward" region of the TC.

It is commonly agreed that most TCTORs occur in the northeast (or front-right) quadrant with extension into the southeast (or back-right) quadrants (Edwards 2012; Schultz and Cecil 2009; Novlan and Gray 1974; McCaul 1991). Novlan and Gray (1974) found that the centroid of all TCTORs from the years 1948-1972 was located at 50° in the earth-relative framework. When they used the motion-relative framework, they found that the centroid shifted from 50° to 80°. McCaul (1991) provided only the motion-relative framework claiming that many of the TCs analyzed had a strong northward component to their motion. His findings supported the notion of the front-right (northeast) quadrant being the preferred sector of TCTOR development. Schultz and Cecil (2009), with a much larger dataset to work with, found agreeing results with the previous studies mentioned. Their findings; however, differed from those of Novlan and

Gray (1974) with respect to the centroid shift when changing frameworks. Schultz and Cecil found that there was a counter-clockwise shift in TCTOR distribution when the framework changed from earth- to motion-relative (Figure 2.2). Regardless of this difference, the preferred sectors were still the front-right (or northeast) sectors. Edwards (2012) utilized both frameworks as well, and his findings supported those of Schultz and Cecil (2009) with respect to the shift in centroid and the preferred sectors previously mentioned. Edwards also suggested that a loosely defined sector is a better classification of where TCTORs are most likely to develop as the variability in TCTOR location increased with larger datasets. He identified the proposed preferred sector as extending from the north-northwest, through northeast quadrant, to roughly southeast of TC center.

The shear-relative framework also presents a similar lopsided distribution when compared to the other two frameworks. TC-scale vertical wind shear, or the environmental shear acting on the whole TC, has been shown to be a major influencer in the spatial distribution of TCTORs within a given TC. Among all sizes of TCs, the majority of TCTORs occur in the downshear region within a given TC, shifting from downshear/downshear-left to downshear-right as the distance from the TC center increases (Figure 2.3) (Schenkel et al. 2020; Paredes et al. 2021). To take it a step further, Schenkel et al. (2020) found that TCTORs are more common in TCs that are experiencing stronger TC-scale vertical wind shear (i.e., greater than 11.2 m/s), and develop more frequently in the downshear-right region.

Aside from the azimuthal distributions, one aspect of the spatial distribution of TCTORs that is commonly addressed is the radius, or range, from the TC center as preferred regions have been identified (McCaul 1991). TCTORs most commonly develop between 200-400 km from the TC center with a secondary maximum closer to the center at the 100 km range (McCaul 1991). Not only is there a general affinity for TCTORs to develop in certain ranges, but different

intensities of TCTORs have different ranges in which they more commonly develop. Schultz and Cecil (2009) found that tornadoes that develop within 200 km of the TC center tend to be weaker, more commonly rating F0 or F1. Along with this, they found that stronger TCTORs develop in more distant ranges on average than weaker TCTORs, although the difference in ranges is roughly 50-100 km.

There have been several studies that have investigated the distribution of TCTORs as a function of distance from the coastline (Novlan and Gray 1974; Schultz and Cecil 2009; Moore and Dixon 2011; Edwards 2012). There is strong agreement and evidence that the majority of TCTORs occur within the first 100-200 km from the coastline with a rapid decrease in TCTOR activity beyond those distances. Most of the TCTORs closest to the coastline are associated with TC landfall and rainbands coming onshore. Schultz and Cecil (2009) also investigated whether stronger TCTORs were more frequent further inland and found that such TCTORs followed similar decreasing counts in frequency with increasing distance from the coastline (Figure 2.4).

2.5 Time of Day

TCTORs can occur at any hour of the day; however, there appears to be a diurnal trend in the number of reported TCTORs that has been noted by several researchers (McCaul 1991; Schultz and Cecil 2009; Moore and Dixon 2011). In both Coordinated Universal Time (UTC) and Local Solar Time (LST), there is a gradual increase in TCTOR counts throughout the day to a late-afternoon/early-evening peak followed by a sharp decline after sunset. Although there is a distinct overall pattern common among the two time references, there are also differences between the two. Using UTC, Moore and Dixon (2011) identified a diurnal pattern in TCTOR frequency with a peak occurring between 2000-2159 UTC and a minimum occurring between 0400-0559 UTC (Figure 2.5). Edwards (2012) reached similar conclusions while using 3-hourly

bins, identifying the 18-21 UTC bin as having the highest number of TCTORs and 05-08 UTC having the fewest. Most other researchers have used LST and have concluded peak TCTOR report times that are slightly earlier. McCaul (1991) reported the peak occurrence being between 15-18 LST using 3-hourly bins, and Schultz and Cecil (2009) found their peak to be 14-17 LST using 1-hourly bins (Figure 2.6).

Possible explanations for the apparent diurnal cycle have included simple daytime heating of the surface (similar to non-TC tornadoes), and a reporting bias where weaker tornadoes do not go reported if little to no damage is reported overnight (Schultz and Cecil 2009). The former possible explanation is addressed by Schultz and Cecil (2009), where they analyzed the increase in both TCTOR and all tornado reports from morning to afternoon. They found that TCTOR reports increased by a factor of four whereas the overall tornado report counts increased by a factor of 12, suggesting that daytime heating plays a lesser role in TCTOR development.

Although there is a general pattern present among all TCTORs that have been studied, is there a significant difference in the time of day between East coast and Gulf coast TCTORs? With the mixed usage of UTC and LST, it can become difficult to interpret any differences between the studies that focused on all TCTORs and the study done by Moore and Dixon (2011), and to further complicate the matter, no study has isolated East coast TCTORs for such analysis. Therefore, a direct comparison between the two coasts must be made using the same time reference.

2.6 Tropical Cyclone Motion

It has been suggested that TC motion, both speed and direction, at landfall plays a crucial role in the development of TCTORs (Novlan and Gray 1974; Gentry 1983; McCaul 1991;

Verbout et al. 2007; Schultz and Cecil 2009). With respect to the translational speed of a TC during landfall, McCaul (1991) identified that there was a preference for TCTOR development in TCs that were moving faster (> 5 m/s) than TCs that produced no tornadoes (3-4 m/s). McCaul noted that this delineation breaks down at speeds greater than 15 m/s (as few TCs produce tornadoes when translating at such speeds). Schultz and Cecil (2009) also analyzed TC translational speed and found results that were consistent with the findings of McCaul (1991), identifying that greater percentages of TCs that produce tornadoes have faster forward motion (≥ 5 m/s) (Figure 2.7).

TC direction at the time of landfall, or when approaching land, seems to have a greater influence on the number of TCTORs that are produced. Novlan and Gray (1974) found that the mean heading of TCs that produced tornadoes was 30°. Gentry (1983) found that most hurricanes had headings between 300° and 30° with little variation between those that produced fewer or more tornadoes. McCaul (1991) used a different style of directional classification, assigning 90° to TCs that made landfall moving perpendicular to the coastline. He then separated the TCs into their respective landfall basins and found that the mean directional heading of TCs along the Gulf coast was approximately 90°. Alternatively, he found that East coast TCs typically make landfall with headings that range between near-parallel to the coast (0° in his system) and perpendicular to the coastline, being strongly skewed toward the smaller heading values. Schultz and Cecil (2009) did not study differences between the East and Gulf coast TC motion but found consistent TCTOR-producing TC headings between 300° and 40° (Figure 2.8).

There are some possible explanations for these trends. With respect to the translational speed, McCaul (1991) found that faster TCs were associated with stronger winds aloft and drier local environments. The stronger upper-level winds help provide increased mesoscale shear

which can support TCTOR development. Regarding the direction of TC motion, the explanation of its associated trend is much more straightforward. With the front-right quadrant of a TC being the preferred sector for TCTOR development, the angle at which the TC makes landfall can be crucial. The Gulf coast TCs studied by McCaul (1991) approached the coastline near-perpendicular which allowed for the preferred TCTOR sector to also move onshore and maximize the time spent onshore. Conversely, when he studied East coast TCs, they approached the coastline with less direct angles, keeping the preferred sector offshore in many cases. This is generally accepted as one reason for lower TCTOR counts in East coast landfalling TCs, but could an environmental factor also be at play for those that do manage to bring the front-right quadrant ashore?

2.7 Tropical Cyclone Intensity

TC intensity has long been thought to be a strong indicator of the potential for TCTOR development, and previous research has supported this notion. TCs that produce TCTORs have been shown to be stronger at landfall than those TCs that do not produce any tornadoes (Novlan and Gray 1974; McCaul 1991; Verbout et al. 2007; Moore and Dixon 2011). Novlan and Gray (1974) found that roughly two-thirds of all TCTORs were produced during the dissipating stages of intense TCs whereas the remainder of TCTORs were produced while the TC was at peak intensity. They noted that TCTOR-producing TCs had a mean minimum central pressure of 955 mb and mean maximum surface winds of 102 knots. This is significantly stronger than TCs that they found did not produce any TCTORs with those TCs having a mean minimum pressure of 975 mb and mean maximum winds of 65 knots. McCaul (1991) supported these previous findings with respect to the maximum winds. He identified TCs that produced at least one tornado had average peak winds of 28.7 m/s, and those that produced greater than eight

tornadoes had average peak wind speeds of 47.1 m/s. In comparison, TCs that produced no tornadoes only had average peak wind speeds of 21.9 m/s. Verbout et al. (2007) took a different approach and analyzed TCTOR outbreaks as a function of TC intensity. Their findings suggested that TCs of Category 2 intensity or greater are more likely to produce TCTOR outbreaks which is consistent with previous studies. Moore and Dixon (2011) concluded that there was no simple or direct correlation between TC intensity and TCTOR production; however, they noted that Category 3 hurricanes produced a substantially larger percentage of TCTORs even though the frequency of Category 3 hurricanes at landfall was much less frequent than weaker systems.

Although correlation does exist between TC intensity and TCTOR production, it has been described as weak (Moore and Dixon 2011) and suggestive that other dynamical factors are at work. The intensity of a given TC at landfall may be a predictor of its potential for TCTOR development, but other factors must be considered. As Novlan and Gray (1974) mentioned, there is a preference for TCTOR production in TCs that are dissipating which begs the question, at what intensity during dissipation are TCTORs favored, if any? Is it possible that the momentum of an intense TC at landfall may persist in the upper levels of the storm as it progresses inland leading to enhanced low-level vertical wind shear in the mesoscale environment of outer rainbands?

2.8 Time from Landfall

It has been well documented in multiple studies that TCTOR development follows a general pattern in relation to the time of TC landfall (McCaul 1991; Schultz and Cecil 2009; Moore and Dixon 2011). The pattern begins with a sharp increase in TCTOR counts within 12-24 hours prior to landfall as TCs near the coastline and outer rainbands move onshore. This is

followed by a peak in TCTOR activity within 12 hours of landfall, and then a gradual decline in activity beyond 24-36 hours after landfall.

McCaul (1991) used 24-hour bins to identify when TCTORs occur in relation to TC landfall. These bins were centered on days from landfall. For example, TCTORs occurring on Day 0 occurred within 12 hours of landfall, either before or after. What he found was a slight increase in TCTOR activity in the two days prior to landfall with a sharp increase and peak in TCTOR activity on Day 0 (+/- 12 hours of landfall). The days following landfall exhibited a rapid decline in activity with most activity ceasing prior to the end of the third day after landfall. Schultz and Cecil (2009) used 12-hour bins instead to identify more temporal detail, separated the data into the core region (≤ 200 km from TC center) and the outer region (> 200 km from TC center), and delineated each bin by tornado F-scale. What they found was that core region TCTORs (of all intensities) occurred more frequently within 12 hours of landfall, both before and after. When they analyzed the outer region TCTORs, they found that there was a broader peak in TCTOR frequency between 12 hours prior to landfall through 24 hours after landfall with a gradual decline after 24 hours. Moore and Dixon (2011) used 1-hour bins when analyzing Gulf coast TCTOR frequency as a function of time from landfall. In doing so, they identified greater variability in frequency than in previous studies, but the overall trend was similar. They identified several clusters of elevated TCTOR activity at 3-4 hours prior to landfall (15% of all TCTOR activity), 1-2 hours after landfall (33%), 12-19 hours after landfall (17%), and 36-41 hours after landfall (9%).

There is general consensus in the literature as to the reasoning for such a distinct pattern in TCTOR frequency as a function of time from TC landfall. TCTORs that develop prior to landfall are the result of outer rainbands moving onshore ahead of the TC center whereas the peak at, or just after, landfall is attributable to the bulk of the TC crossing land which increases

the low-level shear due to friction in a large portion of the storm, particularly in the front-right, or northeast, quadrant.

2.9 Instability Parameters

As TCTORs are commonly confined within certain areas around the TC, it is reasonable to hypothesize that the local environments surrounding the TC (i.e., within the TC circulation) are not identical. The instability parameters that often exhibit pronounced azimuthal and radial variations are convective available potential energy (CAPE), convective inhibition (CIN), lifted condensation level (LCL), and the low- to mid-level relative humidity (RH).

CAPE is well-known to be a required ingredient for tornado development. CAPE can be measured using different lifted parcels which results in different types of CAPE. Common variations include surface-based (SBCAPE), mean-layer (MLCAPE), and most-unstable (MUCAPE). In the mid-latitude environments, each variation of CAPE has its use, and each can have different implications in storm development, but within a TC environment, it is common to find the SBCAPE equivalent to the MUCAPE. Novlan and Gray (1974) suggested that in comparison with their non-TC counterparts, the required CAPE is much lower on average for TCTORs. McCaul (1991) found this to be the case when analyzing TCTOR proximity soundings. He identified that the average surface-based CAPE within the front-right quadrant of the TC, where most TCTORs develop, was 684.2 J/kg. He also noted that SBCAPE increased with range from the TC center, averaging 670 J/kg at radii less than 300 km and 704 J/kg at radii greater than 300 km. McCaul also contoured the mean values of SBCAPE with respect to TC center (Figure 2.9) which suggested that SBCAPE did not increase uniformly with radius, but increased substantially more to the right (or east) of TC center.

More recent case studies (McCaul et al. 2004; Baker et al. 2009; Eastin and Link 2009) have suggested that SBCAPE values may be more variable and larger in magnitude than documented by McCaul (1991). For example, McCaul et al. (2004) speculated that previously derived SBCAPE values may be too small, as SBCAPE exceeded 2000 J/kg near an outer rainband of TS Beryl (1994) that spawned 29 tornadoes. Likewise, from a case study of Hurricane Andrew (1992), McCaul et al. (1993) found that SBCAPE was maximized near the middle of primary rainbands. It was speculated that the proximity soundings used in McCaul (1991) may have been launched in less-than-ideal conditions (i.e., near active convection and/or downwind of the relevant TCTOR). Furthermore, when performing a case study on Hurricane Ivan (2004), Baker et al. (2009) found average front-right quadrant SBCAPE values to be 1562 J/kg within 500 km of TC center. Eastin and Link (2009) used two separate soundings (a NOAA G-IV dropsonde and an operational rawinsonde at Tampa Bay) to determine the convective parameters available for TCTOR development within Hurricane Ivan (2004). They found that dropsonde-based CAPE in the near-supercell environment was relatively low (960 J/kg of MUCAPE, 618 J/kg of MLCAPE) but CAPE from the Tampa rawinsonde (located further from the TC center and relevant supercells) was much larger (> 2300 J/kg). An interesting note from their findings was that the SBCAPE and MUCAPE were equivalent in both soundings.

CIN is another useful parameter for forecasting tornadoes. The role of CIN in the TCTOR framework has rarely been evaluated; however, there appeared to be some consensus between the few case studies (Baker et al. 2009; Eastin and Link 2009). When evaluating the front-right quadrant of Hurricane Ivan (2004), Baker et al. (2009) averaged all soundings within that quadrant and found CIN values to be -10.7 J/kg and -12.3 J/kg in the 0-500 km and 500-750 ranges from TC center, respectively. Eastin and Link (2009), using their two sounding methods in Hurricane Ivan (2004), found that CIN values were similar to those found by Baker et al. The

dropsondes identified a CIN value of -16 J/kg near the observed rainband and a value of -12 J/kg from the Tampa Bay rawinsonde approximately 250 km east-southeast of the rainband.

LCL values can be of importance as they can help identify how close to the surface a cloud base may be (as well as the relative moisture content of the sub-cloud layer). Lower LCLs can result from a reduction in near-surface temperatures and/or an increase in near-surface moisture. In terms of TCTOR development, lower cloud bases support the generation of vertical vorticity nearer to the surface (via the tilting and stretching of shear-induced horizontal vorticity by the air rising through cloud base). Baker et al. (2009) identified a noteworthy difference between LCL heights on the left and right side (with respect to TC motion) of Hurricane Ivan (2004). They found that the right side LCL heights were roughly 200 meters less than those on the left side, suggesting that this reflected the advection of moist maritime air on the right side of the TC. When averaging the front-right quadrant together, they found that LCL heights within 500 km of TC center averaged 380 meters, and the heights were slightly less at 350 meters between 500-750 km from TC center. Eastin and Link (2009) found that their rainband proximity soundings calculated LCLs of 520 meters approximately 50 km west of the observed rainband and 640 meters approximately 220 km east-southeast of the rainband.

TCs require a deep layer of moist air in order to sustain themselves and thrive. While mid-level dry air intrusions normally weaken TCs, such intrusions can be beneficial for TCTOR development (Curtis 2004). Curtis found that LCLs were lower (by 141 meters), the surface to 900 mb RH was larger (> 92%), and the layers above 700 mb were drier (< 82%) in the front-right quadrant of multiple TCs that experienced a dry air intrusion relative to TCs that did not. While no identifiable spatial pattern was found, these results suggested that some dry air may be necessary for TCTOR development through an increase of convective instability by means of

increasing the environmental lapse rate (through a combination of enhanced solar heating of the surface and mid-level evaporational cooling from adjacent rainbands.

2.10 Vertical Shear Parameters

Not only do tornadoes require instability, but also sufficient vertical wind shear (VWS) in the mesoscale environment. Varying degrees of VWS have been found to aid in the development of tornadoes. Within TCs, previous studies have shown that VWS is vital to the development of TCTORs and the most intense VWSs often determine the location of TCTOR activity within a given TC (McCaul 1991; McCaul et al. 2004; Eastin and Link 2009; Schenkel et al. 2020; Paredes et al. 2021). Looking at the spatial distribution of 0-3 km relative helicity, McCaul (1991) found that much of the available helicity was located on the right side of a TC, relative to the TC motion, roughly between 30° and 135° (Figure 2.10). These values were maximized approximately 400 km from the TC center, although the maxima did not cover a large spatial area. He also made note of a distinct shape taken on by hodographs within TCTOR environments. He described this shape as a "loop" or "horseshoe" that is the result of veering winds from the surface through 10 km. McCaul used two different types of proximity soundings which he described as general and close proximity. General proximity soundings were loosely based on the criteria set by Novlan and Gray (1974) which restricted soundings for analysis to those within 100 nautical miles and three hours of a TCTOR. Close proximity sounding criteria were more restrictive, requiring the observed sounding to be within 40-km and two hours of a TCTOR. Using both the general and close proximity soundings, the same "horseshoe" hodograph shape can be seen in Figure 2.11, represented by dark and lighter lines, respectively. For comparison to the traditional mid-latitude supercell environment, McCaul overlaid the close proximity sounding and hodograph with an Oklahoma supercell composite sounding and

hodograph (Figure 2.12). The differences in the hodographs were apparent with the TCTOR hodograph being much more curved and taking on that "horseshoe" shape with significant low-level shear and winds maximized around 2-3 km AGL whereas the Oklahoma supercell hodograph had significant curvature in the lowest 2 km then became straight with maximum winds occurring above 3 km.

McCaul et al. (2004) performed a case study on Tropical Storm Beryl (1994), analyzing the local TCTOR environment that allowed for an outbreak to occur. In their analysis, they found similar hodographs to those seen in Figures 2.11 and 2.12 (close proximity), but with slightly less curvature in the upper levels. They found that 0-3 km helicity values were at least 100 m^2/s^2 with peak values of 250 m^2/s^2 and 0-1 km helicity values peaked greater than 120 m^2/s^2 during the outbreak. Eastin and Link (2009) found similar values using a proximity dropsonde near a tornado-producing rainband of Hurricane Ivan (2004). They found that 0-1 km cell-relative helicity was 185 m^2/s^2 and 0-3 km cell-relative helicity was 233 m^2/s^2. Schenkel et al. (2020) studied the effects of TC-scale VWS and found that in the preferred shear-relative sectors of a TC (downshear left and right), 0-1 km and 0-3 km cell-relative helicity values were maximized within 400 km of TC center in strong TC-scale shear environments. The values of 0-1 km cell-relative helicity within this region ranged anywhere from 0 m^2/s^2 to upwards of 250 m^2/s^2 with medians falling roughly between 30 and 150 m^2/s^2. The 0-3 km cell-relative helicity ranged from 10 m^2/s^2 to over 300 m^2/s^2 with medians ranging from roughly 60 m^2/s^2 to near 200 m^2/s^2. With these favorable sheared environments in mind, Paredes et al. (2021) showed that there was a broader region of favorable helicity values ($\geq$ 100 m^2/s^2) in the downshear region as the size of a TC increases.

2.11 Critical Gaps in Research

The TCTOR climatology is not updated regularly (annually), yet advancements in technology and communication allow for better detection and reporting of TCTORs (Doswell and Burgess 1988). The last comprehensive TCTOR climatology was compiled by Schultz and Cecil (2009). One critical knowledge gap left unaddressed by previous climatologies is TCTOR differences as a function of coastline (Gulf vs. East). Updating the TCTOR climatology and separating the TCTOR data by coastline may allow for some insight into significant spatiotemporal differences in TCTOR production by the landfalling TCs along each coast.

Individual case studies have presented environmental characteristics of specific TCs and their local TCTOR environment using observed proximity soundings. These case studies have exhibited similar results, but also demonstrated that significant variability from one TC to the next can exist. An issue with these studies is their use of observed soundings, which have limited frequency (i.e., rawinsondes are launched at best 6 h intervals during TC landfalls) and limited spatial proximity (i.e., rawinsonde launch sites are sparse and thus proximity soundings are often > 100 km from relevant tornado producing convection). No TCTOR study has yet to take advantage of hourly RUC-RAP model analyses (with 13-40 km spatial resolution). Moreover, a comprehensive statistical analysis with a larger dataset that includes numerous sounding-based instability and shear parameters remains lacking.

Given the apparent discrepancy in the number of TCTORs produced by East and Gulf coast landfalling TCs (McCaul 1991), previous studies have attempted to identify the cause of such discrepancy. Some hypotheses have focused on the TC landfall angle and TC recurvature (Novlan and Gray 1974; McCaul 1991; Verbout et al. 2007; Schultz and Cecil 2009). However, differences in local environmental instability and vertical shear may also be relevant, further motivating a comprehensive statistical analysis between East and Gulf coast TCTOR sounding-

based parameters. Such an analysis may provide crucial information as to whether or not an environmental difference exists between the two coasts, and if that difference, should it exist, be a relevant cause of the dearth of East coast TCTORs.

It should be noted that the Schultz and Cecil (2009) and Moore and Dixon (2011) studies were guides to the climatological analysis performed in this study, and the McCaul (1991) study was a guide to the TCTOR environmental analysis. More details of how the study was conducted are provided in the Data and Methods section.

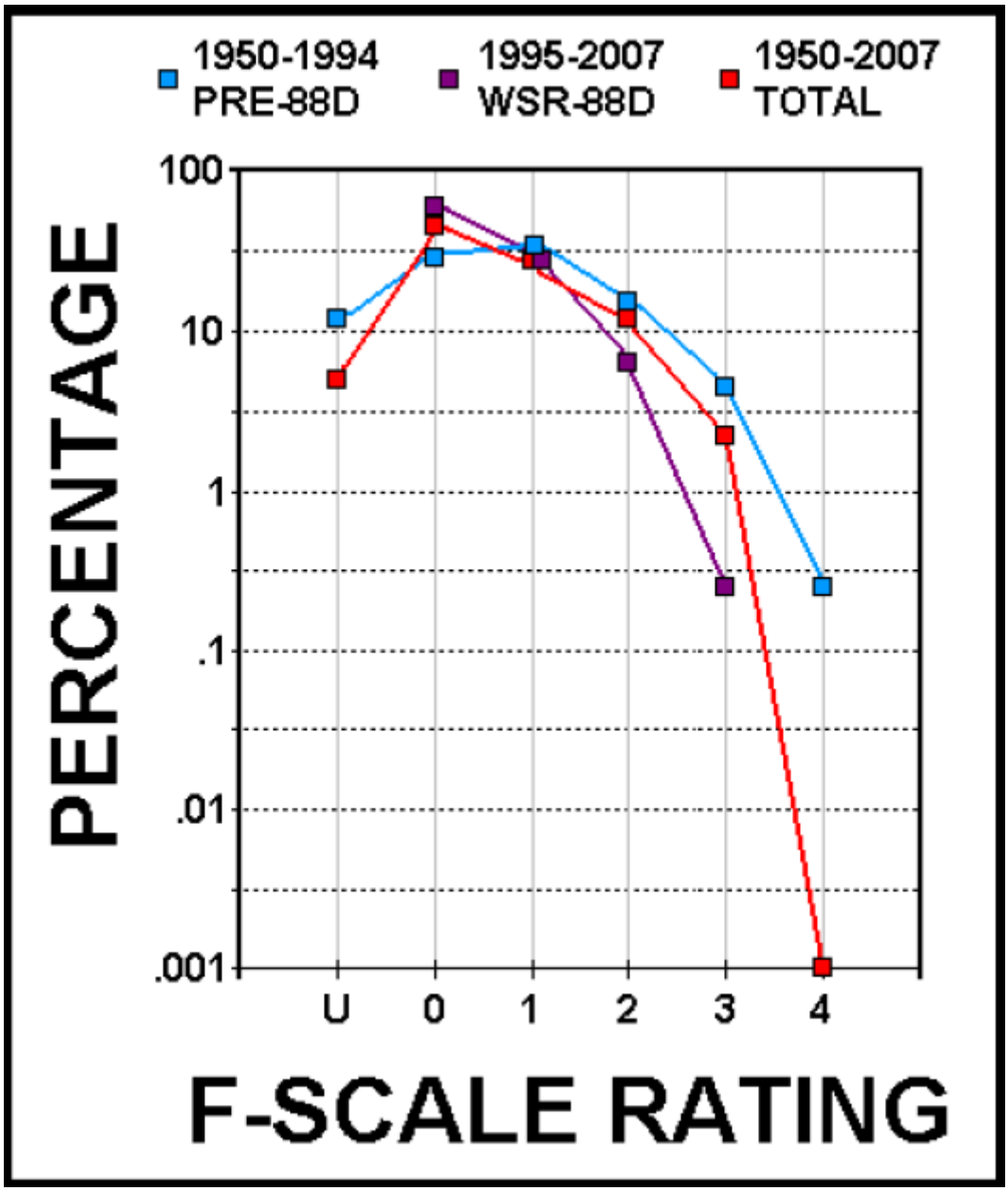

Figure 2.1: Logarithmically scaled line graph of tornado damage-rating distribution, as percentages of each period's total, for time bins preceding (blue) and during (purple) the WSR-88D era, and for the entire period (red). U represents unknown ratings and unrated events, collectively. From data supplied by Schultz and Cecil (2009). From Edwards (2012).

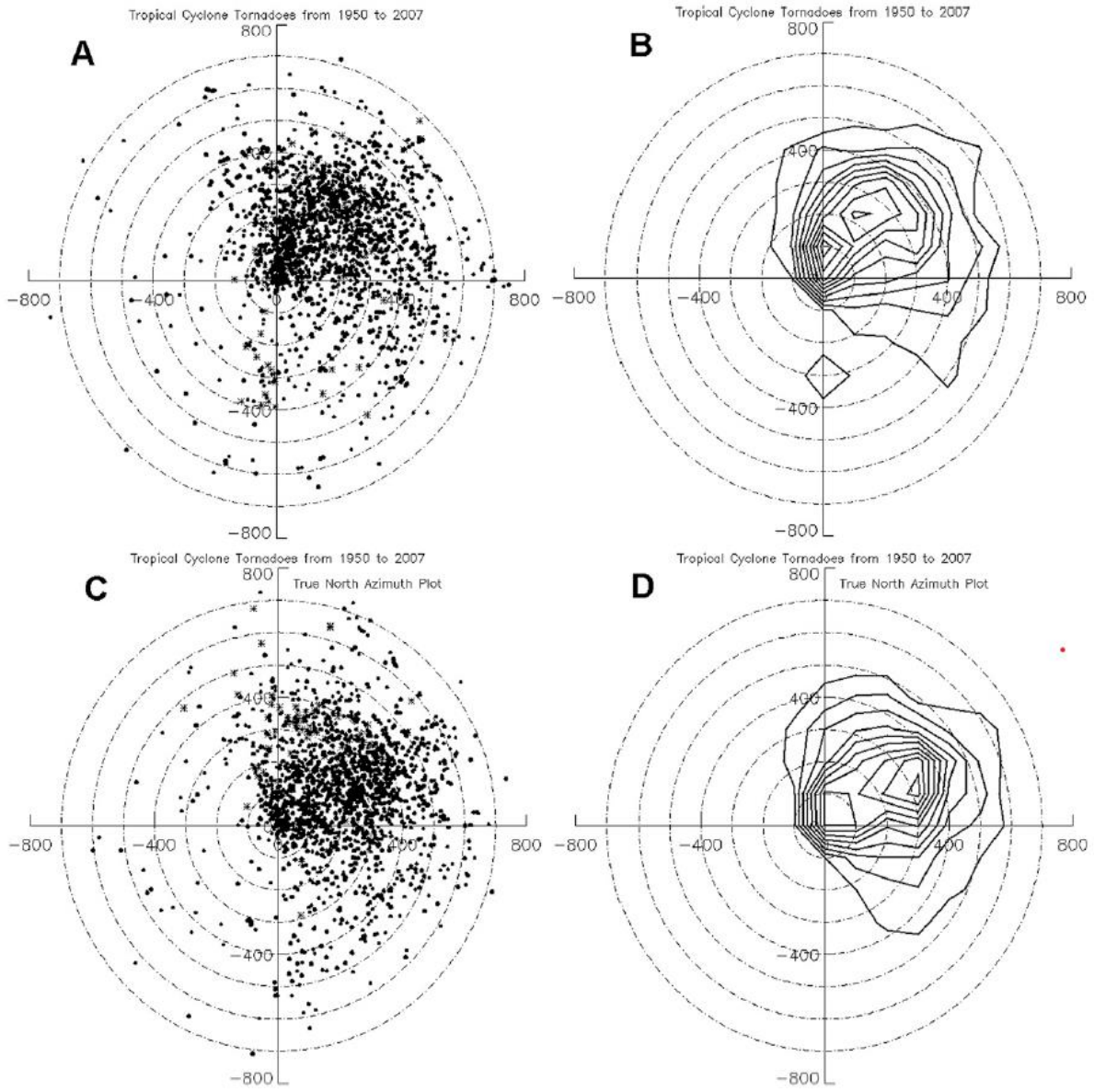

Figure 2.2: Tropical cyclone tornado locations in both storm-relative and Cartesian coordinates. Range rings are in 100-km increments. (a) Locations relative to TC motion vector. (b) 2D histogram of locations relative to TC motion vector, with 100 km x 100 km bin spacing centered on the origin. Contour interval is 10 tornadoes per grid box. (c) Locations relative to true north. (d) As in (b), but relative to true north. From Schultz and Cecil (2009).

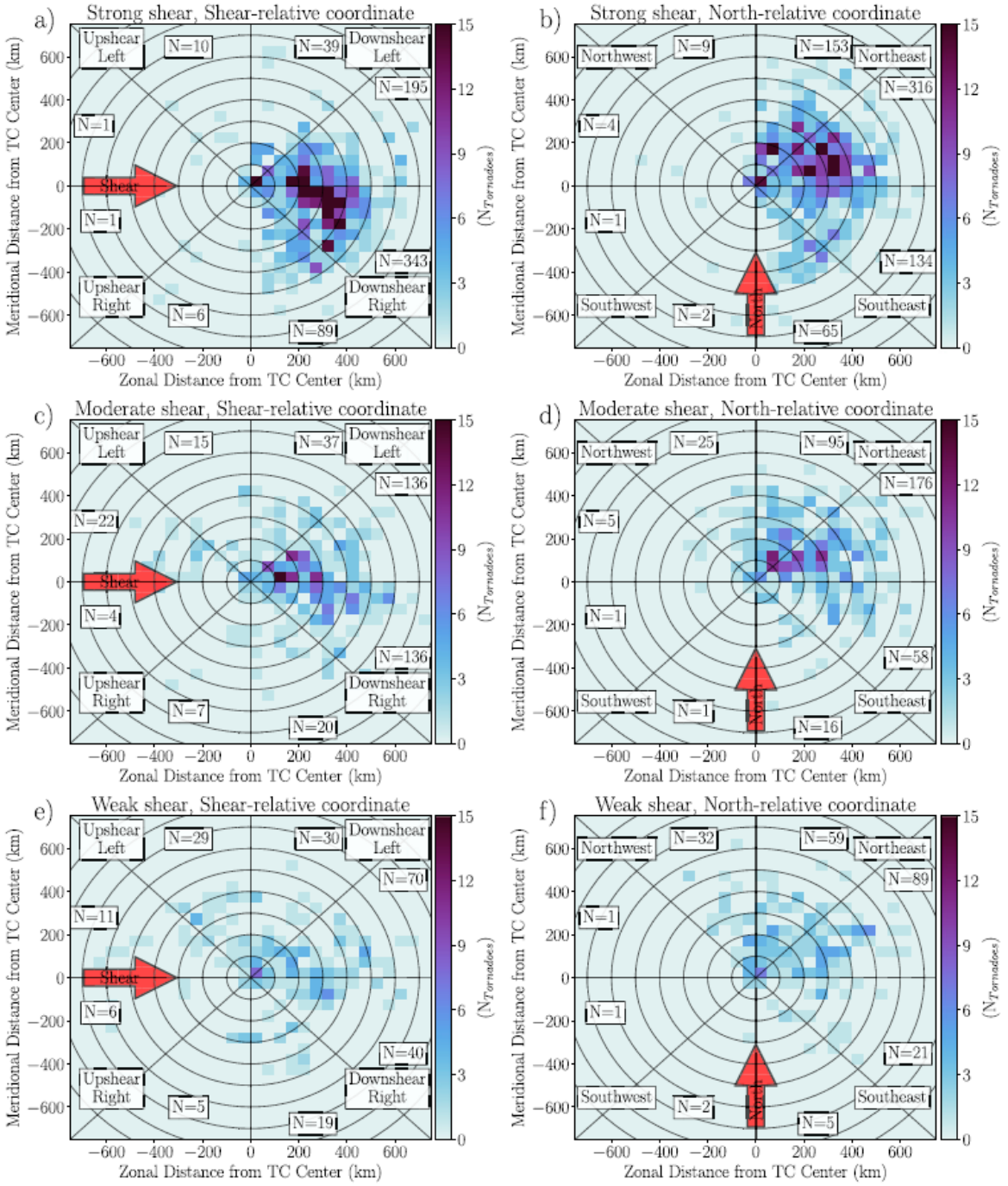

Figure 2.3: Plan view plot of tornado location (N = tornadoes; shaded squares) for TCs in (a),(b) strong; (c),(d) moderate; and (e),(f) weak VWS. Tornado reports in (a), (c), and (e) have been rotated around the TC center such that the VWS vector (red arrow) at the time of tornado occurrence is pointing to the right. The tornado reports in (b), (d), and (f) are plotted relative to true north with the red arrow labeled accordingly. The boxed numbers show the total number of tornadoes in each octant. From Schenkel et al. (2020).

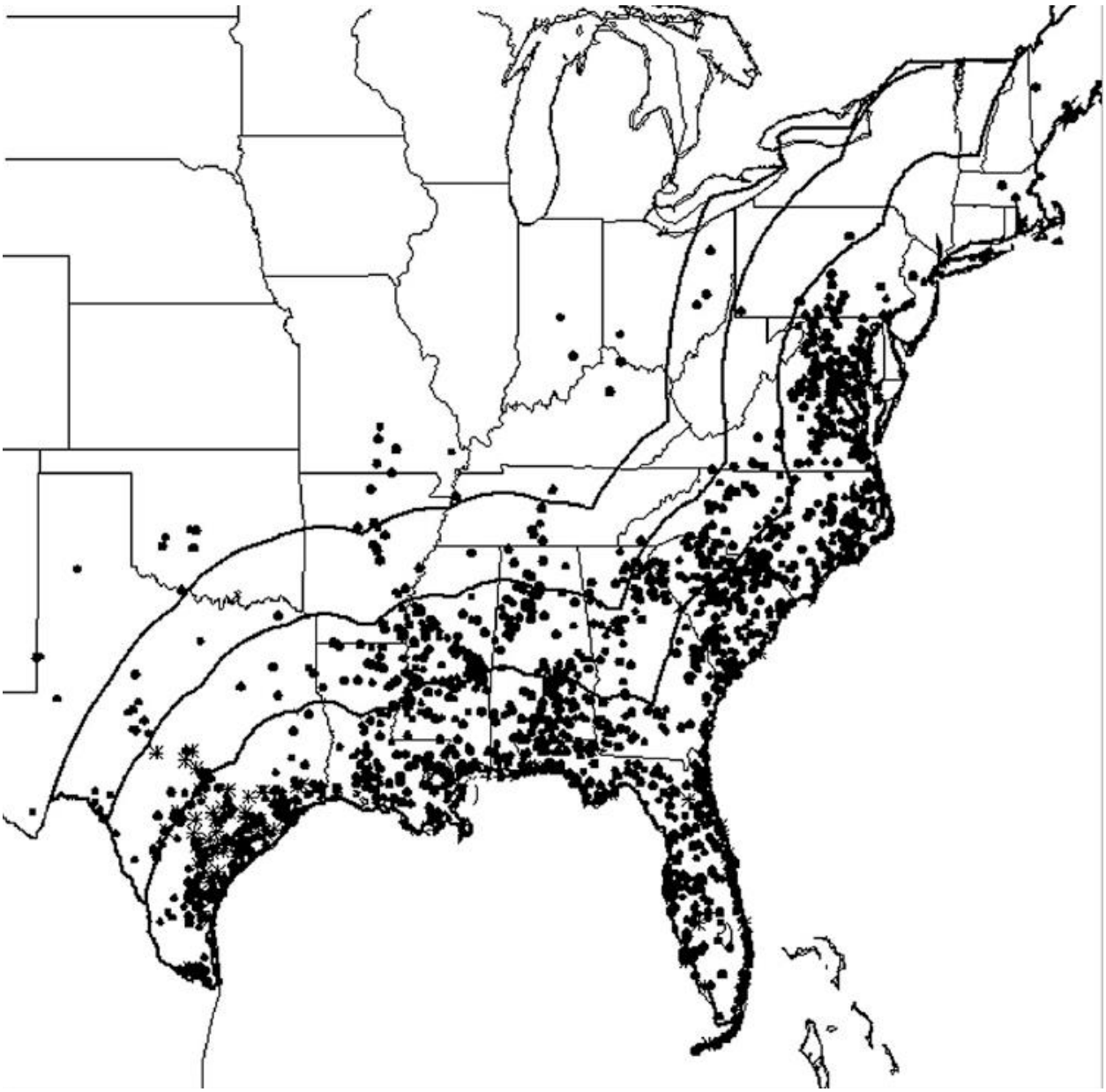

Figure 2.4: The U.S. tornado locations associated with Atlantic basin tropical cyclones, 1950–2007. Range lines moving inland from the coast are associated with the distances of 200, 400, and 600 km. From Schultz and Cecil (2009).

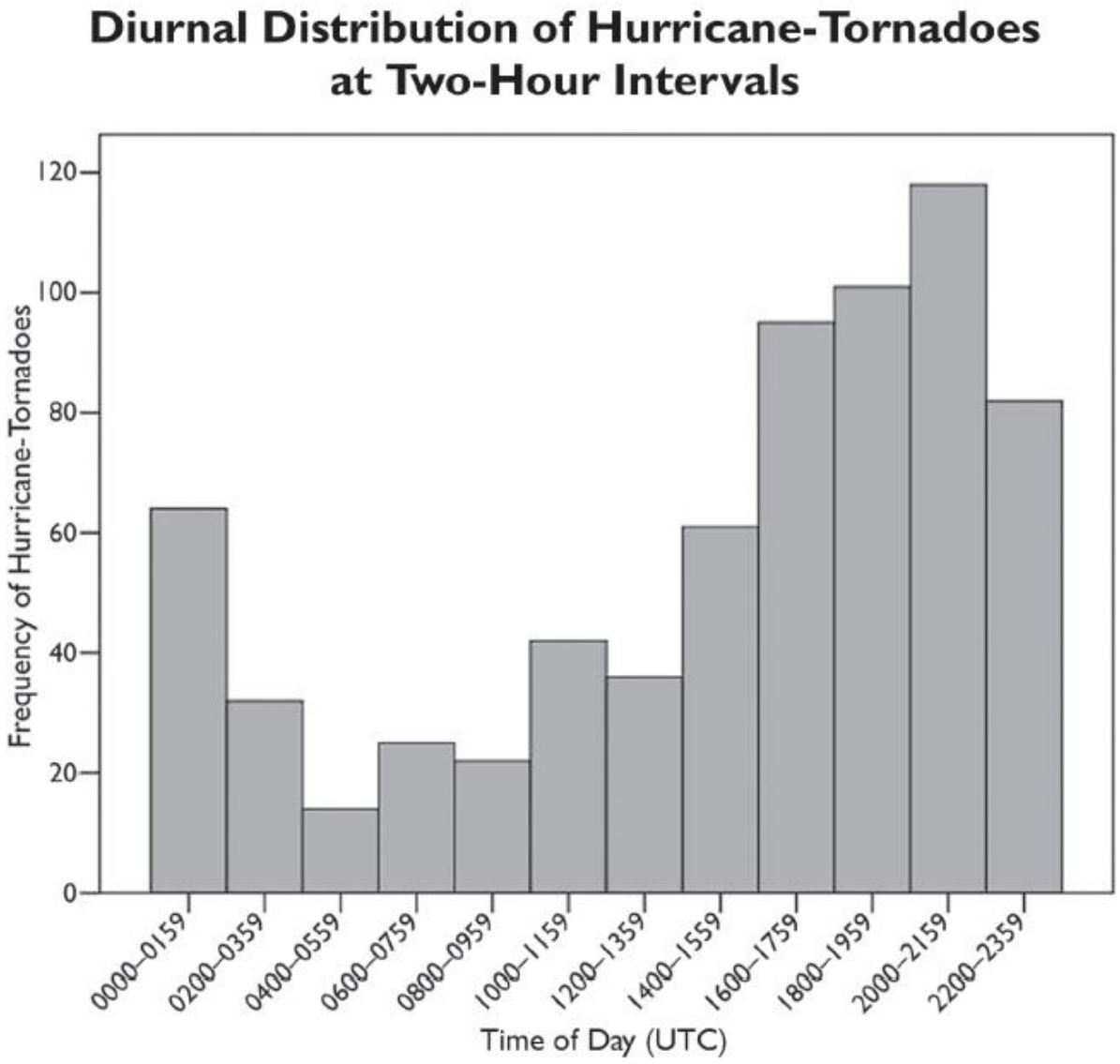

Figure 2.5: The diurnal distribution of Gulf Coast hurricane-tornadoes at two-hour intervals. Coordinated Universal Time (UTC) is five hours ahead of Central Daylight Time and four hours ahead of Eastern Daylight Time. From Moore and Dixon (2011).

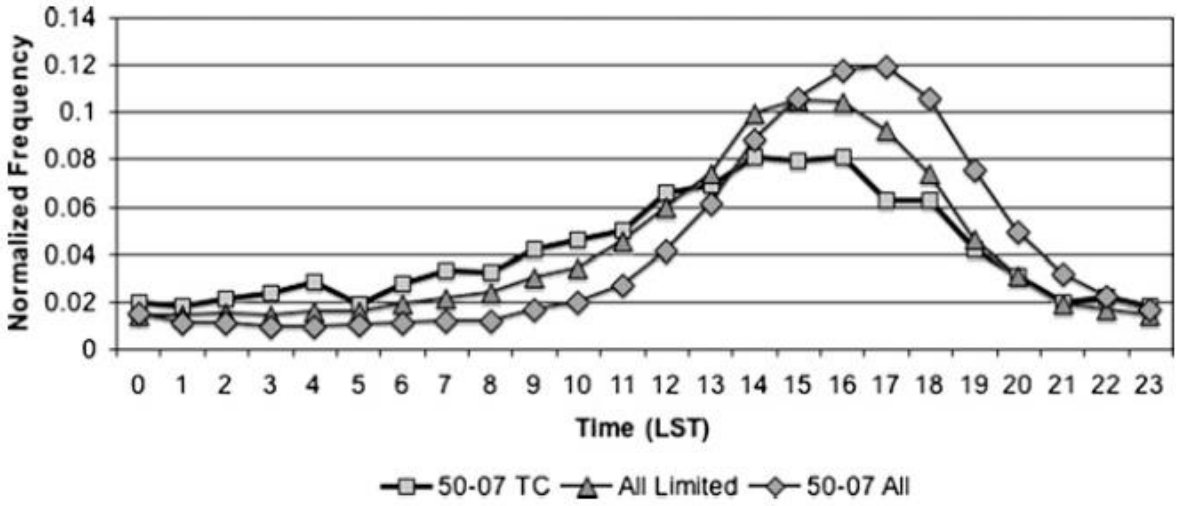

Figure 2.6: Histogram of the local solar time of TC tornadoes (thick black line with squares), all U.S. tornadoes limited by a 400-km distance from the coast and from May to November (black line with triangles), and all U.S. tornadoes (black line with diamonds). From Schultz and Cecil (2009).

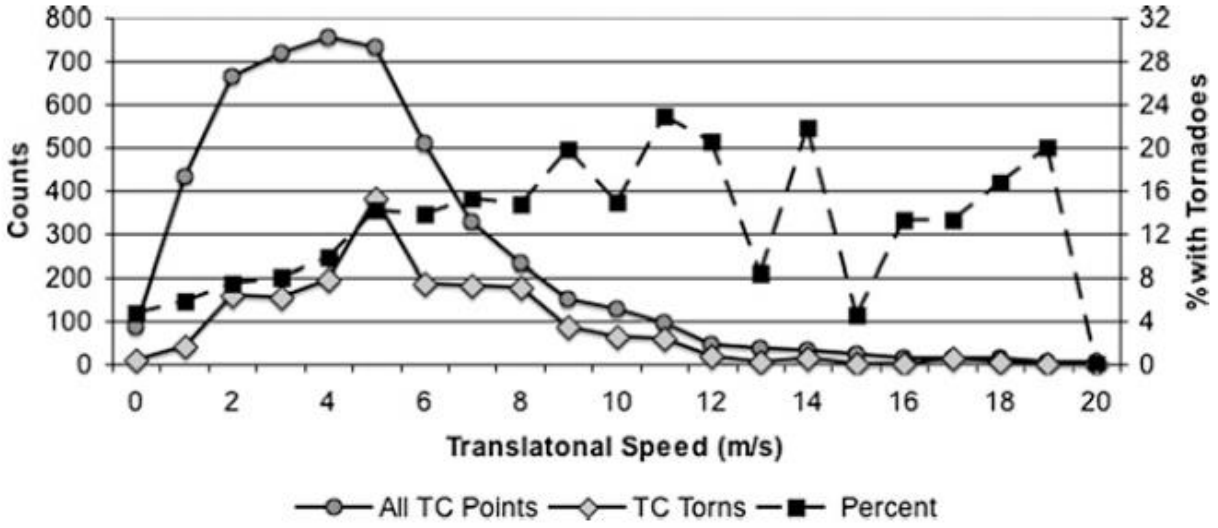

Figure 2.7: As in Fig. 2.8, but for TC translational speed (m/s). The scale between axes is 25:1. From Schultz and Cecil (2009).

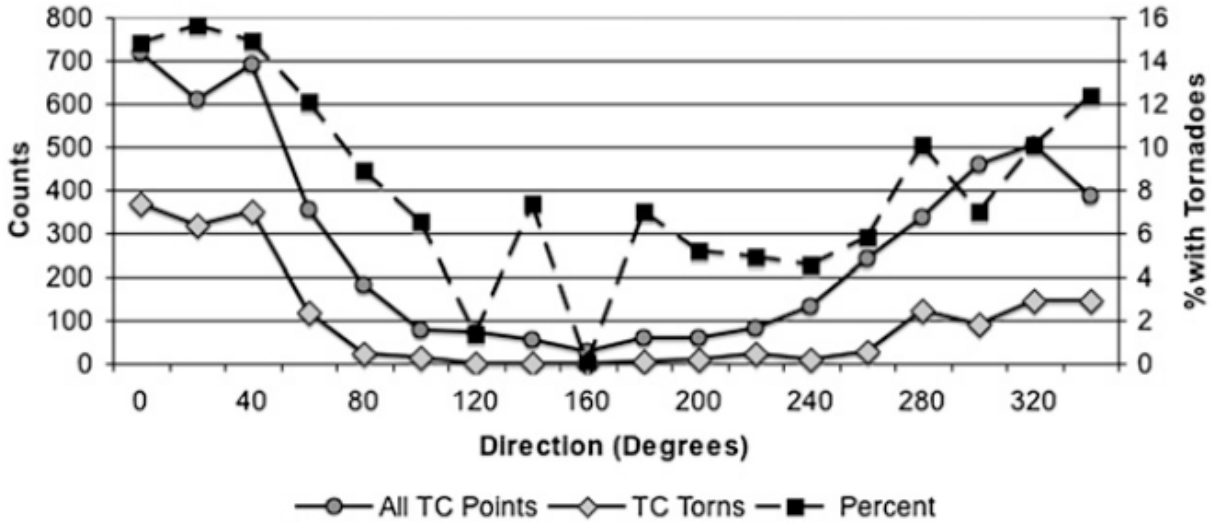

Figure 2.8: Histograms as a function of TC direction of motion: TC tornadoes (solid line with small circles; left axis); 6-hourly time periods with that TC motion, regardless of tornado occurrence (solid line with large circles; left axis); and percentage of all 6-hourly time periods that have associated tornadoes (dashed lines with squares; right axis). Only time periods during which a TC is in the U.S. region (north of 23.58 latitude and west of 70.8 longitude) are included. The scale between axes is 50:1. From Schultz and Cecil (2009).

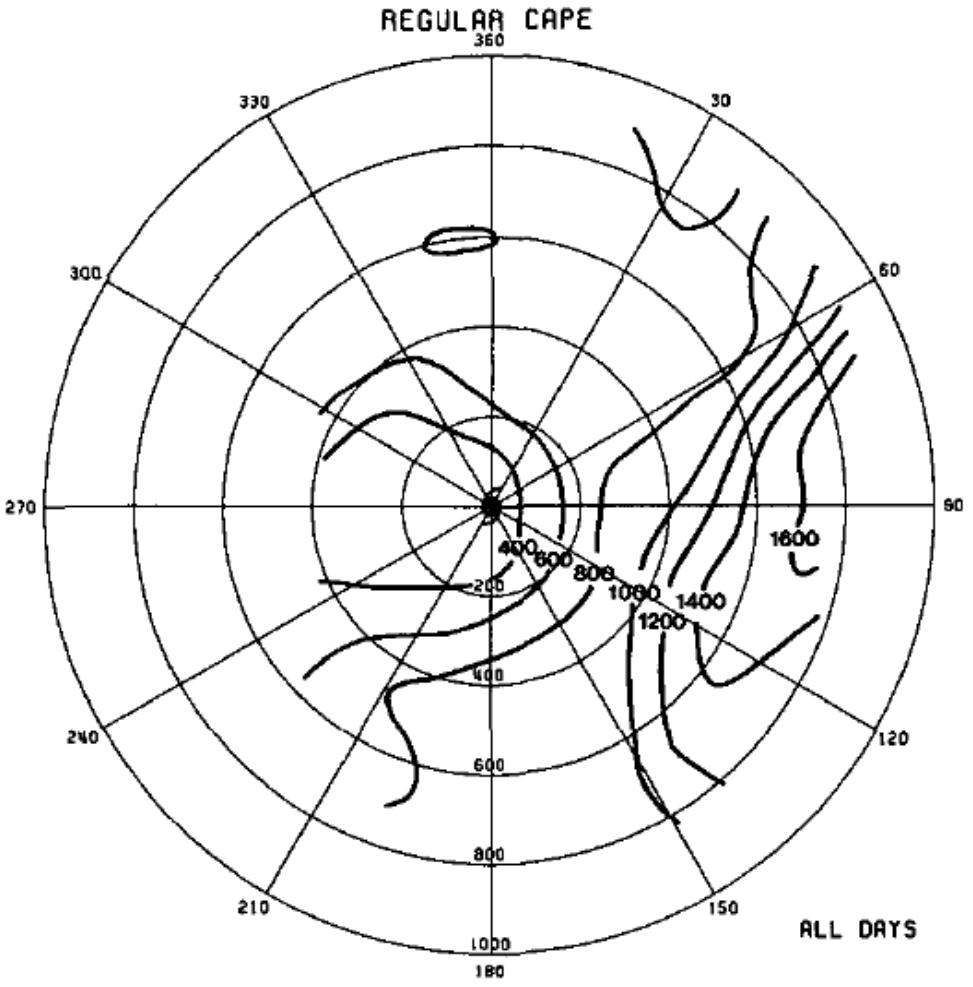

Figure 2.9: Spatial distribution of CAPE for the 1296 hurricane rawinsondes. Objective analysis grid mesh is spaced at 100-km intervals. The hurricane is at the center and is moving toward 360°. Range rings, labeled along the 180° azimuth, are 200 km apart. Units of contours are joules per kilogram. From McCaul (1991).

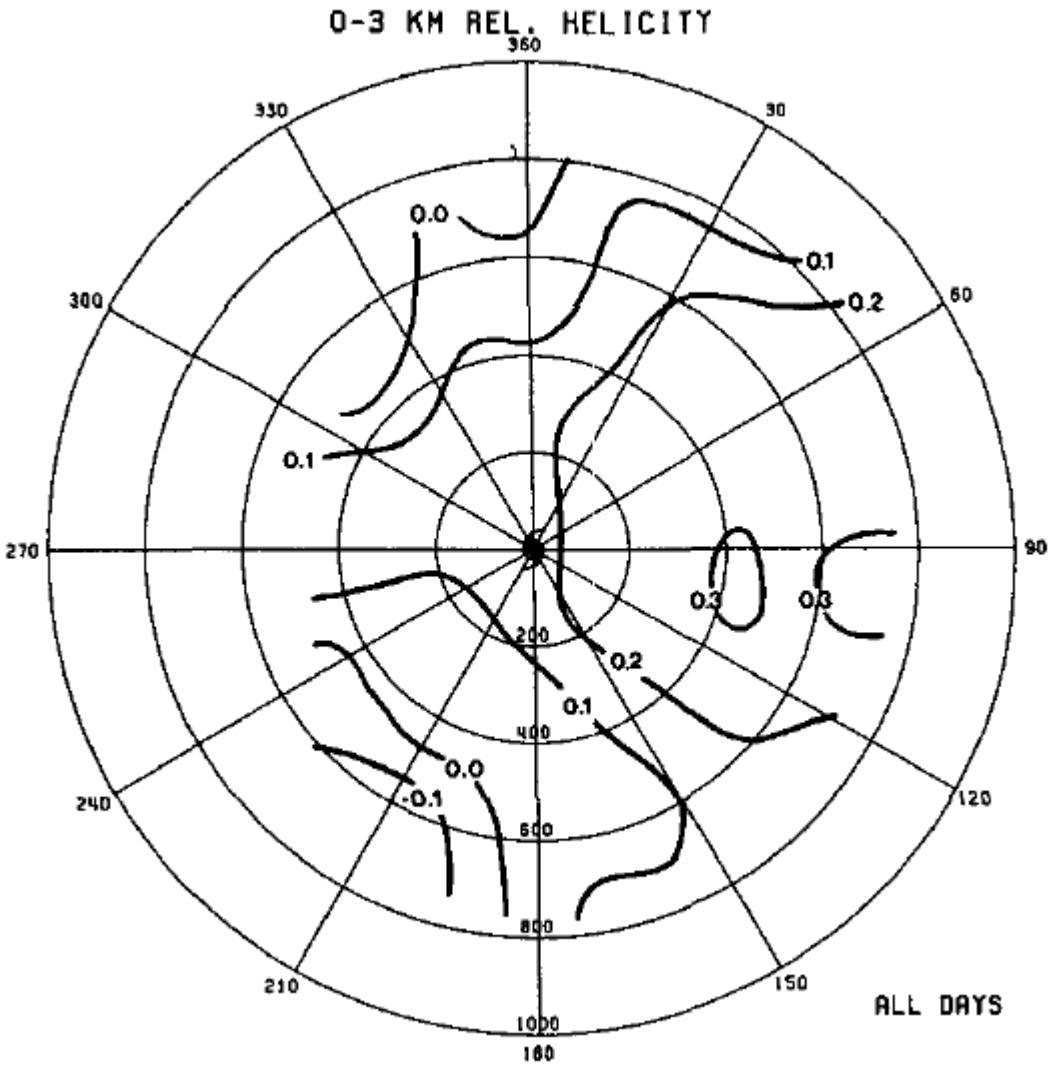

Figure 2.10: Spatial distribution of 0-3 km relative helicity for the 1296 hurricane rawinsondes. Format as in Fig. 2.9. Units of contours are dimensionless. From McCaul (1991).

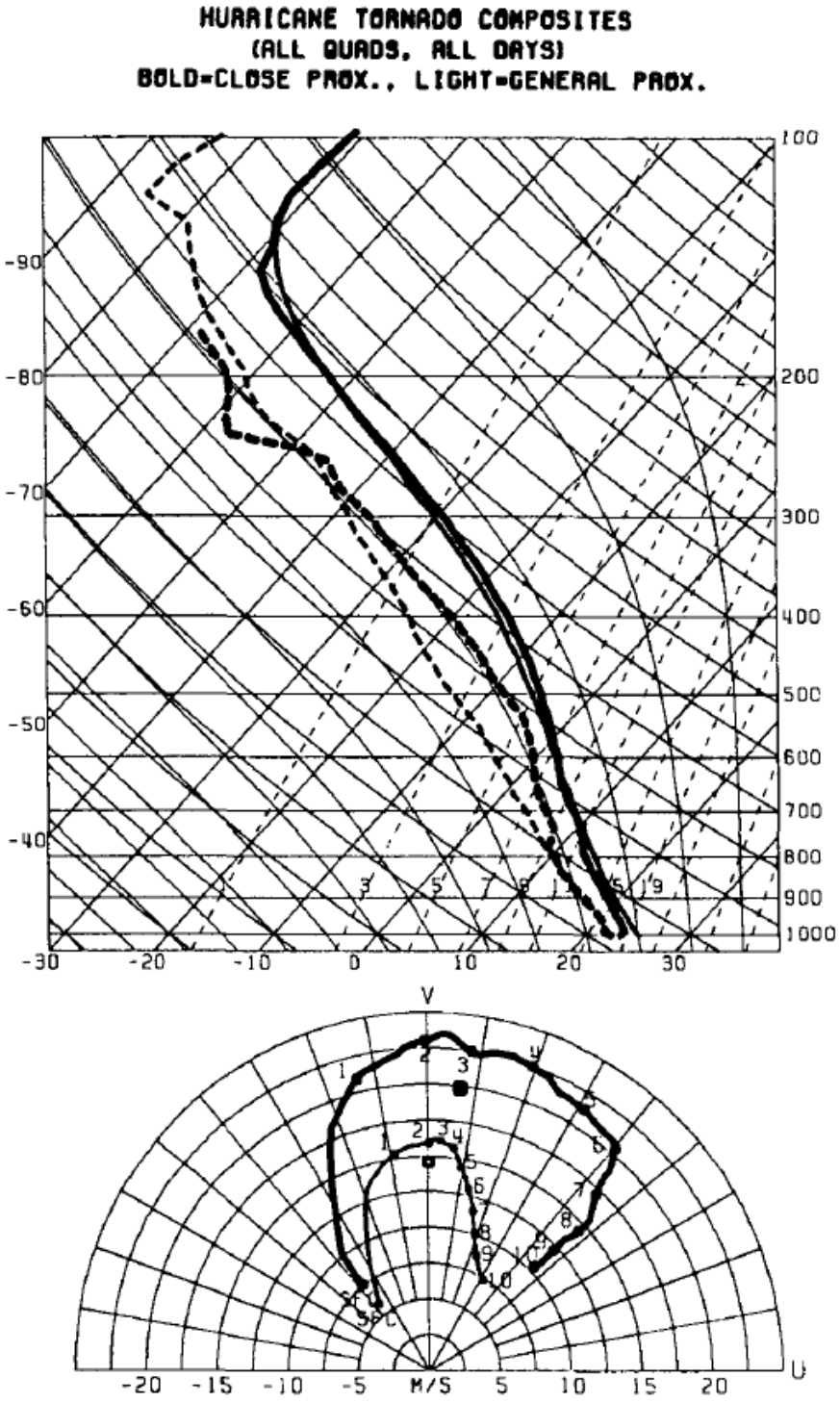

Figure 2.11: Skew T-log p and hodograph diagrams for the composite soundings taken in close proximity (thicker lines) and general proximity (thinner lines) to hurricane tornado events. The U and V components represent the radial and tangential winds relative to hurricane centers at rawinsonde time. Boxes on hodograph diagrams mark 0-6 km mean winds used as estimates of convective cell motion. From McCaul (1991).

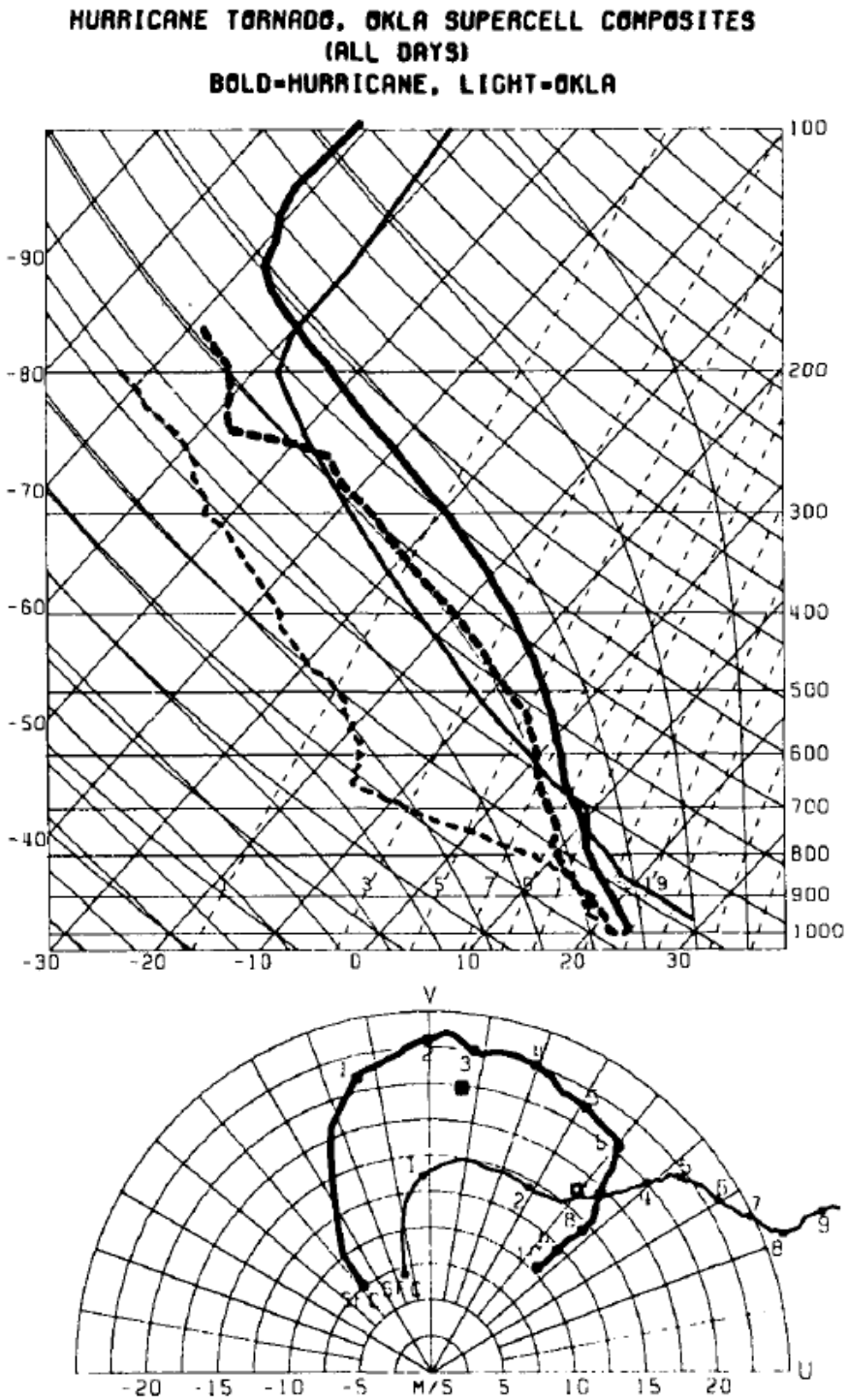

Figure 2.12: Skew T-log p and hodograph diagrams for the hurricane tornado close-proximity composite (thicker lines) and Oklahoma supercell composite of Bluestein and Jain (thinner lines). The U and V components of the Oklahoma composite are relative to true zonal and meridional directions. Boxes mark 0-6 km mean winds. From McCaul (1991).

Chapter 3: Data and Methodology

3.1 Introduction

This chapter will discuss the data sources and methodologies used to perform the analyses required to develop and complete the study. Section 3.2 covers the HURDAT2 database. Section 3.3 focuses on the ONETOR database. Section 3.4 discusses the details of how the TCTOR database was constructed. Section 3.5 looks at how the RUC-RAP model analyses data was utilized for TCTOR proximity sounding analysis. Section 3.6 details how the Goldilocks Zone is defined and how it was created to isolate the TCTOR inflow environment. Section 3.7 reviews the convective parameters that were computed to analyze the TCTOR environments. Section 3.8 describes the construction of composite synoptic maps using RUC-RAP model analyses data. Section 3.9 discusses the methodology of determining and classifying TC landfall angles.

3.2 HURDAT2

The HURDAT2 database is the official archive of Atlantic basin TC activity. The database is maintained by the National Hurricane Center and updated annually after careful post-season reanalysis (https://www.nhc.noaa.gov/data/#hurdat). For each TC, the database contains the storm's location (latitude and longitude), intensity (minimum sea level pressure and maximum sustained surface wind speed), and radii of selected surface wind magnitudes (64 knots, 50 knots, 34 knots) in each quadrant (northeast, southeast, southwest, and northwest) at 6-hour intervals throughout the TC's lifetime. Special record identifiers denote specific events that do not align with the 6-hour intervals, such as landfall, closest approach to the coast without landfall, and change in system status (i.e., extratropical transition).

Each TC within the HURDAT2 dataset was analyzed to determine if it made landfall on a US coastline or passed within 750 km of a US coastline as either a tropical depression, tropical storm, or hurricane, during the years 1950 through 2019. The identified TCs were then separated into two groups based on "landfall" coast: East coast or Gulf coast. For this project, the East coast is defined as the coastline that extends from the US-Canada border to the southern tip of Florida at a longitude of 88.2W. The Gulf coast is defined as the coastline that extends from the same longitude (88.2W) to the US-Mexico border. TCs that made landfall on both coastlines were included in each subset. Specific landfall times and locations for the years 1969 through 1983 were missing from the HURDAT2 dataset, so a manual analysis of National Hurricane Center season track maps was performed to separate TCs into their respective landfall basins during those years.

3.3 ONETOR

The ONETOR dataset contains all reported tornadoes in the United States during the years 1950-2019. The database is maintained by the Storm Prediction Center and is updated regularly after careful post-event confirmation of each reported tornado (https://www.spc.noaa.gov/wcm/#data). Data provided for each confirmed tornado includes the date and time of the tornado converted to UTC, the starting latitude and longitude, intensity measured using the Fujita/Enhanced Fujita Scale, casualties and monetary damage values.

There are some inherent sources of error/uncertainty within the ONETOR database. The large increase in the number of reported tornadoes over the years has been commonly attributed to advancements in technology and detection capabilities. Verbout et al. (2007) found that the number of reported tornadoes of F1 intensity or greater has remained relatively constant over

time whereas the number of reported F0 intensity tornadoes has increased. Schultz and Cecil (2009) noted that lower F-scale counts may have been impacted by a variety of factors, including unreliable or multiple reports. They also described the difficulty in assessing accurate damage ratings for TCTORs as the damage caused by such tornadoes occurs within the swath of damage caused by the TC itself.

3.4 TCTOR Database

In order to develop an updated database of TCTORs, the HURDAT2 and ONETOR datasets were combined to determine which tornadoes occurred within TC circulations that were impacting the US between 1950 and 2019. First, all reported tornadoes were analyzed to see if they occurred during the lifetime of a previously identified East coast or Gulf Coast TC (a temporal filter). Next, following the methods of Schultz and Cecil (2009), a tornado was considered inside the TC circulation if the tornado was within 750 km of the TC center (a spatial filter). The TC center at the time of the reported tornado was determined through simple linear interpolation between the 6-hour TC locations in the HURDAT2 database. If a tornado passed both temporal and spatial filters, several parameters were calculated to facilitate direct comparison with Schultz and Cecil (2009) and Moore and Dixon (2011), including tornado range from the TC center, the earth-relative azimuth of the tornado from the TC center, the TC motion-relative azimuth of the tornado from the TC center, and tornado time relative to the TC landfall time (or closest passage time; based on the respective time denoted in the HURDAT2 database). The TC motion vector at specific times (e.g., when a given tornado was reported) was determined through simple linear interpolation between the two HURDAT2 storm locations encompassing the tornado report time. Data for each tornado was then exported to the Gulf coast

or East coast TCTOR database, determined by the landfalling basin associated with its parent TC. If a TC made landfall in both basins, individual tornadoes were separated based on the nearest in time landfall location.

Between the years 1950 and 2005, each tornado was cross-checked with the TCTOR database compiled by Schultz and Cecil (2009) to see if it was consistent with their vetted results. Schultz and Cecil assessed tornadoes that occurred three hours prior to and after each 6-hourly HURDAT2 observation, while this database focused on tornadoes that occurred between each HURDAT2 observation, resulting in slight discrepancies between the two databases for the years 1950-2005. Because specific landfall times were not available for the years 1969-1983, the TCTORs that occurred during those years use the time from landfall determined by Schultz and Cecil.

After the 1950-2019 East coast and Gulf coast TCTOR databases were complete, all TCTORs that occurred at a distance greater than 500 km from the TC center were analyzed using radar data, synoptic maps, and satellite imagery to confirm a physical relationship between the TC and the tornado. This quality control measure removed four TCTORs from the East coast database and six from the Gulf coast database. Following quality control, 373 East coast and 1,942 Gulf coast TCTORs were included in the study.

3.5 RUC-RAP Analysis

To assess the local tornado environment and provide a way to compare environments between East coast and Gulf coast landfalling TCs, the Rapid Update Cycle/Rapid Refresh (RUC-RAP) 20-km model analyses were used to extract representative proximity soundings near each tornado. This assessment covered all TCTORs that occurred from 2005-2019 (i.e., the

period covered by the RUC-RAP archive). For East coast landfalling TCs, 100 TCTORs occurred between 2005 and 2019 while Gulf coast landfalling TCs produced 667 TCTORs during the same period. To assess the evolving local environment of the tornadoes, the RUC-RAP analyses were obtained to include the hour of the tornado as well as the two hours prior to the tornado time. Data was not available for certain days (or the files were corrupted), namely data for Katrina (August 31, 2005), Bill (June 17, 2015), and Dolly (July 23-24, 2008).

3.6 Goldilocks Zone

In order to adequately analyze the local tornado environment within the RUC-RAP data, an appropriate inflow region had to be identified relative to each reported tornado. In TCs, typical inflow angles (relative to a given range ring in the cylindrical coordinate system) can range from 0° to 20° (Powell 1982). In relation to non-TC severe weather events, Potvin et al. (2010) identified a spatiotemporal range where sampling of the proximity environment provided the most insight into tornadic development potential. Named the "Goldilocks Zone," or GZ, they identified a region between 40-km and 80-km away from the severe weather event and between 0 and 2 hours prior to the event as being the most beneficial when assessing tornadic risk. Potvin et al. (2010) focused solely on supercells that produced significant tornadoes (rated EF2-EF5) which can influence their local environment at ranges of 10-40 km; however, the supercells that produce TCTORs (often rated EF0-EF2) are frequently smaller and less intense than their mid-latitude counterparts and are less likely to influence the environment at such distances. Therefore, the original GZ has been modified for the TC framework so that the local TCTOR environment could be adequately assessed using a range that is closer to the TCTOR event. Combining the findings of Powell (1982) and Potvin et al. (2010), the GZ of each TCTOR was

calculated as the region between 0° and 20° off tangent of the radial ring, and between 20-km and 60-km away from the location of the TCTOR (Figure 3.1).

Once the GZ was identified, a custom Python script filtered through the RUC-RAP grid columns to isolate those columns that fell within the GZ of each TC tornado. Typically, 2-4 columns were present within the GZ for each TCTOR. The columns were then averaged together to produce a mean GZ sounding, and this process was repeated for the hour of the tornado, one hour prior to the tornado, and two hours prior to the tornado. This led to 3 soundings being generated for each TCTOR, totaling 2,301 soundings.

3.7 Convective Parameters

A total of 39 convective parameters were calculated using SHARPpy (Blumberg et al. 2017) for each averaged GZ sounding that was processed. These parameters are grouped into four categories: instability, vertical shear, humidity, and composite parameters.

The computed instability parameters are comprised of the lifted condensation level (LCL), the level of free convection (LFC), the equilibrium level (EL), three different variations of convective available potential energy (CAPE) and convective inhibition (CIN), as well as Downdraft CAPE (DCAPE) and lapse rates at two different layers. Surface-based CAPE and CIN are calculated by using the surface temperature and dewpoint. Mean-layer CAPE and CIN are calculated using the mean temperature and dewpoint in the lowest 100 mb. Most-unstable CAPE and CIN utilize the most unstable parcel within the lowest 300 mb. Each of these variations are useful in certain situations and no one variation fits all circumstances. Surface-based CAPE and CIN are useful when the surface layer is the most unstable, which is common in tropical air masses. Should it not be the most unstable layer, the most-unstable CAPE and CIN indicate the pressure level (or AGL height) at which the air is most favorable. The mean-layer

helps to remove any uncertainty or variation within the lowest 100-mb of the troposphere which may provide better insight into the instability where inversions or other abnormal lapse rates may be present near the surface. The surface-based and mean-layer CAPE values within the 0-3 km AGL layer were also calculated to help analyze the lower-tropospheric instability. Knowing that TCTORs commonly develop within miniature supercells (Eastin and Link 2009; Schenkel et al. 2020), the instability confined in the lower troposphere may be more indicative of a favorable environment. Two different lapse rates were derived from each sounding as well. The first being between the 0-3 km layer and the second being between the 700-500 mb layer in order to determine surface and mid-level instability, respectively.

Based on the work of Thompson et al. (2007), the effective inflow layer, and its associated upper and lower boundaries was derived from the soundings. Included in this is half of the effective storm depth. Further expanding on their work, the effective vertical wind shear (VWS) was calculated along with the BRN Shear and VWS in the 0-1 km, 0-3 km, and 0-6 km layers. These different layers of shear were chosen as they serve different purposes. The 0-6 km layer can help identify storm mode; however, it may not be as beneficial within a TC environment. Compared to a cold-core mid-latitude system where maximum winds are near the tropopause, TCs have maximum winds near the surface that decrease with height and, depending on the range, reverse direction with the upper-level anticyclone. This difference in vertical wind structure could lead to values that underestimate the TCTOR potential. The 0-3 km and 0-1 km identify low-level shear which could lead to mesocyclone and tornado development, but could also suffer from similar errors as the 0-6 km layer. Using storm motion based on the work of Bunkers et al. (2000), the storm-relative helicity (SRH) was calculated in multiple layers including the 0-500 m AGL layer, 0-1 km AGL layer, 0-3 km AGL layer, and the effective

inflow layer. The SRH layers also have different implications for tornado development. The 0-3 km layer provides insight into the potential for supercell development whereas Rasmussen (2003) found that the 0-1 km layer was a better predictor of tornadic supercells versus non-tornadic supercells. He suggested that a smaller layer could be even more beneficial to forecasting tornadic potential. The 0-500 m layer provides a near-surface assessment of the potential for rotating updrafts.

Surface-based and mean-layer equivalent potential temperatures were calculated using the surface temperature and dewpoint, and the mean temperature and dewpoint in the lowest 100 mb, respectively. The mean relative humidity (RH) was also calculated in the lowest 100 mb layer, the 0-2 km AGL layer, the 2-4 km AGL layer, and the 4-6 km AGL layer. Curtis (2004) found that mid-level dry intrusions are commonly associated with TCTOR outbreaks. There have been no previous studies that analyze the local RH directly, so these different layers will provide a new look into the local moisture environment using Curtis (2004) as a guide.

Multiple composite parameters were also calculated and most of them are commonly used in mid-latitude sounding analysis. The supercell composite parameter (SCP) and significant tornado parameter (STP) were both calculated using fixed and effective layers based on the work of Thompson et al. (2007). These two were developed using databases of Great Plains supercells, and as such they are commonly used for those events. However, as noted by Eastin and Link (2009) and Schenkel et al. (2020), the supercells that produce TCTORs are structurally different and smaller than those that frequently develop in the Great Plains. Understanding this, these parameters may not be as beneficial in forecasting TCTOR events. Along with the two variations of SCP and STP, the Sherburn Parameter, based on the work of Sherburn and Parker (2014), was also calculated using the fixed (0-3 km AGL) and effective

layer shears. This composite parameter is designed to be used in high-shear low-CAPE environments which could make it useful within a TCTOR environment as there is typically very high shear and relatively lower CAPE (Novlan and Gray 1974; McCaul 1991; Baker et al. 2009; Eastin and Link 2009).

To determine the statistical significance of any differences in the convective parameters between the East and Gulf coasts, a two-sample t-test was performed for each calculated parameter. This test assumes that the two samples are independent and possess near-normal distributions. Statistical significance was determined using the 5% confidence level, and the calculations were achieved using the SciPy library (Virtanen et al. 2020) within a custom Python script.

3.8 Synoptic Maps

Understanding the synoptic pattern surrounding localized severe weather events can provide useful information into the development of such events, and TCTORs are no exception. Composite synoptic maps of select parameters were created using the already available RUC-RAP model analyses between 2005 and 2019. The selected parameters included those used to identify potential supercell development (e.g., CAPE, SRH) or those identified as significantly different between the East and Gulf coast TC environments including surface-based 0-3 km CAPE and 0-1 km bulk shear (see the sounding analysis section below for more). To compare and contrast "typical" TCTOR synoptic patterns for each coastline, TC-relative composites across a near-synoptic portion of the RUC-RAP model domain were constructed using all relevant hourly analyses when a TCTOR was reported. More specifically, using the HURDAT2 dataset, the latitude and longitude of each TC at landfall was compared to the available grid points within the RUC-RAP domain. The nearest grid point to the TC landfall position was used

as the TC center. To build the overall domain, all grid points within the following ranges were included for each TC and subsequently averaged across all TCs: 3000 km to the west, 3000 km to the north, 1000 km to the east, and 1000 km to the south. To accommodate the model boundaries, if the TC landfall point was located too close to a model boundary (i.e., less than 1000 km), the TC "center" was adjusted so that the model boundary was the edge of the mean domain. The overall synoptic composite domain was 4000 km by 4000 km, with the mean TC center offset 1000 km south and east from the domain center in order to display the dominant westward-moving synoptic pattern that the average TC encountered at the time of each TCTOR event. Due to limitations of the available parameters within the native RUC-RAP data across the entire study period, a large number of desired parameters had to be calculated at each grid point within the domain. This was originally attempted in Python, however, because of the slow nature of Python and time constraints on the project, custom Fortran scripts were utilized in conjunction with Python to perform the calculations with much less computation time.

3.9 Landfall Angles

TCs can have vastly different impacts depending on the angle at which they make landfall relative to the coastline. These landfall angles can determine where TCTORs develop and how much coastal real estate is impacted by the most severe quadrant of a TC. Consider Figure 3.2 which provides two separate TC landfall scenarios for the East coast. TC "A" is moving due north at landfall, and thus only a small fraction of the right-front quadrant (orange shading) will be placed over land and fewer TCTORs would be expected. In contrast, TC "B" is moving due west at landfall which places the entirety of the TCTOR-favorable, right-front quadrant over land, therefore greater TCTOR production would be expected. Figure 3.3 also provides two Gulf coast TC landfall scenarios similarly to Figure 3.2. Along the Gulf coast, both TC "A" and "B"

have motion vectors with strong northward components, but “A” is moving towards the north-northwest along the western coastline while “B” is moving towards the north-northeast along the eastern coastline. An examination of the orange-shaded area, or right-front quadrant, both scenarios bring most of this quadrant ashore. The more significant difference is the TC location as the orientation of the coastline itself varies dramatically across the basin. While the right-front quadrant in both TCs moves ashore, the onshore flow of TC “A” will be greater than that of TC “B” due to the landfall angle and orientation of the coastline, all else being equal. This difference may result in greater shear across the right-front quadrant in TC “A”, and thus greater potential for TCTOR development. The most influential factor in determining the TC landfall angle is the synoptic pattern as it dictates the TC track, and thus the angle at which it will make landfall. Because of this, it is reasonable to hypothesize that the synoptic pattern may contribute significantly to TCTOR production, therefore, an analysis of the synoptic pattern is warranted.

For each TC that made landfall along the East or Gulf coast of the US between the years 1950 and 2019, the landfall angle was determined by first placing a straight line between the two 6-hourly observations that bracketed the landfall. The orientation of this line in relation to the gross coastline (manually measured) was designated as the landfall angle. A landfall angle perpendicular to the coastline was designated 0°. If the orientation of the line was to the right of perpendicular, it was denoted as a positive landfall angle up to +90° (parallel with the coastline), and lines to the left were denoted as negative angles (Figure 3.4). To account for TCs that made landfall on either coastline, each landfall was considered a separate event and placed within the respective coastline analysis. For TCs that had multiple landfalls on the same coastline, landfalls

that resulted in TCTOR events were considered separate events. Landfalls that did not result in any TCTOR events were not included in the analysis.

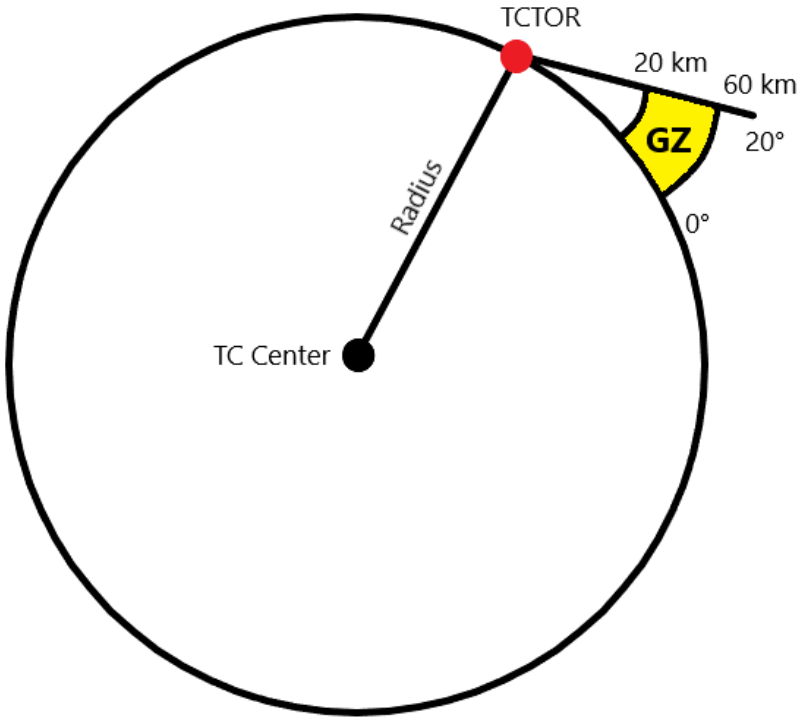

Figure 3.1: Diagram representing the location of the Goldilocks Zone in relation to the TC center and TCTOR initiation location, denoted by GZ and yellow shading.

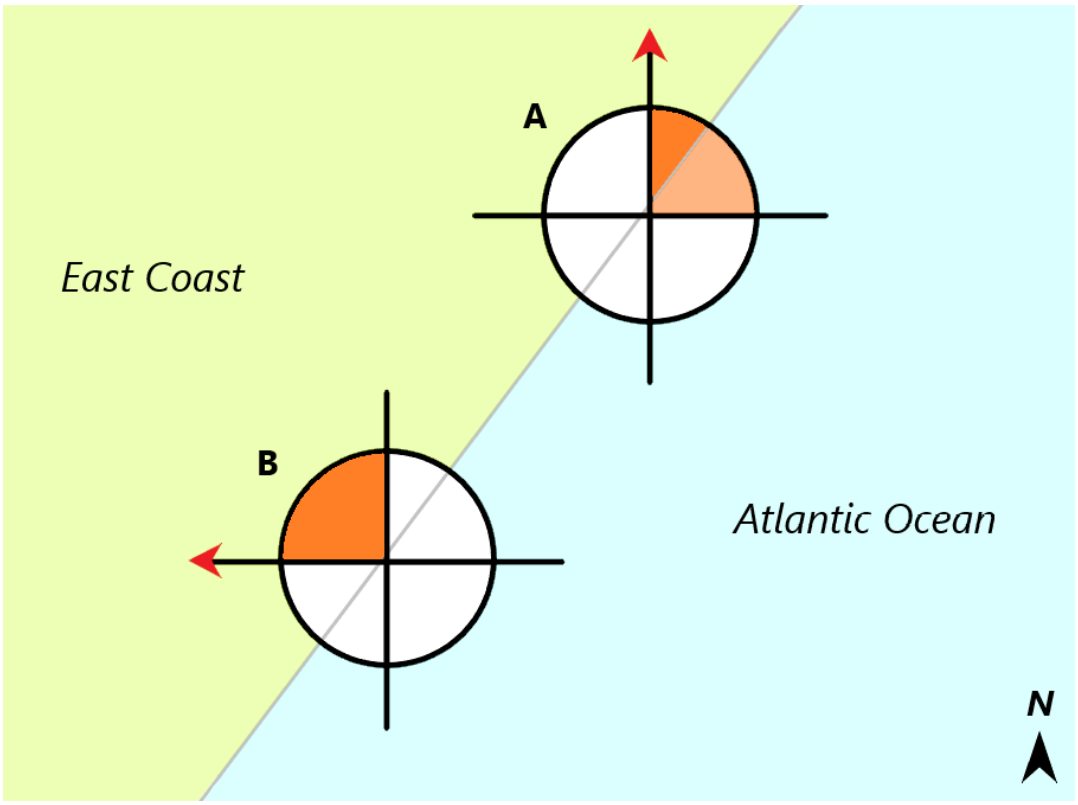

Figure 3.2: Conceptual model of how landfall angle differences, or TC motion (denoted by red arrows) relative to the coastline orientation, impacts the location of the right-front quadrant (orange shading) along the East coast. A and B are two TCs moving due North and West, respectively.

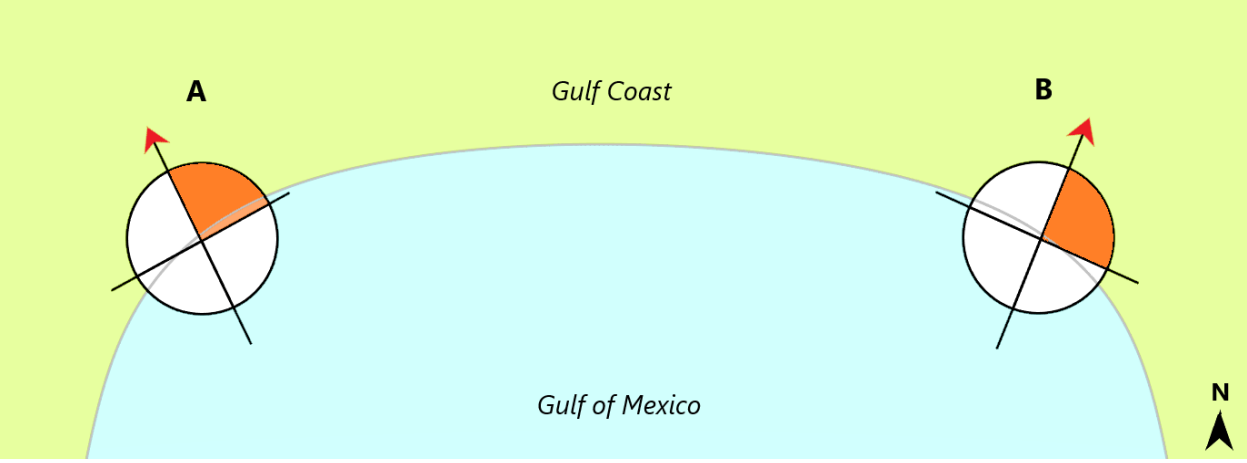

Figure 3.3: Conceptual model of how landfall angle differences, or TC motion (denoted by red arrows) relative to the coastline orientation, impacts the location of the right-front quadrant (orange shading) along the Gulf coast. A and B are two TCs moving due North-Northwest and North-Northeast, respectively.

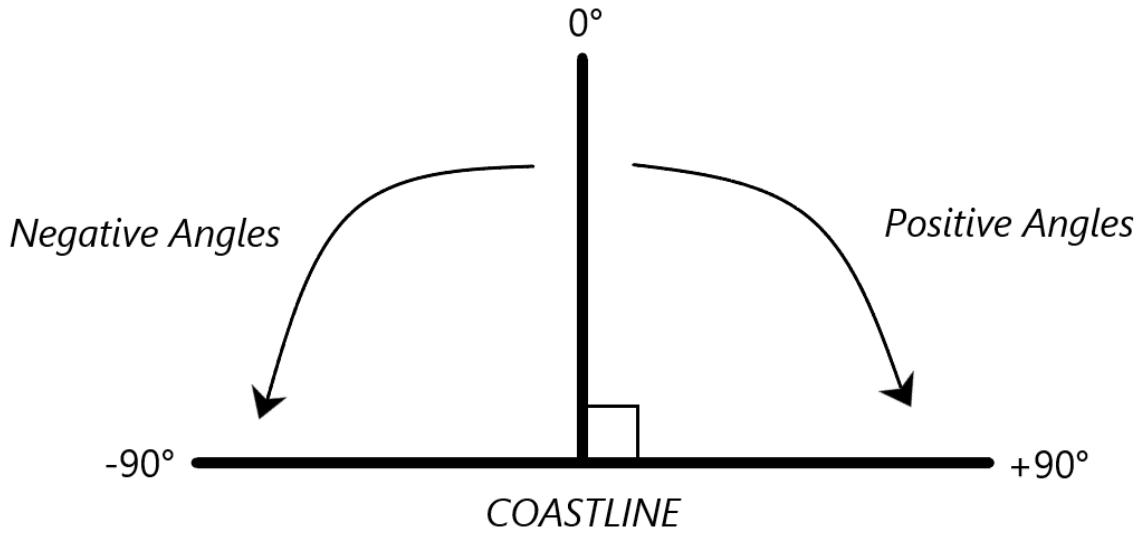

Figure 3.4: Conceptual diagram displaying the methodology for determining and classifying the TC landfall angles during analysis.

Table 3.1: List of computed environmental parameters. List includes the abbreviation, full name or description of the parameter, and pertinent studies that either introduced the parameter or analyzed the parameter as it relates to TCTOR development.

Abbreviation	Full Parameter Description	Relevant Studies
LCL	Lifted Condensation Level	Baker et al. (2009); Eastin and Link (2009)
LFC	Level of Free Convection	
EL	Equilibrium Level	
SBCAPE	Surface-Based Convective Available Potential Energy computed using the surface parcel	McCaul (1991); McCaul et al. (1993); McCaul et al. (2004); Baker et al. (2009); Eastin and Link (2009)
SBCAPE03	Surface-Based Convective Available Potential Energy in the 0-3 km AGL layer computed using the surface parcel	Baker et al. (2009); Eastin and Link (2009)
SBCIN	Surface-Based Convective Inhibition computed using the surface parcel	Baker et al. (2009); Eastin and Link (2009)
MLCAPE	Mean-Layer Convective Available Potential Energy computed using the mean parcel in the lowest 100 mb	Eastin and Link (2009)
MLCAPE03	Mean-Layer Convective Available Potential Energy in the 0-3 km AGL layer computed using the mean parcel in the lowest 100 mb	
MLCIN	Mean-Layer Convective Inhibition computed using the mean parcel in the lowest 100 mb	
MUCAPE	Most-Unstable Convective Available Potential Energy computed using the most-unstable parcel in the lowest 300 mb	Doswell and Rasmussen (1994); Eastin and Link (2009)
MUCIN	Most-Unstable Convective Inhibition computed using the most-unstable parcel in the lowest 300 mb	

LR03	Lapse Rate through the 0-3 km layer	
LR700500	Lapse Rate through the 700-500 mb layer	
SBTHE	Surface equivalent potential temperature	Eastin and Link (2009)
MLTHE	Mean-Layer equivalent potential temperature computed using the mean of the lowest 100 mb	
MLRH	Mean Relative Humidity in the lowest 100 mb layer	
RH02	Mean Relative Humidity in the 0-2 km AGL layer	
RH24	Mean Relative Humidity in the 2-4 km AGL layer	
RH46	Mean Relative Humidity in the 4-6 km AGL layer	
DCAPE	Downdraft Convective Available Potential Energy computed using the 700 mb pressure level	
EFFBOT	Bottom of the Effective Inflow Layer	Thompson et al. (2007)
EFFTOP	Top of the Effective Inflow Layer	Thompson et al. (2007)
EFFDEP	Depth of the Effective Inflow Layer	Thompson et al. (2007)
STMHLF	Half of the Effective Storm Depth	Thompson et al. (2007)
SHEAR01	Vertical Shear magnitude in the 0-1 km AGL layer	Baker et al. (2009); Eastin and Link (2009)
SHEAR03	Vertical Shear magnitude in the 0-3 km AGL layer	
SHEAR06	Vertical Shear magnitude in the 0-6 km AGL layer	McCaul (1991); Baker et al. (2009); Eastin and Link (2009)
BRNSHEAR	BRN Shear	Weisman and Klemp (1982); McCaul (1991); Eastin and Link (2009)

EFFSHEAR	Effective Shear	Thompson et al. (2007)
SRH05	Storm-Relative Helicity in the 0-500 m AGL layer computed using Bunkers et al. (2000) cell motion	Bunkers et al. (2000)
SRH01	Storm-Relative Helicity in the 0-1 km AGL layer computed using Bunkers et al. (2000) cell motion	Bunkers et al. (2000); Rasmussen (2003); Baker et al. (2009); Eastin and Link (2009)
SRH03	Storm-Relative Helicity in the 0-3 km AGL layer computed using Bunkers et al. (2000) cell motion	Bunkers et al. (2000); McCaul (1991); Baker et al. (2009); Eastin and Link (2009)
SRHEFF	Storm-Relative Helicity in the Effective Inflow Layer computed using Bunkers et al. (2000) cell motion	Bunkers et al. (2000); Thompson et al. (2007); Eastin and Link (2009)
SCPFIX	Supercell Composite Parameter computed using fixed layers	Thompson et al. (2003); Baker et al. (2009); Eastin and Link (2009)
SCPEFF	Supercell Composite Parameter computed using effective layers	Thompson et al. (2012); Baker et al. (2009)
STPFIX	Significant Tornado Parameter computed using fixed layers	Thompson et al. (2003); Baker et al. (2009); Eastin and Link (2009)
STPEFF	Significant Tornado Parameter computed using effective layers	Thompson et al. (2012); Baker et al. (2009)
SHERBS3	Sherburn Parameter computed using fixed layer shear	Sherburn and Parker (2014)
SHERBE	Sherburn Parameter computed using effective layer shear	Sherburn and Parker (2014)

Chapter 4: Results

4.1 Introduction

This chapter will cover and discuss the preliminary results of this research. Section 4.2 covers the 70-year TC climatology. Section 4.3 details the TC landfall angle climatology. Section 4.4 discusses the TCTOR decadal distributions. Section 4.5 covers the TCTOR annual seasonality. Section 4.6 focuses on the TCTOR activity per TC. Section 4.7 details the relationship between TCTORs and TC intensity. Section 4.8 describes the relationship between TCTORs and TC intensity at landfall. Section 4.9 covers the TCTOR spatial distribution. Section 4.10 discusses the TCTOR azimuthal distribution within a TC-relative framework. Section 4.11 details the TCTOR distributions as a function of the time of day. Section 4.12 focuses on the local TCTOR environment analysis. Section 4.13 covers the synoptic environment surrounding TCTOR events.

4.2 Tropical Cyclone Climatology

One of the primary objectives of this research was to update the TCTOR climatology record to include the most recent 12 years of data. Part of doing so included reviewing the climatology of TCs that were pertinent to the project. To be considered pertinent for the project, a TC must have made landfall on, or had a close encounter with, either the East or Gulf coast of the United States between the years 1950 and 2019, and produced at least one tornado. Using these guidelines, 54 TCs were identified as having impacted the East coast and 145 TCs were identified as having impacted the Gulf coast. These TCs were then counted within 10-year bins and their frequency in relation to all landfalling TCs was calculated per decade in order to provide a direct comparison between the two coastlines.

For the East coast (Figure 4.1), all landfalling TCs between 1950 and 1989 produced at least one TCTOR. However, beginning in the 1990s, there was a rapid decline in the frequency of TCTOR-producing TCs with respect to all East coast landfalling TCs. Interestingly, the most recent decade exhibited the lowest frequency of tornado-producing TCs with less than 40% of landfalling TCs producing at least one tornado. The increased frequencies prior to the 1990s may be attributed to the difficulty associated with distinguishing TC and tornado damage without additional sources of confirmation, such as Doppler radar which was not implemented until the 1990s.

As for the Gulf coast (Figure 4.2), there are some similarities and differences that are notable. As a whole, unlike the East coast, there was little variability in the frequency of Gulf coast tornado-producing TCs through the 1990s. The frequencies through the 1990s were, on average, greater than those among East coast TCs as more than 80% of landfalling Gulf coast TCs produced at least one tornado. There was a decrease in tornado-producing TC frequency similar to the East coast after the 1990s, but of lesser magnitude. This distribution highlights the notion that Gulf coast landfalling TCs, on average, produce tornadoes more frequently than those making landfall on the East coast.

4.3 Tropical Cyclone Landfall Angles

TCs tend to follow common paths as they approach US coastlines, but any slight deviation from those generalized paths, along with the orientation of the coastline itself, can lead to dramatic differences in TCTOR production and impacts. As noted above, the angle at which a TC makes landfall determines whether the TCTOR favorable right-front quadrant remains offshore or falls entirely onshore for an extended period. Because the orientation of the East and

Gulf coasts are noticeably different, it is expected that the average TC making landfall on either coastline would have different landfall angles as well. For the years 1950-2019, the mean landfall angle for East coast TCs was +34° (i.e., 34° to the right of perpendicular with the coastline) with a median angle of +30° (Figure 4.3). For Gulf coast TCs (Figure 4.4), the mean landfall angle was approximately +1° with a median angle of 0° (i.e., perpendicular to the coastline). Figures 4.5 and 4.6 display the spatial distribution of the two landfall angle bins for the East and Gulf coast, respectively. In Figure 4.5, East coast landfalling TCs appear to have an even distribution of landfall angles along the entire coastline as no particular region has a noticeable affinity for landfall angles greater than or less than the mean of +30°. On the other hand, for Gulf coast TCs (Figure 4.6), positive landfall angles were slightly more frequent along the western portion of the Gulf coastline while negative landfall angles were slightly more common along the eastern Gulf coastline. Using the Mississippi River Delta to divide the Gulf coastline into western and eastern regions, approximately 55% of positive landfall angles occurred in the western region and 55% of negative landfall angles occurred in the eastern region.

To investigate why the modest spatial differences might be present, the seasonality of the landfall angles for each coastline was analyzed. Figures 4.5 through 4.8 show the monthly frequency of landfalling TCs delineated by each coastline's respective mean landfall angle. East coast landfall seasonality (Figures 4.7 and 4.8) appears to be similar between the two landfall angle bins with the majority of landfalls occurring in August and September, the peak of the Atlantic Hurricane season. While only a few landfalls occurred outside of this peak, there is no clear preference for certain landfall angles at varying times of the year. By contrast, the Gulf coast landfall seasonality (Figures 4.9 and 4.10) is noticeably different between the two landfall

angle bins. The negative landfall angles were most frequently observed during the peak of the hurricane season in August and September with a quasi-normal distribution around the peak. The positive landfall angle seasonality was not as straightforward as a secondary peak in June was present and comparable in magnitude to the peak in September. This secondary peak suggests that positive landfall angles along the Gulf coast are more likely to occur in the early portion of the hurricane season. This is likely due to the climatology of TC development and dominant steering mechanisms throughout the Atlantic basin during a typical season. Early season TCs in the Gulf of Mexico are steered primarily by the Bermuda ridge which is located closer to the US, and mid-latitude troughs are less frequent, so northerly to northwesterly TC motion is commonly observed with landfalls occurring more frequently along the northwestern Gulf coast. This region of the Gulf coast has a general northeast-to-southwest orientation which, when combined with the previously described TC motion, positive landfall angles are more common. Closer to peak hurricane season, the Bermuda ridge is located further east and digging troughs gradually increase in frequency, so later season Gulf coast TCs have a more northerly to northeasterly motion at landfall. This motion steers these TCs towards the eastern region of the Gulf coast which has a general northwest-to-southeast orientation, resulting in negative landfall angles.

4.4 TCTOR Decadal Distribution

After a basic climatology was performed on the tornado-producing TCs alone, the TCTOR climatology could be addressed. To provide a similar look at how the number of TCTORs has trended over time, the counts of TCTORs were separated into 10-year bins and their frequency was calculated with respect to landfalling TCs. A total of 373 East coast and 1,942 Gulf coast TCTORs were identified for analysis.

Along the East coast, a single peak of TCTOR frequency was noted in the 1970s where the number of TCTORs per landfalling TC was approximately 12 (Figure 4.11). The anomalous TCTOR production of the 1970s was likely a result of Hurricane David (1979) which produced 34 TCTORs alone whereas the six tornado-producing TCs in the 1980s collectively produced 15 TCTORs, resulting in a minimum TCTOR frequency in the 1980s. Outside of the two extrema, the TCTOR counts per landfalling TC were fairly consistent, averaging between 4 and 6 with a slight increase in the three decades in which Doppler radar was utilized. The minimal increase in recent TCTOR frequencies could be related to increased tornado-detection capabilities and technological advancements (Doswell and Burgess 1988).

As for the Gulf coast, the majority of TCTOR decadal frequencies were larger in magnitude than along the East coast, and a more obvious long-term trend was able to be identified (Figure 4.12). The 2000s exhibited the greatest TCTOR production with more than 20 tornadoes per landfalling TC. There appeared to be an increase of TCTOR production between 1950 and 2009, unlike the East coast which exhibited more consistent TCTOR frequencies. In the 2010s a decline in TCTOR production was observed with an average of 11 TCTORs per landfalling TC, and this decline coincided with a decrease in the frequency of tornado-producing TCs. However, when considering the two decades prior to the peak in the 2000s, the lower frequency in the 2010s appears to be consistent with those observed in the previous decades, suggesting that the 2000s may have truly been anomalous, skewing the perception of a long-term increase in TCTOR frequency.

4.5 TCTOR Seasonality

The seasonality of TCTORs was analyzed using a monthly frequency, normalized by the number of landfalling TCs for a given coastline. Unsurprisingly, the general trend along both the East and Gulf coasts was similar to TC climatology with all TCTOR events occurring between May and November, including a notable peak in TCTOR activity in August and September, the peak of the Atlantic Hurricane Season. The East coast frequencies (Figure 4.13) showed a gradual increase in TCTOR activity prior to peaking in September; however, the Gulf coast had an additional spike in activity in June (Figure 4.14). This early season spike for the Gulf coast is not overly surprising as the sea surface temperatures in the Gulf of Mexico warm quickly and the development of early season TCs in the Gulf of Mexico are not uncommon. Aside from the increased Gulf coast TCTOR frequency in June, the distributions are roughly similar although the magnitudes of Gulf coast TCTOR frequencies are greater.

With TC landfall angles in mind, could there be a connection between the seasonalities of TCTOR frequency and landfall angles? The seasonality of TC landfall angles is largely dictated by the dominant synoptic steering patterns which determine how much of the TC's right-front quadrant is over land. For the East coast, both landfall angle bins (Figures 4.7 and 4.8) show dominant peaks in August and September that are roughly similar in magnitude. Because those two months are the peak of the Atlantic Hurricane Season, the East coast TCTOR frequency during those two months is also greatest. While these seasonality patterns are similar, they provide little insight into the relationship between the landfall angle and TCTOR production along the East coast. There was, however, a more insightful relationship between the seasonality patterns along the Gulf coast. Negative landfall angles along the Gulf coast (Figure 4.9) were most frequently observed during the peak of the hurricane season with a magnitude in September

that was greater than the positive landfall angles. Similar to the East coast, the negative Gulf coast landfall angles do not provide much insight as the distribution followed a similar pattern to the TCTOR monthly distribution. On the other hand, positive Gulf coast landfall angles (Figure 4.10) were very frequent in the early season with an expected peak in activity during the peak season. This peak in June coincides with a peak in Gulf coast TCTOR activity that is not matched in the negative landfall angle distribution. Interestingly, the positive landfall angles, if too large, could prevent a large portion of the right-front quadrant from moving ashore. However, if the angle does permit the right-front quadrant to move ashore, either in part or whole, the onshore flow would be maximized in this region leading to enhanced shear. This suggests that the landfall angle seasonality does play a significant role in TCTOR production.

4.6 TCTOR Activity per Tropical Cyclone

It is well-known that not all TCs produce tornadoes, and among those that do there is large variability in the number of tornadoes produced (Novlan and Gray 1974; McCaul 1991; Verbout et al. 2007; Moore and Dixon 2011). Tables 4.1 and 4.2 display the number of tornadoes produced by East coast and Gulf coast landfalling TCs. Some TCs, such as Katrina (2005), are displayed on both tables as they made landfall along both coastlines during their lifetime. Included in these tables is the name of the TC, the date of landfall along the respective coastline, the TC intensity at the time of landfall, and the number of TCTORs that were produced. These tables support previous research that suggests significant variability in the number of TCTORs produced per TC.

This variability can be seen in the differences between a few notable TCs along both the East and Gulf coasts. Along the East coast, Hurricane Hugo (1989) made landfall as a Category 4 hurricane in South Carolina, yet only produced two TCTORs. A weaker, yet similarly notable

East coast TC, was Hurricane Florence (2018). Florence made landfall in North Carolina as a Category 1 hurricane and produced 44 TCTORs. Several differences exist between these two TCs. As previously mentioned, the intensity of each TC at landfall was very different with Hugo (1989) and Florence (2018) making landfall as Category 4 and Category 1 hurricanes, respectively. Along with intensity, the forward motion of each hurricane was quite different. Hugo (1989) was a rapid TC with forward speeds greater than 12 m/s while travelling towards the northwest whereas Florence (2018) was much slower, only translating at speeds as low as 1 m/s with directional motion towards the south and west after landfall.

Two notable Gulf coast TCs that exhibited such variability were Hurricane Ivan (2004) and Hurricane Michael (2018). These two hurricanes both made landfall as major hurricanes, Category 4 and Category 5, respectively. These two hurricanes also had similar translational speeds at landfall, roughly 6-7 m/s. However, Hurricane Ivan (2004) produced 118 TCTORs and Michael (2018) produced only 16. Ivan had a dry air intrusion present at the time of landfall and was experiencing increased vertical wind shear from an approaching mid-latitude trough. Michael on the other hand, had no dry air intrusion at the time of landfall and minimal vertical wind shear. Michael did have an interaction with a weak shortwave trough which did enhance Michael's outflow. These examples reveal not only the variability in TCTOR production between TCs, but also the different factors that could influence TCTOR production. Those factors include, but are not limited to, the TC intensity, the TC forward motion, dry air intrusions, TC-scale vertical wind shear, and mid-latitude trough interactions.

4.7 TCTORs and Tropical Cyclone Intensity

As previously mentioned, there was large variation in the number of TCTORs produced per TC, but there is consensus that more intense hurricanes often produce more tornadoes

(Novlan and Gray 1974; McCaul 1991; Verbout et al. 2007; Moore and Dixon 2011). When stratifying the frequency of TCTORs by Saffir-Simpson intensity ratings, most previous studies focused on the TC intensity at landfall rather than at the time of the tornado (which may occur 1-2 days after landfall after the TC weakened significantly). Figures 4.15 and 4.16 display the frequency of TCTORs stratified by the Saffir-Simpson TC intensity at the time of the tornado, separated into East and Gulf coasts, respectively.

For the East coast, the frequency of TCTORs was skewed dramatically towards weaker TCs. At the time of the TCTORs, nearly 60% of all tornadoes were produced by TCs of either tropical depression or tropical storm strength with the largest fraction of tornadoes produced by TCs of tropical storm strength. As TC intensity increased, there was a sharp decline in TCTOR frequency. A similar trend was observed for the Gulf coast, whereby roughly 70% of all TCTORs were produced by TCs of less than hurricane intensity. Again, as TC intensity increased to hurricane strength, there was a sharp decrease in TCTOR frequency, but within the five hurricane intensities, only a casual decrease was observed. With Gulf coast landfalling TCs, the majority of TCTORs occurred when the TC is of tropical depression strength.

These results suggest that stratifying TCTOR frequencies by TC intensity at landfall may be misleading as not all TCTORs occur at that time, but can occur days before or after landfall.

4.8 TCTORs and Tropical Cyclone Intensity at Landfall

To mimic the previous studies that focused on TC intensity at landfall, a similar analysis was performed with the updated TCTOR database to provide a direct comparison with those studies and identify any differences between the two methodologies. It has been noted that TCTORs are more frequently associated with TCs that are stronger at landfall, but the correlation

between the two has not been conclusive (Novlan and Gray 1974; McCaul 1991; Verbout et al. 2007; Moore and Dixon 2011). Novlan and Gray (1974) found that TCs that produced TCTORs were more intense at landfall, based on minimum surface pressure and maximum wind speed, than those that did not produce any. McCaul (1991) supported this finding, noting that TCs with at least one TCTOR had maximum wind speeds that were greater, on average, compared to TCs that did not produce any. He also found that TCs that produced more than 8 TCTORs had average maximum wind speeds that were more than double the maximum wind speeds of TCs with no TCTOR production. Taking a statistical approach, Verbout et al. (2007) found that TCs that were Category 2 or greater at landfall were more likely to be associated with TCTOR outbreaks. Moore and Dixon (2011), while only looking at Gulf coast hurricanes, found that hurricanes of Category 3 intensity produced the most TCTORs with a gradual increasing trend in TCTOR production per TC with an increase in TC intensity.

Figures 4.17 and 4.18 provide the frequency of TCTORs with respect to TC intensity at landfall for the East and Gulf coasts, respectively. A simple, visual comparison of the two charts shows little commonality between the separate distributions. East coast TCTORs were most frequently associated with TCs of Category 2 intensity at landfall, accounting for nearly half of all TCTOR events along the East coast. Category 3 and greater intensity TCs accounted for less than 20% of all East coast TCTOR events which does not align with the findings of previous studies. This distribution suggests that along the East coast, weaker TCs more frequently produce TCTORs.

Figure 4.18 shows a much less straightforward distribution of TCTOR frequencies for the Gulf coast. There are two distinct peaks in TCTOR frequency for landfalling TCs of tropical storm and Category 3 hurricane intensity, with the largest frequency of TCTORs being

associated with landfalling tropical storms, accounting for approximately 33%. In contrast, of the remaining Gulf coast TCTOR events, roughly one-third of all TCTOR-producing TCs along the Gulf coast were of intensity Category 3 or greater between the years 1950-2019. This continues to challenge the generalized notion that stronger TCs at landfall produce more TCTORs as the majority of Gulf coast TCTORs were spawned by TCs that were weaker, on average, at landfall. However, if the data were restricted to TCs of hurricane intensity, the results would align better with those of Moore and Dixon (2011), which highlighted the highest frequency of TCTOR events with Gulf coast Category 3 hurricanes.

When analyzing the TCTOR frequencies with respect to TC intensity, either at landfall or at the time of the TCTOR, there appears to be a negative correlation between the two. A possible explanation for such a relationship is that stronger TCs may create an environment that is too sheared, preventing any potential convection from becoming sufficiently organized. While the apparent negative correlation may be of some use, there are many more factors that must be considered in TCTOR development in addition to TC intensity, especially in the mesoscale environment.

4.9 TCTOR Spatial Distribution

TCTORs produced by East coast TCs were much fewer in number than those produced by Gulf coast TCs and impacted a much smaller area of the coastal United States. Figures 4.19 and 4.20 show the initiation locations of all TCTORs from 1950-2019 that were produced by East coast and Gulf coast landfalling TCs, respectively. The majority of East coast TCTORs were located within the states that border the Atlantic Ocean, with only a few exceptions. There was also not much extension inland, with the most western East coast TCTOR occurring in southeast Tennessee. However, the Gulf coast TCTORs were much more widespread across

much of the Southeastern US with extension into the Midwest and Mid-Atlantic regions as well. The widespread nature of Gulf coast TCTORs was related to the TC tracks. Many Gulf coast TCs had relatively northward motion that became northeastward as they encountered mid-latitude troughs. In both cases, it is clear that much of TCTOR activity was concentrated closer to the coastline which aligns with previous studies (Novlan and Gray 1974; Schultz and Cecil 2009; Moore and Dixon 2011; Edwards 2012).

4.10 TCTOR Azimuthal Distribution

With the inclusion of the past 12 years of TCTOR data, there is little change, if any, to the TCTOR locations relative to the TC center (see Figure 2.2). In both the earth- and motion-relative frameworks including all TCTORs (Figures 4.21 and 4.22), the majority continued to be found within the Northeast, or right-front, quadrant, consistent with many previous researchers' findings (Novlan and Gray 1974; McCaul 1991; Verbout et al. 2007; Schultz and Cecil 2009; Moore and Dixon 2011). When changing the reference framework from earth- to motion-relative, there was a slight shift towards 0° in the densest TCTOR locations.

The findings became more intriguing as they were delineated by coastline. In the earth-relative framework, East coast TCTORs were primarily located on the northern side of the TC with the majority of them found between 0° and 45° and within 400 km of TC center (Figure 4.23). Within the same framework, Gulf coast TCTORs were also primarily found within 400 km of TC center, but the densest region of TCTORs was found at an azimuthal range between 45° and 90° from true north (Figure 4.24). When using the motion-relative framework, both East and Gulf coast TCTORs shifted counter-clockwise. East coast TCTORs became more concentrated between 315° and 45°, centered on 0° (Figure 4.25), while the Gulf coast TCTORs became concentrated between 0° and 45° (Figure 4.26). The East coast patterns were starkly

different from the overall pattern commonly observed. East coast TCTORs appeared to favor the regions more northward and in the direction of the TC motion vector. This may be related to the TC angle of landfall along the East coast and where the onshore flow is maximized relative to that angle. The Gulf coast projections mimicked the patterns seen in the overall dataset as the number of Gulf coast TCTORs comprised the majority of the total TCTOR count.

4.11 TCTOR Time of Day

It is well-documented that TCTORs are more common during the afternoon and evening hours (Novlan and Gray 1974; Gentry 1983; McCaul 1991; Verbout et al. 2007; Schultz and Cecil 2009; Moore and Dixon 2011; Edwards 2012), but the hourly ranges that are presented among previous studies varied in some degree and did not all use a similar time reference (i.e., Universal Time Coordinated or Local Solar Time were commonly used, but not consistently). To assist in comparing the local environment in which TCTORs develop, Local Solar Time (LST) was used to provide the 3-hourly mean of TCTOR counts at each hour. LST focuses on the physical location of interest and determines the Sun's position in the sky at each TCTOR time, allowing for a more direct comparison between the East and Gulf coasts which have varying time zones.

East coast TCTORs had a fairly straightforward distribution with TCTORs being most frequent between the hours of 10 and 19 LST, peaking between 13 and 15 LST (Figure 4.27). There was a slight decline during the overnight hours with an interesting minor uptick in frequency around 5 LST. These findings were consistent with previous studies that suggested that diurnal heating plays a significant role in TCTOR development. The Gulf coast TCTORs showed a much cleaner distribution throughout the day (Figure 4.28). There was a single distinct peak that maximizes at 15 LST (which was slightly later in the local day than that of East coast

TCTORs). There was also a more gradual increase in activity beginning around 6 LST and a sharper decrease in activity that leveled off around 22 LST. Overall, the East coast TCTORs appeared to occur slightly earlier in the day than those of the Gulf coast and most activity occurred within a narrower window than Gulf coast TCTORs.

4.12 TCTOR Local Environment Analysis

Local TCTOR environments have been analyzed in a number of studies using a variety of methods which has led to inconsistent results and difficulty in discerning which findings were the most applicable to the typical local upstream environment of a tornado-producing TC supercell (McCaul 1991; McCaul et al. 2004; Baker et al. 2009; Eastin and Link 2009). McCaul (1991) studied a large sample of TCTOR proximity soundings that highlighted high shear, low CAPE environments, yet noted in a later study (McCaul et al. 2004) that the previously studied proximity soundings may not have adequately sampled the environment in which TCTORs were developing, resulting in observed CAPE values that were lower than hypothesized. Case studies such as those conducted by Baker et al. (2009) and Eastin and Link (2009) also found that the observed CAPE in their proximity soundings was greater than values originally reported by McCaul (1991), further suggesting that the sampling may not have been ideal.

Through the use of the TC-modified Goldilocks Zone (GZ), the nearby inflow region of TCTOR-producing supercells was able to be consistently analyzed across 867 TCTOR events. For each event, the hour of the event (Hour 0) and the two preceding hours (Hours 1 and 2) were included to assess the evolution of each analyzed convective metric. Box and whisker plots were used to depict each metric's distribution between the two coastlines and across the three hours of interest (see Figs 4.31-4.69), while a Student's t-test provided information regarding the significance of any differences in the distribution means. Table 4.3 provides the list of metrics

with their associated t-statistic and p-value. Positive (negative) t-statistics indicate larger (smaller) East coast metric values, respectively.

Of the 39 convective metrics analyzed, the number of significantly different metrics at the 5% confidence level ranged between 18 and 28 depending on the hour of interest, with Hour 2 having the fewest and Hour 1 having the most. While there are notable variations between the three hours, there are also several metrics consistently different between the coastlines at all three hours. Those consistently different metrics include the LCL, LFC, EL, SBCAPE, SBCIN, SBCAPE03, MLCAPE, MLCIN, MLCAPE03, MUCIN, MLRH, RH02, bulk shear in all three layers, effective inflow bulk shear, BRNSHEAR, SRH in all layers, fixed-layer SCP, and 0-3 km Sherburn Parameter.

Using the Hour 0 analysis time to compare the coastlines directly, the East coast TCTOR environments consistently had lower LCL heights (259 m compared to 410 m, Fig. 4.31), lower LFC heights (565 m compared to 1187 m, Fig. 4.32), and greater EL heights (13246 m compared to 12635 m, Fig. 4.33), than the environments of the Gulf coast TCTORs. Being calculated using a surface-based parcel, these metrics are heavily influenced by the low-level temperature and moisture profiles. Lower LCL heights indicate a surface environment that has more moisture which would contribute to lower LFC heights in a conditionally unstable environment in the low-mid levels. Elevated EL heights could be suggestive of cooler temperatures in the upper levels, but in the framework of lower LCL and LFC heights, they are likely related as a surface parcel reaches the LFC and begins to follow the pseudo-adiabatic profile sooner, allowing for a more positively buoyant parcel. As one might expect, the various types of CAPE and CIN showed patterns consistent with such differences in the LCL, LFC, and EL, most notably the SBCAPE was larger (1791 J/kg compared to 1518 J/kg, Fig. 4.34) and SBCIN was

smaller (-7 J/kg compared to -20 J/kg, Fig. 4.35) for East coast TCTOR environments (Table 4.4).

As previously mentioned, it appears that variations in the low-level moisture played a significant role in determining the multiple stability differences. When examining relative humidity differences through multiple layers, the only significant differences were between the lowest 100-mb mean mixed-layers and 0-2 km layers where means were greater for East coast TCTORs than for Gulf coast TCTORs. To understand this difference, the spatial distribution of each coast's TCTORs must be considered. East coast TCTORs during the study period were, on average, closer in proximity to the coast than those associated with Gulf coast TC landfall. Examining Figures (Figures 4.19 and 4.20, respectively), the difference in the spatial distribution is apparent as several Gulf coast TCTORs were observed much further inland than most East coast TCTORs. Being further removed from the coastline, low-level moisture is less readily available through surface fluxes, likely leading to the disparity between the two datasets.

Moving away from the thermodynamic parameters, a number of kinematic parameters were also found to be significantly different between the two coastlines. When comparing the general shape of the hodographs in the East and Gulf coast composite soundings (Figures 4.29 and 4.30, respectively), the shape matches the classic "horseshoe-like" curvature noted in McCaul (1991). What differentiates the two coastlines is the magnitude of the bulk shear in the layers that are commonly assessed: 0-1 km, 0-3 km, 0-6 km, and effective inflow layer. The East coast TCTOR environments, on average, had lower bulk shear magnitudes in each layer with the most significant difference in the 0-3 km layer (Figure 4.56) where the mean value on the East coast was 15.69 m/s compared to 18.85 m/s among Gulf coast TCTOR environments. Not only were the East coast bulk shear magnitudes less than the Gulf coast, but the BRN shear (Figure

4.58) was also of much lesser magnitude among East coast TCTORs with a mean value of 8.04 m^2/s^2 compared to 30.58 m^2/s^2 among Gulf coast TCTOR environments. The reasoning for this disparity may be attributed to the angle at which TCs make landfall on either coastline. With the strongest winds located in the front-right/northeast quadrant of the TC (Schenkel et al. 2020, 2021), any time this quadrant moves over land, the bulk shear and BRN shear values will be larger than if it remains offshore. Moreover, while at the surface where friction is decelerating the low-level winds, the mid-level winds remain unimpeded, resulting in larger shear magnitudes across the different parameters. Should the strongest quadrant remain offshore, a weaker vertical wind profile, despite similar surface interactions, will have reduced shear magnitudes. Gulf coast TCs make landfall at a mean angle of 0° whereas East coast TCs make landfall at a mean angle of +30° (see Section 3.9 - Landfall Angles for details). This allows for the northeast (strongest wind) quadrant of Gulf coast TCs to also be onshore, resulting in stronger vertical shear while the same northeast quadrant of East coast TCs is not always onshore (and experiencing increased friction), resulting in weaker vertical shear. Furthermore, these discrepancies in landfall angle and low-to-mid level wind profiles also impact the SRH in the 0-500 m, 0-1 km, 0-3 km, and effective inflow layers (see Figures 4.60-4.63). The SRH in each of these layers was greater in Gulf coast TCTOR environments than in East coast TCTORs, and the differences increased from 116 m^2/s^2 to 253 m^2/s^2 as the layer depth increased from 0-500 m to 0-3 km, respectively. SRH is a measure of the curvature of the low-level wind profile with veering winds relative to storm motion producing larger values. Streamwise vorticity is horizontal vorticity, generated by vertical wind shear, that is inline with the storm inflow. Larger SRH values (increased veering winds with height) indicate that increased streamwise vorticity is ingested in the storm's updraft which leads to vertical cyclonic rotation and thus can be an

indicator for tornadic development (Davies-Jones 1984). Therefore, lesser SRH values along the East coast would result in less streamwise vorticity available to be ingested into the developing miniature supercell, and potentially fewer TCTOR events. However, while the mean East coast SRH values were less than the Gulf coast values at all hours and levels, they do exceed 100 m^2/s^2 (Table 4.4) which is sufficient for rotating updrafts.

With regard to composite parameters, the fixed-layer SCP and the 0-3 km Sherburn parameter (Sherburn and Parker 2014) were also impacted by the vertical wind shear discrepancies, as both parameters were significantly larger in Gulf coast TCTOR environments (3.65 and 0.83, respectively) than those of East coast TCTORs (0.97 and 0.7, respectively). The fixed-layer SCP includes the MUCAPE (Fig. 4.40), 0-3 km bulk shear (Fig. 4.56) and 0-3 km SRH (Fig. 4.62). The two kinematic parameters within the SCP equation were both significantly greater in the Gulf coast TCTOR environments than those along the East coast which negated the insignificant difference in MUCAPE values between the two coastlines (see Tables 4.3 and 4.4). The 0-3 km Sherburn parameter assesses the significant severe event risk within high-shear, low-CAPE environments and calculates this risk based on the 0-3 km bulk shear (Fig. 4.56), 0-3 km lapse rate (Fig. 4.42), and the 700-500 mb lapse rate (Fig. 4.43). Of these three parameters, the only one that was significantly different between the two coastlines was the 0-3 km bulk shear magnitude (Tables 4.3 and 4.4). The 700-500 mb lapse rate was nearly identical between the two coastlines, and the East coast 0-3 km lapse rates were slightly greater than the Gulf coast, but the differences were not significant. While the Gulf coast TCTOR environments had larger SHERBS3 values, the difference between the two coastline means was only 0.11, and both coastline means were well below the 25th percentile of SHERB3 value of approximately 1 for tornadic events studied by Sherburn and Parker (2014) (see their Figure 13a). Another caveat is

that their study only focused on non-tropical significant severe events with tornadoes of EF-2 intensity or greater. These caveats caution the direct interpretation of these results when assessing the utility of this parameter within TCTOR environments.

While several of these metrics are significantly different between the two coastlines, many of the significant differences may not be practically applied within operational forecasting. For example, at all analysis hours, SBCIN was significantly less on the East coast than on the Gulf coast (Fig. 4.35), however, these differences were, on average, around 15 J/kg. Another similar example is the 0-1 km bulk shear which was also significantly less in East coast TCTOR environments (Fig. 4.55), but the mean differences at all analysis hours was approximately 1.5 m/s. In the hours leading up to a TCTOR event, deciphering these quantitatively small differences in the mesoscale environment can be challenging, therefore, not all statistically significant differences may be beneficial in forecasting TCTOR risk. Other metrics that fall into this category include SBCAPE03, MLCIN, MLCAPE03, MUCIN, MLTHE, RH02, SHEAR01, SHEAR06, EFFSHEAR, SRH05, STPEFF, SHERBS3, and SHERBE (Table 4.4). However, there are a number of metrics that differ significantly between the two coastlines and may be used operationally. The more useful metrics are those that had quantitative differences in their mean values that are outside the realm of "noise" or calculation variability. These metrics include LCL, LFC, SBCAPE, MLCAPE, BRNSHEAR, SRH01, SRH03, SCPFIX, and SCPEFF. Because the mean values of these parameters are so different at all analysis hours, different threshold values would be required to quantify similar TCTOR risk across the two coastlines. Understanding which metrics are more pragmatic in the hours leading up to a TCTOR event can provide the Storm Prediction Center valuable insight into the potential for TCTOR development, and thus they would be able to communicate the threat with adequate lead time.

4.13 Synoptic Map Analysis

Previous studies have found certain synoptic features and convective metrics that contribute to TCTOR production in landfalling TCs. Verbout et al. (2007), when analyzing Texas landfalling TCs, found that tornado outbreak cases occurred more frequently when landfalling TCs interacted with a 500-mb trough located to the north-northwest over the northern Plains along with the presence of significant low- and deep-layer shear (surface-850 mb and surface-500 mb, respectively). Curtis (2004) noted that mid-level dry air intrusions also contributed to TCTOR outbreaks. In light of these findings, to understand how certain convective metrics differed between the East and Gulf coasts, composite synoptic maps were developed for each coastline. Along with the delineation between coastline, each coastline's TCs were further subdivided into two groups: TCs with landfall angles greater than the mean landfall angle for its respective coastline, and TCs with landfall angles less than the mean. This allowed for comparisons not only between the East and Gulf coasts, but also within each coastline to determine whether the angle at which a TC makes landfall has any impact on the spatial patterns of both significant convective metrics and TCTOR events. Using the results from the proximity TCTOR sounding analysis as a guide, a select set of the significantly different parameters (between coasts) were chosen for this analysis, including SBCAPE, SBCIN, 0-2 km relative humidity, and 0-1 km and 0-3 km bulk shear magnitudes. Other basic synoptic parameters, such as the 200-, 500-, and 850-mb heights and winds, 2-4 km and 4-6 km relative humidity, and surface equivalent potential temperature were also analyzed to either aid in interpretation of the synoptic pattern or to expand on the findings of previous studies.

Isobaric Heights and Winds

Beginning with the East coast composite synoptic wind patterns, there are some notable differences between East coast TCs with landfall angles greater than +30° (i.e., storms moving due north toward a southwest to northeast oriented coastline, hereinafter "north-moving") and less than +30° (i.e., storms moving due west toward a southwest to northeast oriented coastline, hereinafter "west-moving") through each of the three analyzed isobaric levels.

At the 200-mb level, for north-moving TCs, there was a deeper trough located north of the mean TC location with an associated jet streak on the east side of the trough (Figure 4.70). A stronger ridge was also observed to the west-southwest of the TC which, in combination with the aforementioned trough, aided to steer the mean TC towards the north and east. The TCTOR locations were also situated in proximity to the right-entrance region of the 200-mb jet, which could be an additional source of lift to aid in TCTOR production. In contrast, for west-moving TCs (Figure 4.71), the 200-mb flow pattern is much less amplified and more zonal in nature, although a weak ridge can be seen roughly 1500 km to the west of TC center. Along with the general pattern difference, the upper-level wind magnitudes are also weaker than the environments surrounding north-moving TCs and displaced further north from the TC itself, resulting in less significant interactions.

At the 500-mb level, the height and wind patterns surrounding north- and west-moving TCs (Figures 4.72 and 4.73, respectively) show mid-level ridging to the west of the TC center, however, for north-moving TCs, an additional weak ridge can be seen on the eastern edge of the TC. This additional ridge, although weaker, may have helped to contribute to the north to northeast steering flow as it is in closer proximity to the TC itself. The 500-mb height and wind patterns for both north- and west-moving TCs exhibited jet streaks to the north-northeast of the

mean TC center, however, for north-moving TCs, this jet streak is closer in proximity to the TC and greater in magnitude. There was also a more amplified flow to the north of north-moving TCs compared to a more zonal pattern for west-moving TCs, mimicking the 200-mb flow patterns.

At the 850-mb level (Figures 4.74 and 4.75), the dual-ridge pattern can be seen in both landfall angle types. For north-moving TCs (Figure 4.74), the western ridge is stronger than for west-moving TCs. An interesting finding is that the eastern ridge was stronger for west-moving TCs (Figure 4.75) than the eastern ridge in proximity to north-moving TCs (Figure 4.74), suggesting that the strength of the lower-level ridges and their locations relative to the TC center were aiding in the steering flow at the time of landfall. When looking at the magnitude of the wind speeds, North-moving TCs were also much stronger, on average, than their west-moving counterparts which is significant as the steering flow layer varies depending on the strength of the TC (Velden and Leslie 1991). The low-level ridging to the east of west-moving TCs (Figure 4.75) may have provided more influence in bringing the preferred quadrant ashore along with a more favorable environment for TCTOR development. Along with impacting the steering flow, the dual ridges may have impacted the TC wind speeds as well. For example, the eastern ridge provides additional southern flow to the eastern region of the TC which would increase vertical wind shear as the TC makes landfall. Any additional wind shear could lead to more TCTOR development given sufficient instability. As indicated by the black dots in both figures, the west-moving TCs have a broader spatial distribution of TCTOR events as the preferred quadrant was able to move onshore whereas the TCTORs associated with north-moving TCs are heavily focused to the north of TC center as the preferred quadrant may have only partially moved onshore, if at all.

The Gulf coast composite synoptic maps have some apparent differences not only between TCs with landfall angles greater than 0° (hereinafter "northwest-moving") and less than 0° (hereinafter "northeast-moving") two landfall types, but also when compared to the East coast landfalls. The 200-mb level heights and winds patterns for Gulf coast northwest-moving TCs (Figure 4.76) and northeast-moving TCs (Figure 4.77) show some notable differences. The upper-level flow for northwest-moving TCs exhibited a less amplified pattern when compared to that of northeast-moving TCs, and the wind magnitudes are generally weaker. There is a stronger jet streak to the northeast of the mean TC center of northwest-moving TCs which places the TCTOR locations in proximity to the right-entrance region of the jet (Figure 4.76). This collocation of TCTORs and the right-entrance region of the upper-level jet was observed in both East and Gulf coast datasets for TCs with landfall angles greater than the respective mean. An interesting difference between these two figures is observed height differences. The heights surrounding northwest-moving TCs were much lower than those surrounding northeast-moving TCs which highlights the seasonality of Gulf coast TCs and their respective landfall angles as northwest-moving TCs more frequently occurred in the early season when the atmosphere had only begun to warm (i.e., higher heights), whereas the northeast-moving TCs occurred later in the season after the atmosphere had warmed throughout its depth (i.e., lower heights).

At the 500-mb level, ridges become more apparent. For northwest-moving TCs (Figure 4.78), dual ridges were observed with one being located approximately 2500 km to the west of TC center and another much closer to the east of TC center. Northeast-moving TCs also showed a dual-ridge feature on either side of the TC center (Figure 4.79) with similar relative magnitudes to the ridges identified near northwest-moving TCs (Figure 4.78). A key difference is the location of the western ridge as it is located to the TC's southwest at a distance of 500-1000 km.

There was also a trough located to the northwest of the mean northeast-moving TC (Figure 4.79) instead of a ridge in the same location for northwest-moving TCs (Figure 4.78), and a moderate jet streak located roughly 2500 km north of the TC center.

The 850-mb level maps for both landfall bins (Figures 4.80 and 4.81) show several similarities. For both northwest- and northeast-moving TCs, a broad trough was observed to the TC's northwest and a ridge was located on the TC's eastern flank. For northwest-moving TCs (Figure 4.80), the ridge was nearly due east of the TC center allowing for more northward steering flow. In contrast, northeast-moving TCs (Figure 4.81) experienced a ridge that was located to the east-northeast of TC center, resulting in an easterly component to the steering flow. The TCTOR locations and counts were impacted based on the landfall angle due to the steering flow patterns. Gulf coast northwest-moving TCs produced more TCTORs (1106) that were more concentrated within the northeast quadrant and closer to the TC center whereas the northeast-moving TCs produced fewer TCTORs (825) that were nearly equally distributed between the eastern quadrants. This discrepancy was likely due to which quadrants were onshore and experiencing increased vertical wind shear due to friction with the land surface. Due to the increased vertical shear, TCTOR development was more likely to occur in the quadrants with larger portions onshore.

Bulk Shear

With respect to the spatial distribution of bulk shear magnitudes, there are again some notable differences between both landfall angle types at both coastlines. Along the East coast, 0-1 km shear magnitudes are noticeably larger for north-moving TCs than west-moving TCs (Figures 4.82 and 4.83, respectively). Directly comparing these with the Gulf coast TCs (Figures

4.84 and 4.85), the region of maximum 0-1 km shear is located in the northeast quadrant whereas for East coast TCs it is located due north of TC center. This is likely a result of the landfall angles and orientation of the East coast which results in the northeast quadrant (with the strongest winds) oftentimes remaining offshore; therefore, the strongest shear values are located in the northern region of the TC instead of the typical northeast quadrant. In an opposite pattern from the East coast TCs, the Gulf coast northwest-moving TCs (Figure 4.84) had weaker 0-1 km shear values compared to the northeast-moving TCs (Figure 4.85). Along both coastlines, in the landfall bin with the maximum 0-1 km shear magnitudes, the majority of TCTORs occurred outside of the maxima, most frequently in the 12-15 m/s range, suggesting that the ideal 0-1 km shear magnitudes for TCTOR development may not be the largest observed magnitudes during a TC landfall. This feature of TCTOR environments implies that shear does not contribute to TCTOR development in isolation, but instead suggests that instability must be a contributing factor alongside shear.

When analyzing the 0-3 km shear magnitudes, the spatial patterns mimic the 0-1 km shear distributions for both coastlines (Figures 4.86-4.89). For both north- and west-moving East coast TCs (Figures 4.86 and 4.87, respectively), the TCTOR event locations were situated in regions of 0-3 km shear magnitudes of 15-18 m/s with TCTORs remaining outside of the region of maximum shear. Similar TCTOR counts were found for north- and west-moving East coast TCs (190 and 178, respectively), which, based solely on the local 0-3 km shear patterns, is not unexpected. For northwest- and northeast-moving Gulf coast TCs (Figures 4.88 and 4.89, respectively), there is an interesting difference between the 0-3 km shear pattern compared to the 0-1 km shear pattern. The region in which Gulf coast TCTORs developed in both landfall angle bins was collocated with the region of maximum 0-3 km shear magnitudes which is unlike the 0-

1 km shear maps. For Gulf coast TCs, the maximum 0-3 km shear values were greater than the East coast TCs (approximately 19-20 m/s and 17-18 m/s, respectively), and the Gulf Coast TCTOR events were most frequently located in regions of 18-20 m/s shear. Although the 0-3 km shear patterns were similar between northwest- and northeast-moving Gulf coast TCs, the TCTOR counts were not similar (1106 and 825, respectively), suggesting that Gulf coast TCTOR counts are impacted by another environmental characteristic.

Relative Humidity

Significant differences were found in the 0-2 km mean relative humidity profiles between the two coastlines, and therefore the spatial distribution of the mean relative humidity in the 0-2 km layer. Because of the potential importance of mid-level dry air intrusions noted by Curtis (2004), the 2-4 km, and 4-6 km layers were also assessed. For north- and west-moving East coast TCs (Figures 4.90 and 4.91, respectively), the 0-2 km relative humidity values within the contours of the TC itself were similar between the two, although there was significantly drier air within the ridge to the west of north-moving TCs. Although a ridge exists in a similar location in both TC groups, the ridge was much stronger for north-moving TCs which supports the notion of drier air in place. There was also evidence of drier air being advected into the southern edge of the north-moving TCs, however it is far removed from the TCTOR locations (Figure 4.90). For north- and west-moving East coast TCs (Figures 4.92 and 4.93, respectively), there is a striking difference in the 2-4 km relative humidity patterns between the two classifications. It is important to note that the low-level dry air advection seen in north-moving TCs was not simply surface based, but continued through the low-to-mid levels of the troposphere (Figure 4.92). On average, the TCs themselves had very high relative humidity values in their immediate

environment, but the advection of drier air on the southern flank of north-moving TCs is able to be seen in more than one level. This advection of drier air into the southern region, and subsequently the eastern region, of these TCs is consistent with one of the two primary patterns of mid-level dry air advection noted by Curtis (2004) which led to tornado outbreaks. West-moving TCs were surrounded by a much more moist environment in the 2-4 km layer and their respective TCTORs occurred in regions of high relative humidity (Figure 4.93). The 4-6 km layer mean relative humidity patterns for north- and west-moving East coast TCs (Figures 4.94 and 4.95, respectively) did not show significantly different patterns compared to the 0-2 km and 2-4 km layers while continuing to highlight TCTOR event occurrence within regions where the mean relative humidity was greater than 80%.

The spatial patterns of 0-2 km, 2-4 km, and 4-6 km mean relative humidities for Gulf coast TCs did not show much variability between the two landfall types (Figures 4.96-4.101). For the 0-2 km layer, there was little difference between the relative humidity spatial distribution and magnitudes of northwest- and northeast-moving TCs (Figures 4.96 and 4.97, respectively). What was different was that the region of relative humidity surrounding the TCs was larger in size and slightly smaller in magnitude than that of the East coast TCs. The 2-4 km and 4-6 km layers for Gulf coast TCs (Figures 4.98-4.99 and Figures 4.100-4.101, respectively) also did not show major differences between the landfall types, however, when compared to their respective East coast layer maps, the Gulf coast ambient environment exhibited greater relative humidity values on average with less significant dry air advection into the TC, if any. Similar to the East coast maps, Gulf coast TCTOR locations were most frequently located in regions where the relative humidity in each of the three layers was greater than 75%, supporting the notion that

TCTORs require sufficient moisture through the mid-levels of the troposphere to support buoyant updrafts.

Thermodynamic Parameters

Certain varieties of CAPE were identified as being statistically different from East coast and Gulf coast TCTOR events. Composite synoptic maps of 0-3 km surface-based CAPE (SBCAPE03), surface-based CAPE (SBCAPE) and surface-based CIN (SBCIN) were constructed for each landfall angle types for each coastline. For north-moving East coast TCs (Figure 4.102), the TCTOR events were located outside of the maximum SBCAPE03 regions. They were located along a gradient where SBCAPE03 values were ranging from 100-125 J/kg. In contrast, the TCTORs associated with west-moving TCs (Figure 4.103) were located in regions of maximum SBCAPE03 values which could suggest that the landfall angle impacts the amount of temperature and moisture advection within the preferred quadrant for TCTOR development as it moves ashore. The SBCAPE spatial distributions for the two landfall angle types (Figures 4.104 and 4.105) were similar to the SBCAPE03 spatial patterns. For north-moving TCs (Figure 4.104), the TCTOR locations were not in regions with large SBCAPE values, but rather in a gradient region where SBCAPE values ranged from roughly 700-1000 J/kg. In contrast, the TCTORs associated with west-moving TCs (Figure 4.105) were located in regions where SBCAPE values were larger, ranging from approximately 1000-1500 J/kg. Within the context of both SBCAPE03 and SBCAPE, sharp gradients of both parameters were present regardless of landfall angle, and a large fraction of TCTORs developed within this baroclinic boundary region. This finding suggests that a surface-based baroclinic-boundary among East coast TCs may help provide additional shear and lift in regions where modest, yet

sufficient, instability exists which may enhance TCTOR development. There were no significant differences between the TCTOR locations in relation to the SBCIN spatial pattern between the two landfall bins (Figures 4.106 and 4.107). In both landfall types, TCTORs developed in regions where SBCIN was generally less than 50 J/kg.

An assessment of these thermodynamic parameters for the Gulf coast showed similar results in the relationship between TCTOR location and spatial patterns of the parameters, but magnitudes of these parameters were, on average, less than those found for the East coast. For Gulf coast northwest-moving and northeast-moving TCs (Figures 4.108 and 4.109, respectively), TCTORs appeared to be located more frequently near gradients of SBCAPE03 rather than in regions of maximum SBCAPE03 values. The ambient environment of northwest-moving TCs (Figure 4.108) exhibited much lower SBCAPE03 values than that of northeast-moving TCs (Figure 4.109), with the majority of TCTORs having developed in a region of 75-100 J/kg compared to a much wider range of values between 75-175 J/kg. When reviewing the overall composite values of SBCAPE03 for the Gulf and East coasts, the mean East coast values were larger than the mean Gulf coast values. There were similar spatial distributions of SBCAPE for both northwest- and northeast-moving TCs in relation to TCTOR locations (Figures 4.110 and 4.111, respectively). The TCTORs in both landfall angle bins were in an environment with SBCAPE values ranging from 600-1500 J/kg. East coast TCTORs developed in slightly larger SBCAPE environments, but there was more variability dependent on the landfall angle whereas the Gulf coast environments appeared to be more uniform regardless of landfall angle. For the Gulf coast TCs, the SBCIN patterns in proximity to TCTOR locations did not reveal any significant differences between either landfall angle type (Figures 4.112 and 4.113) or in comparison to the East coast TCs (Figures 4.106 and 4.107) although the values were slightly

more elevated, ranging between 50-70 J/kg. While the SBCIN patterns did not differ significantly at the TCTOR locations, in relation to the TC itself, the East coast TCs ot either landfall type had larger values of SBCIN immediately west of TC center and in closer proximity than the Gulf coast TCs.

Summary of Synoptic Differences

In terms of the synoptic wind patterns, there are some similarities between the two coastlines but also some notable differences. Similarities include the presence of a 200-mb jet streak positioned to the northeast of both north-moving East coast and northwest-moving Gulf coast TCs (Figures 4.70 and 4.76, respectively). Although the magnitudes differed, the respective TCTORs were located in the proximity of the right entrance region of this jet which likely provided additional lift within the right-front quadrant of both TCs. The differences begin to appear with the 500-mb level where a ridge can be identified to the west of TCs in both landfall bins of either coastline, but its location in relation to the TC varied. The 500-mb ridge for Gulf coast northwest-moving TCs was located approximately 2500 km to the west (Figure 4.78), however, for northeast-moving TCs, the ridge was much closer, approximately 750 km to the southwest (Figure 4.79). For East coast TCs, there was more consistency in the location of the ridge being nearly due west of TC center, however, for north-moving TCs, the ridge was slightly closer (~2000 km, Figure 4.72), whereas the ridge was approximately 2500 km away from the TC center (Figure 4.73). A more significant difference between the two coastlines was identified at the 850-mb level as the East coast TCs, regardless of landfall types, were in the proximity of a ridge that was located approximately 1000-2000 km to the west (Figures 4.74 and

4.75). In contrast, relative to TC center, there was a trough positioned to the west of Gulf coast TCs where East coast TCs were experiencing a ridge.

The 0-1 km and 0-3 km shear patterns were roughly similar for both landfall types of either coastline. Therefore, more significant differences were identified between the coastlines rather than between the two landfall types. For East coast TCs, the maximum shear values, in both layers, were located to the north of the mean TC center and weaker in magnitude than those of Gulf coast TCs. The maximum shear values for Gulf coast TCs was located east of TC center and were larger in magnitude and spatial extent. Just as intriguing, East coast TCTOR locations were also positioned just outside of the maximum shear values whereas the Gulf coast TCTOR locations were collocated with the maximum shear values.

Relative humidity patterns were notably different between the East and Gulf coasts. East coast TCs, especially north-moving TCs, experienced more significant dry air surrounding the TC in all levels than Gulf coast TCs. Although East coast TCs did experience dry air advection into the southern and eastern regions of the TC that resembled TCTOR-favorable patterns identified by Curtis (2004), there were still far fewer TCTORs associated with East coast TCs than Gulf coast TCs. Also, the East coast TCTORs developed in regions with high relative humidity, suggesting that any dry air intrusion may not have directly impacted the immediate TCTOR environment. The environment surrounding Gulf coast TCs was much more moist in all levels, and similarly, TCTORs developed in regions of high relative humidity.

The thermodynamic properties presented some interesting results as the TCTOR locations for both coastlines were not collocated with regions of maximum SBCAPE or SBCAPE03, but rather along sharp gradients of both parameters. These gradients likely represent surface boundaries that develop as TCs make landfall, and the developing boundaries

may support TCTOR development through localized regions of enhanced lift and/or shear. What was less interesting, and somewhat expected, was the SBCIN spatial distribution for both coastlines. The SBCIN values for both coastlines were minimal throughout the TCTOR-preferred regions, and therefore were likely not a significant factor in TCTOR development.

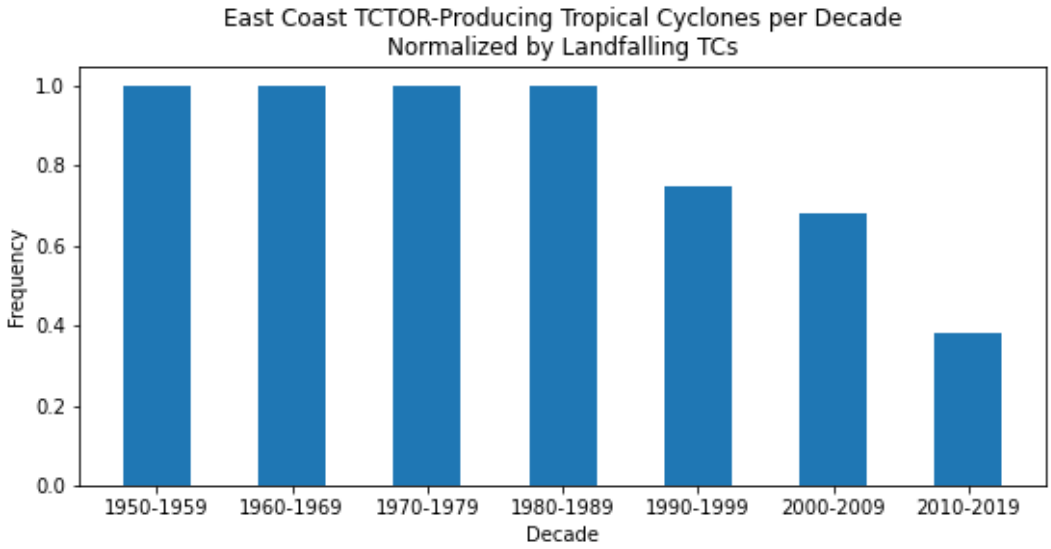

Figure 4.1: Histogram displaying the frequency of East coast tornado-producing TCs by decade, normalized by all landfalling East coast TCs.

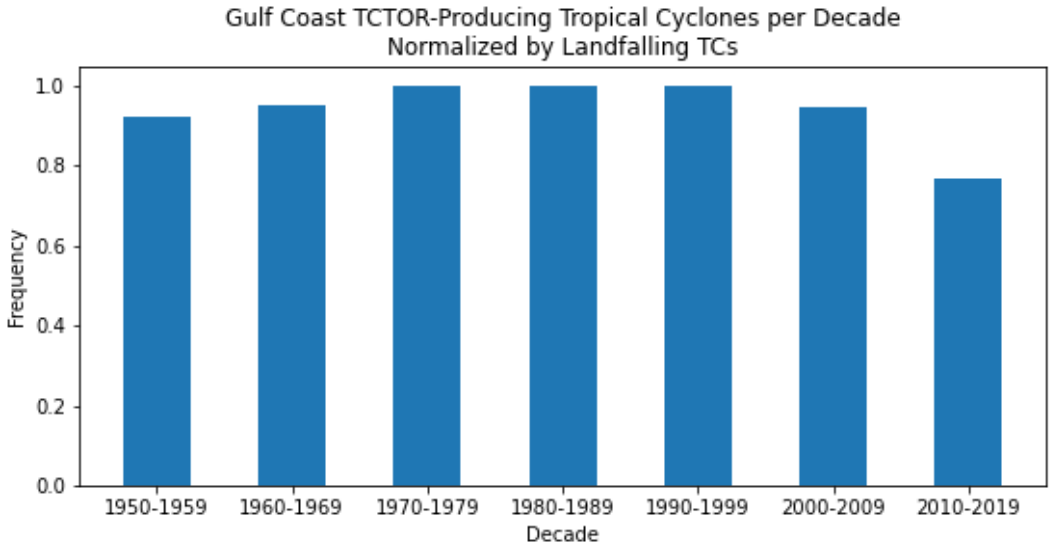

Figure 4.2: Histogram displaying the frequency of Gulf coast tornado-producing TCs by decade, normalized by all landfalling Gulf coast TCs.

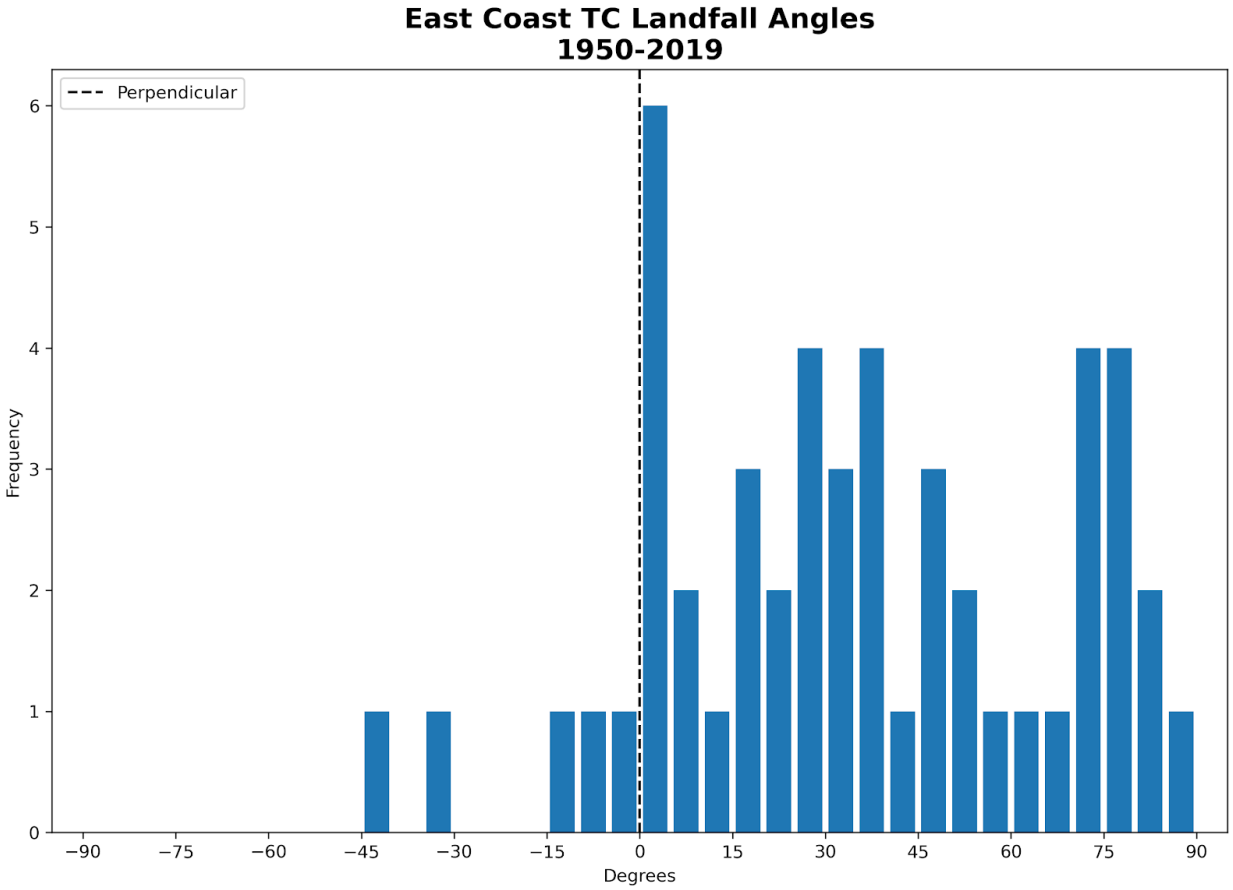

Figure 4.3: Histogram displaying 1950-2019 East coast TC landfall angles. Vertical black dashed line indicates a perpendicular landfall angle.

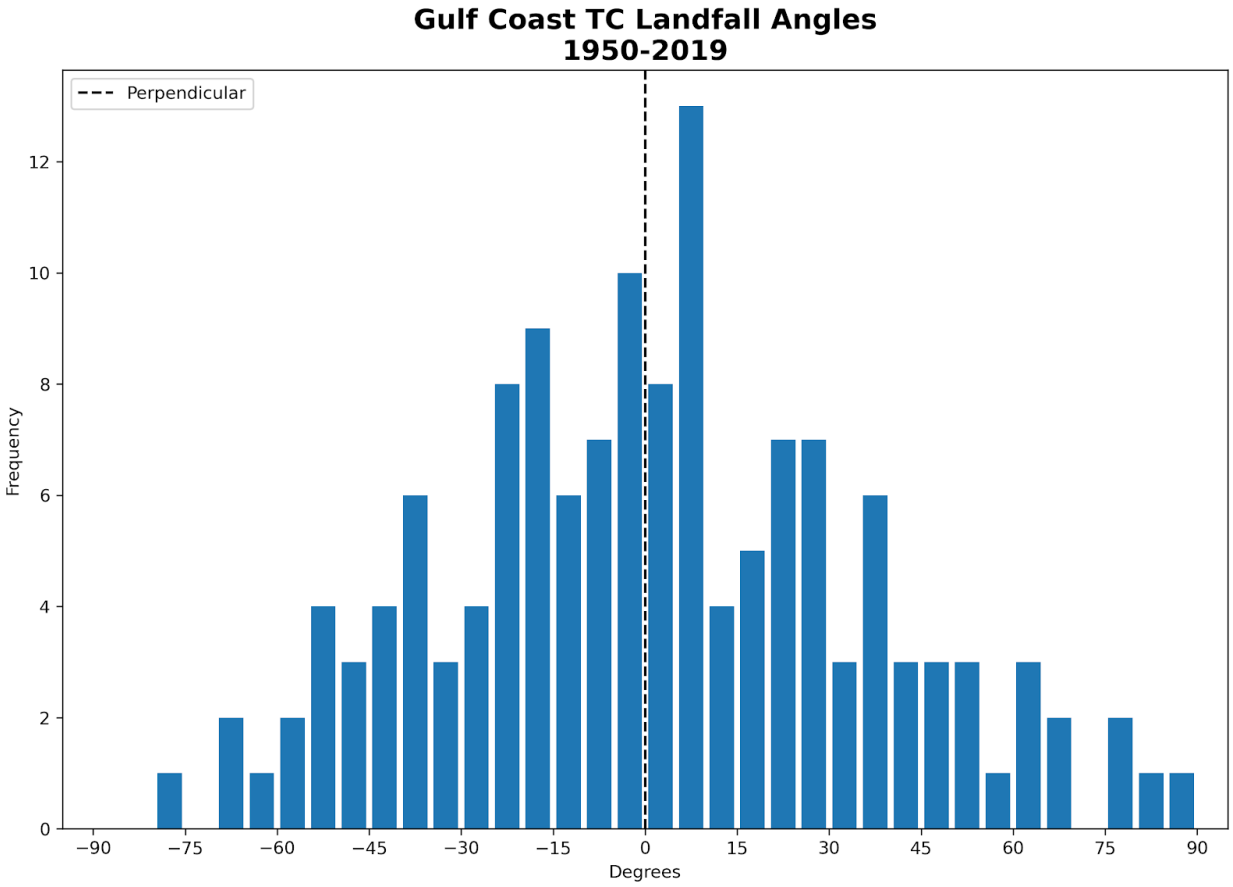

Figure 4.4: Histogram displaying 1950-2019 Gulf coast TC landfall angles. Vertical black dashed line indicates a perpendicular landfall angle.

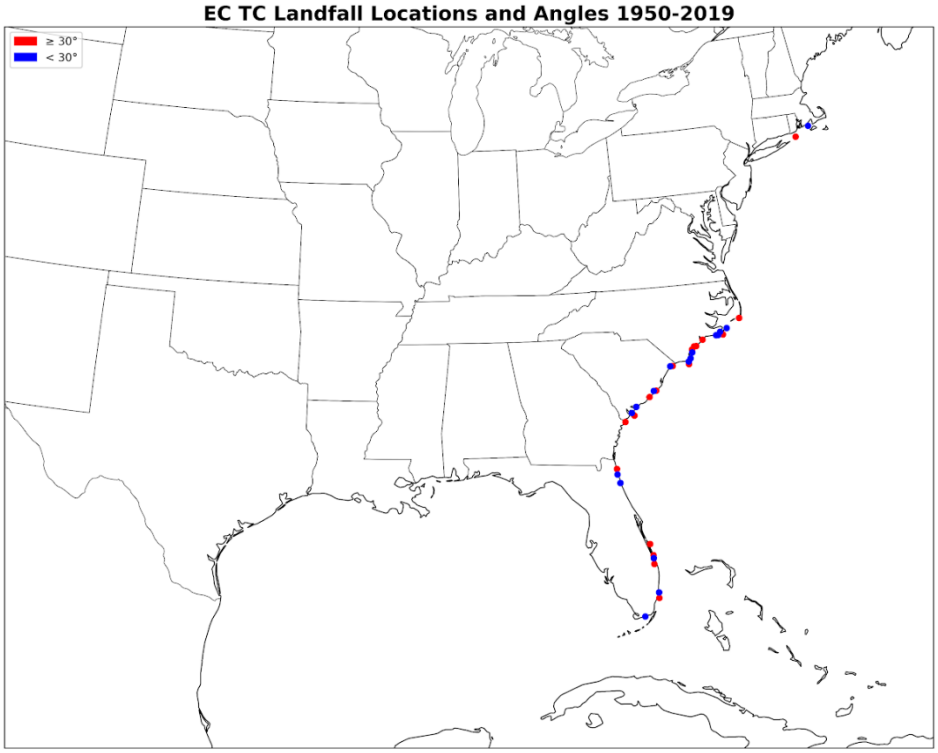

Figure 4.5: East Coast TC landfall locations and angles for the years 1950-2019. Red dots indicate landfall angles greater than or equal to the mean (+30°); blue dots indicate landfall angles less than the mean.

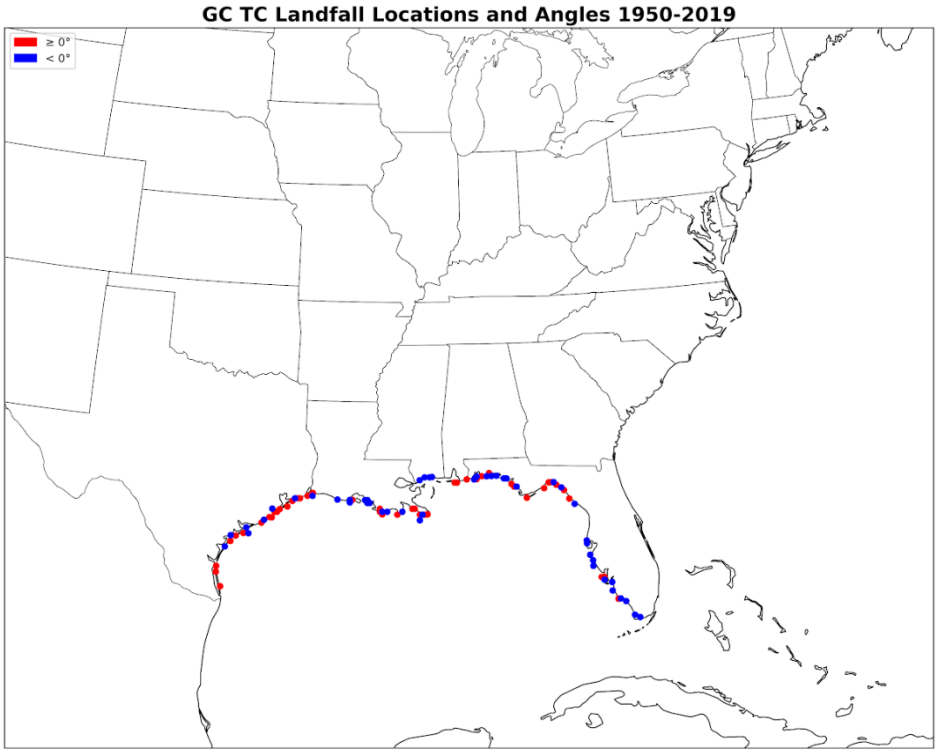

Figure 4.6: Gulf Coast TC landfall locations and angles for the years 1950-2019. Red dots indicate landfall angles greater than or equal to the mean (0°); blue dots indicate landfall angles less than the mean.

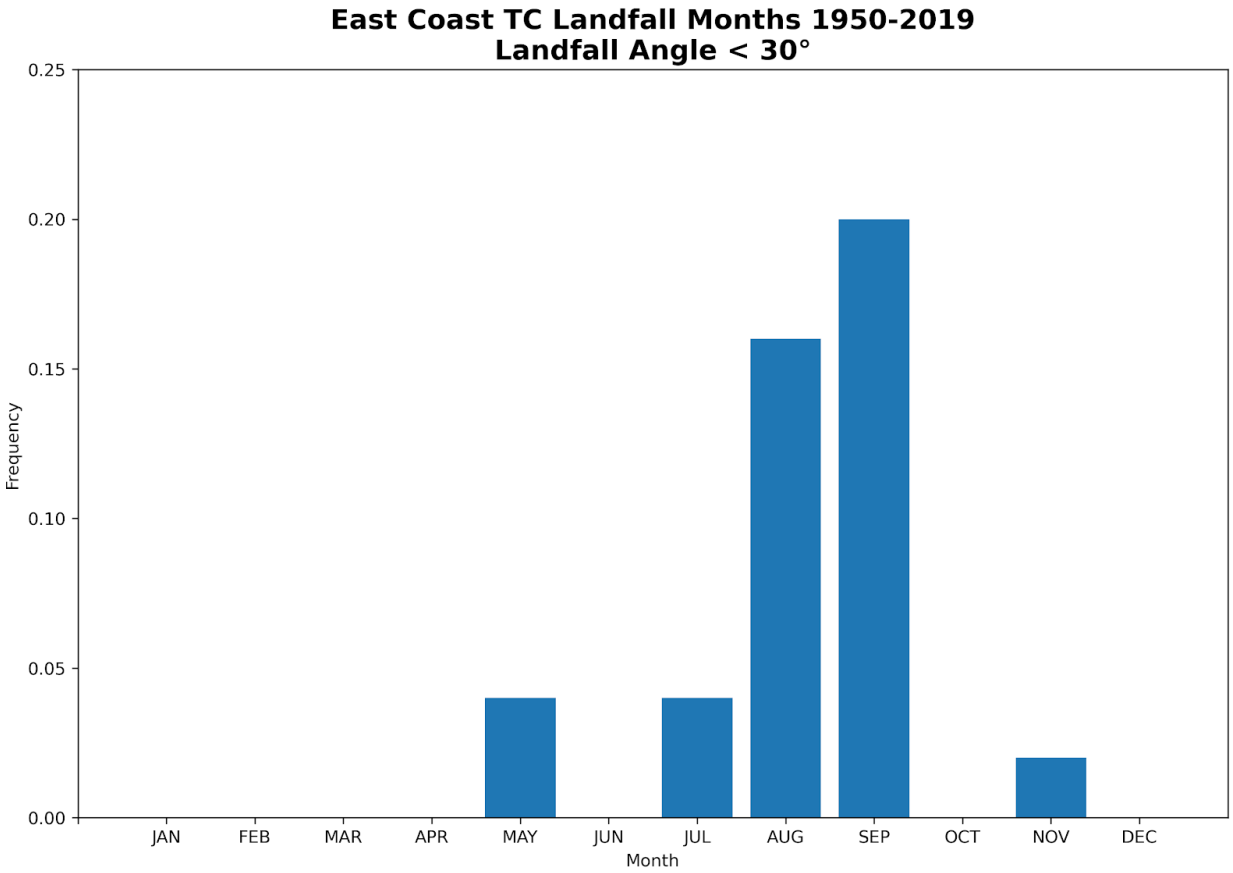

Figure 4.7: East Coast TC landfall frequencies by month of the year for TCs with landfall angles less than the mean (+30°).

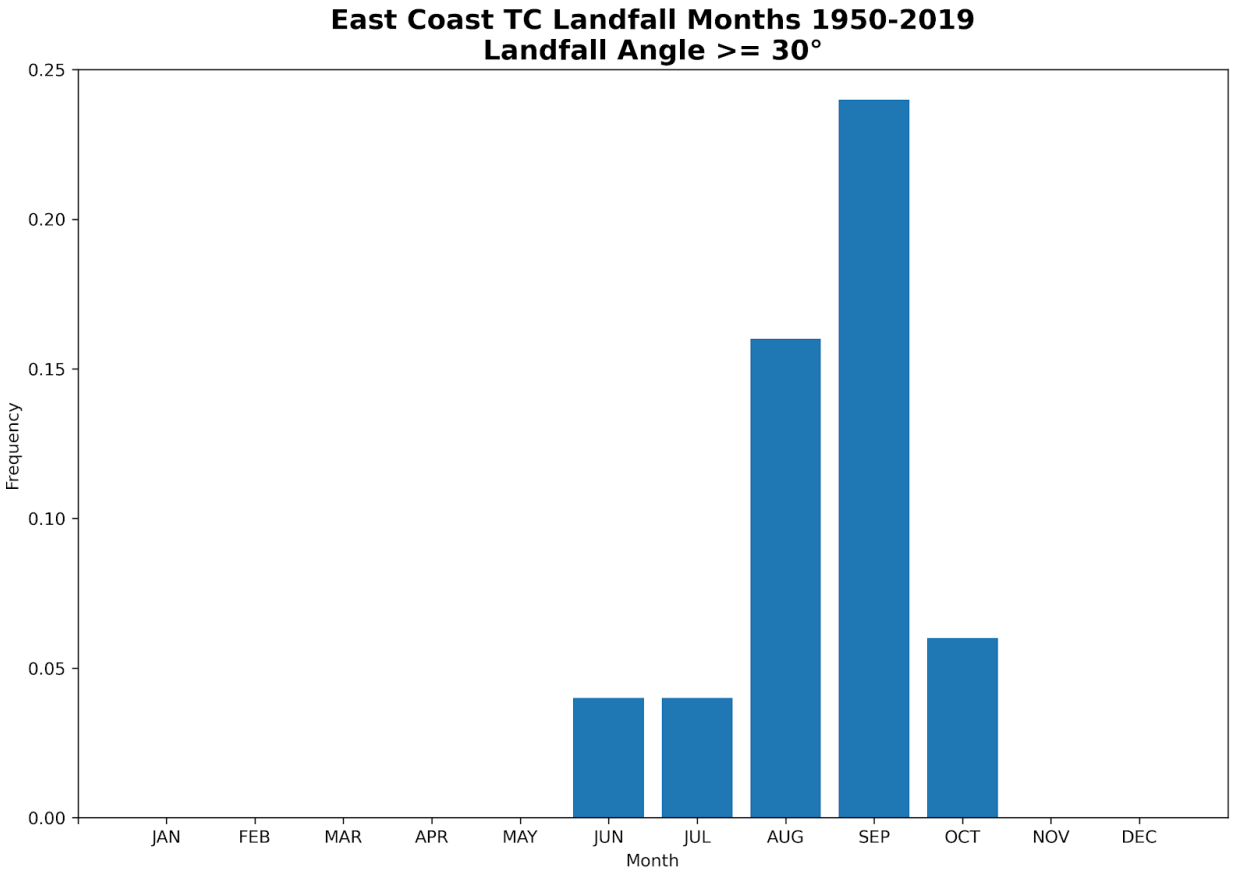

Figure 4.8: East Coast TC landfall frequencies by month of the year for TCs with landfall angles greater than or equal to the mean (+30°).

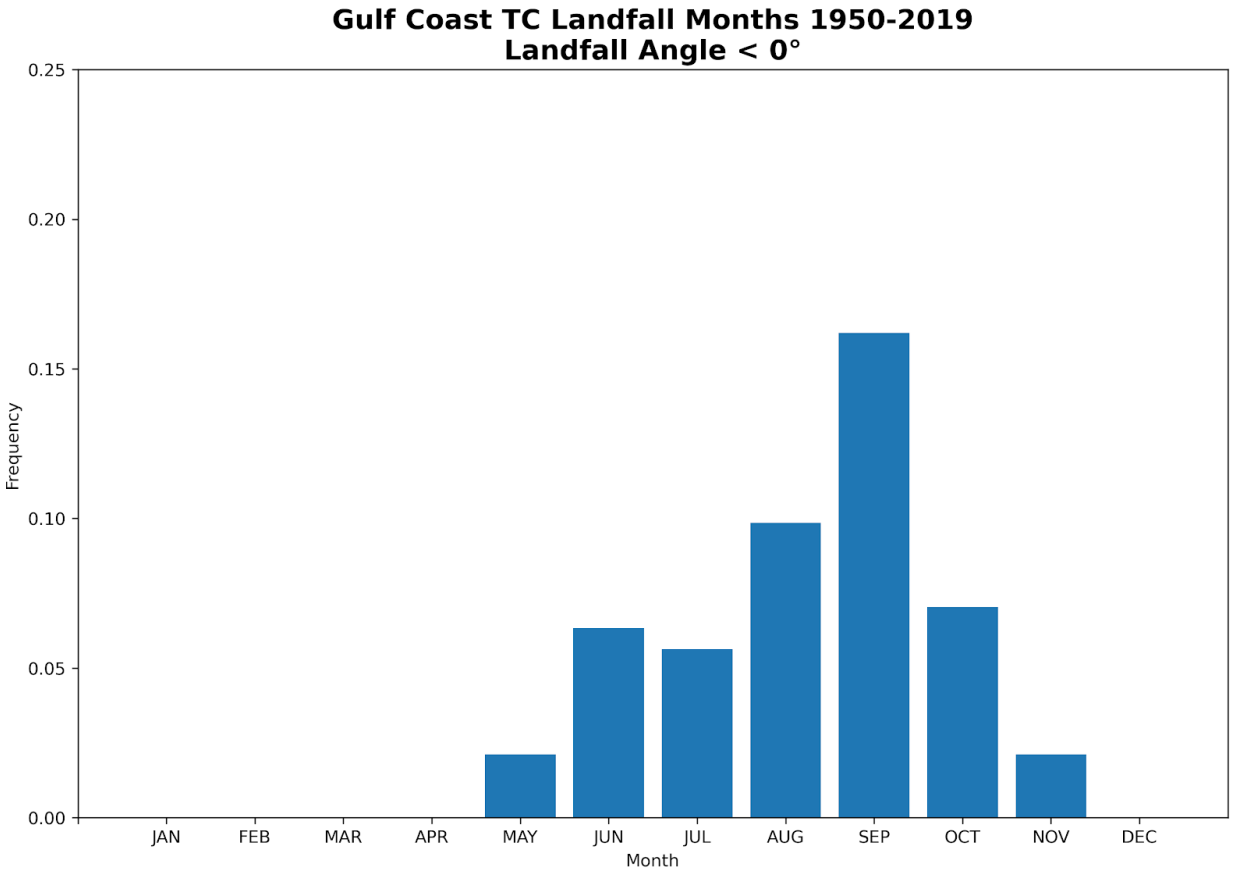

Figure 4.9: Gulf Coast TC landfall frequencies by month of the year for TCs with landfall angles less than the mean (0°).

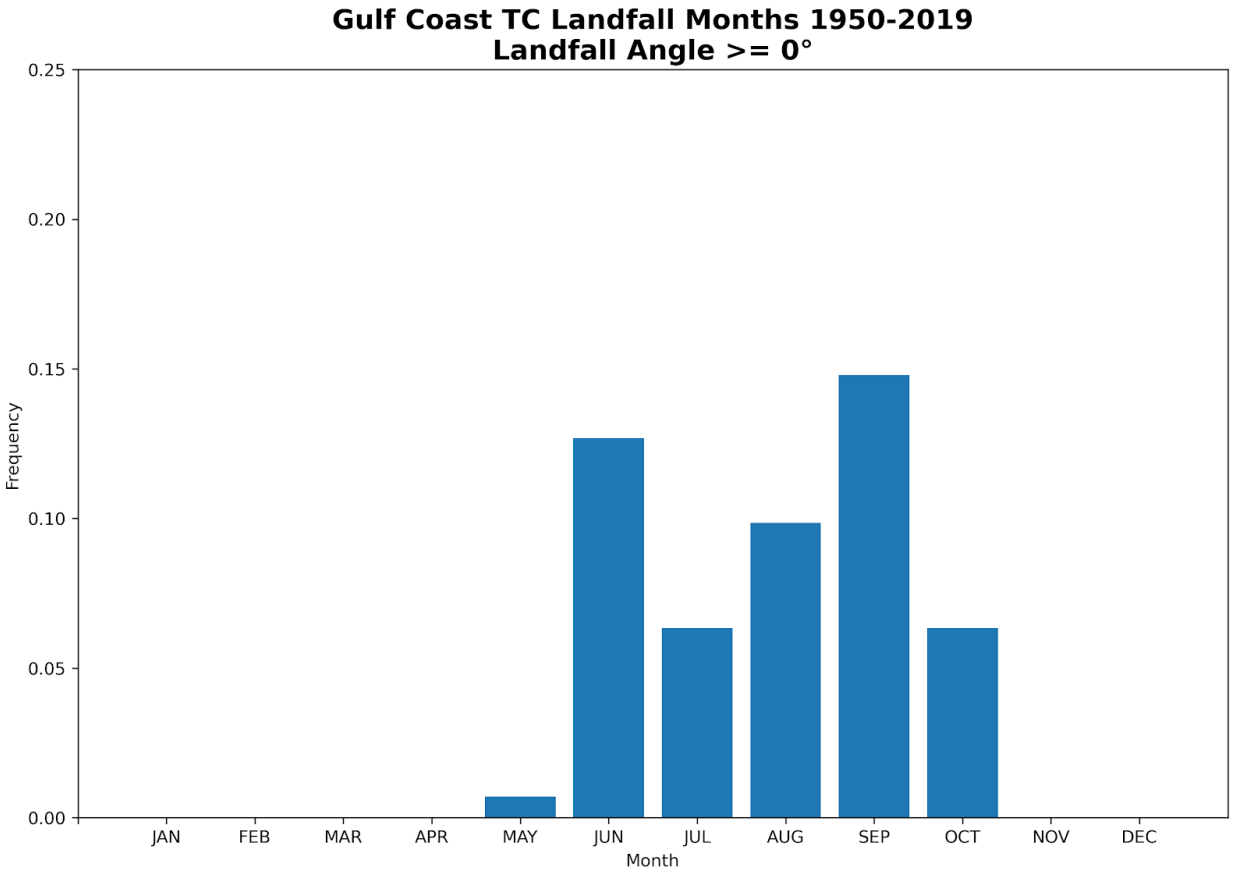

Figure 4.10: Gulf Coast TC landfall frequencies by month of the year for TCs with landfall angles greater than or equal to the mean (0°).

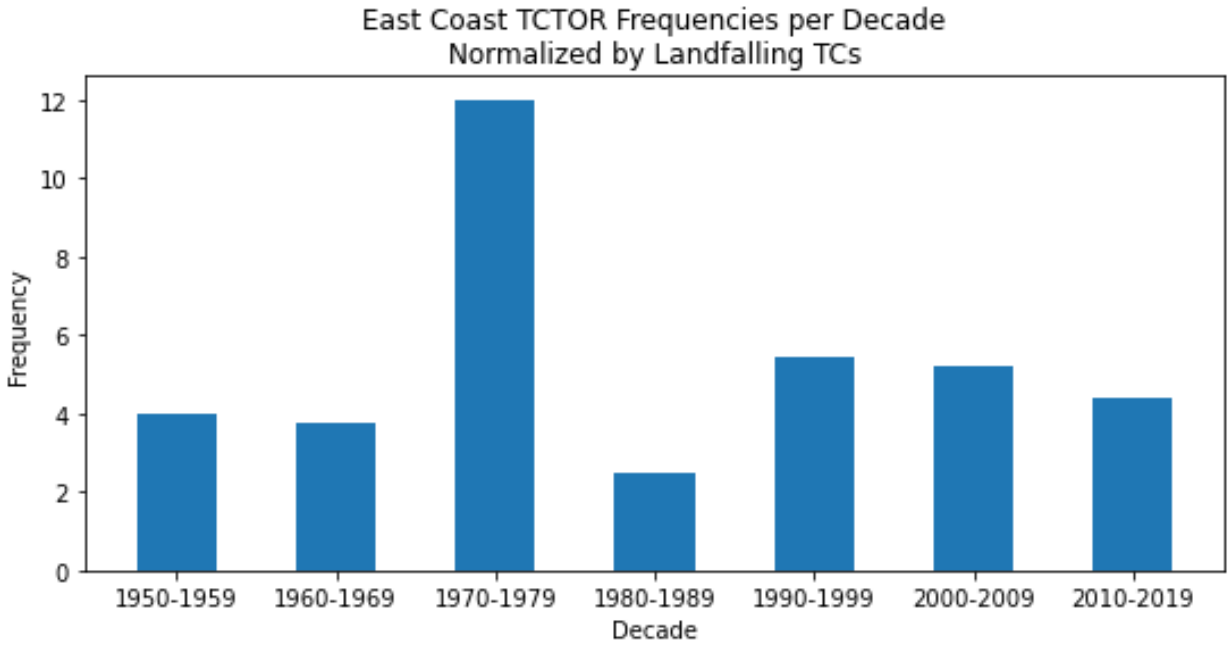

Figure 4.11: Histogram displaying the frequency of East coast TCTORs by decade, normalized by landfalling East coast TCs.

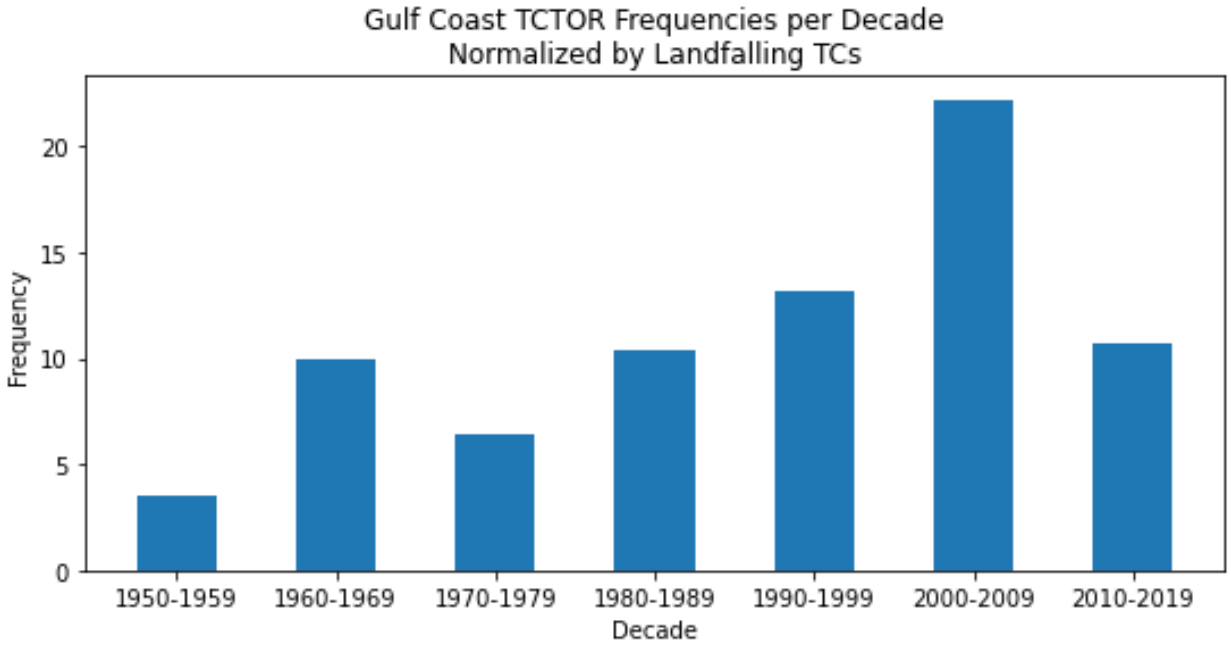

Figure 4.12: Histogram displaying the frequency of Gulf coast TCTORs by decade, normalized by landfalling Gulf coast TCs.

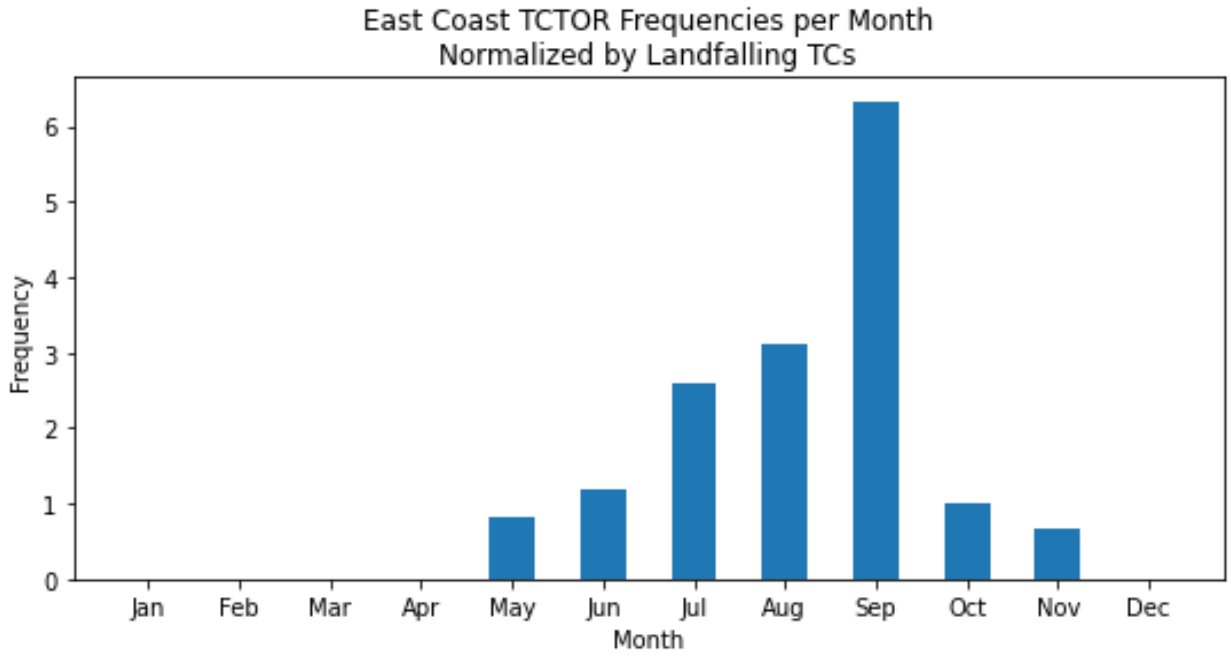

Figure 4.13: 1950-2019 East coast TCTOR frequencies by month of the year, normalized by East coast landfalling TCs.

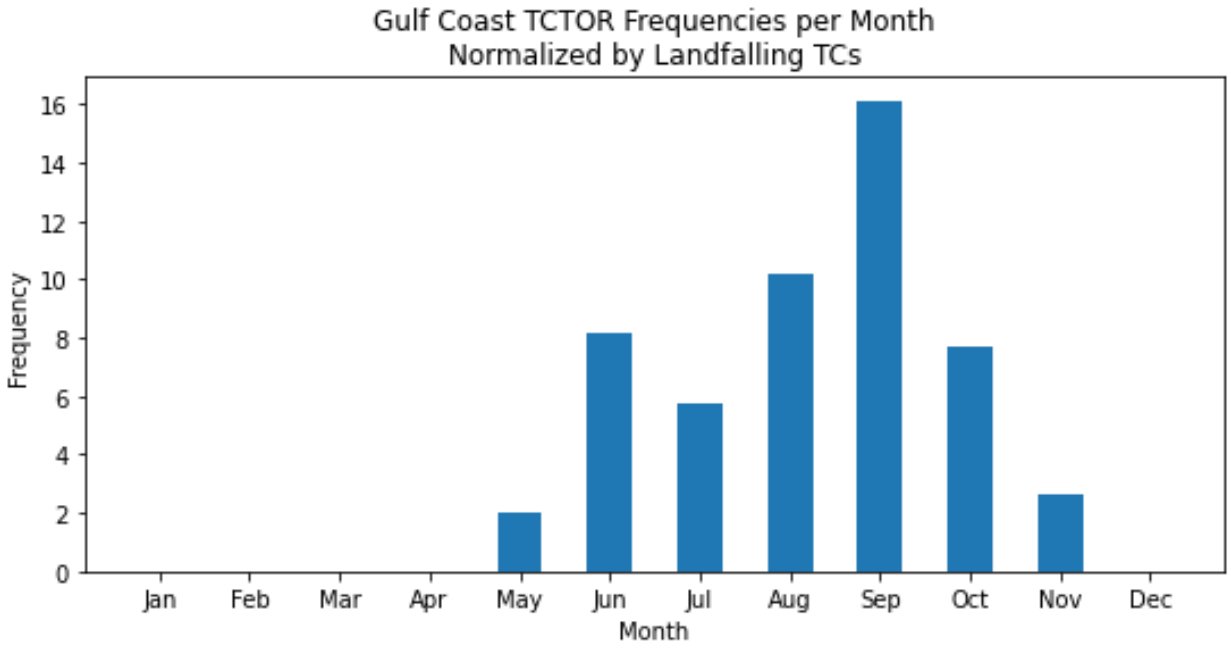

Figure 4.14: 1950-2019 Gulf coast TCTOR frequencies by month of the year, normalized by Gulf coast landfalling TCs.

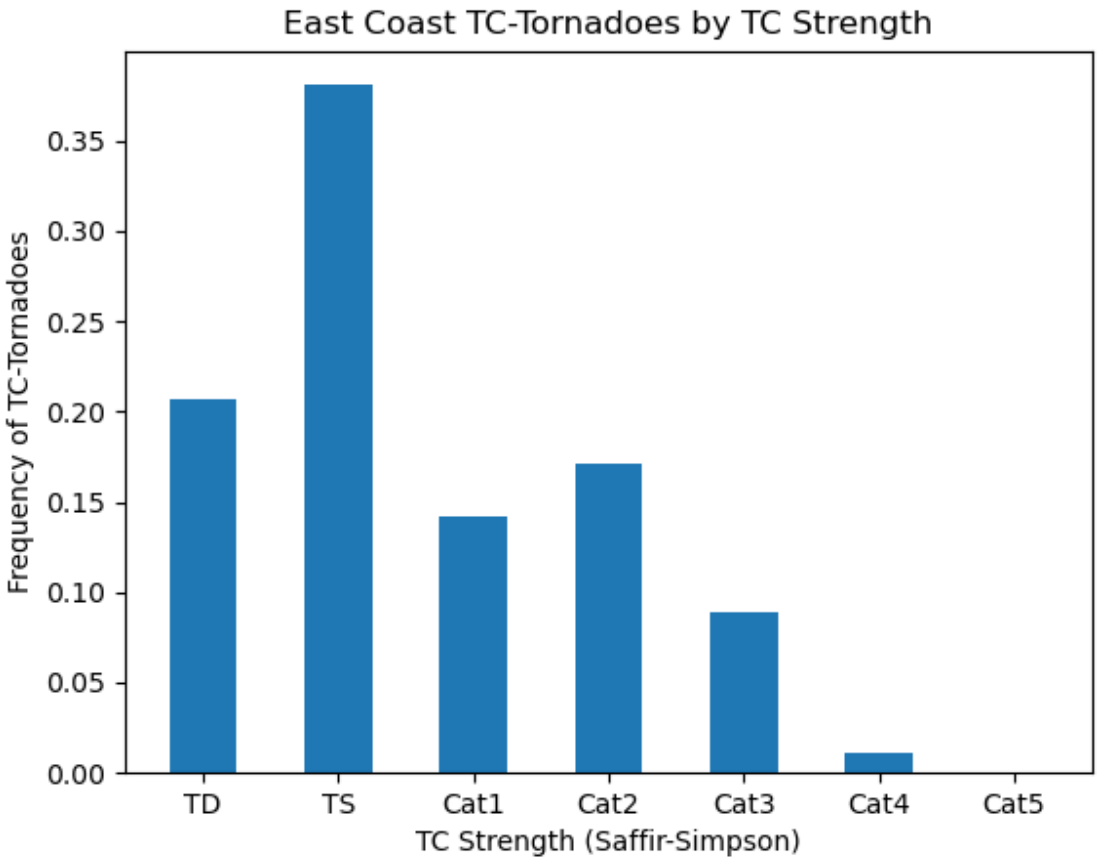

Figure 4.15: Histogram displaying the frequency of East coast TCTORs delineated by TC intensity using the Saffir-Simpson scale.

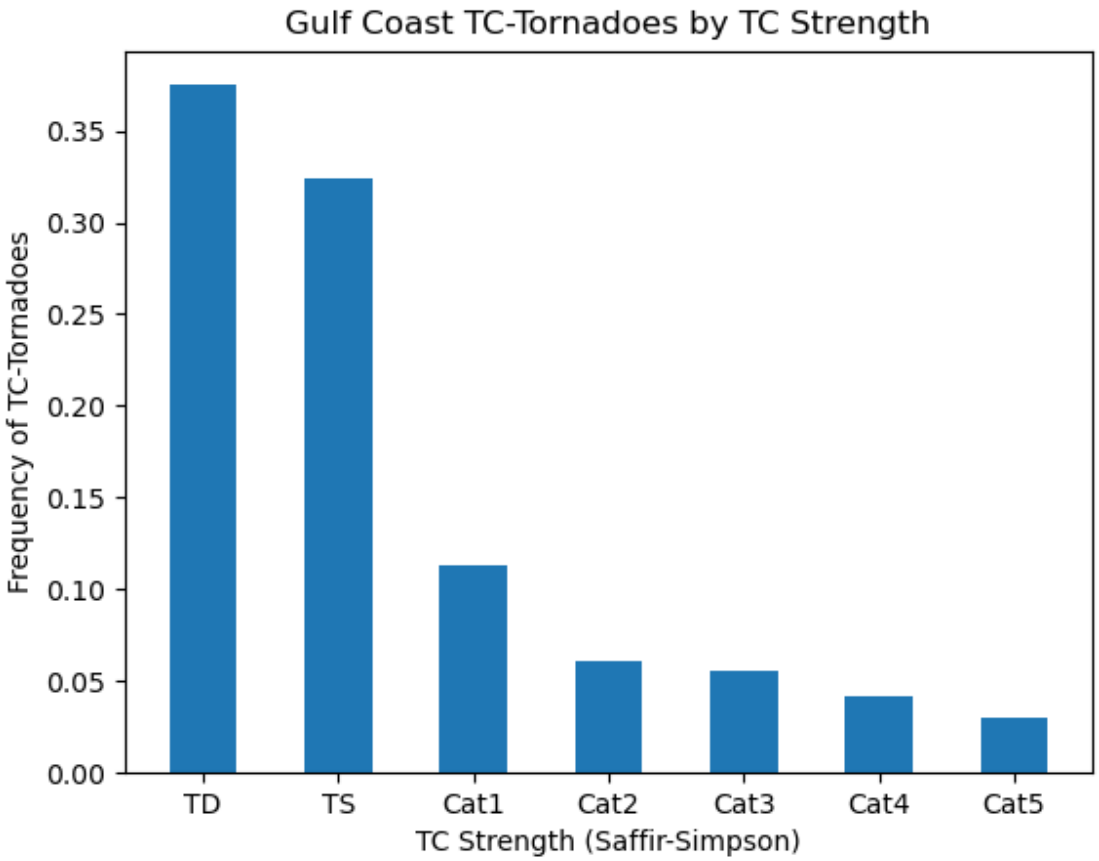

Figure 4.16: Histogram displaying the frequency of Gulf coast TCTORs delineated by TC intensity using the Saffir-Simpson scale.

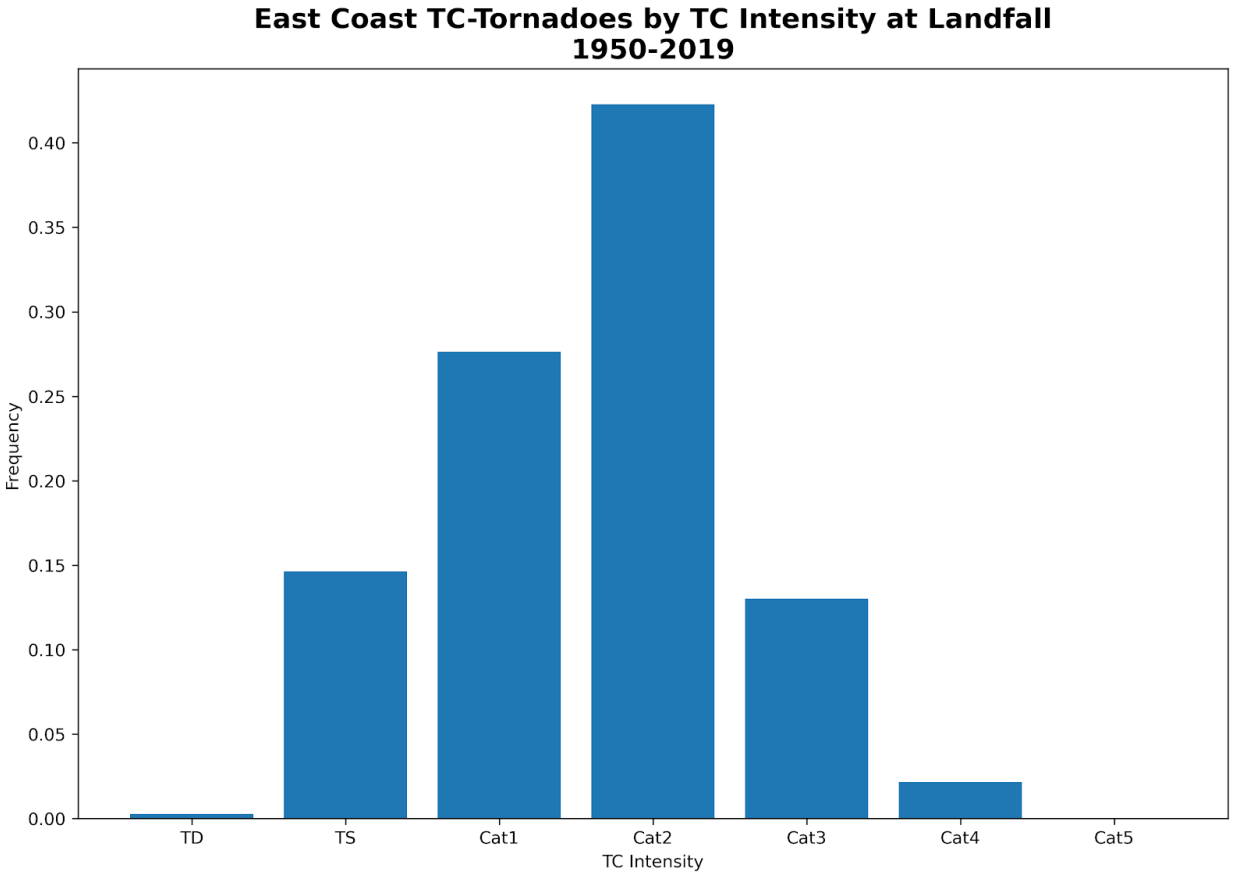

Figure 4.17: Histogram displaying the frequency of East coast TCTORs delineated by TC intensity at landfall using the Saffir-Simpson scale.

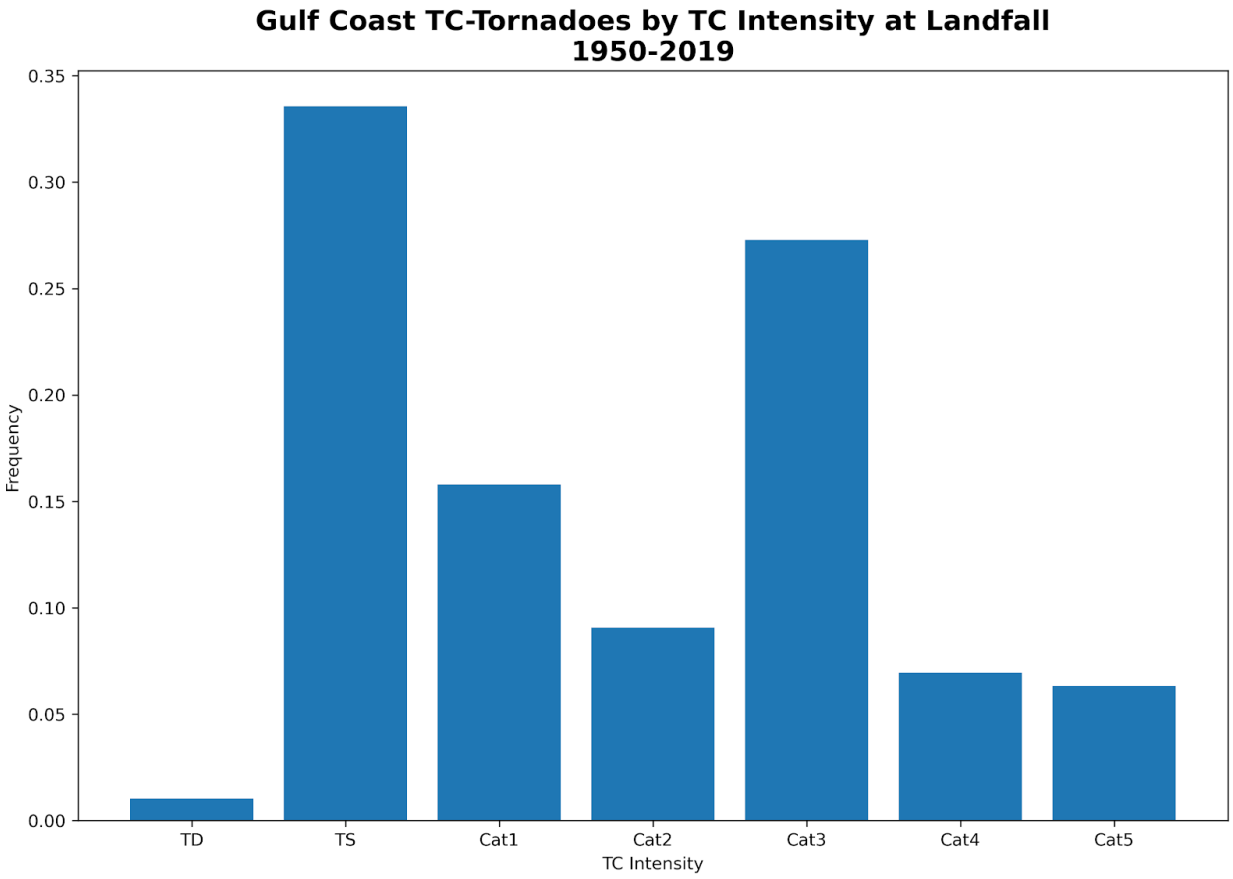

Figure 4.18: Histogram displaying the frequency of Gulf coast TCTORs delineated by TC intensity at landfall using the Saffir-Simpson scale.

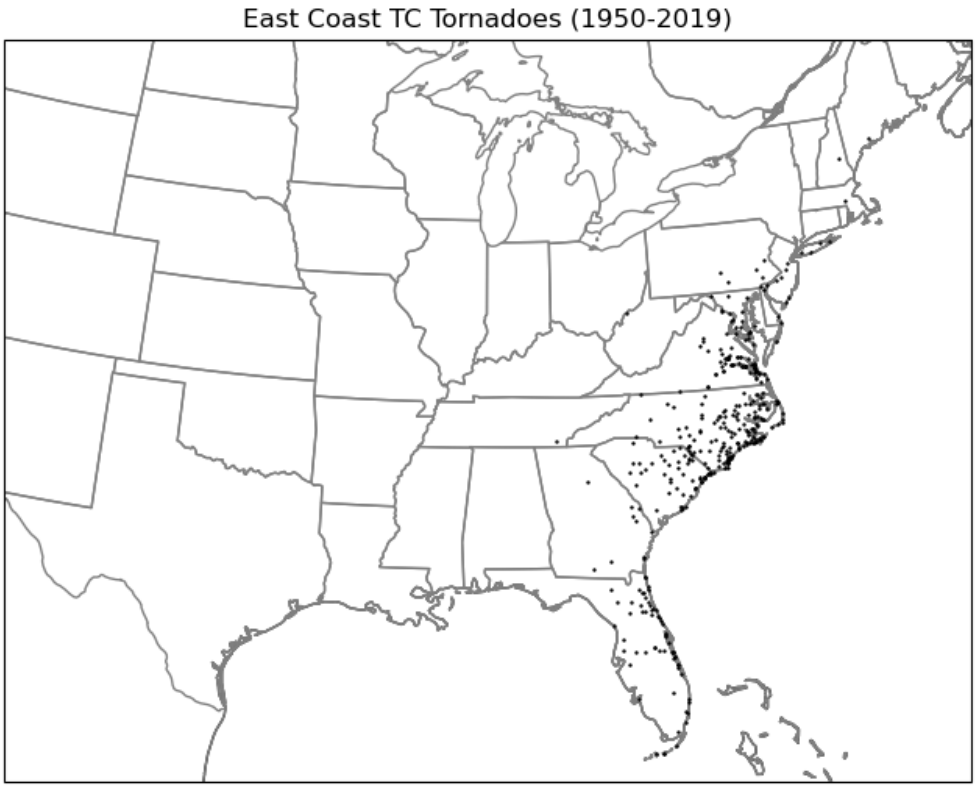

Figure 4.19: Map showing all East coast TCTOR initiation locations (black dots) between the years 1950-2019.

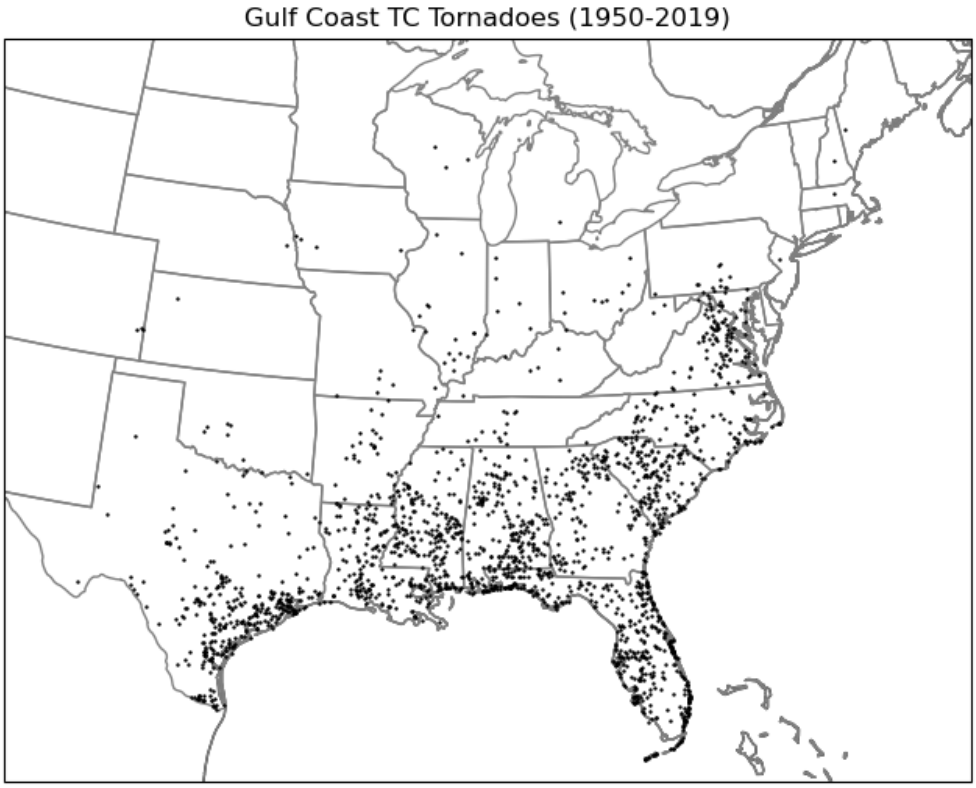

Figure 4.20: Map showing all Gulf coast TCTOR initiation locations (black dots) between the years 1950-2019.

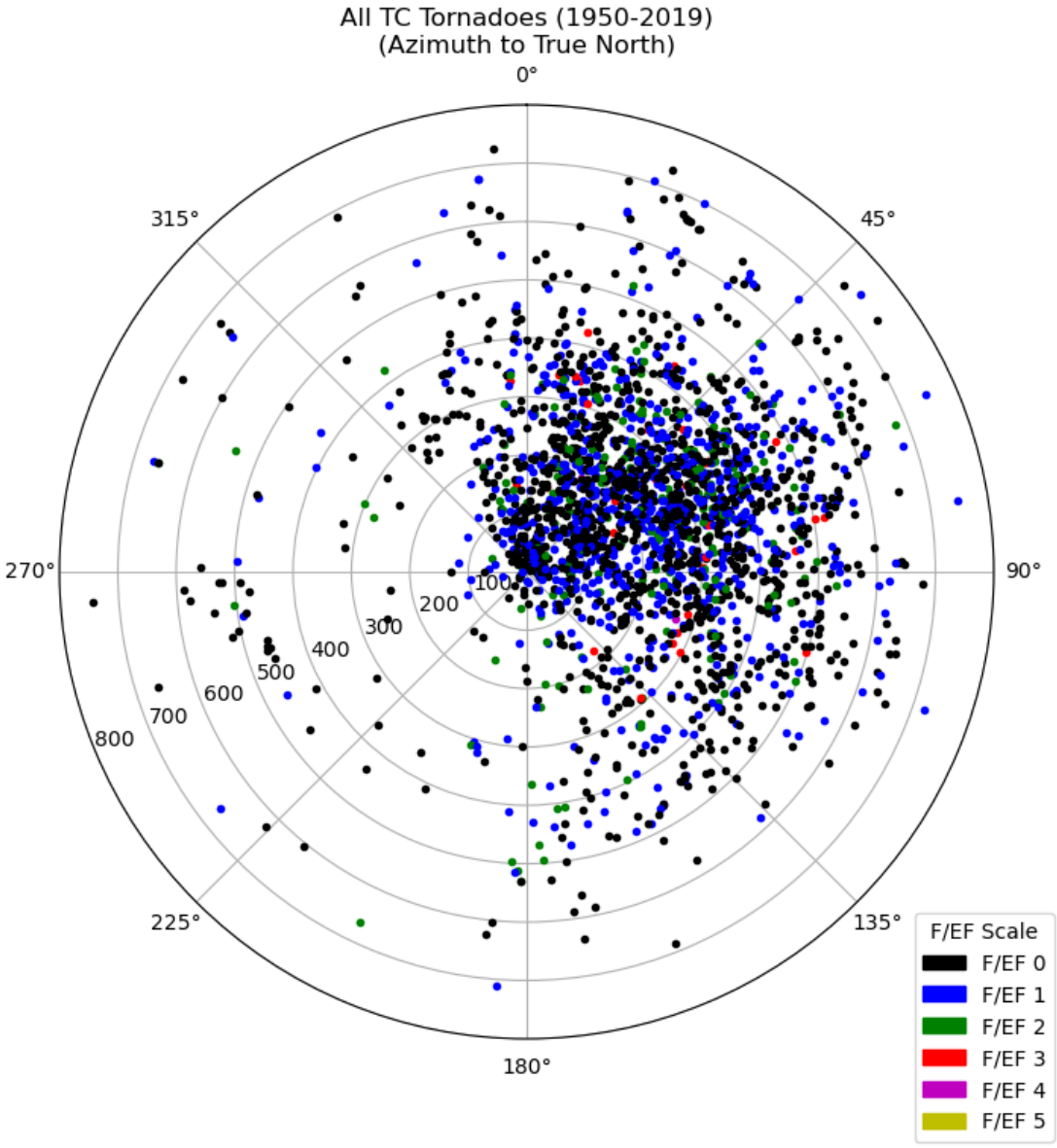

Figure 4.21: All TCTOR initiation locations between the years 1950-2019 in an earth-relative framework with TC center at the center of the plot. Range rings are in 100-km increments. Color denotes TCTOR intensity using the F/EF-scale.

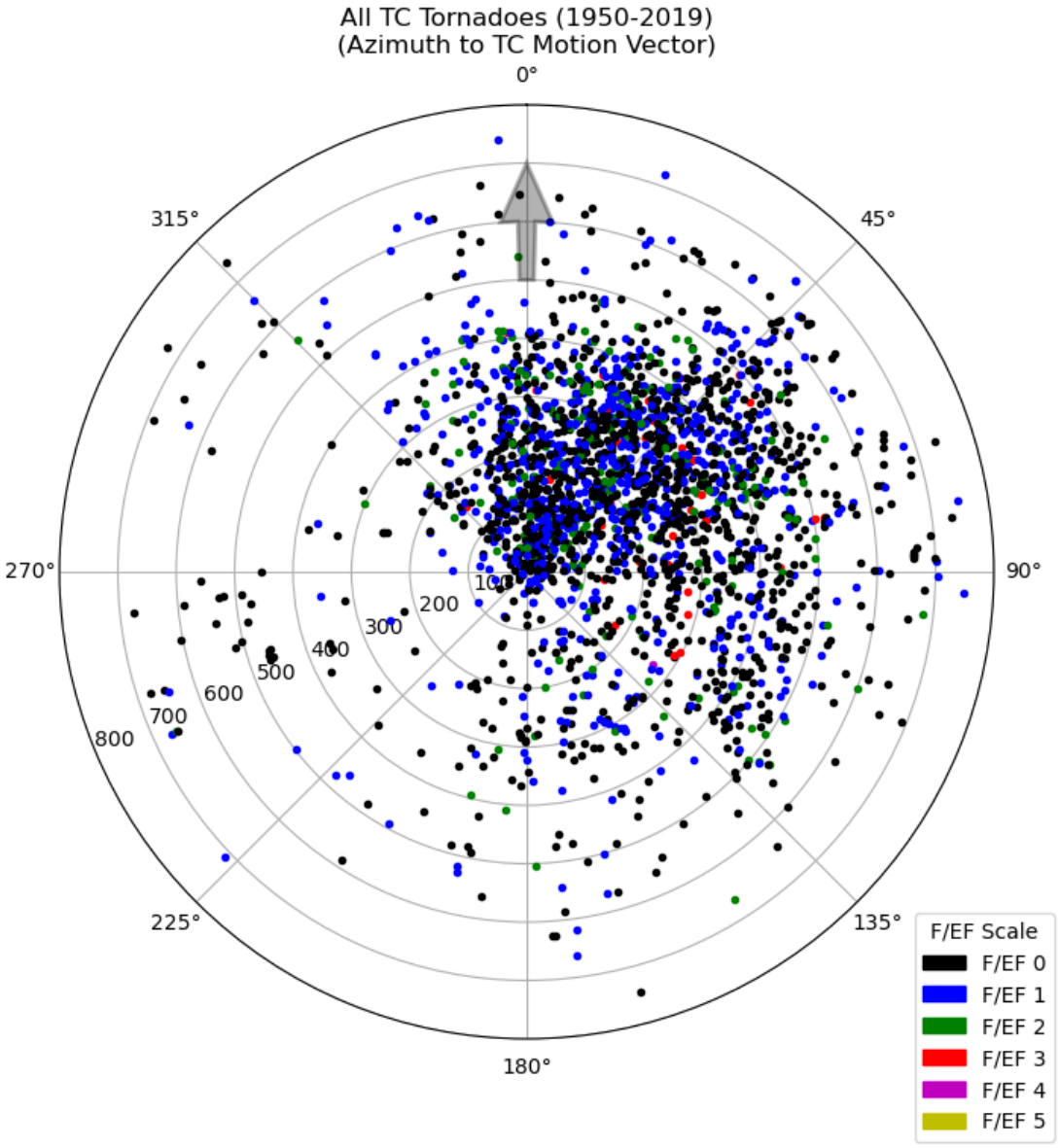

Figure 4.22: All TCTOR initiation locations between the years 1950-2019 in a TC motion-relative framework with TC center at the center of the plot. TC motion denoted by gray arrow at 0°. Range rings are in 100-km increments. Color denotes TCTOR intensity using the F/EF-scale.

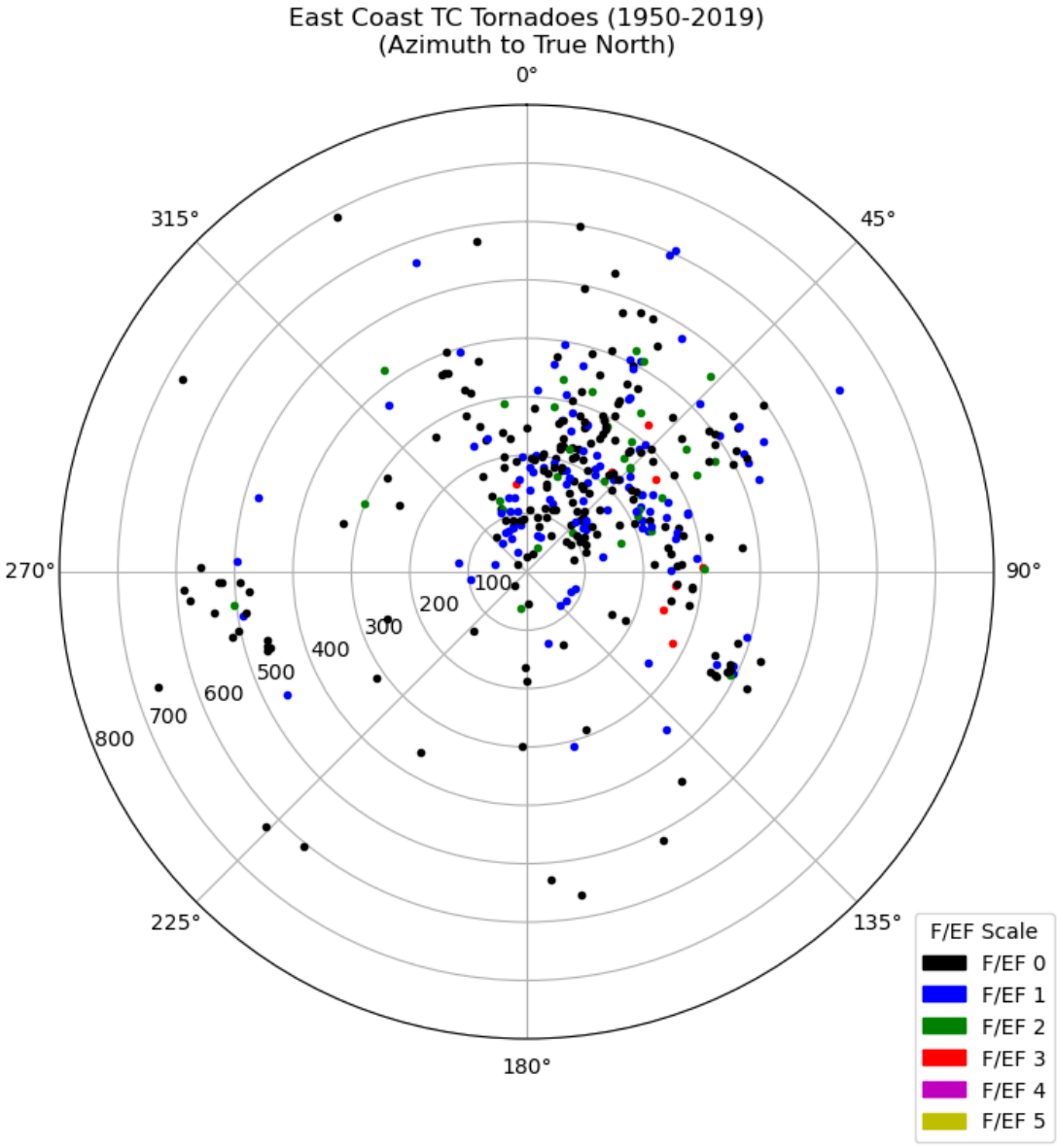

Figure 4.23: All East coast TCTOR initiation locations between the years 1950-2019 in an earth-relative framework with TC center at the center of the plot. Range rings are in 100-km increments. Color denotes TCTOR intensity using the F/EF-scale.

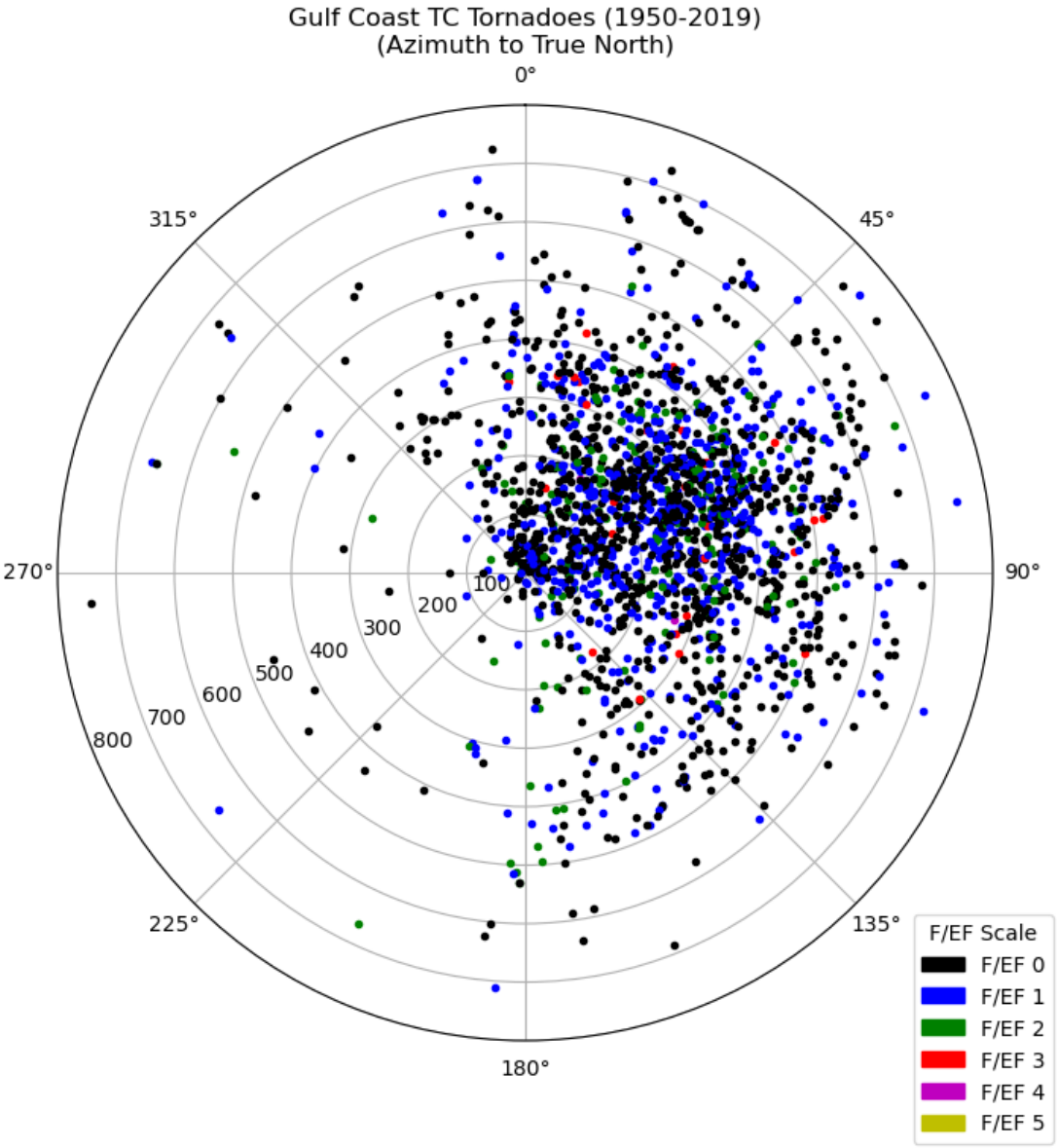

Figure 4.24: All Gulf Coast TCTOR initiation locations between the years 1950-2019 in an earth-relative framework with TC center at the center of the plot. Range rings are in 100-km increments. Color denotes TCTOR intensity using the F/EF-scale.

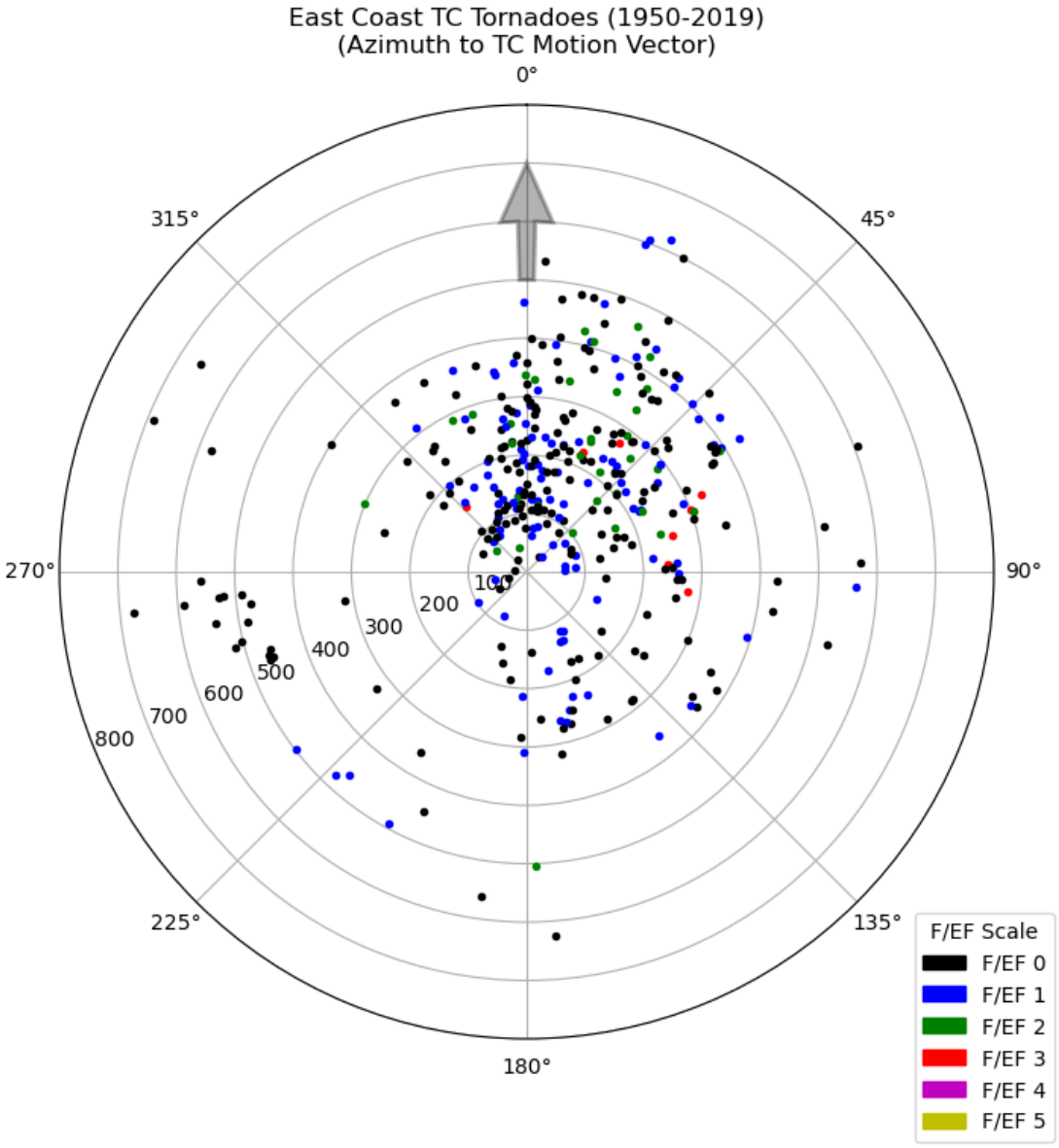

Figure 4.25: All East coast TCTOR initiation locations between the years 1950-2019 in a TC motion-relative framework with TC center at the center of the plot. TC motion denoted by gray arrow at 0°. Range rings are in 100-km increments. Color denotes TCTOR intensity using the F/EF-scale.

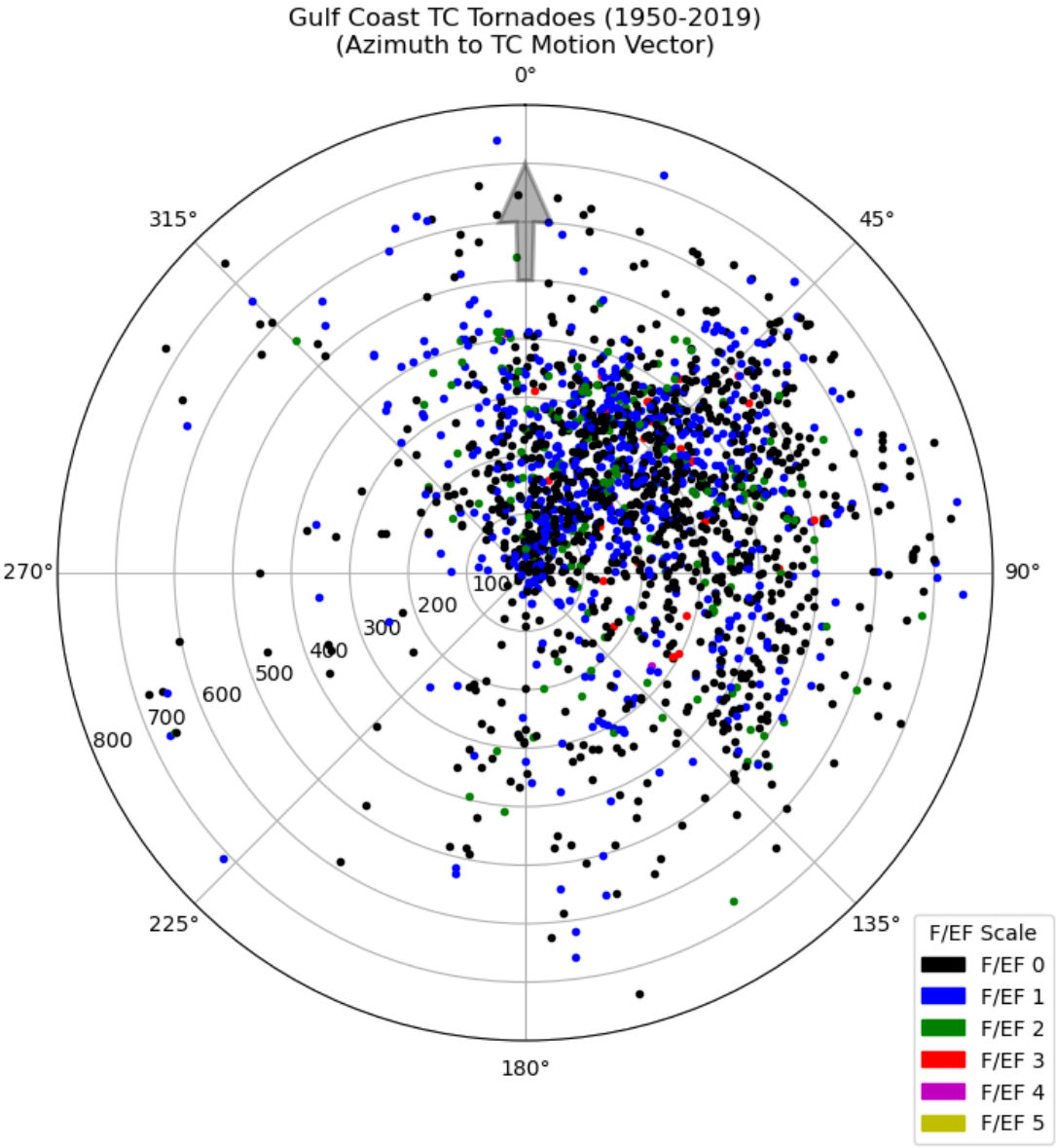

Figure 4.26: All Gulf coast TCTOR initiation locations between the years 1950-2019 in a TC motion-relative framework with TC center at the center of the plot. TC motion denoted by gray arrow at 0°. Range rings are in 100-km increments. Color denotes TCTOR intensity using the F/EF-scale.

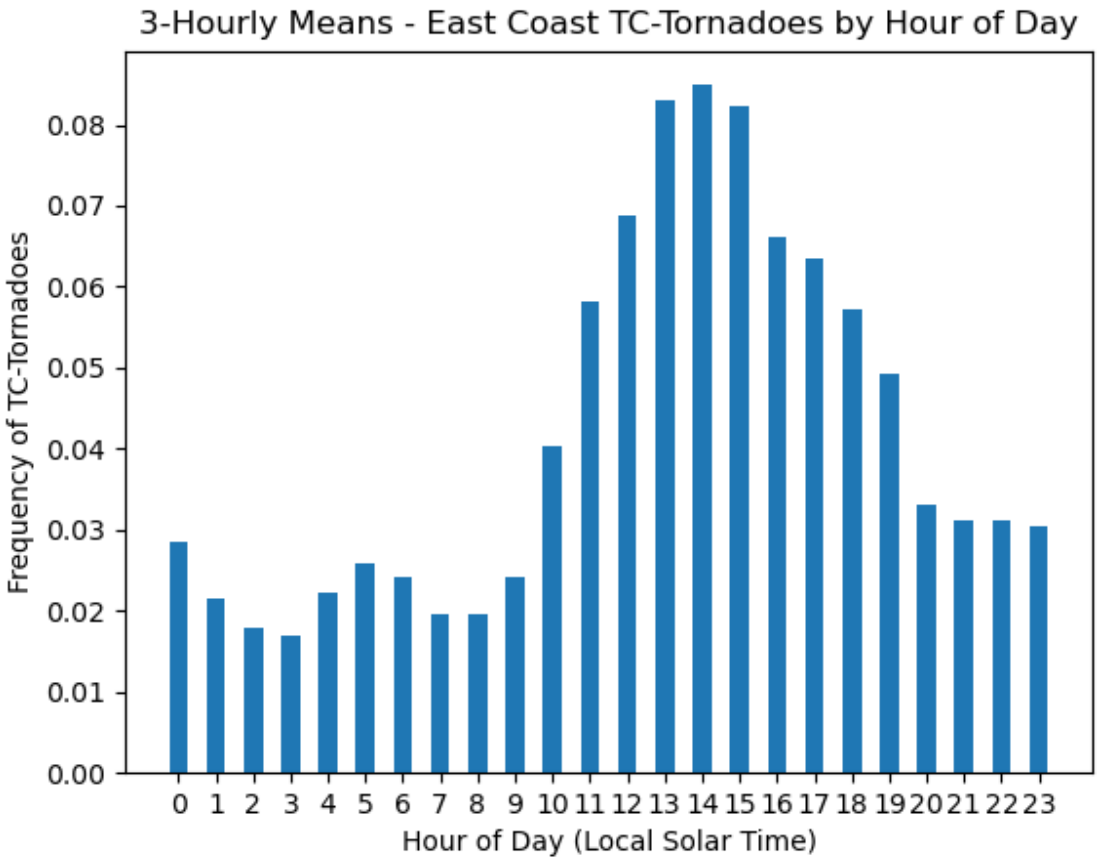

Figure 4.27: Histogram of East coast TCTOR frequency by hour of day using local solar time (LST). Hourly bins are calculated using a 3-hourly mean centered on the hour of interest.

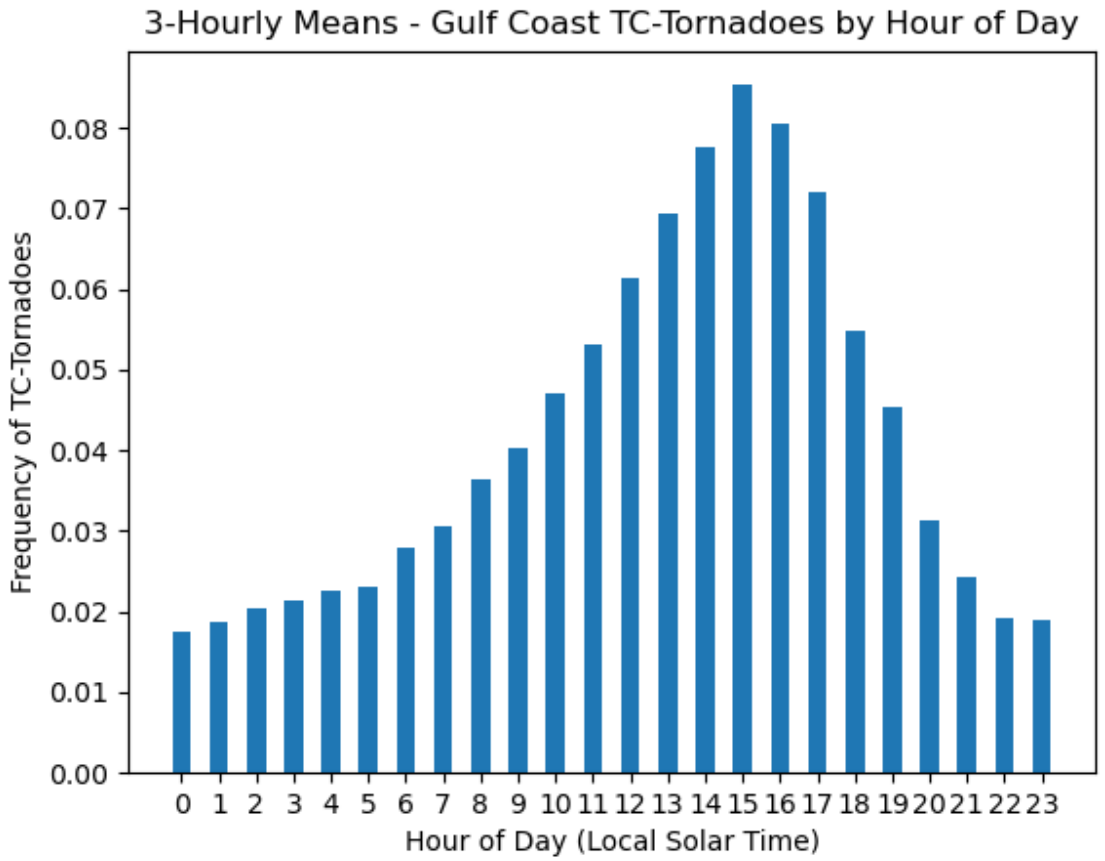

Figure 4.28: Histogram of Gulf coast TCTOR frequency by hour of day using local solar time (LST). Hourly bins are calculated using a 3-hourly mean centered on the hour of interest.

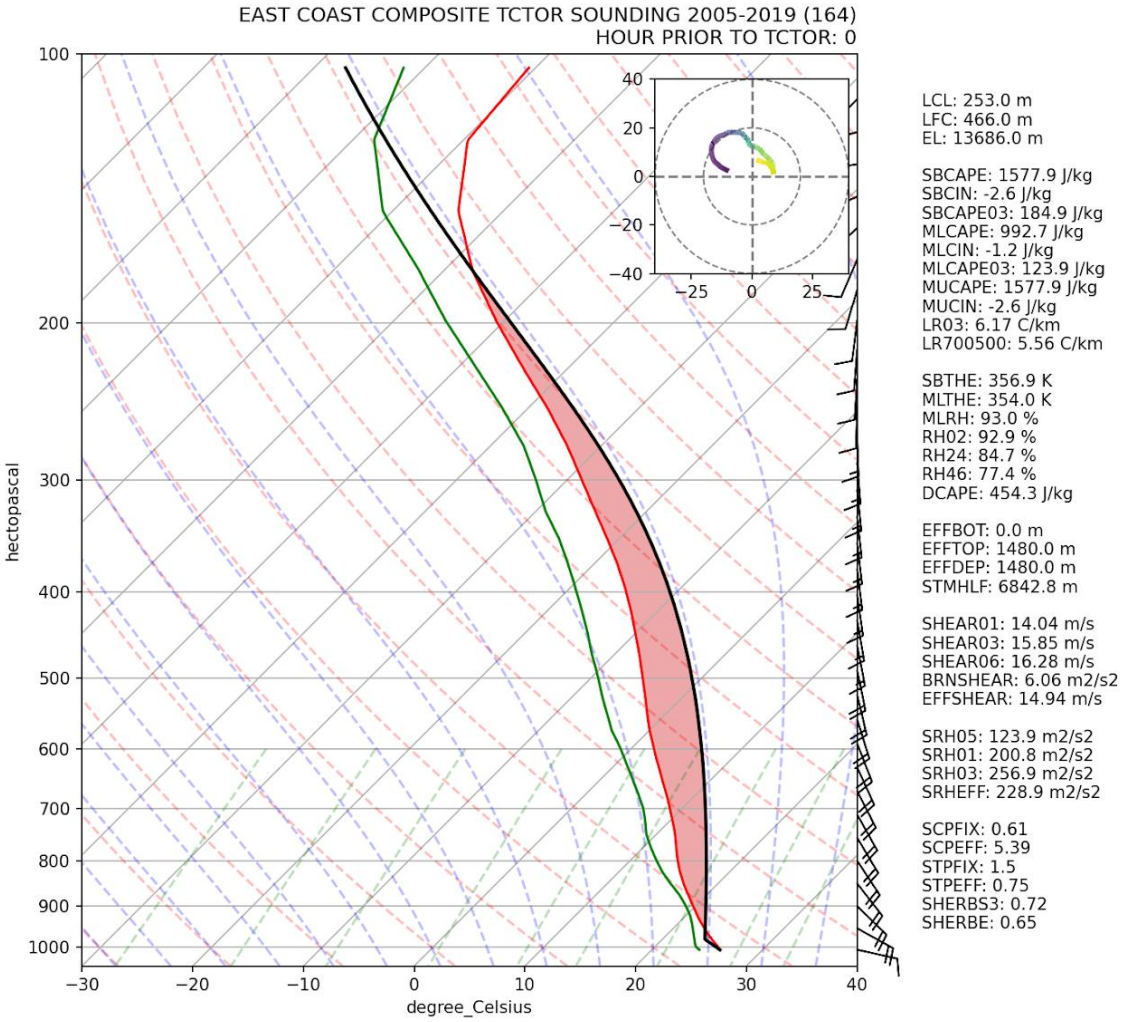

Figure 4.29: 2005-2019 East Coast composite TCTOR sounding and associated convective metrics at the hour of the TCTOR.

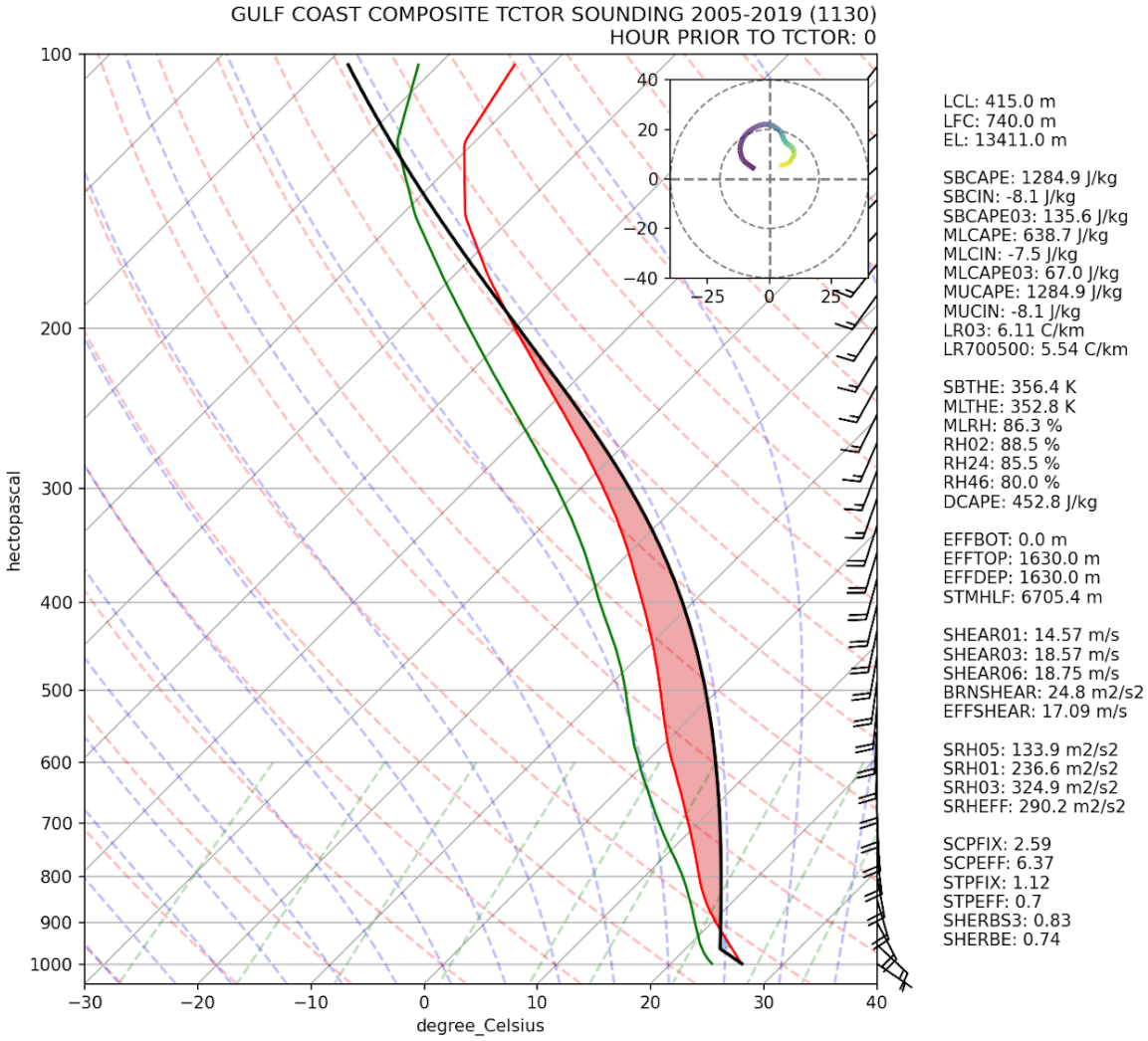

Figure 4.30: 2005-2019 Gulf Coast composite TCTOR sounding and associated convective metrics at the hour of the TCTOR.

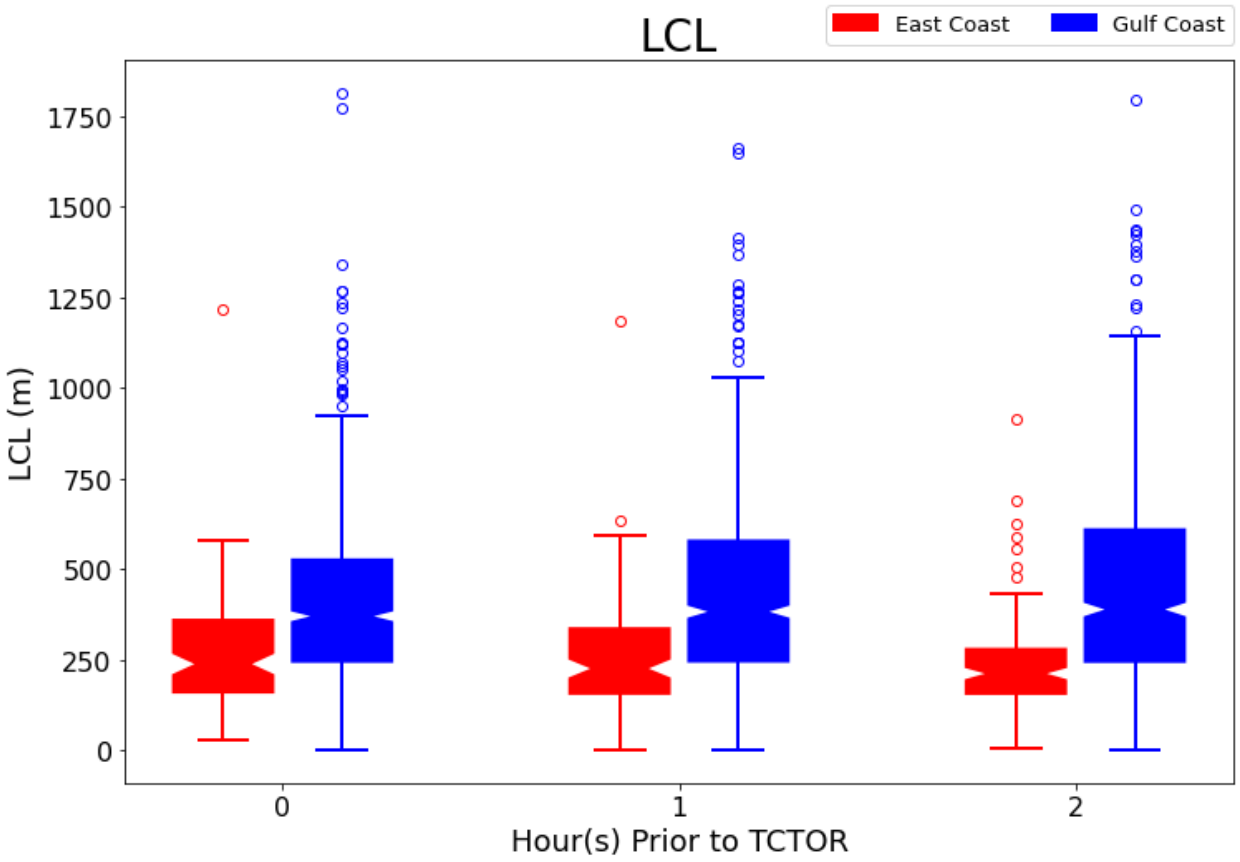

Figure 4.31: Lifted Condensation Level heights box and whisker plots for the East (red) and Gulf (blue) coast TCTOR events separated by hour of analysis prior to TCTOR.

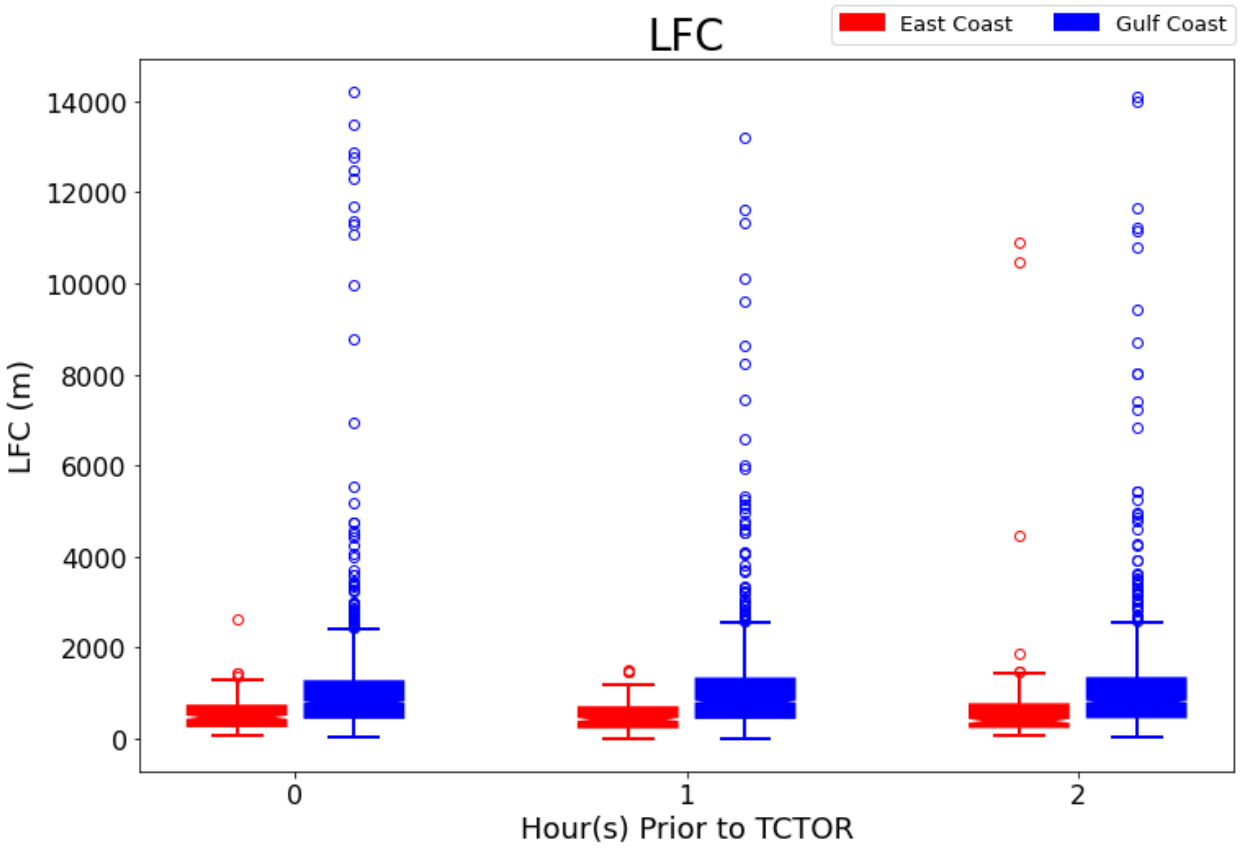

Figure 4.32: Level of Free Convection heights box and whisker plots for the East (red) and Gulf (blue) coast TCTOR events separated by hour of analysis prior to TCTOR.

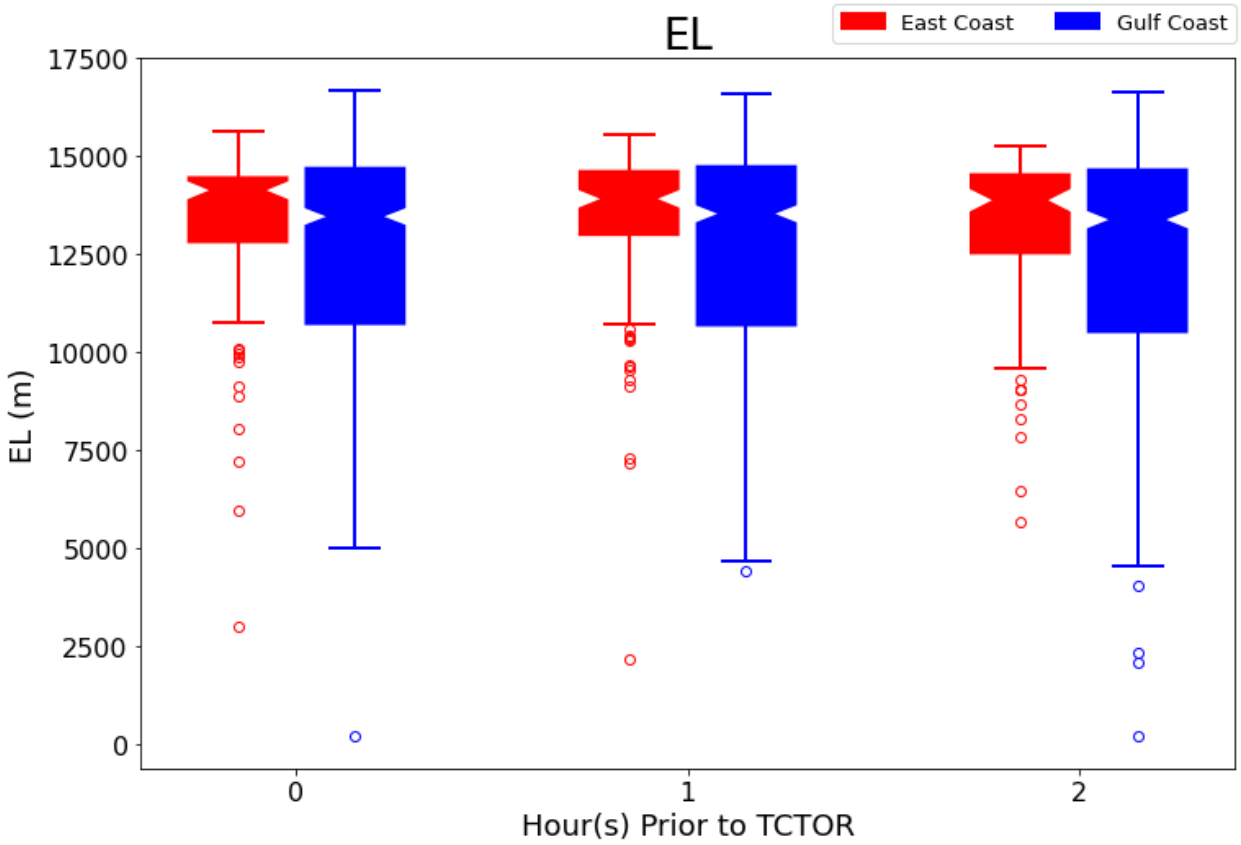

Figure 4.33: Equilibrium Level heights box and whisker plots for the East (red) and Gulf (blue) coast TCTOR events separated by hour of analysis prior to TCTOR.

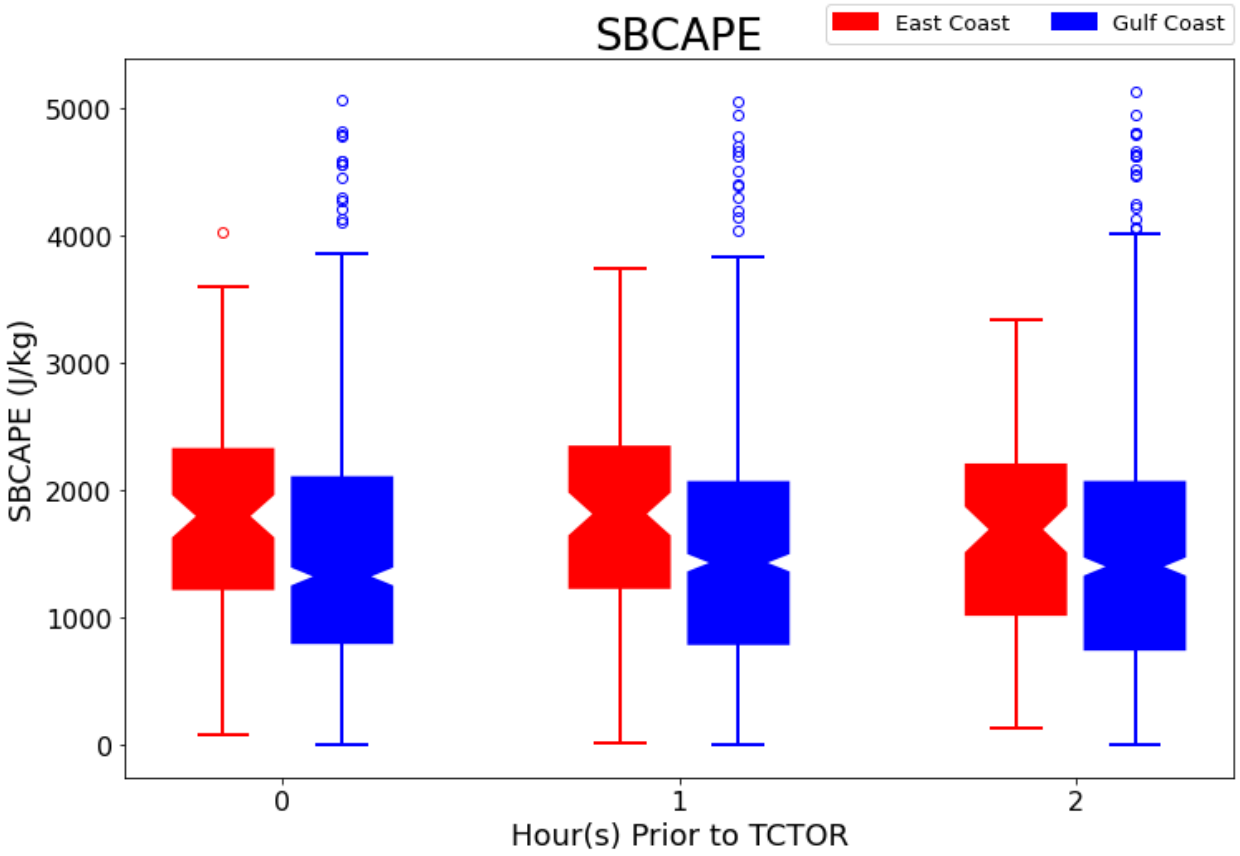

Figure 4.34: Surface-Based CAPE box and whisker plots for the East (red) and Gulf (blue) coast TCTOR events separated by hour of analysis prior to TCTOR.

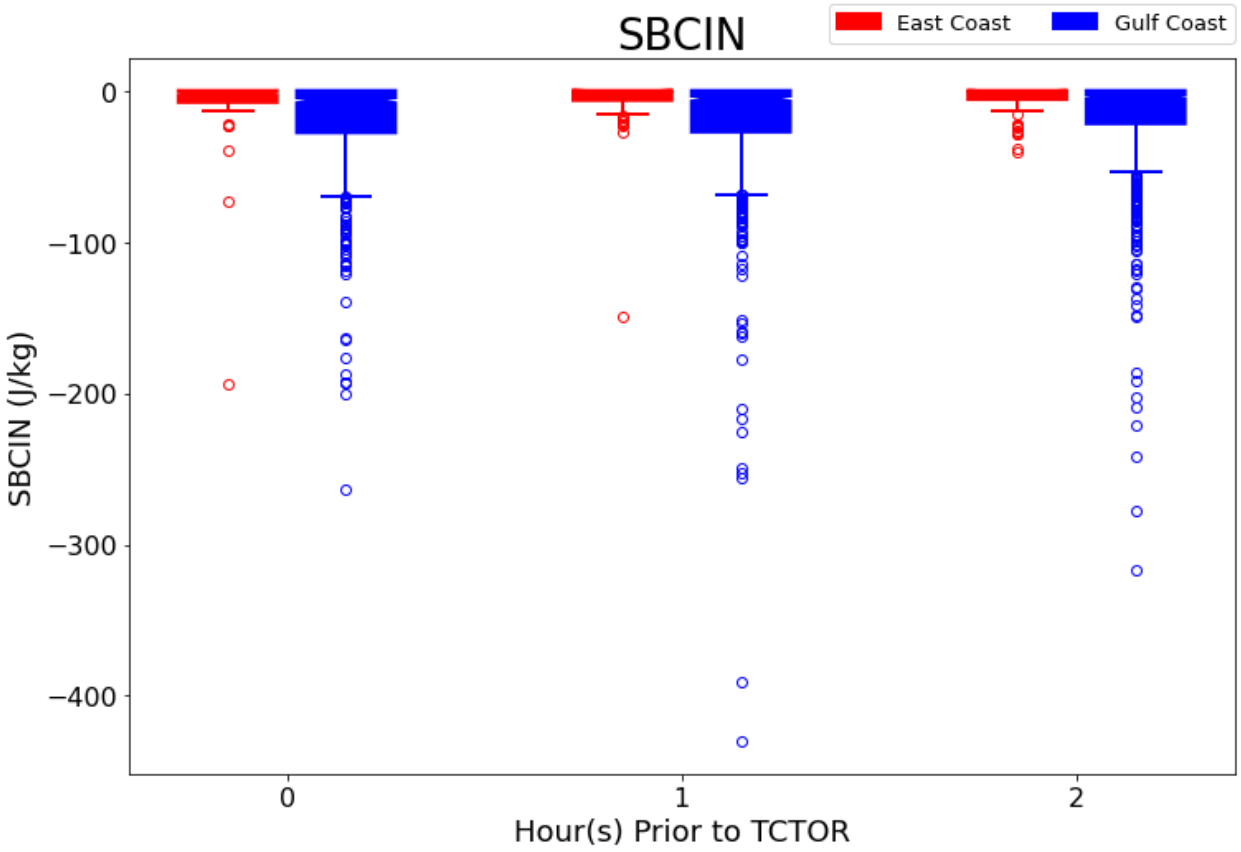

Figure 4.35: Surface-Based CIN box and whisker plots for the East (red) and Gulf (blue) coast TCTOR events separated by hour of analysis prior to TCTOR.

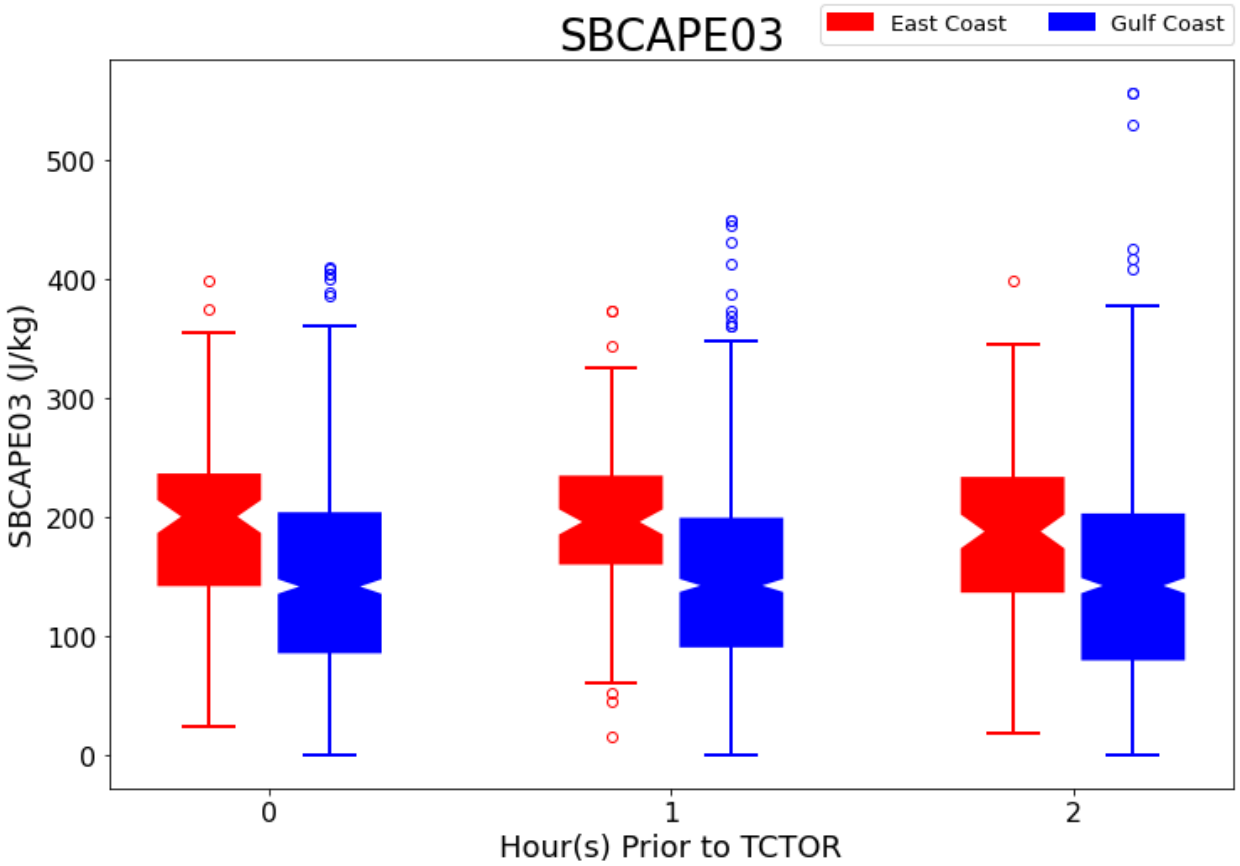

Figure 4.36: 0-3 km Surface-Based CAPE box and whisker plots for the East (red) and Gulf (blue) coast TCTOR events separated by hour of analysis prior to TCTOR.

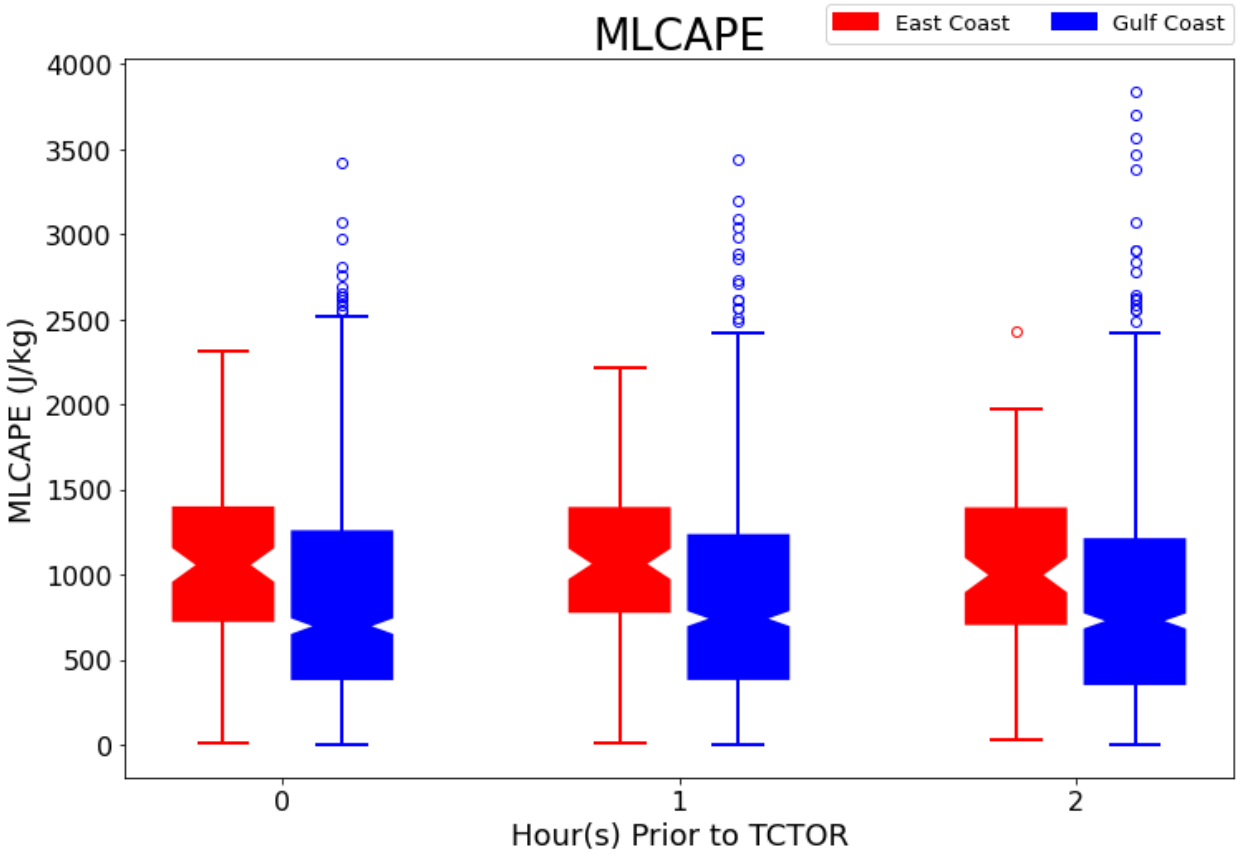

Figure 4.37: Mean Mixed-Layer CAPE box and whisker plots for the East (red) and Gulf (blue) coast TCTOR events separated by hour of analysis prior to TCTOR.

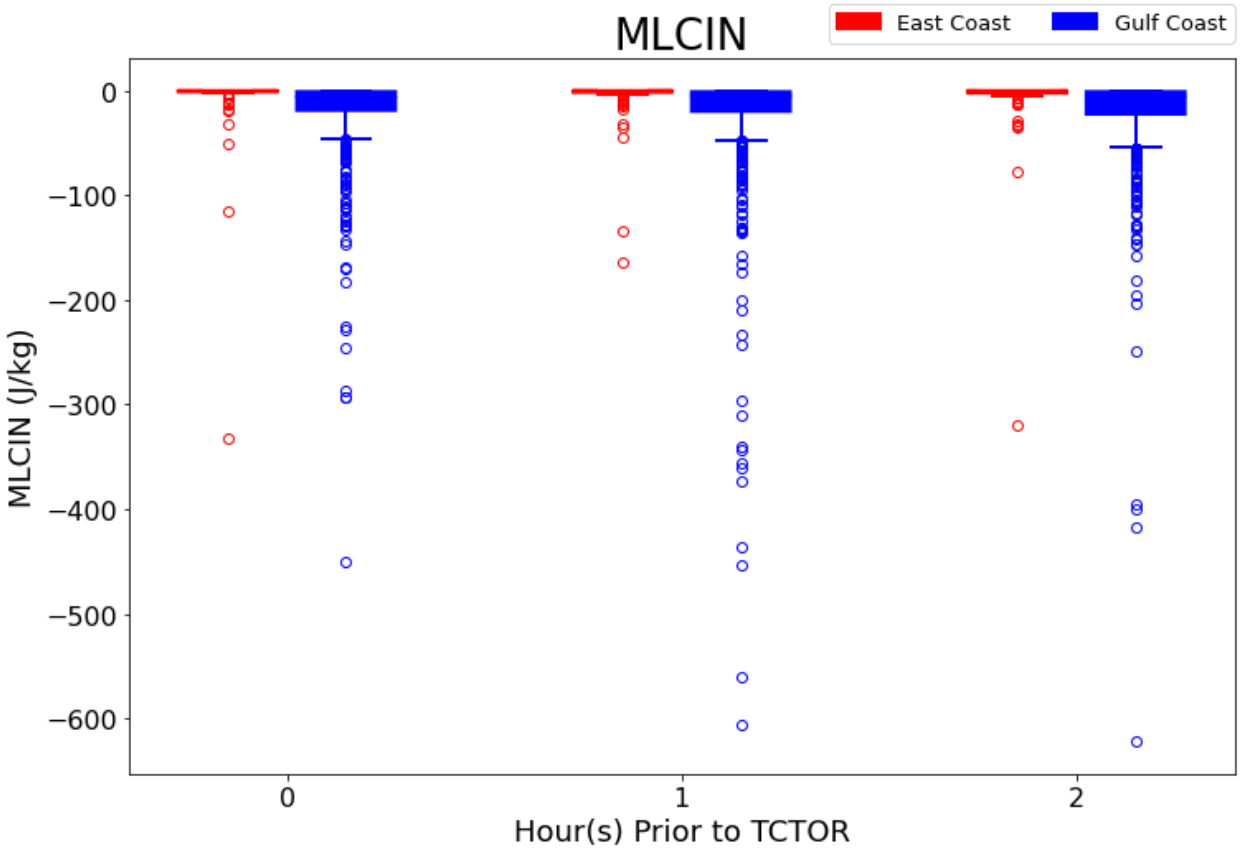

Figure 4.38: Mean Mixed-Layer CIN box and whisker plots for the East (red) and Gulf (blue) coast TCTOR events separated by hour of analysis prior to TCTOR.

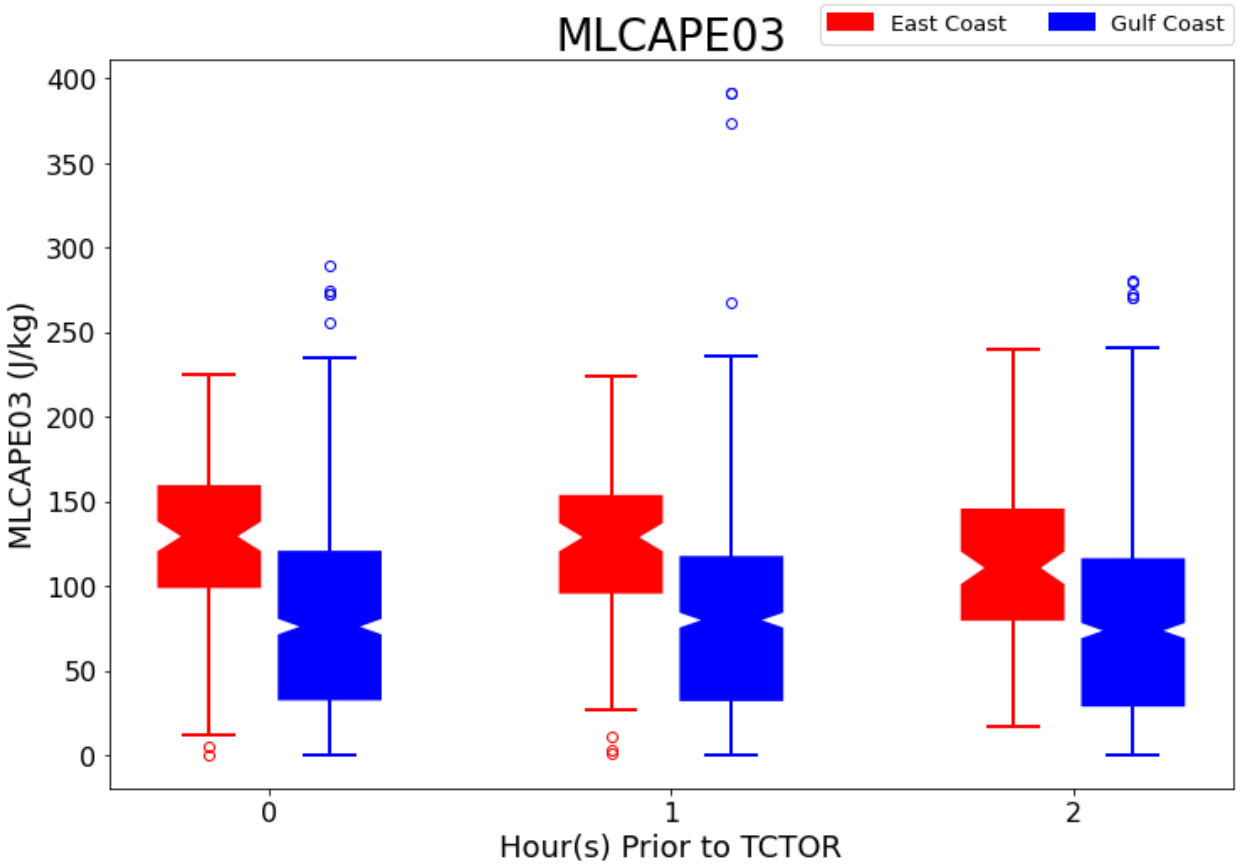

Figure 4.39: Mean Mixed-Layer 0-3 km CAPE box and whisker plots for the East (red) and Gulf (blue) coast TCTOR events separated by hour of analysis prior to TCTOR.

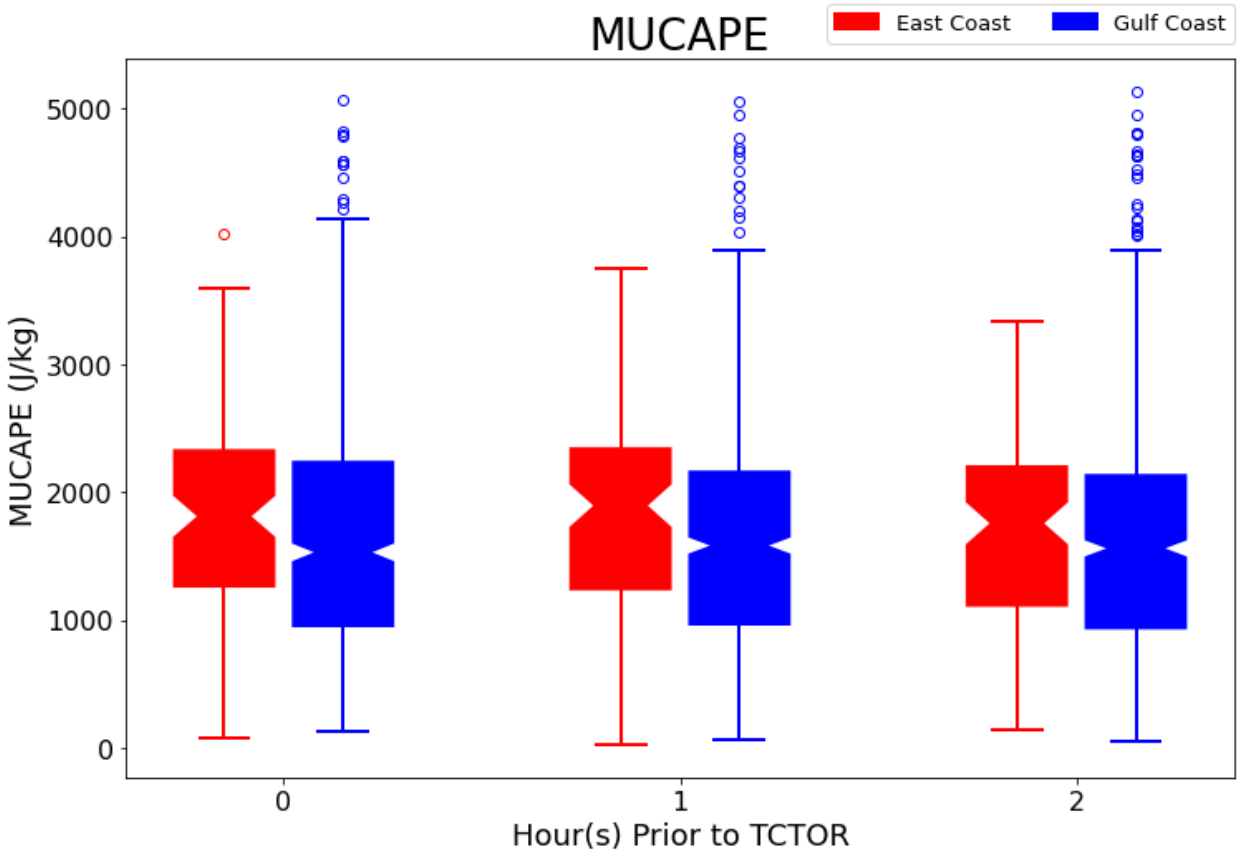

Figure 4.40: Most Unstable CAPE box and whisker plots for the East (red) and Gulf (blue) coast TCTOR events separated by hour of analysis prior to TCTOR.

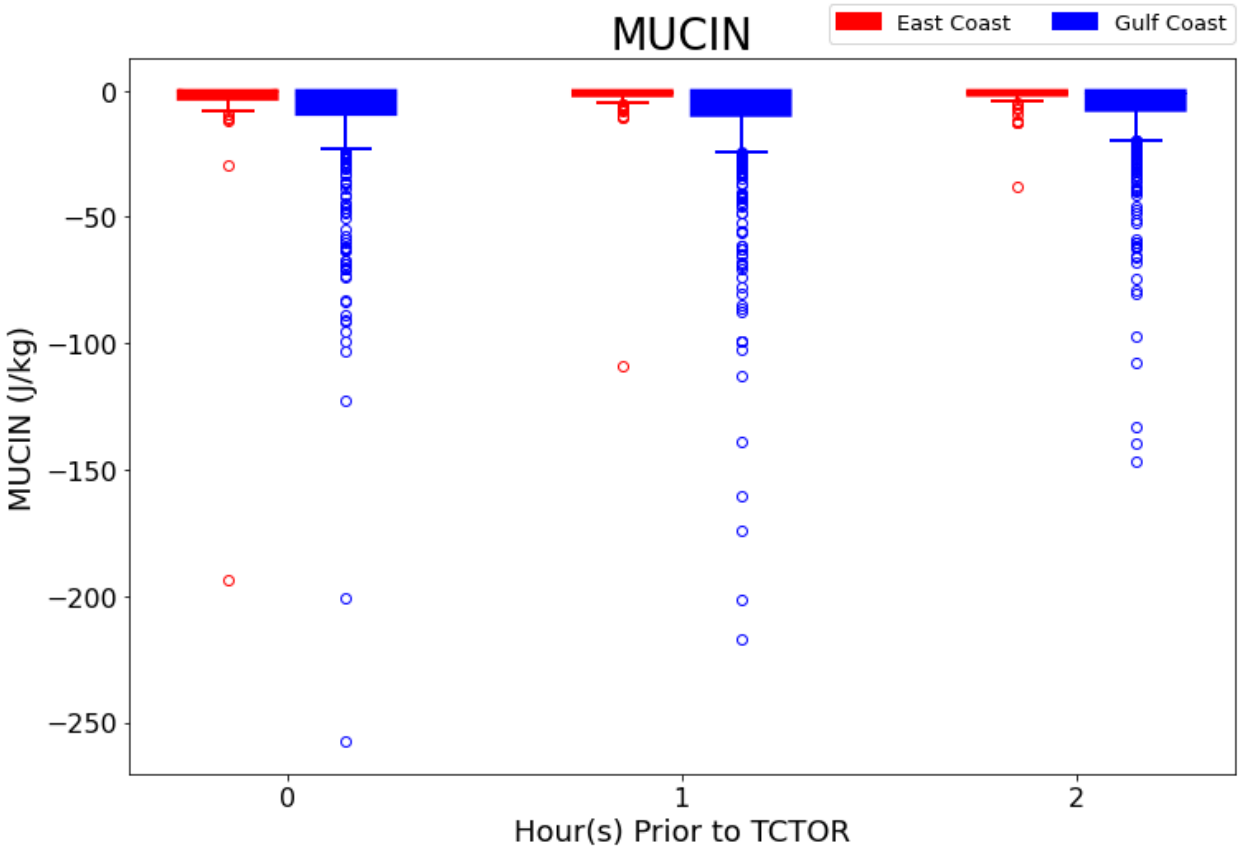

Figure 4.41: Most Unstable CIN box and whisker plots for the East (red) and Gulf (blue) coast TCTOR events separated by hour of analysis prior to TCTOR.

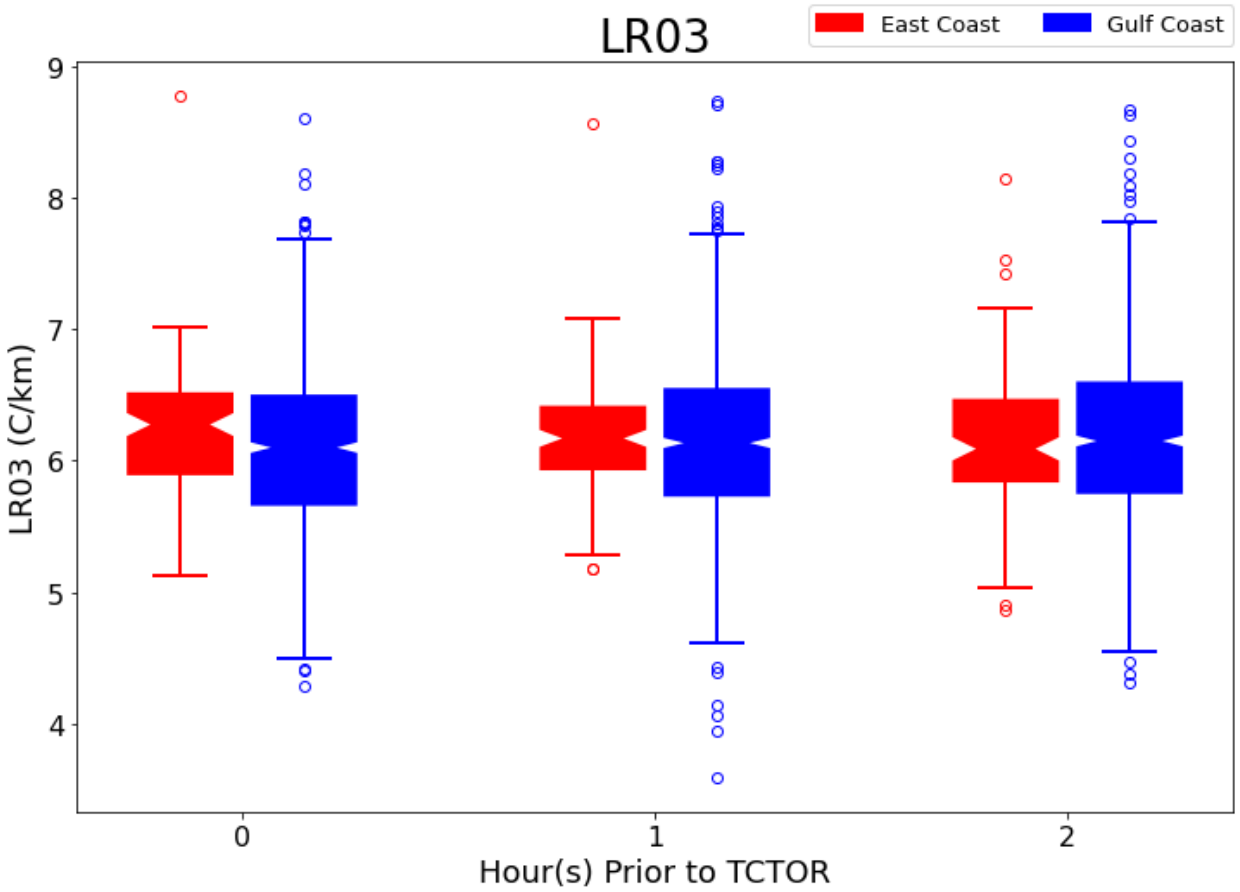

Figure 4.42: 0-3 km Lapse Rate box and whisker plots for the East (red) and Gulf (blue) coast TCTOR events separated by hour of analysis prior to TCTOR.

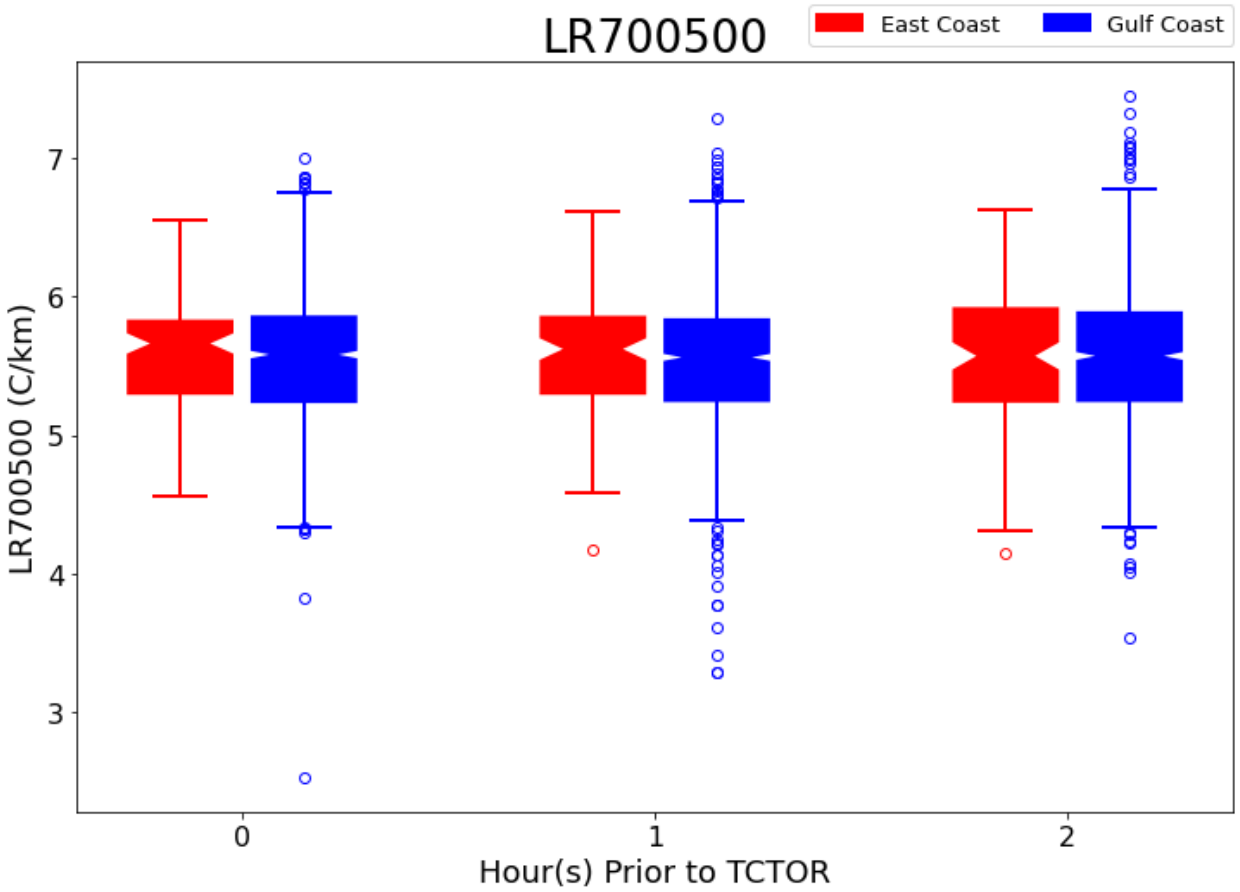

Figure 4.43: 700-500 mb Lapse Rate box and whisker plots for the East (red) and Gulf (blue) coast TCTOR events separated by hour of analysis prior to TCTOR.

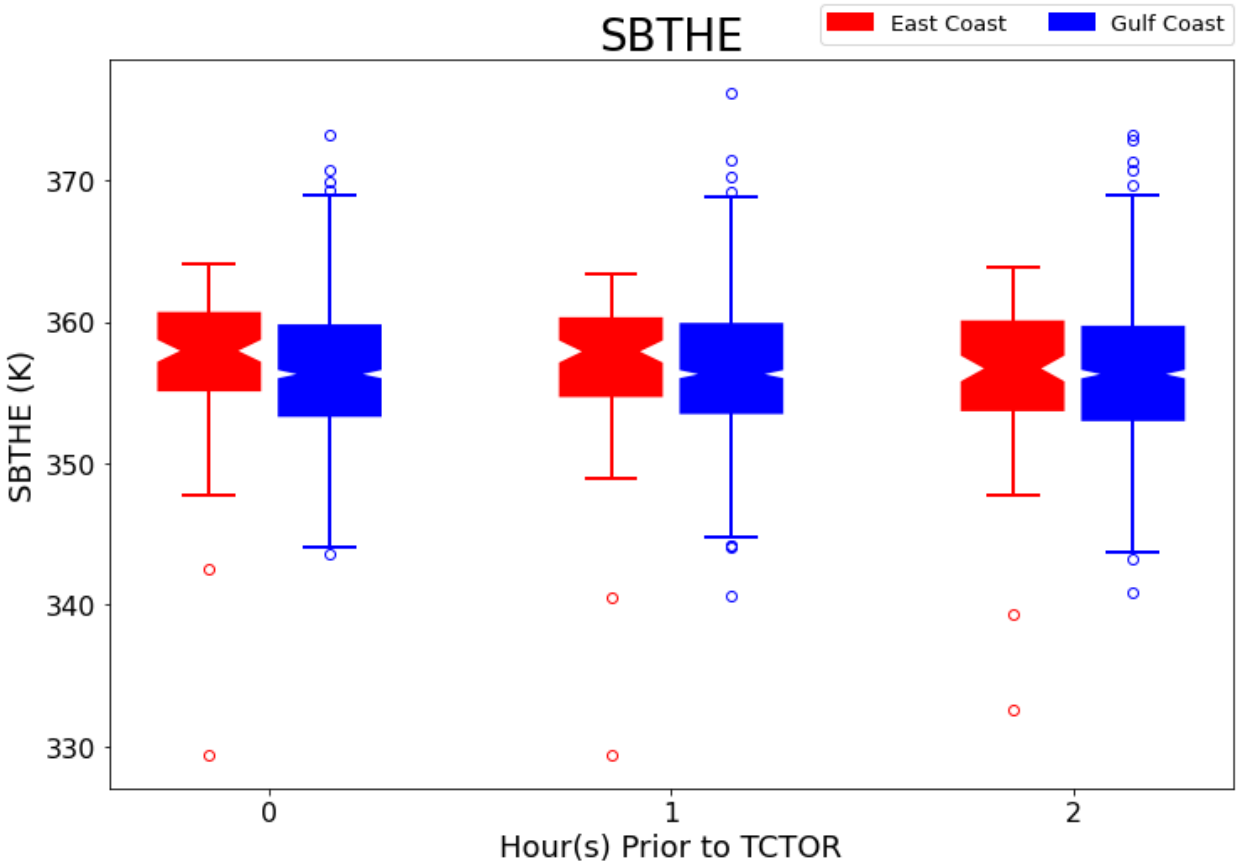

Figure 4.44: Surface-Based Equivalent Potential Temperature box and whisker plots for the East (red) and Gulf (blue) coast TCTOR events separated by hour of analysis prior to TCTOR.

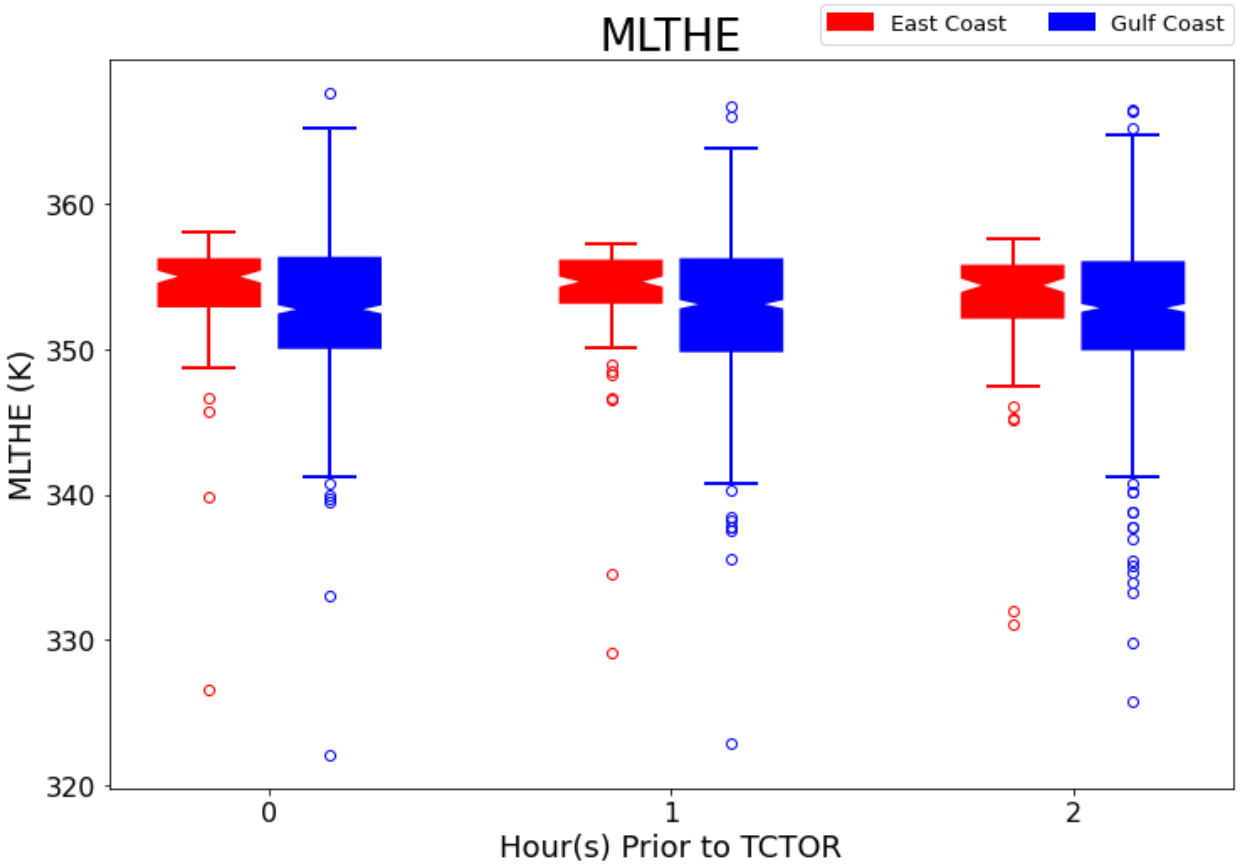

Figure 4.45: Mean Mixed-Layer Equivalent Potential Temperature box and whisker plots for the East (red) and Gulf (blue) coast TCTOR events separated by hour of analysis prior to TCTOR.

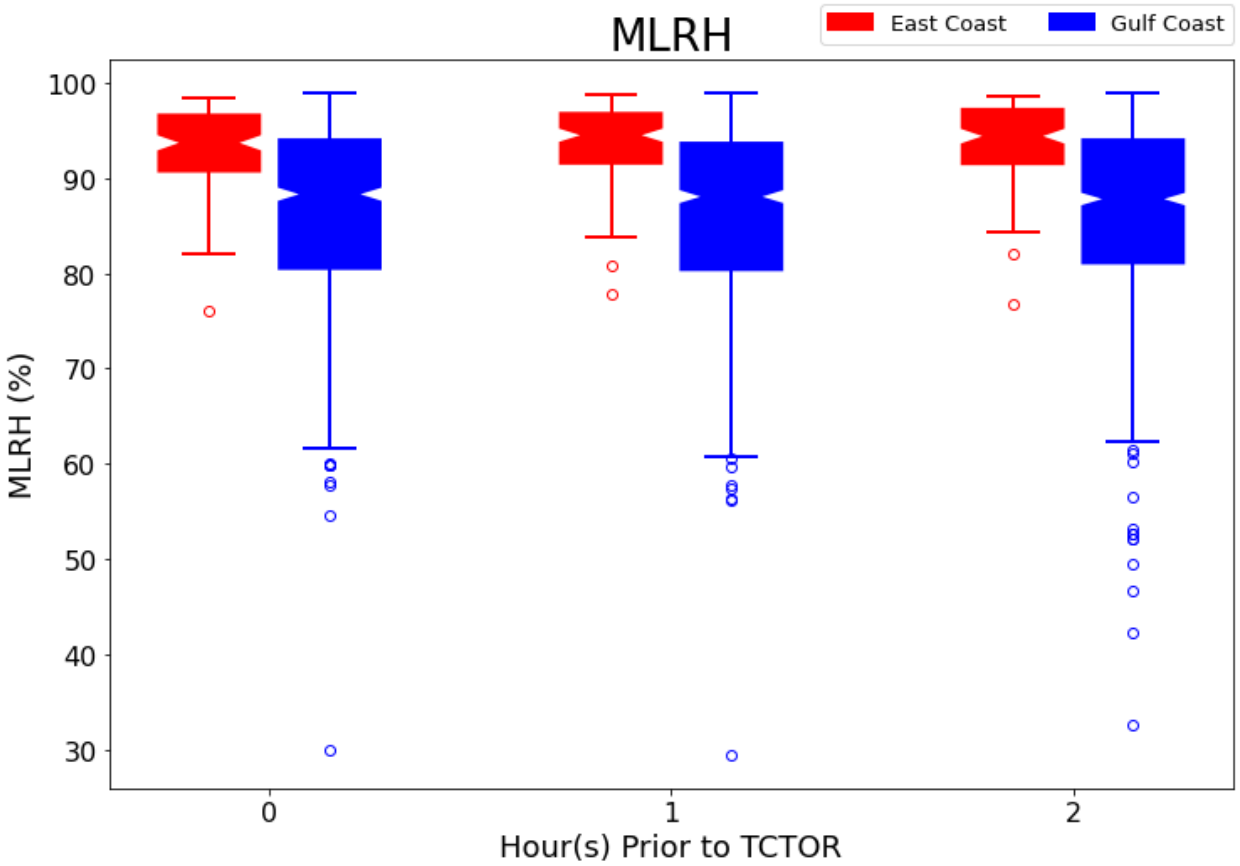

Figure 4.46: Mean Mixed-Layer Relative Humidity box and whisker plots for the East (red) and Gulf (blue) coast TCTOR events separated by hour of analysis prior to TCTOR.

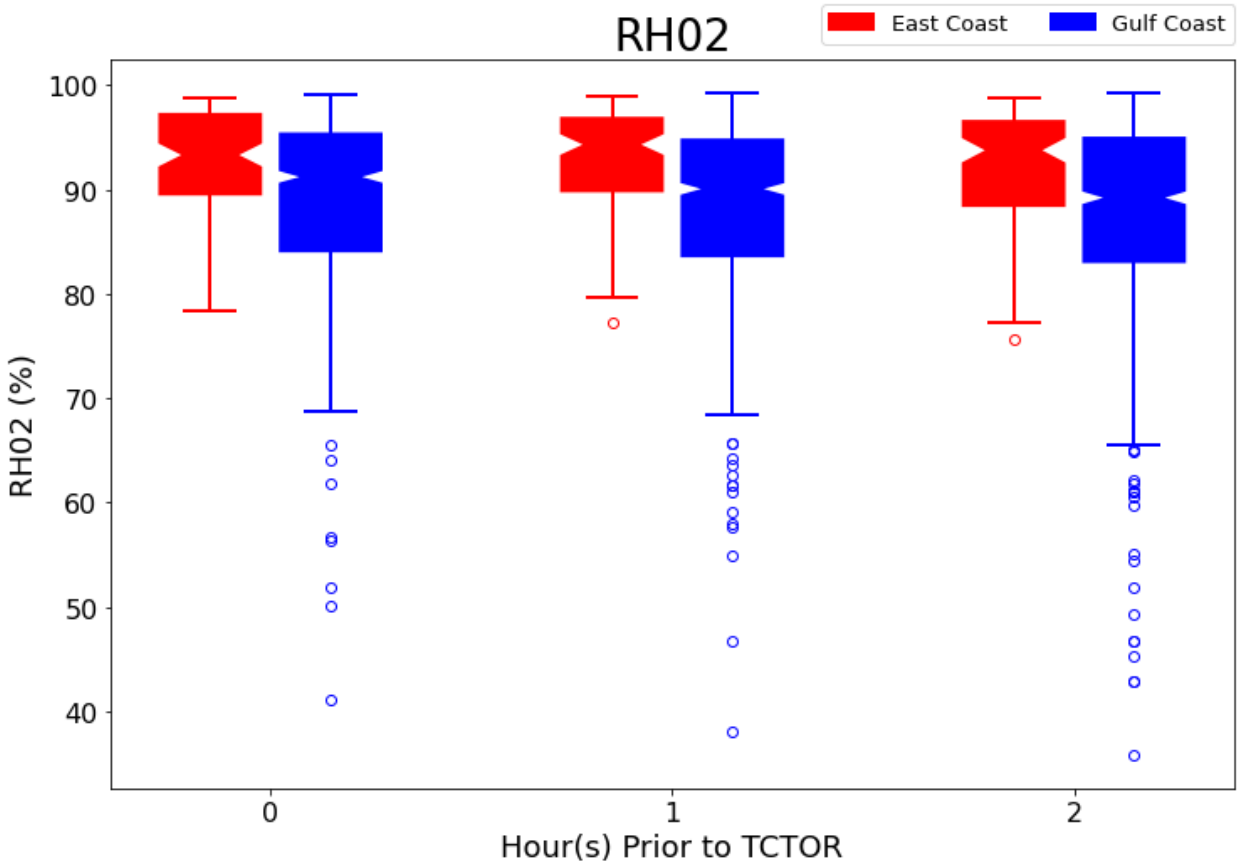

Figure 4.47: 0-2 km Relative Humidity box and whisker plots for the East (red) and Gulf (blue) coast TCTOR events separated by hour of analysis prior to TCTOR.

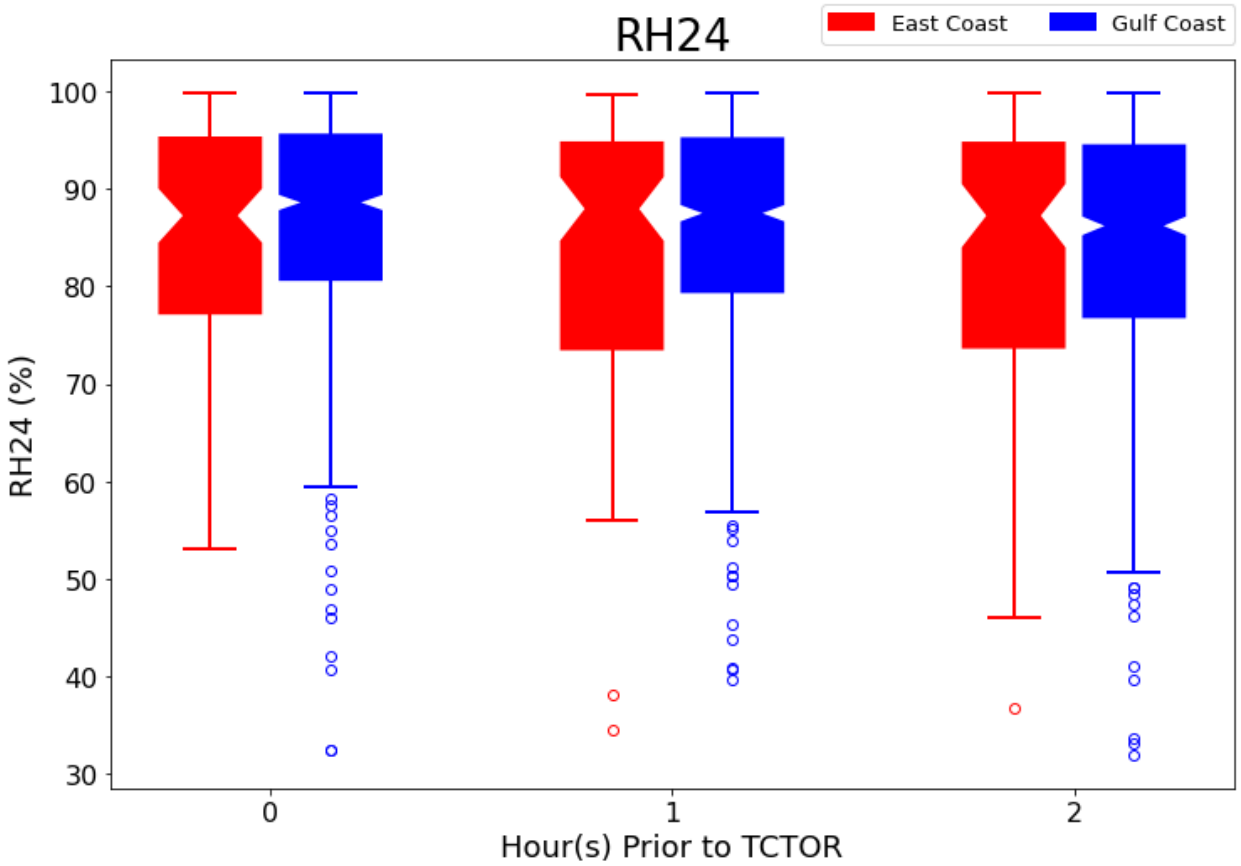

Figure 4.48: 2-4 km Relative Humidity box and whisker plots for the East (red) and Gulf (blue) coast TCTOR events separated by hour of analysis prior to TCTOR.

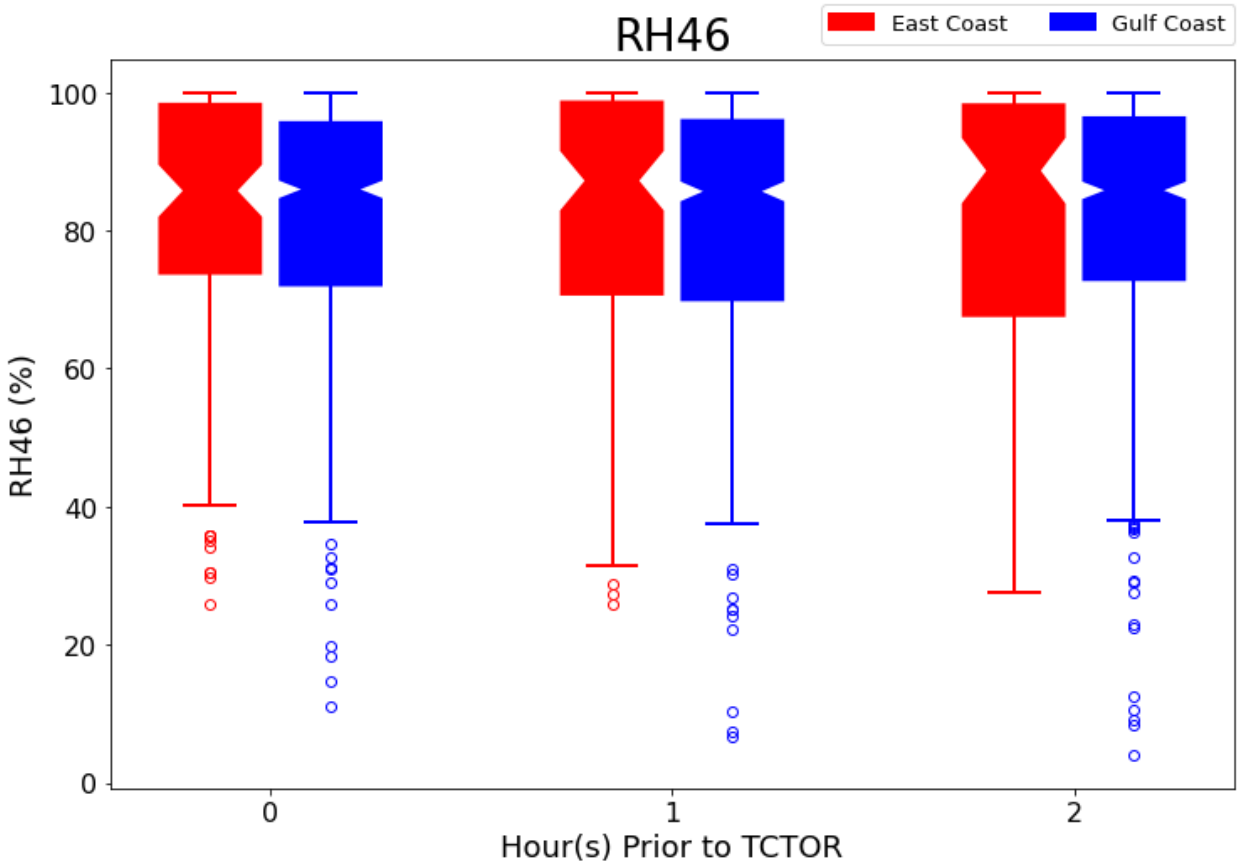

Figure 4.49: 4-6 km Relative Humidity box and whisker plots for the East (red) and Gulf (blue) coast TCTOR events separated by hour of analysis prior to TCTOR.

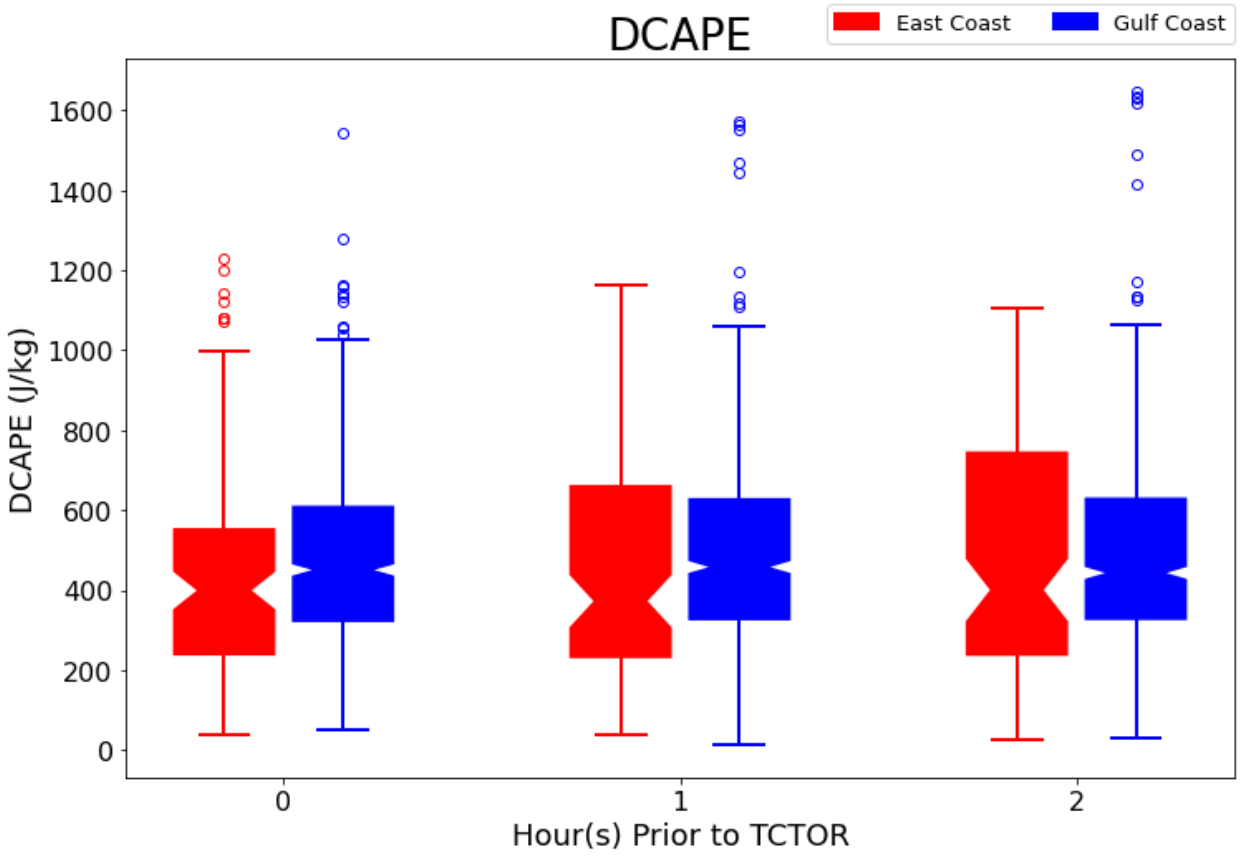

Figure 4.50: Downdraft CAPE box and whisker plots for the East (red) and Gulf (blue) coast TCTOR events separated by hour of analysis prior to TCTOR.

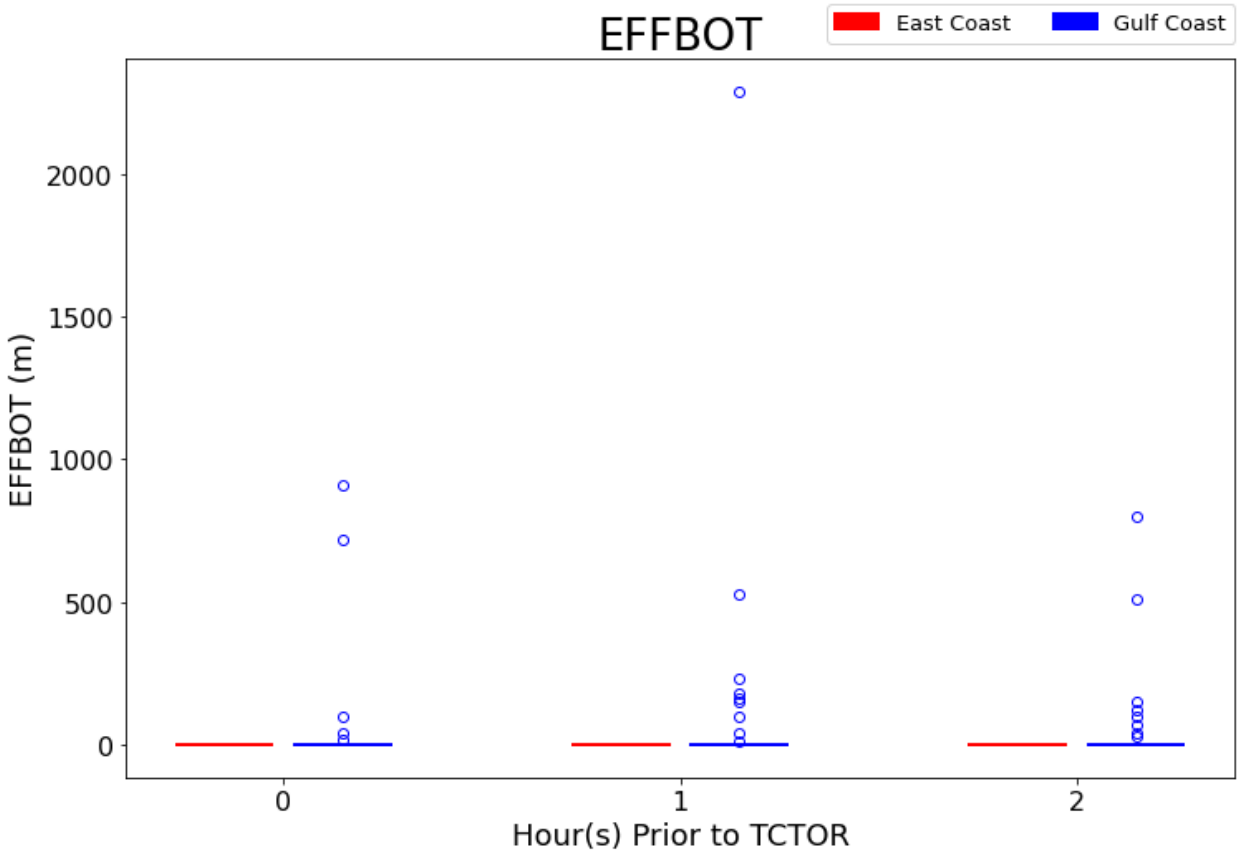

Figure 4.51: Height of the Effective Inflow Layer bottom box and whisker plots for the East (red) and Gulf (blue) coast TCTOR events separated by hour of analysis prior to TCTOR.

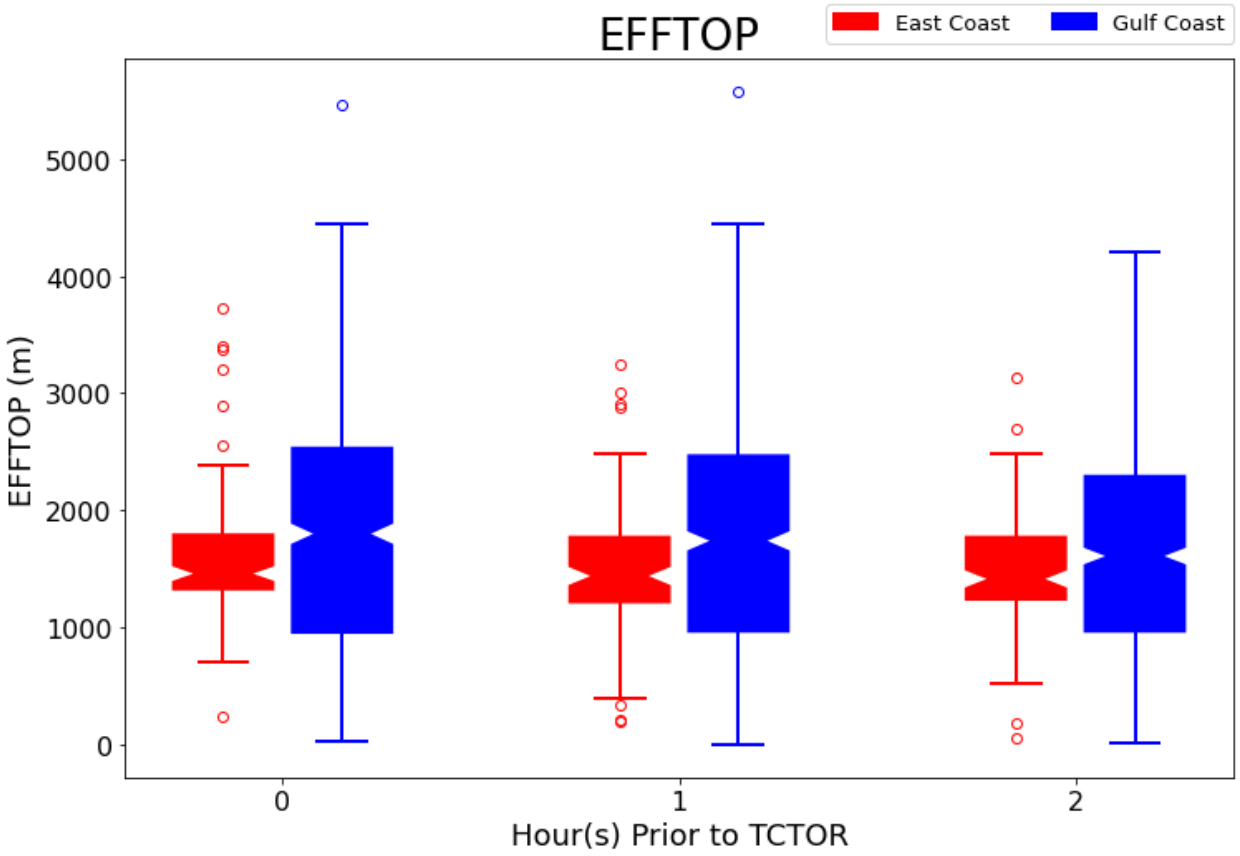

Figure 4.52: Height of the Effective Inflow Layer top box and whisker plots for the East (red) and Gulf (blue) coast TCTOR events separated by hour of analysis prior to TCTOR.

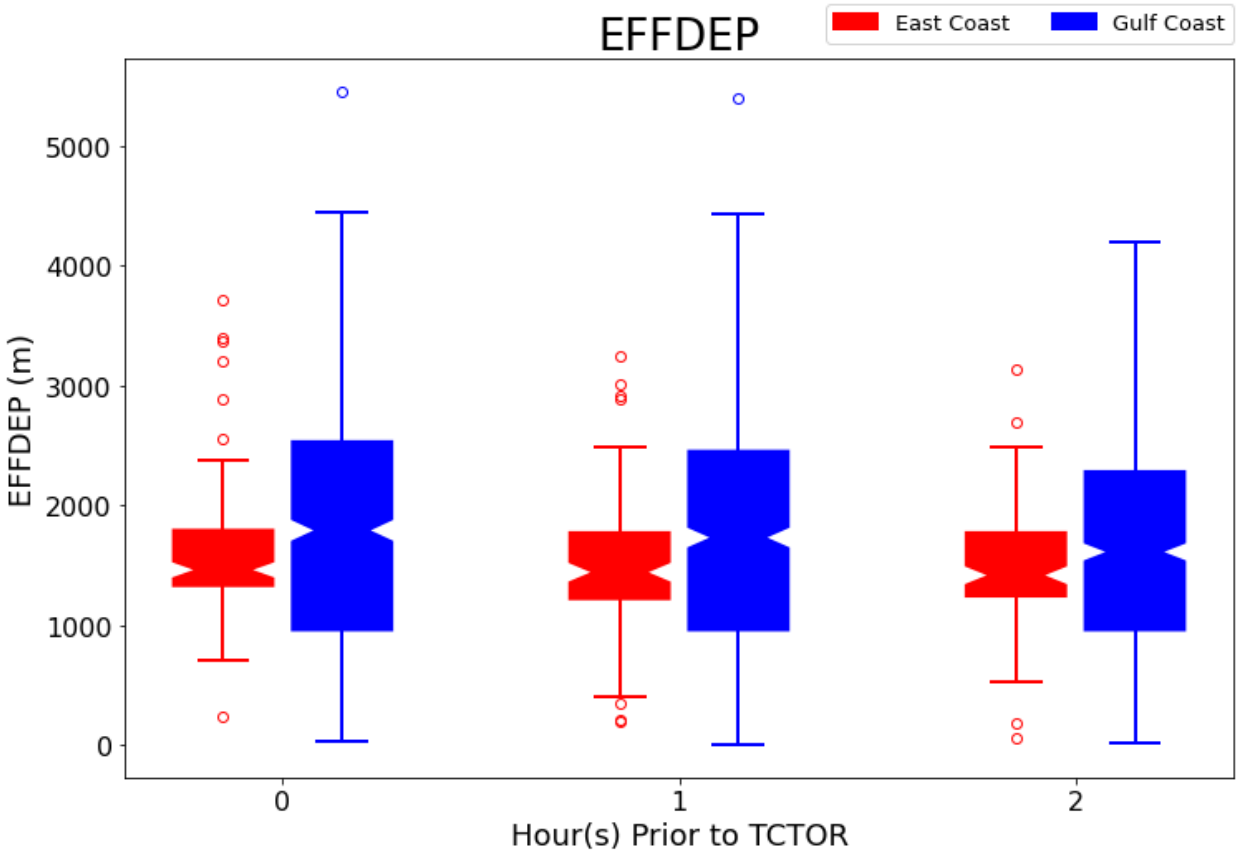

Figure 4.53: Depth of the Effective Inflow Layer box and whisker plots for the East (red) and Gulf (blue) coast TCTOR events separated by hour of analysis prior to TCTOR.

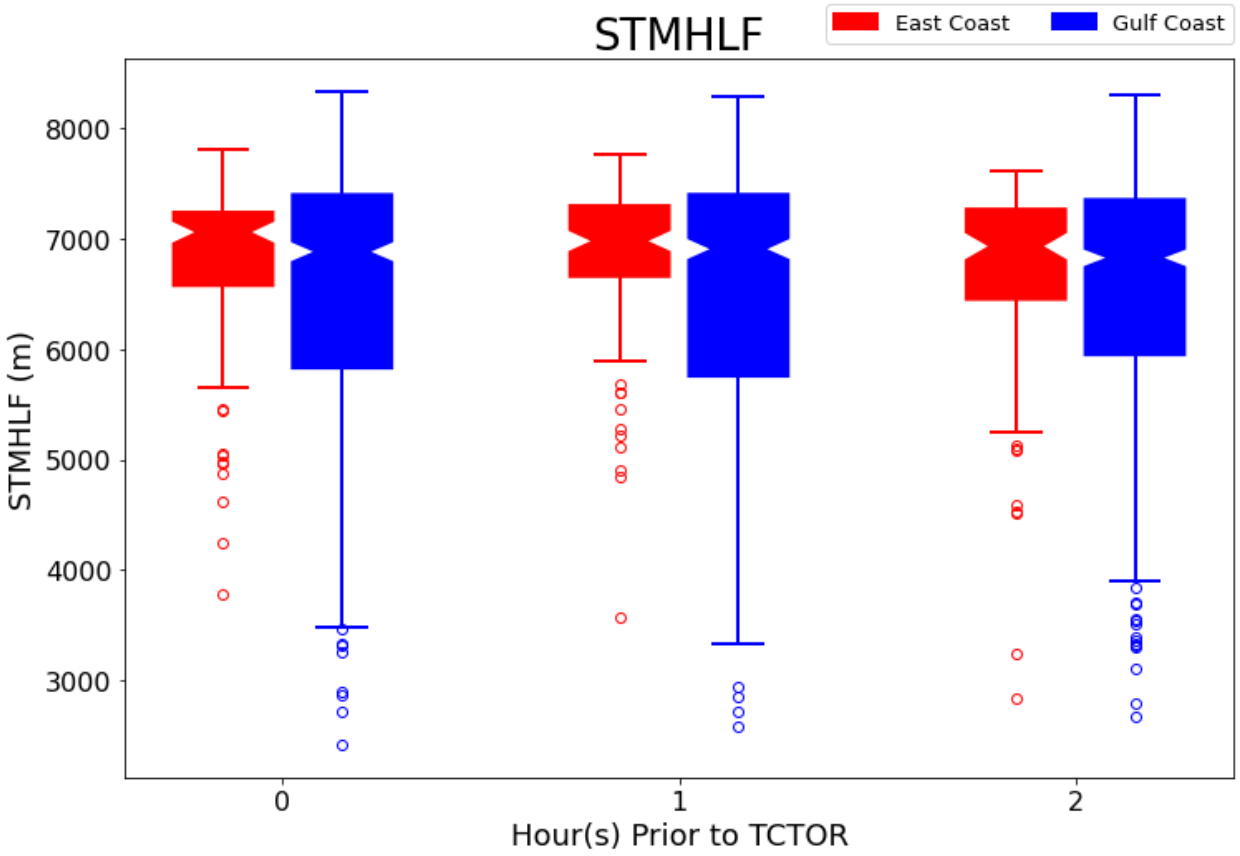

Figure 4.54: Half of the storm height box and whisker plots for the East (red) and Gulf (blue) coast TCTOR events separated by hour of analysis prior to TCTOR.

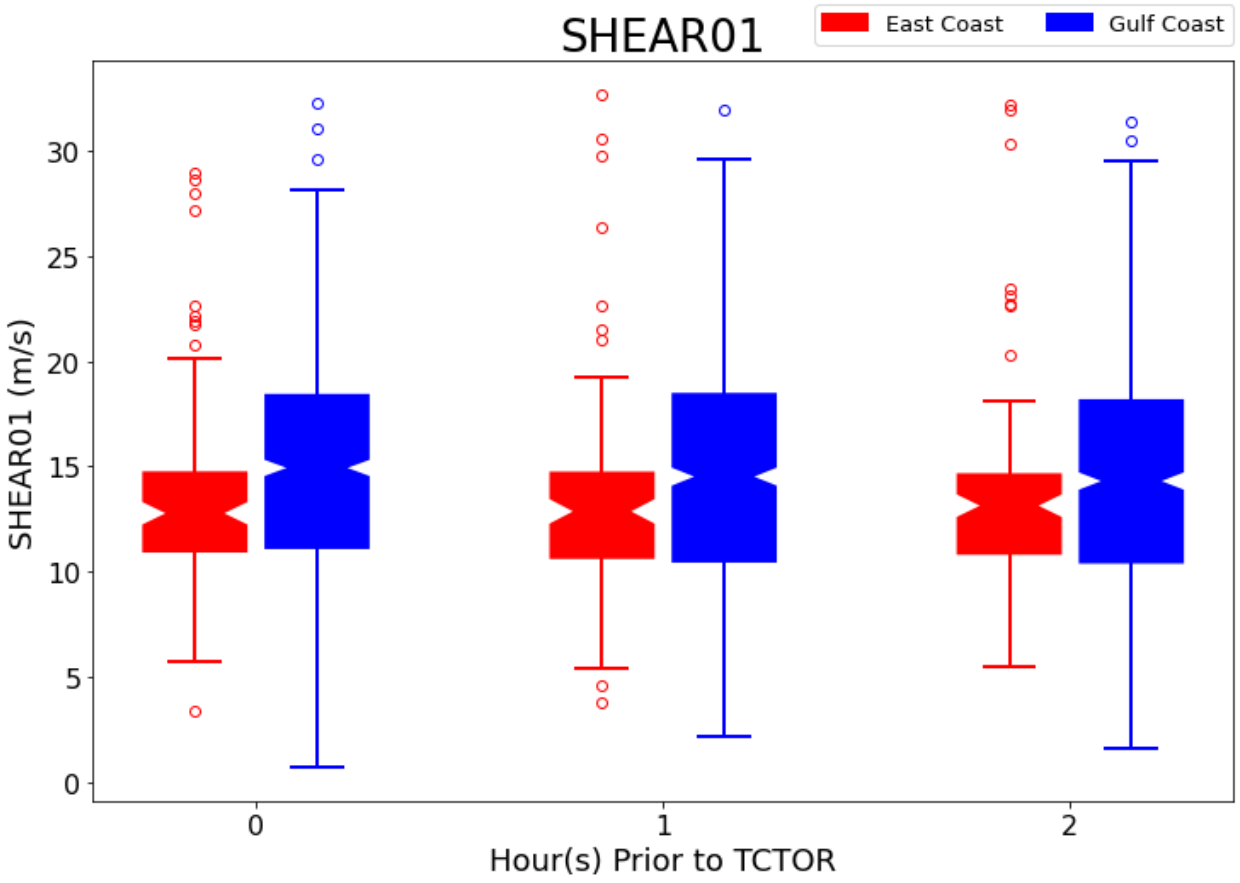

Figure 4.55: 0-1 km Bulk Shear box and whisker plots for the East (red) and Gulf (blue) coast TCTOR events separated by hour of analysis prior to TCTOR.

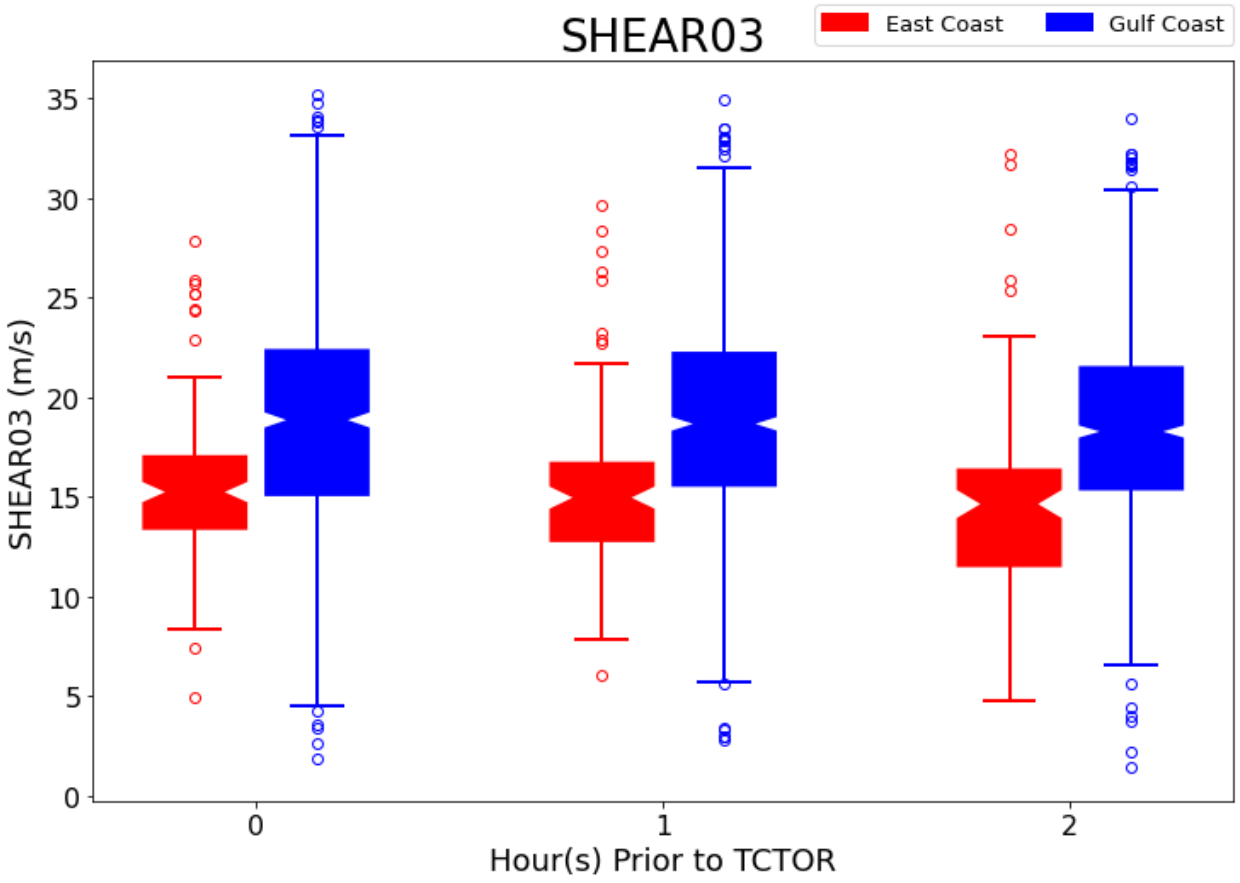

Figure 4.56: 0-3 km Bulk Shear box and whisker plots for the East (red) and Gulf (blue) coast TCTOR events separated by hour of analysis prior to TCTOR.

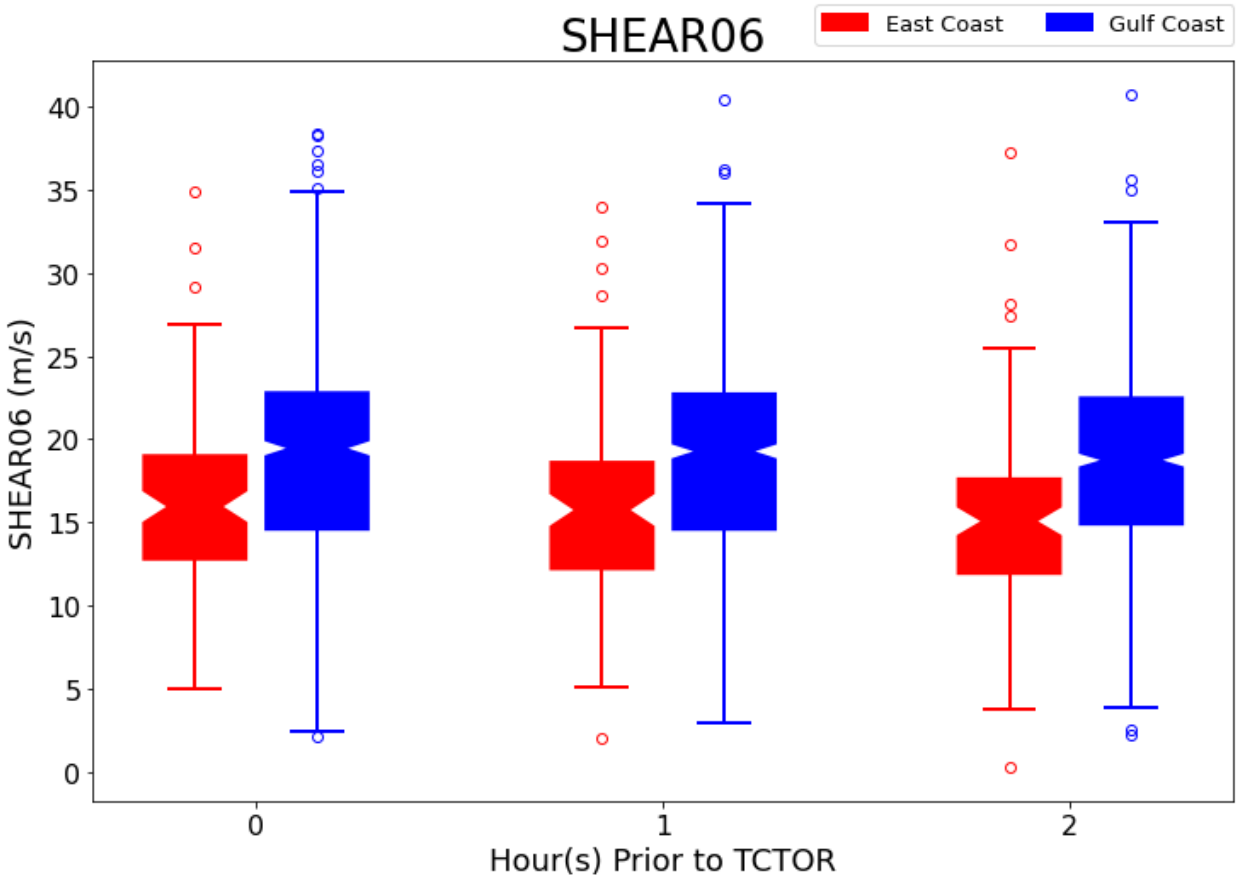

Figure 4.57: 0-6 km Bulk Shear box and whisker plots for the East (red) and Gulf (blue) coast TCTOR events separated by hour of analysis prior to TCTOR.

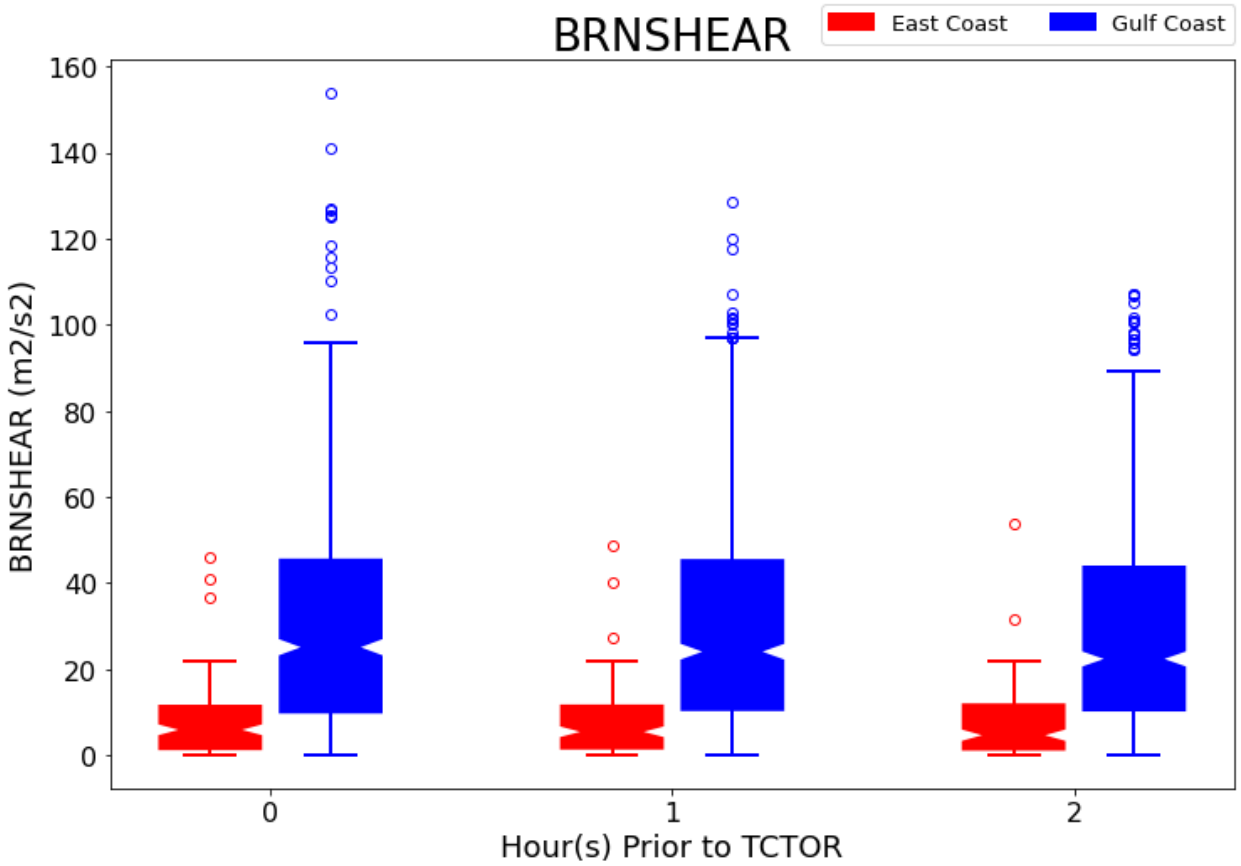

Figure 4.58: BRN Shear box and whisker plots for the East (red) and Gulf (blue) coast TCTOR events separated by hour of analysis prior to TCTOR.

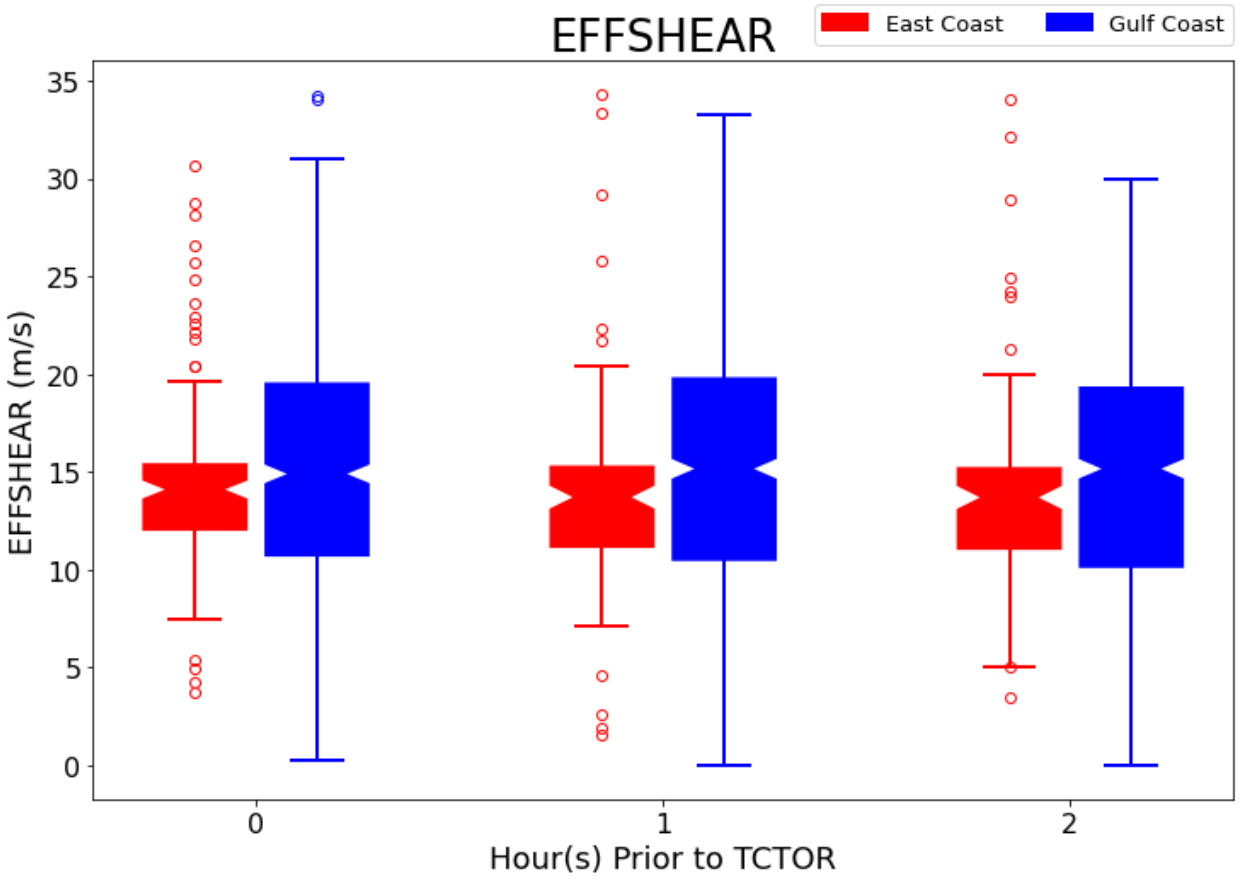

Figure 4.59: Effective Inflow Layer Bulk Shear box and whisker plots for the East (red) and Gulf (blue) coast TCTOR events separated by hour of analysis prior to TCTOR.

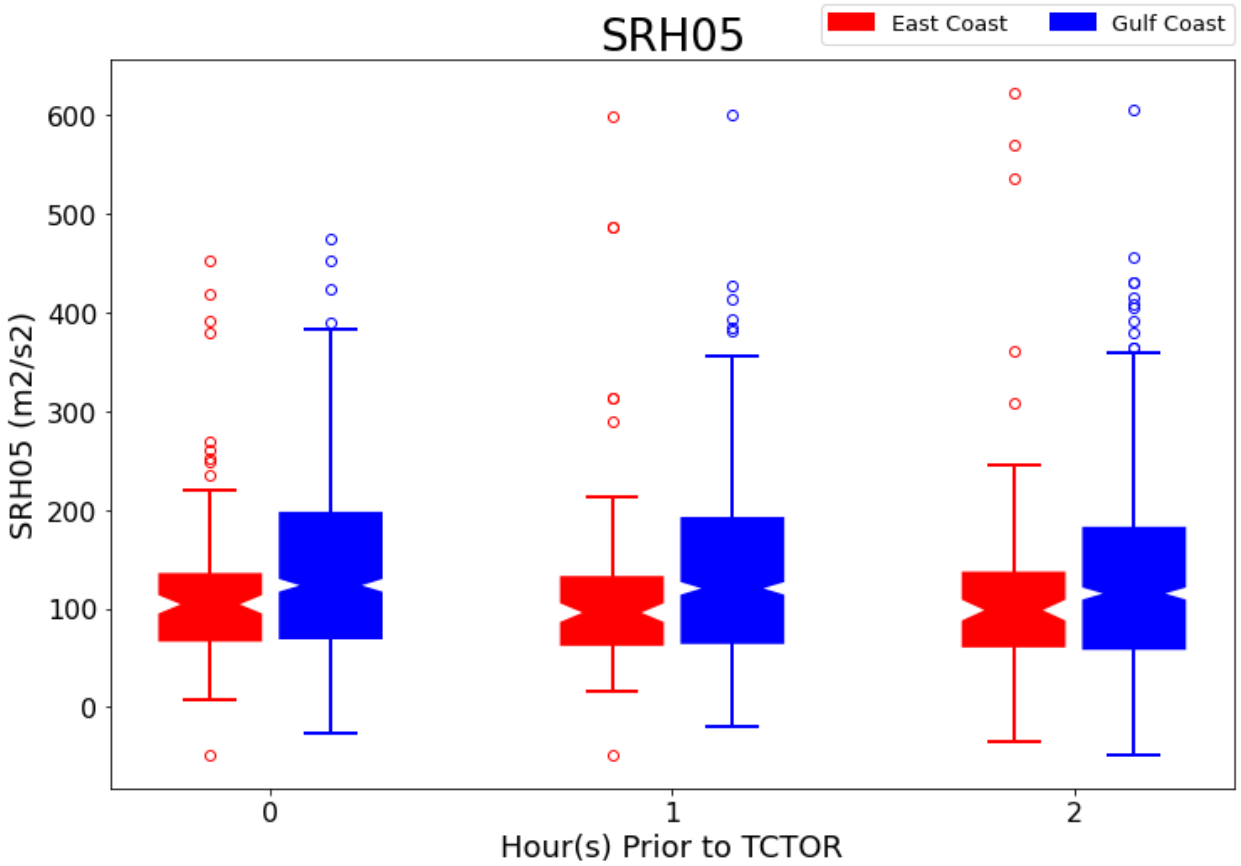

Figure 4.60: 0-500 m Storm Relative Humidity box and whisker plots for the East (red) and Gulf (blue) coast TCTOR events separated by hour of analysis prior to TCTOR.

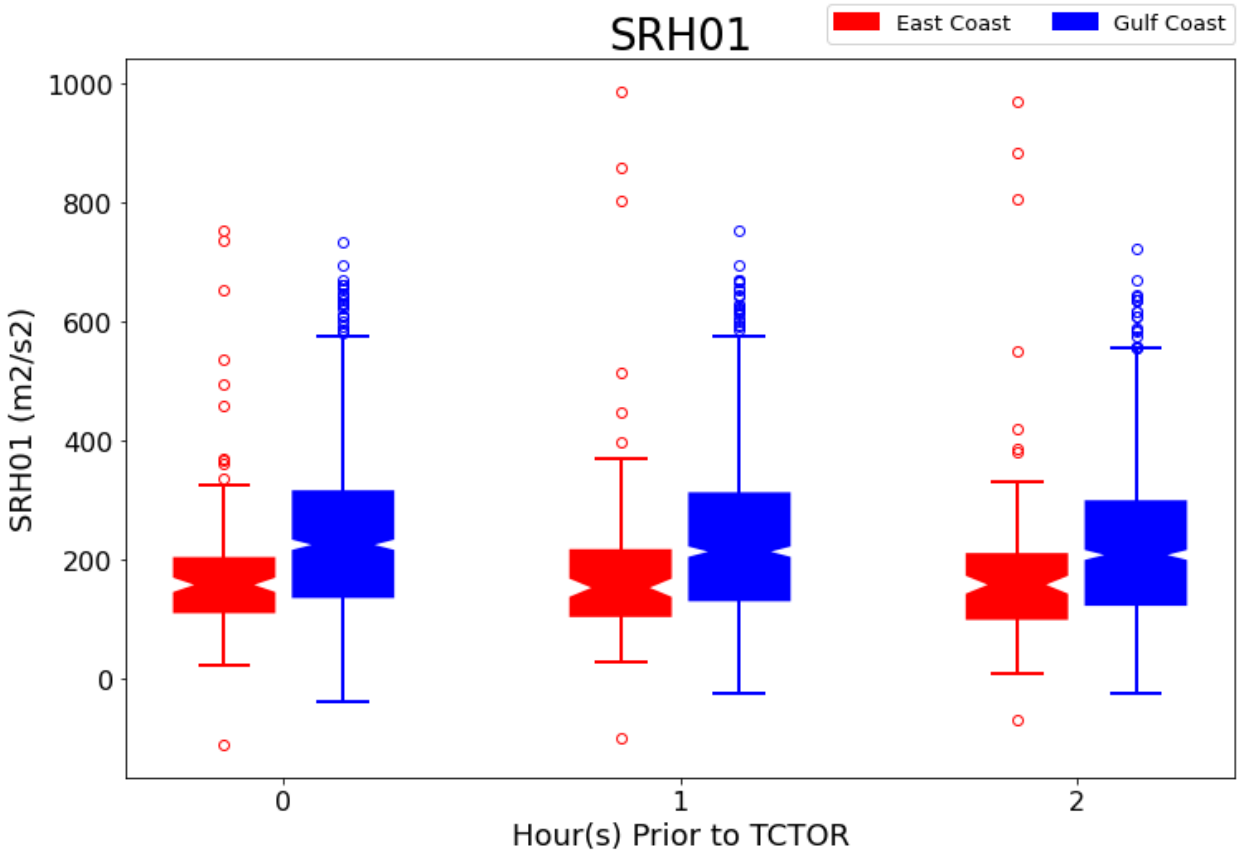

Figure 4.61: 0-1 km Storm Relative Humidity box and whisker plots for the East (red) and Gulf (blue) coast TCTOR events separated by hour of analysis prior to TCTOR.

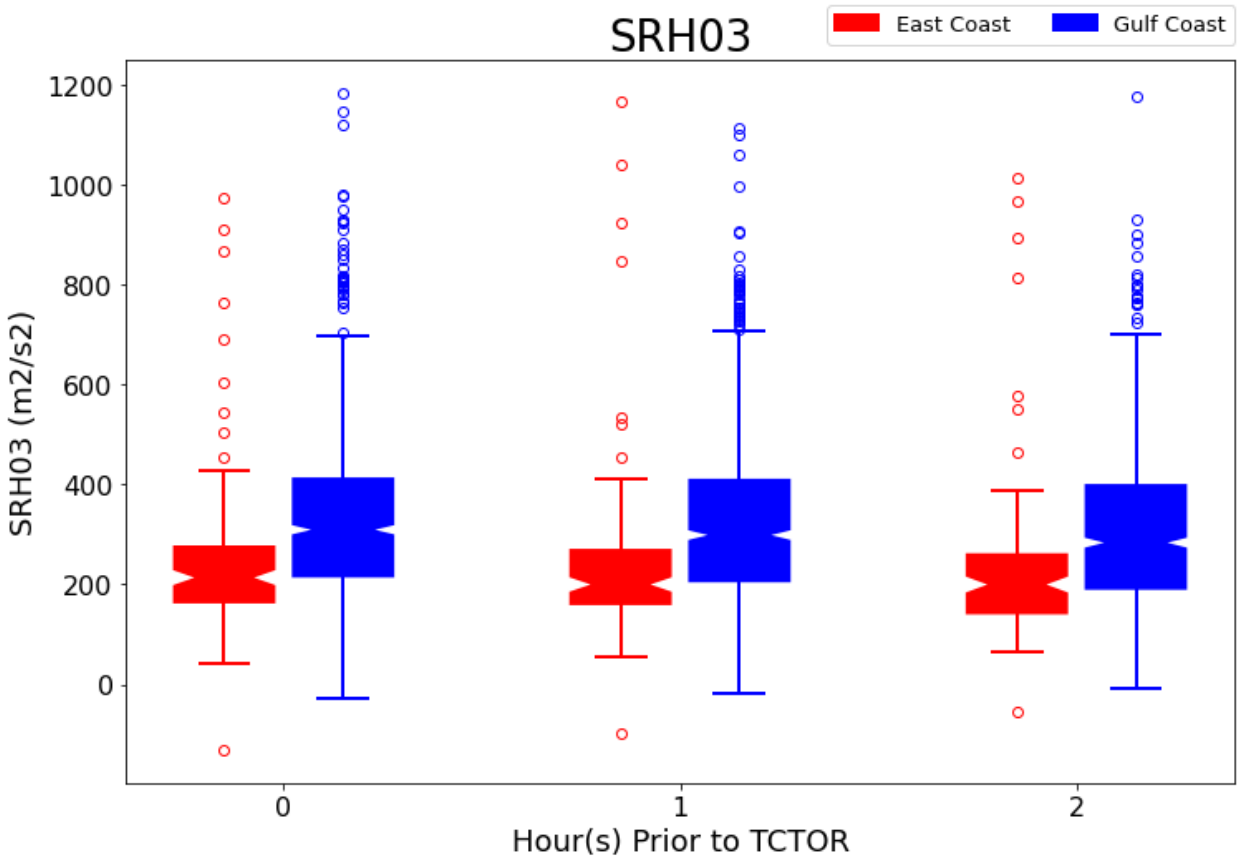

Figure 4.62: 0-3 km Storm Relative Humidity box and whisker plots for the East (red) and Gulf (blue) coast TCTOR events separated by hour of analysis prior to TCTOR.

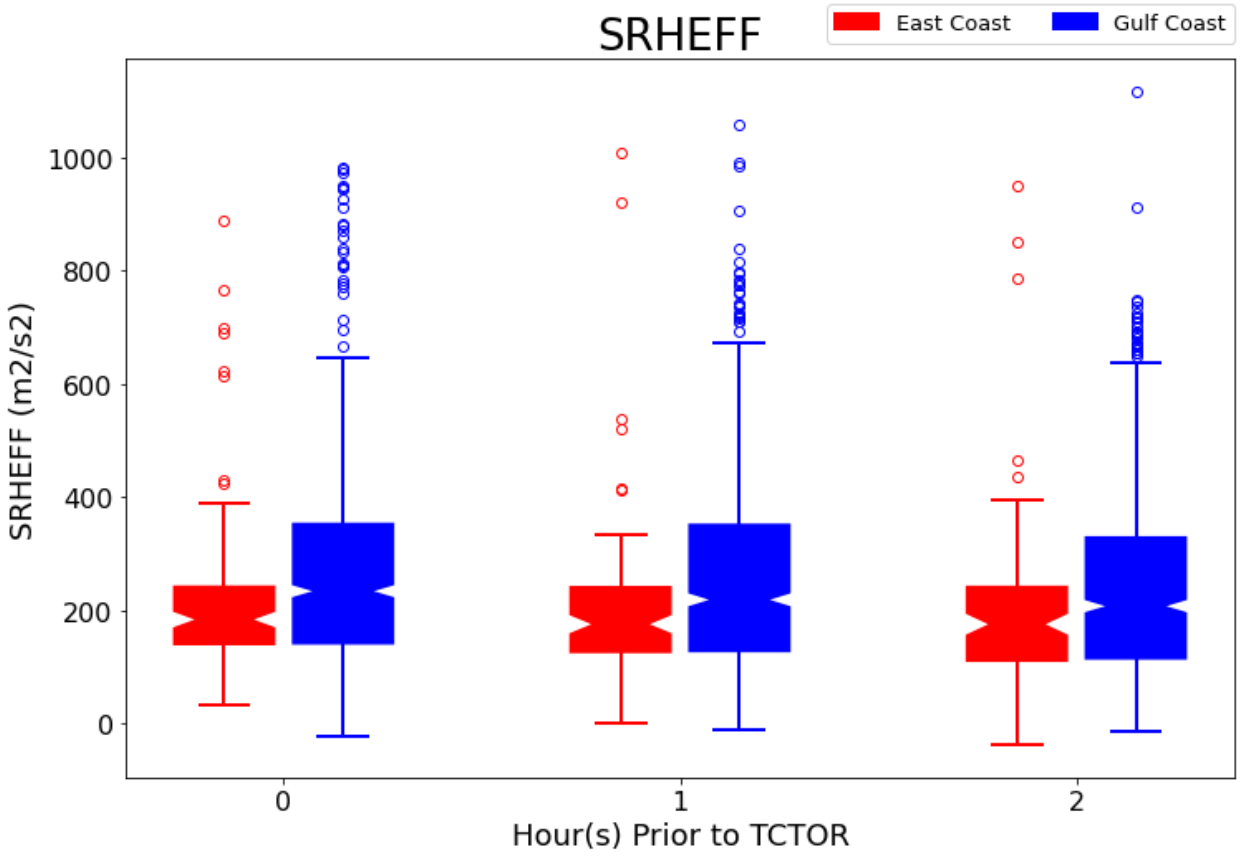

Figure 4.63: Effective Storm Relative Humidity box and whisker plots for the East (red) and Gulf (blue) coast TCTOR events separated by hour of analysis prior to TCTOR.

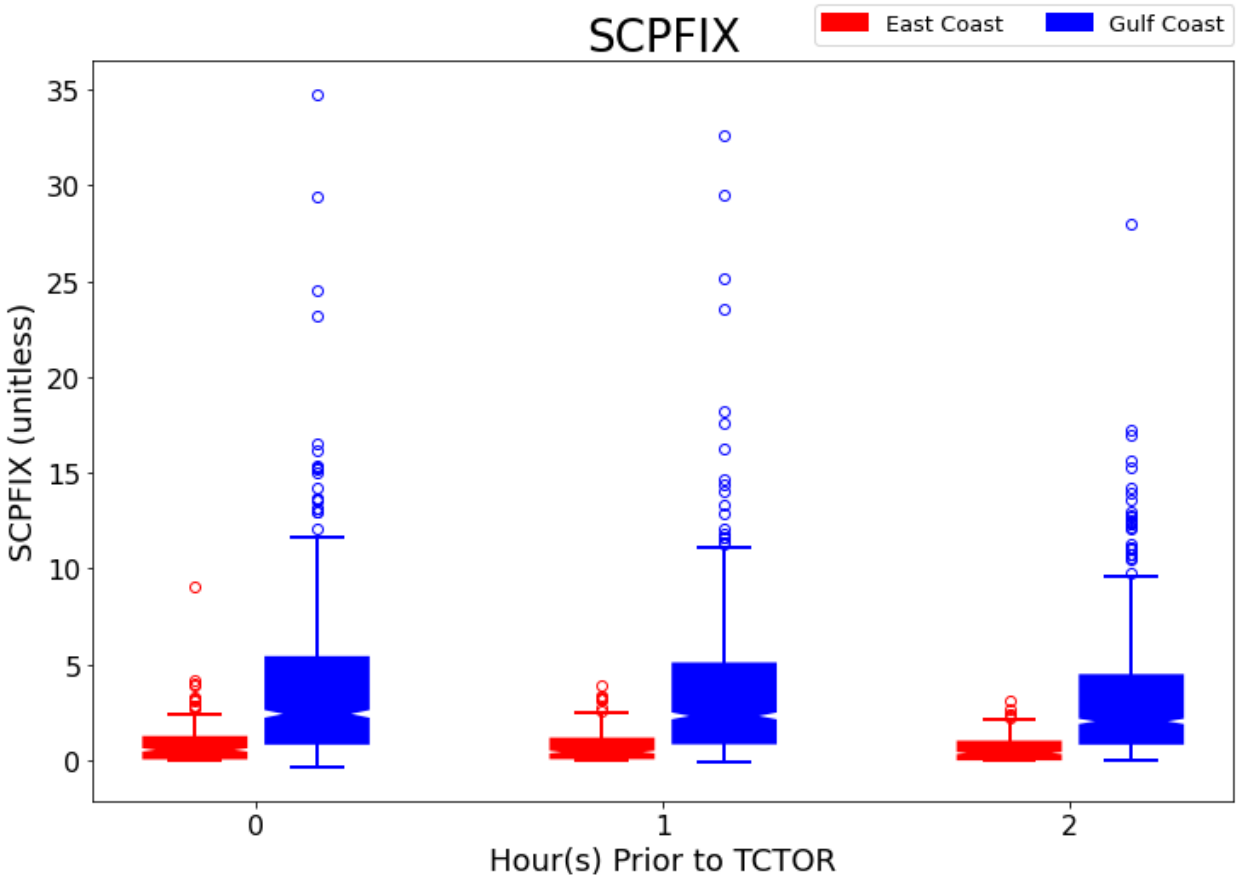

Figure 4.64: Fixed-Layer Supercell Composite Parameter box and whisker plots for the East (red) and Gulf (blue) coast TCTOR events separated by hour of analysis prior to TCTOR.

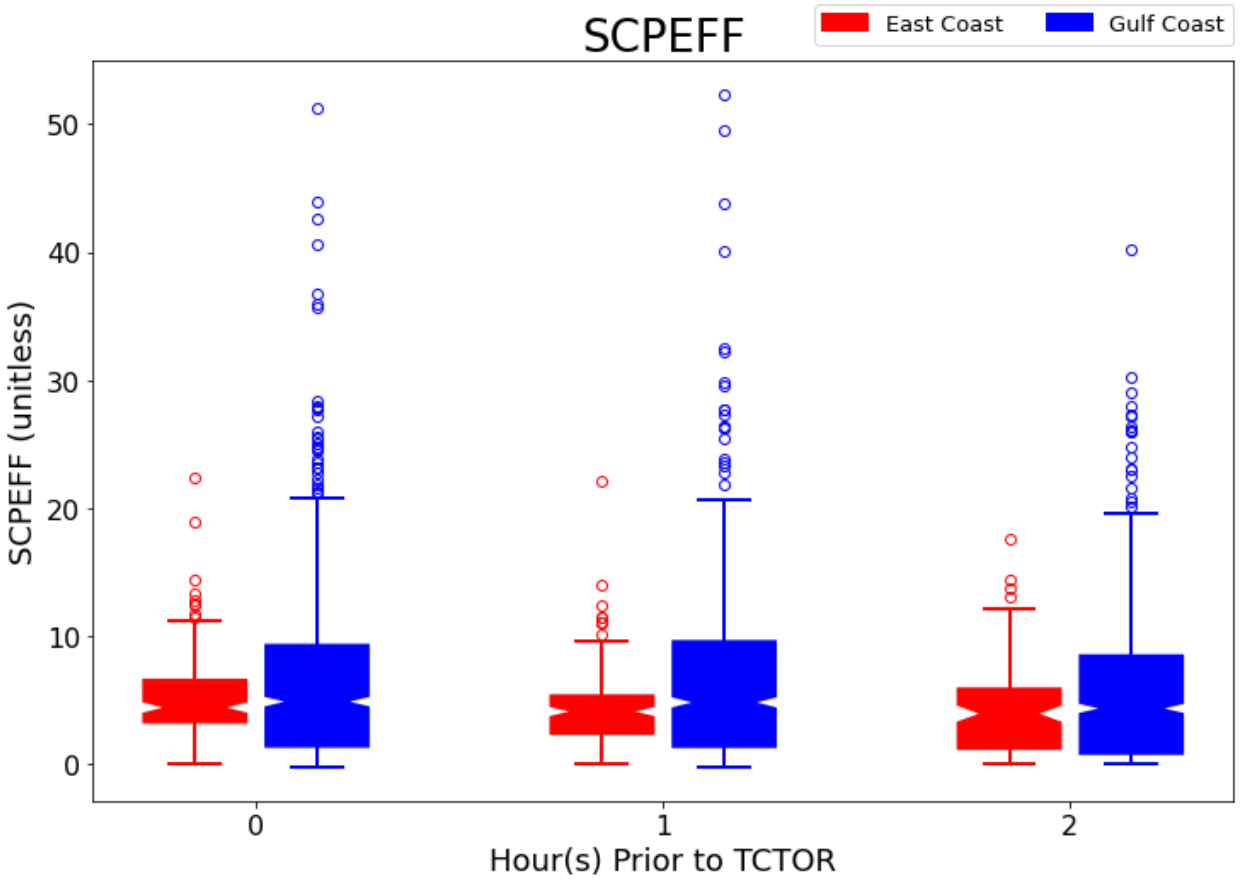

Figure 4.65: Effective Supercell Composite Parameter box and whisker plots for the East (red) and Gulf (blue) coast TCTOR events separated by hour of analysis prior to TCTOR.

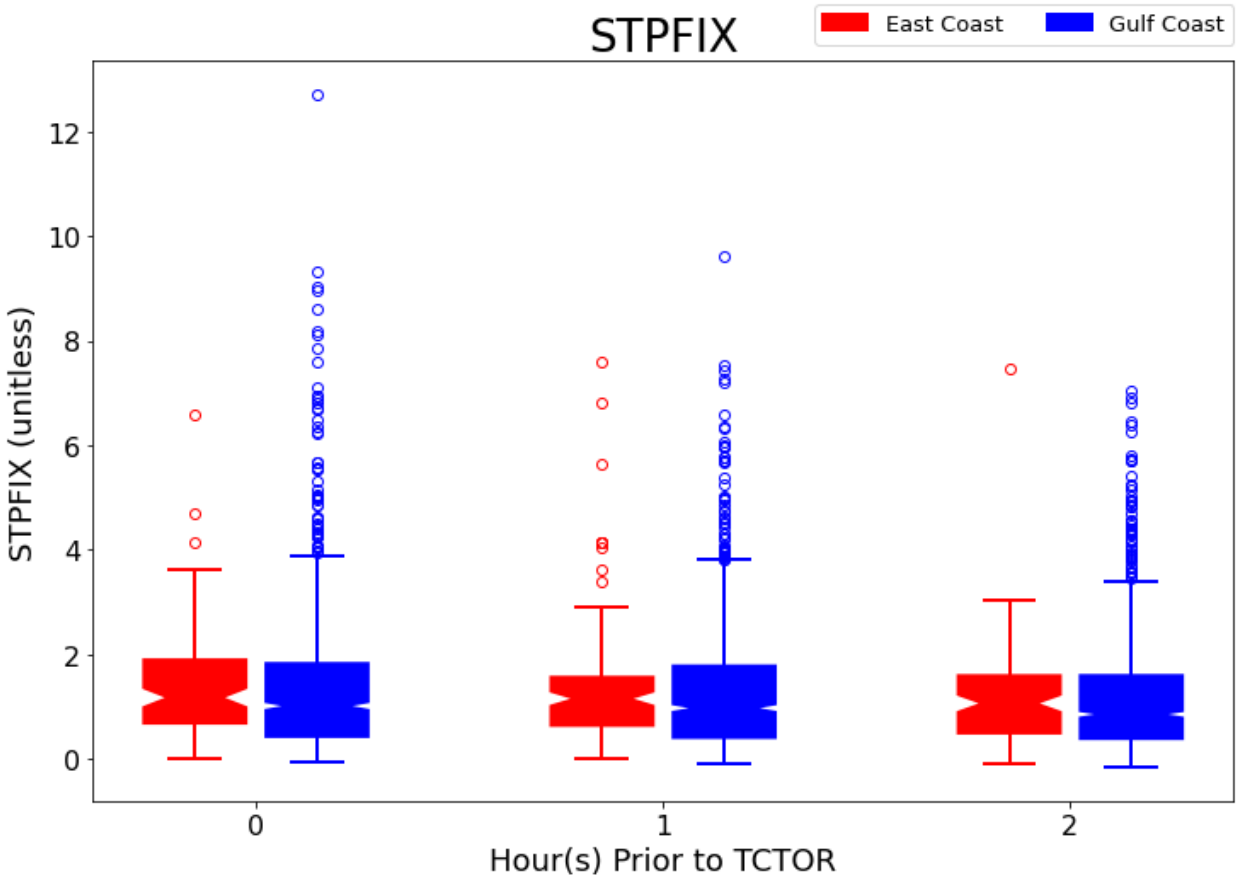

Figure 4.66: Fixed-Layer Significant Tornado Parameter box and whisker plots for the East (red) and Gulf (blue) coast TCTOR events separated by hour of analysis prior to TCTOR.

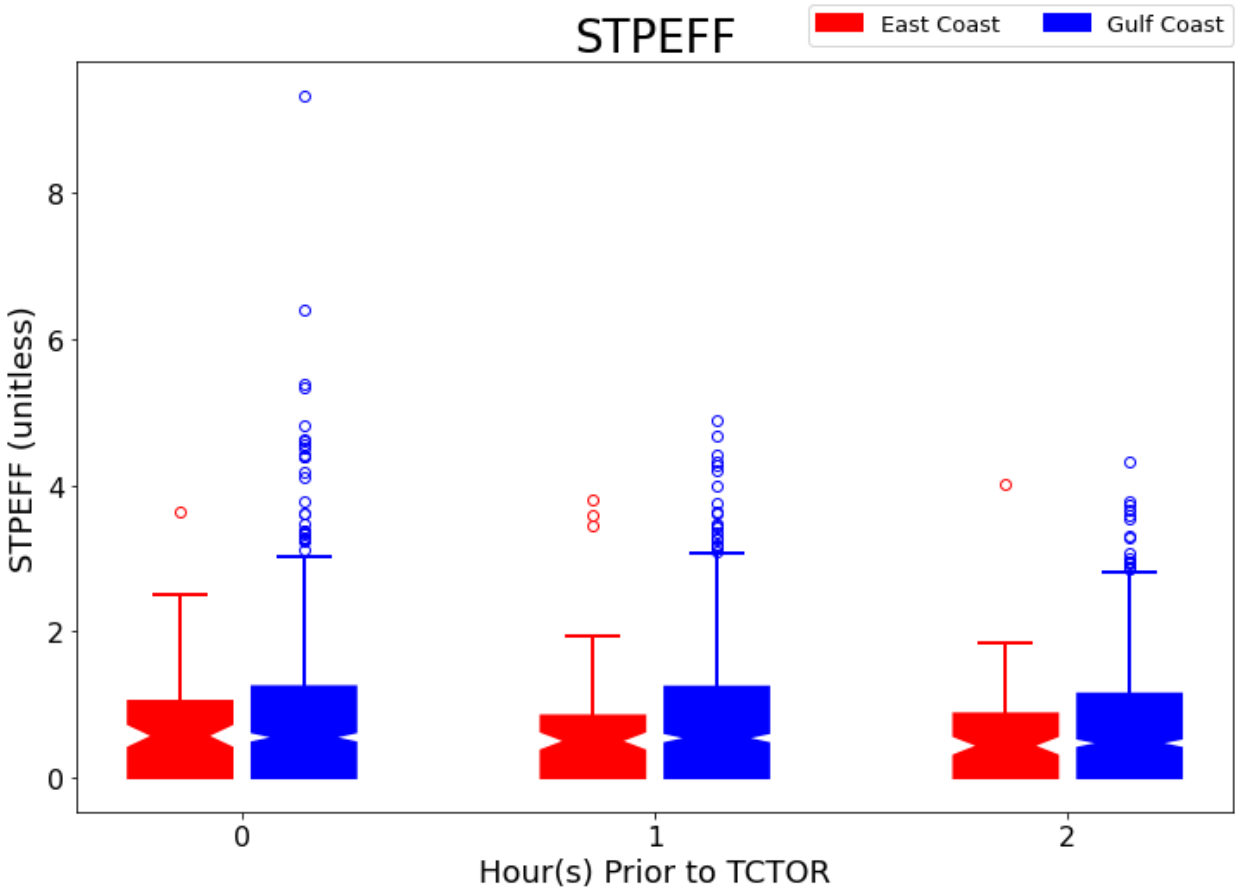

Figure 4.67: Effective Significant Tornado Parameter box and whisker plots for the East (red) and Gulf (blue) coast TCTOR events separated by hour of analysis prior to TCTOR.

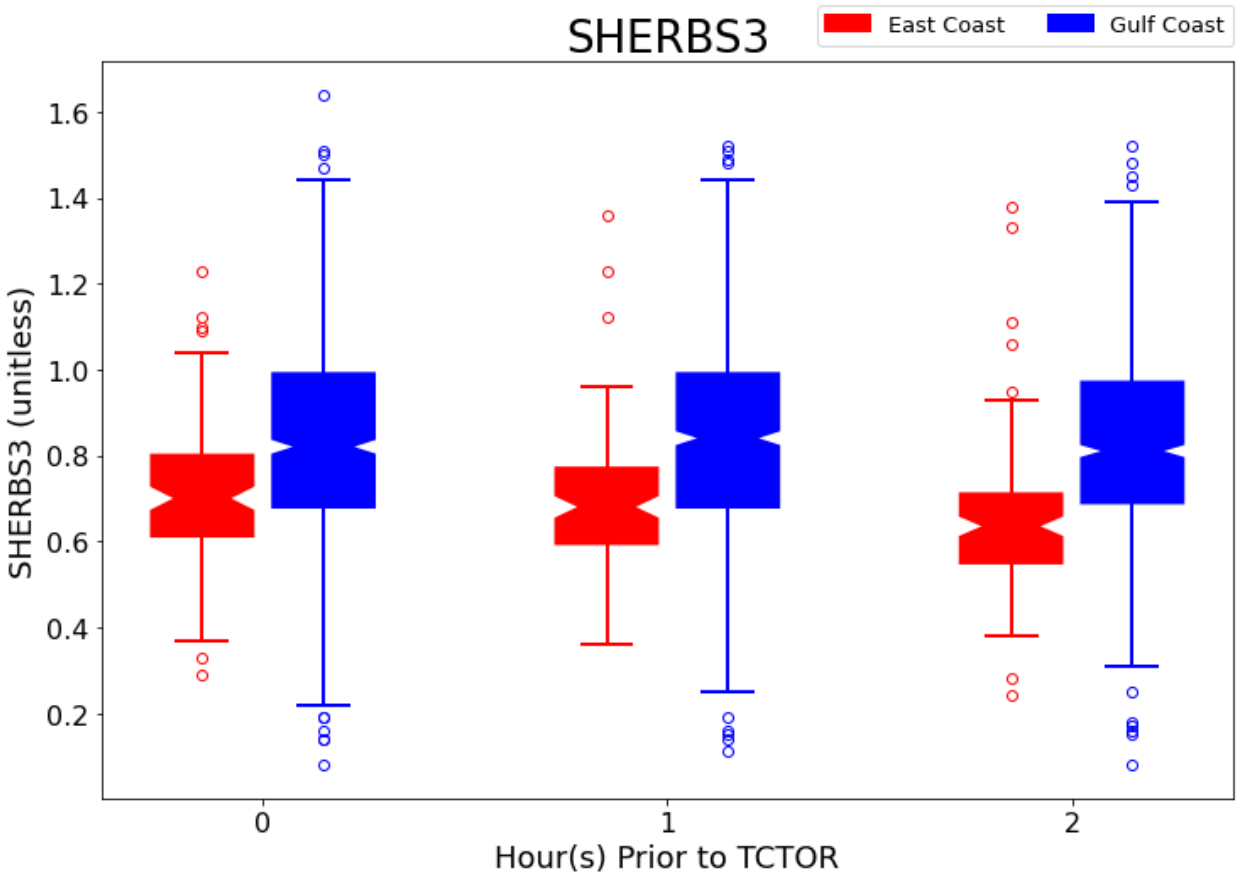

Figure 4.68: 0-3 km Sherburn Parameter (Sherburn and Parker 2014) box and whisker plots for the East (red) and Gulf (blue) coast TCTOR events separated by hour of analysis prior to TCTOR.

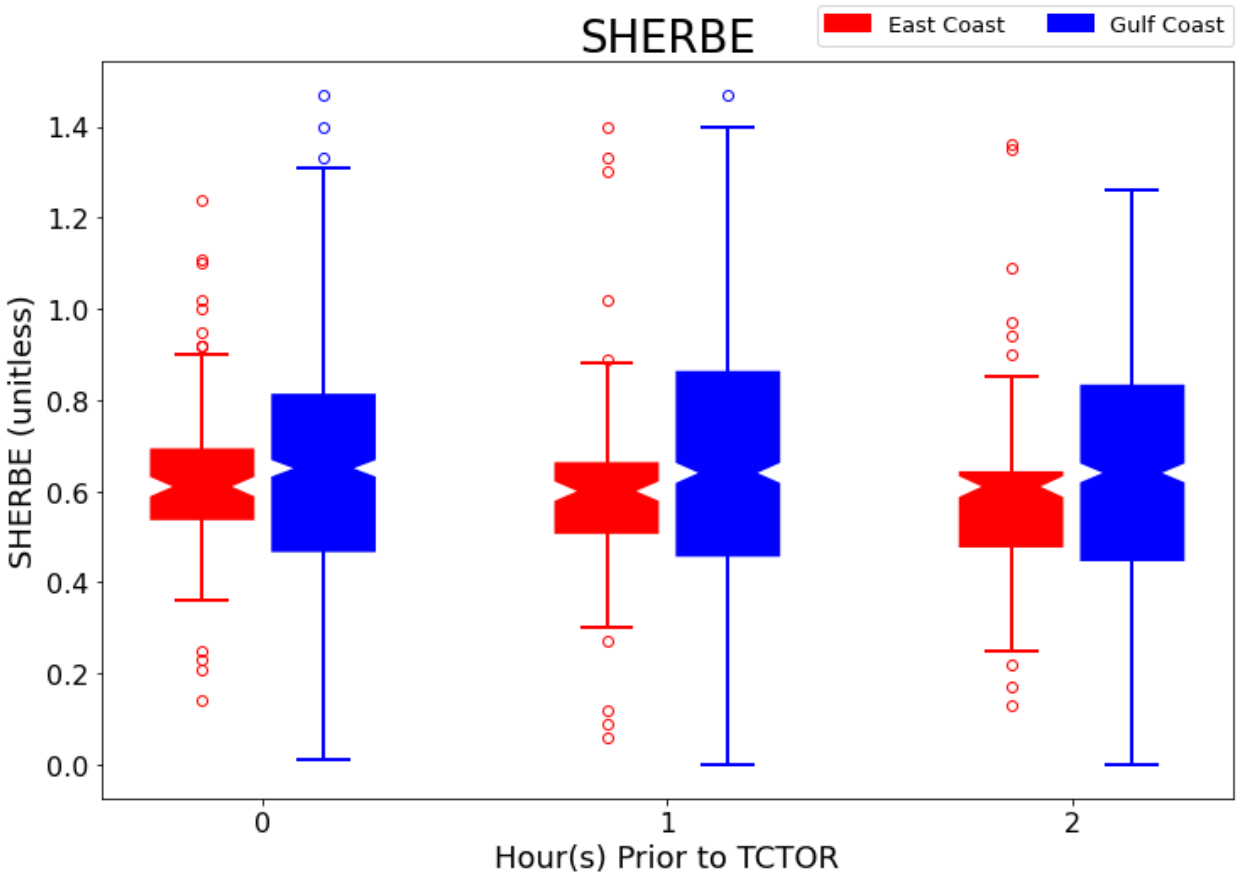

Figure 4.69: Effective Sherburn Parameter (Sherburn and Parker 2014) box and whisker plots for the East (red) and Gulf (blue) coast TCTOR events separated by hour of analysis prior to TCTOR.

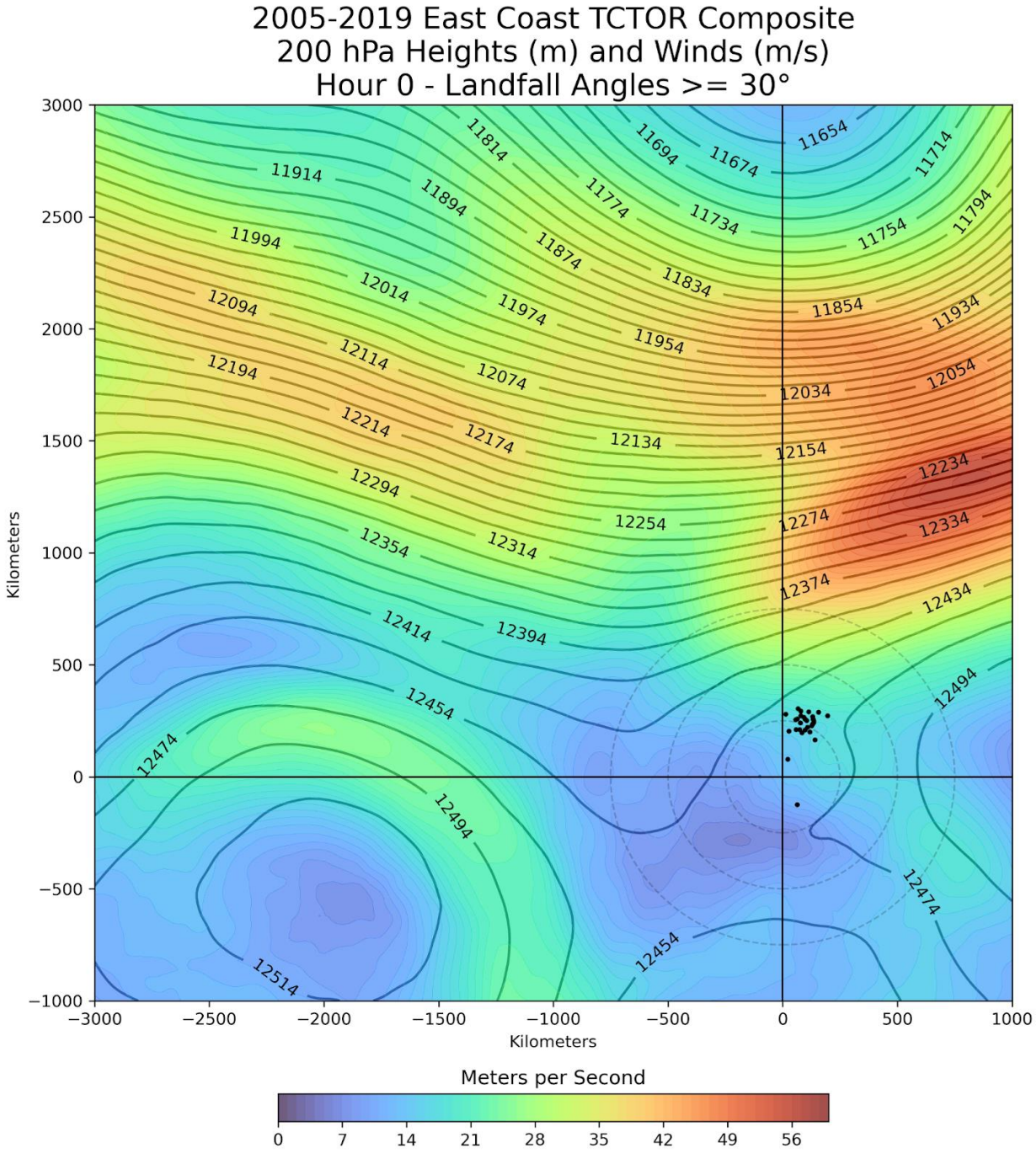

Figure 4.70: 2005-2019 East Coast Composite 200-mb Heights (m) and Winds (m/s) at the time of TCTOR occurrence including TCs with a landfall angle >= 30°. Black dots indicate TCTOR locations. Crosshairs are approximate composite TC center. Light gray dashed circles are range rings at distances 250, 500, and 750 km from TC center.

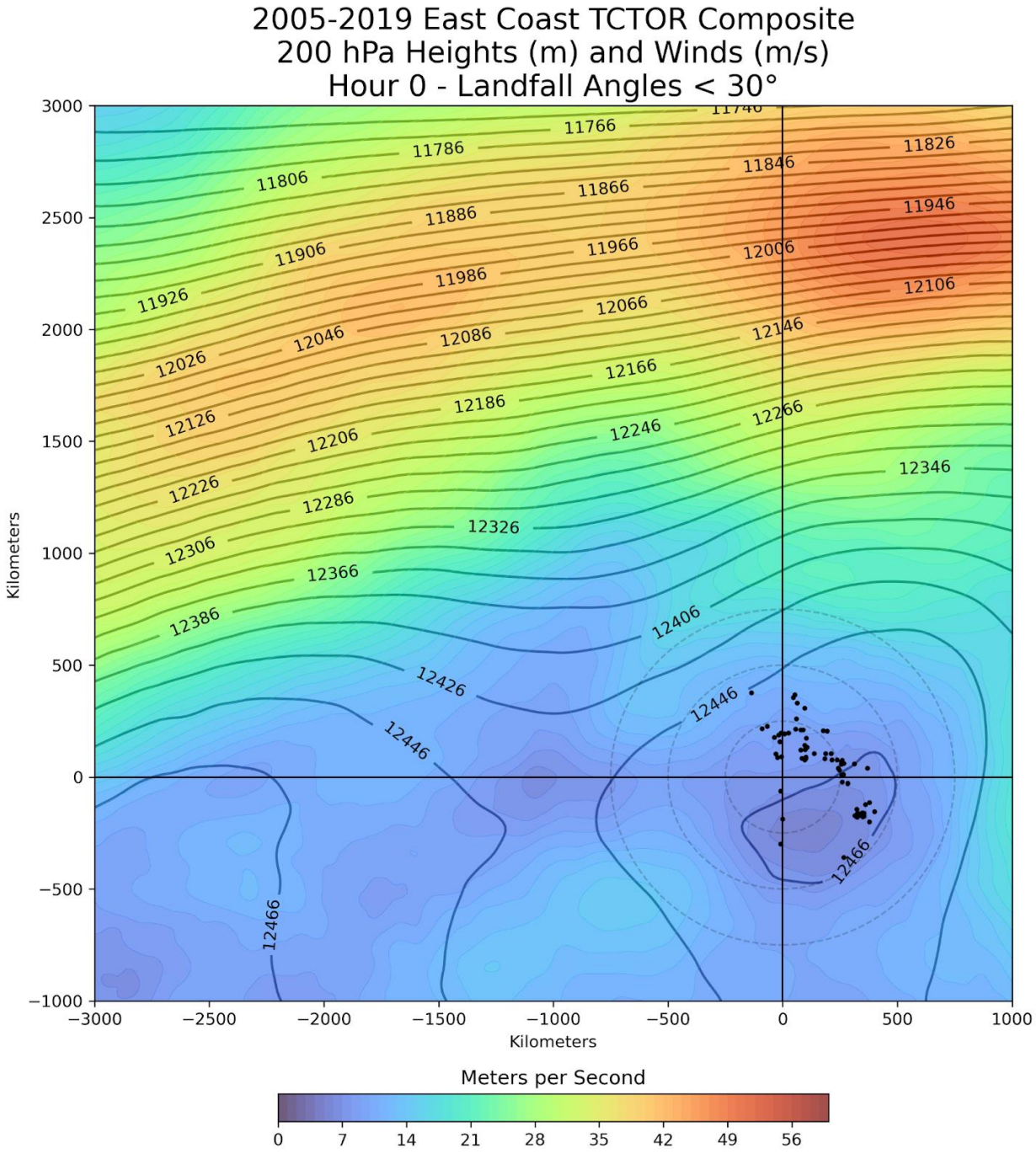

Figure 4.71: 2005-2019 East Coast Composite 200-mb Heights (m) and Winds (m/s) at the time of TCTOR occurrence including TCs with a landfall angle < 30°. Black dots indicate TCTOR locations. Crosshairs are approximate composite TC center. Light gray dashed circles are range rings at distances 250, 500, and 750 km from TC center.

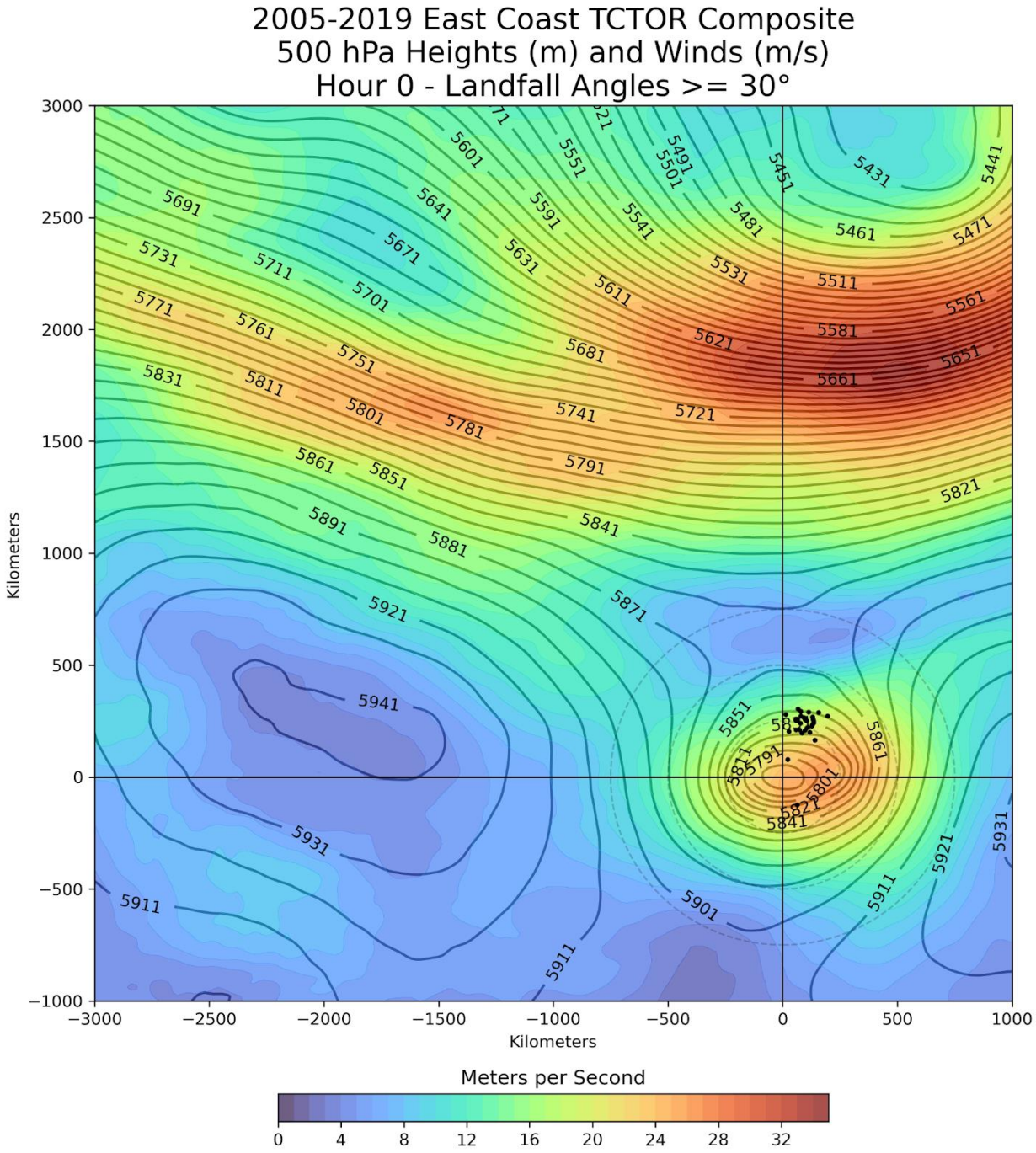

Figure 4.72: 2005-2019 East Coast Composite 500-mb Heights (m) and Winds (m/s) at the time of TCTOR occurrence including TCs with a landfall angle >= 30°. Black dots indicate TCTOR locations. Crosshairs are approximate composite TC center. Light gray dashed circles are range rings at distances 250, 500, and 750 km from TC center.

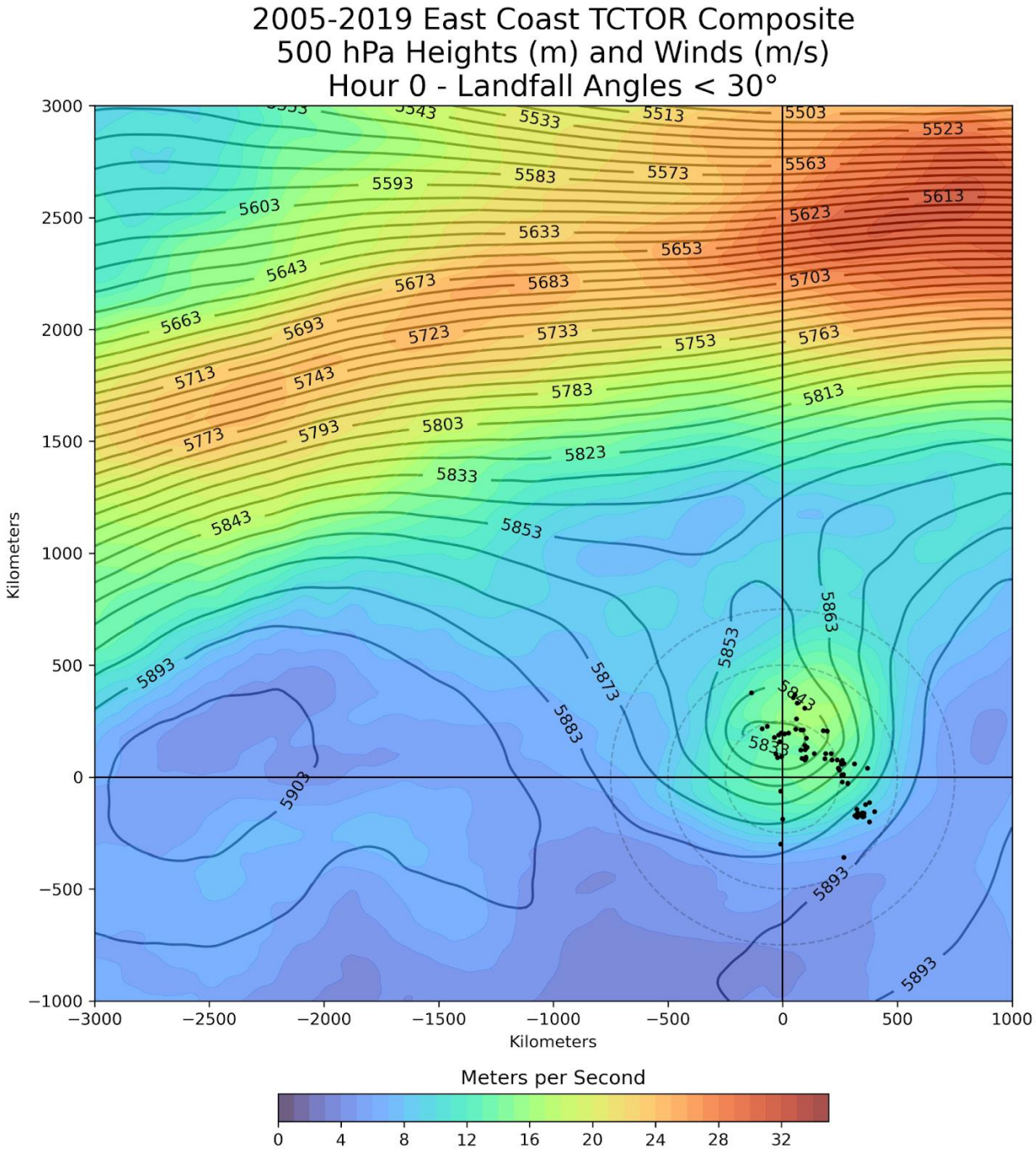

Figure 4.73: 2005-2019 East Coast Composite 500-mb Heights (m) and Winds (m/s) at the time of TCTOR occurrence including TCs with a landfall angle < 30°. Black dots indicate TCTOR locations. Crosshairs are approximate composite TC center. Light gray dashed circles are range rings at distances 250, 500, and 750 km from TC center.

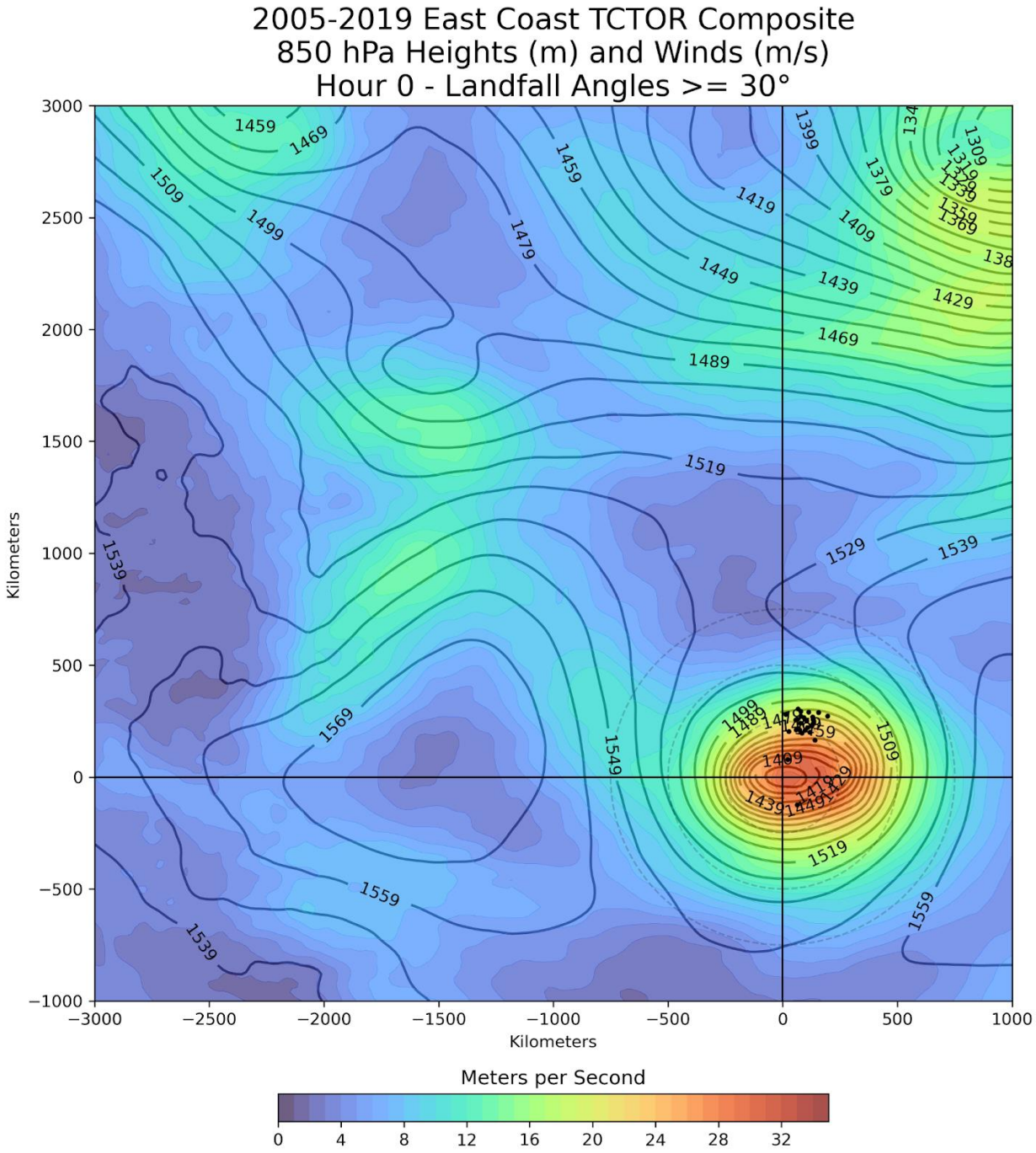

Figure 4.74: 2005-2019 East Coast Composite 850-mb Heights (m) and Winds (m/s) at the time of TCTOR occurrence including TCs with a landfall angle >= 30°. Black dots indicate TCTOR locations. Crosshairs are approximate composite TC center. Light gray dashed circles are range rings at distances 250, 500, and 750 km from TC center.

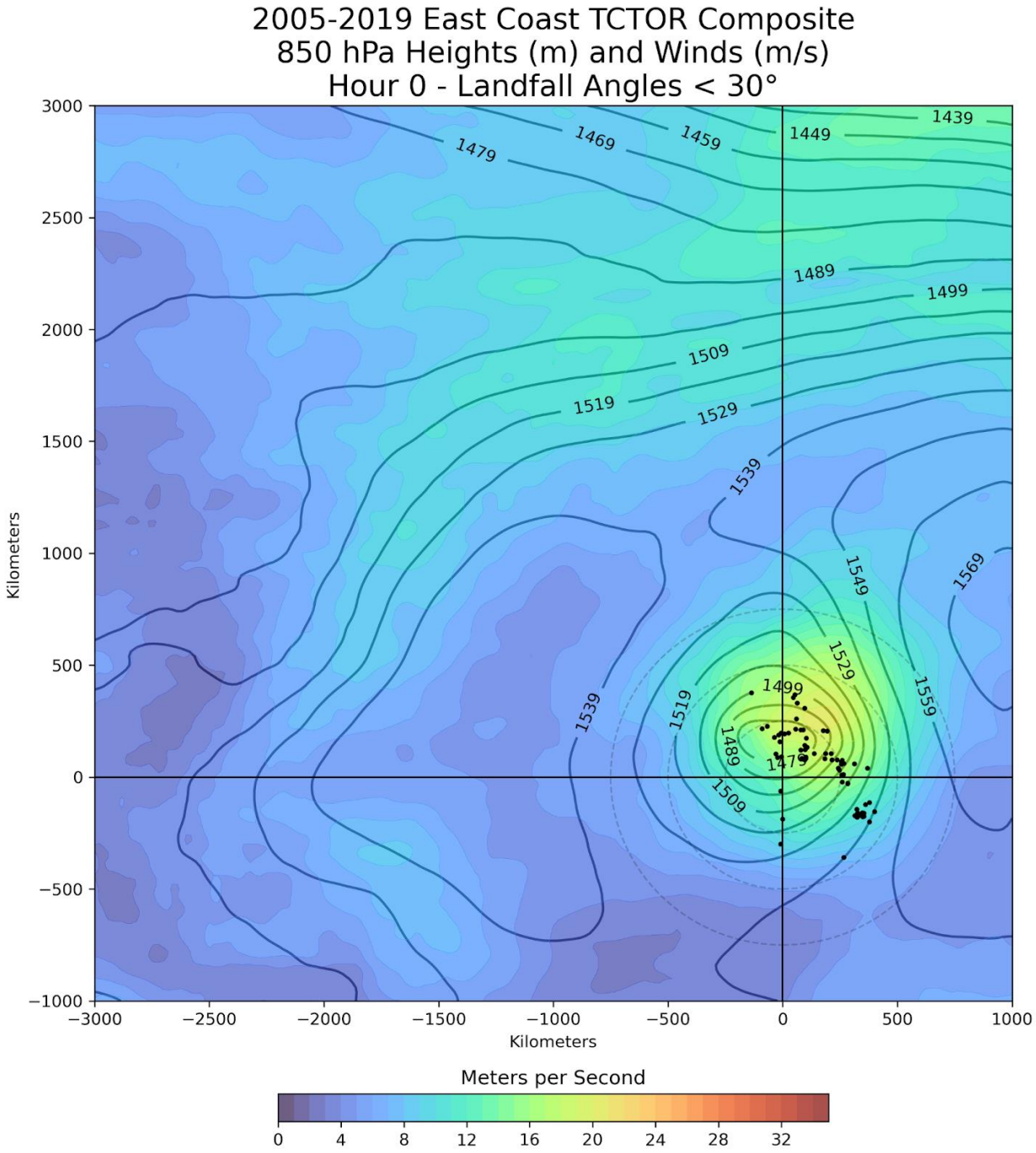

Figure 4.75: 2005-2019 East Coast Composite 850-mb Heights (m) and Winds (m/s) at the time of TCTOR occurrence including TCs with a landfall angle < 30°. Black dots indicate TCTOR locations. Crosshairs are approximate composite TC center. Light gray dashed circles are range rings at distances 250, 500, and 750 km from TC center.

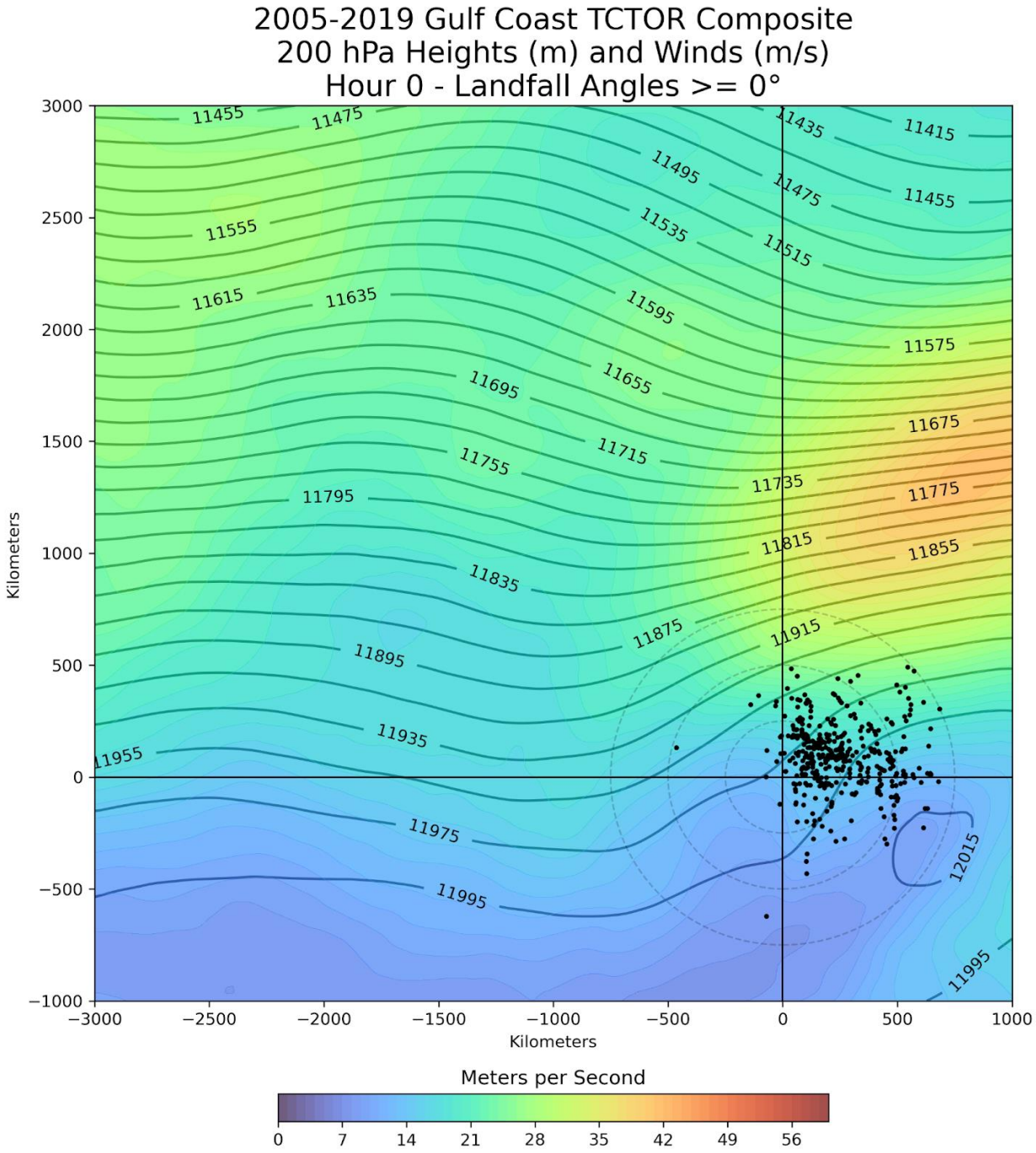

Figure 4.76: 2005-2019 Gulf Coast Composite 200-mb Heights (m) and Winds (m/s) at the time of TCTOR occurrence including TCs with a landfall angle >= 0°. Black dots indicate TCTOR locations. Crosshairs are approximate composite TC center. Light gray dashed circles are range rings at distances 250, 500, and 750 km from TC center.

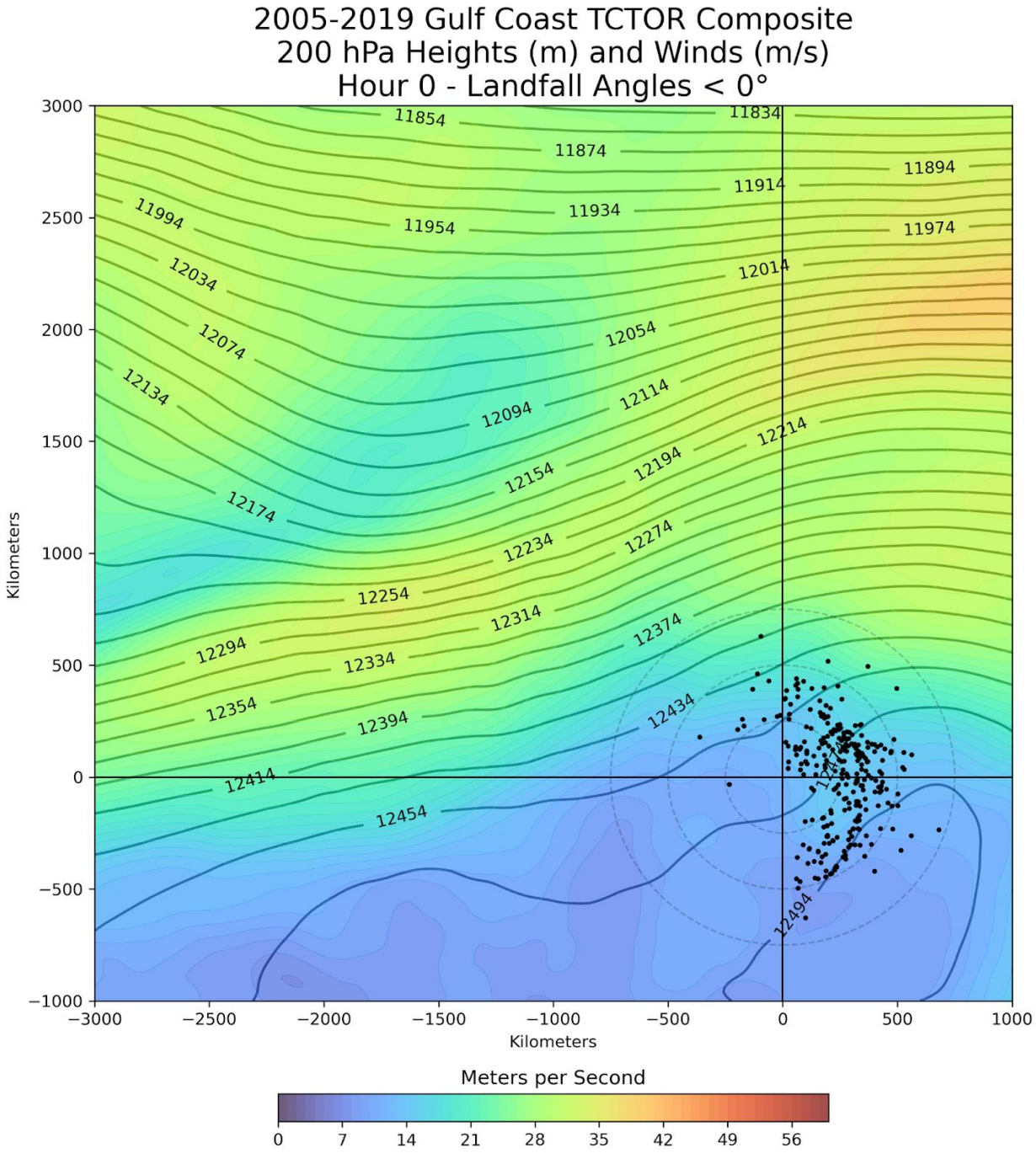

Figure 4.77: 2005-2019 Gulf Coast Composite 200-mb Heights (m) and Winds (m/s) at the time of TCTOR occurrence including TCs with a landfall angle < 0°. Black dots indicate TCTOR locations. Crosshairs are approximate composite TC center. Light gray dashed circles are range rings at distances 250, 500, and 750 km from TC center.

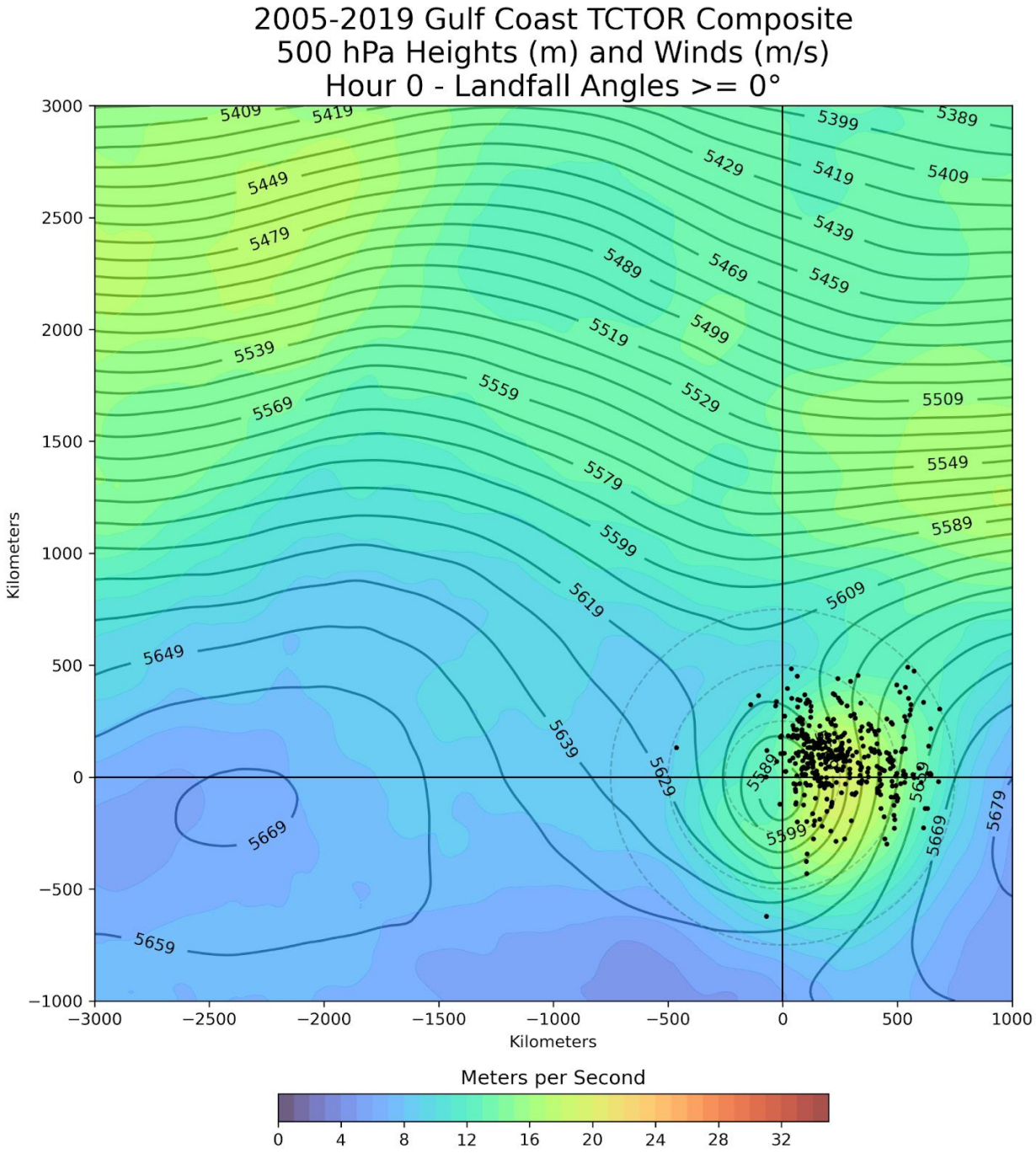

Figure 4.78: 2005-2019 Gulf Coast Composite 500-mb Heights (m) and Winds (m/s) at the time of TCTOR occurrence including TCs with a landfall angle >= 0°. Black dots indicate TCTOR locations. Crosshairs are approximate composite TC center. Light gray dashed circles are range rings at distances 250, 500, and 750 km from TC center.

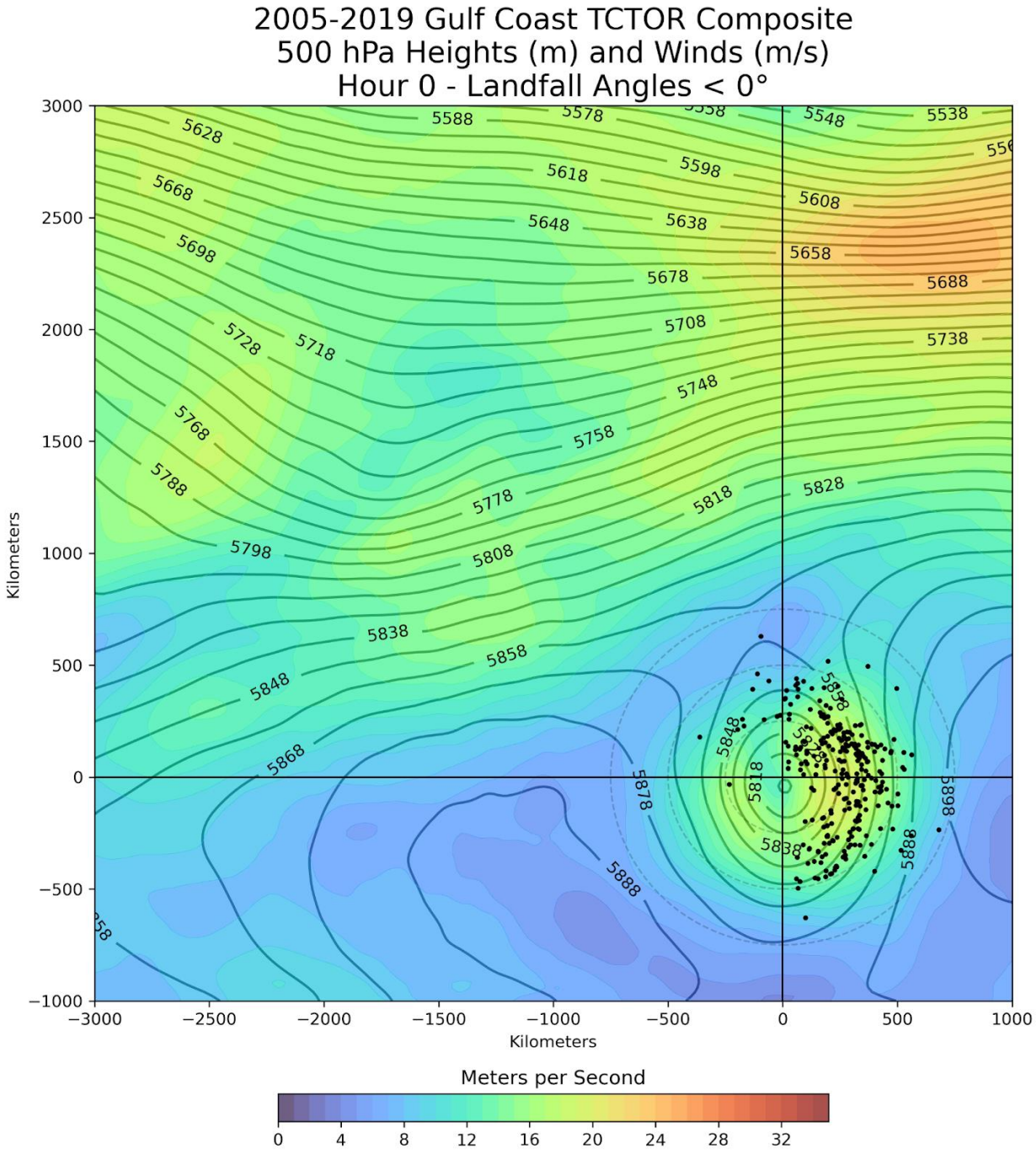

Figure 4.79: 2005-2019 Gulf Coast Composite 500-mb Heights (m) and Winds (m/s) at the time of TCTOR occurrence including TCs with a landfall angle < 0°. Black dots indicate TCTOR locations. Crosshairs are approximate composite TC center. Light gray dashed circles are range rings at distances 250, 500, and 750 km from TC center.

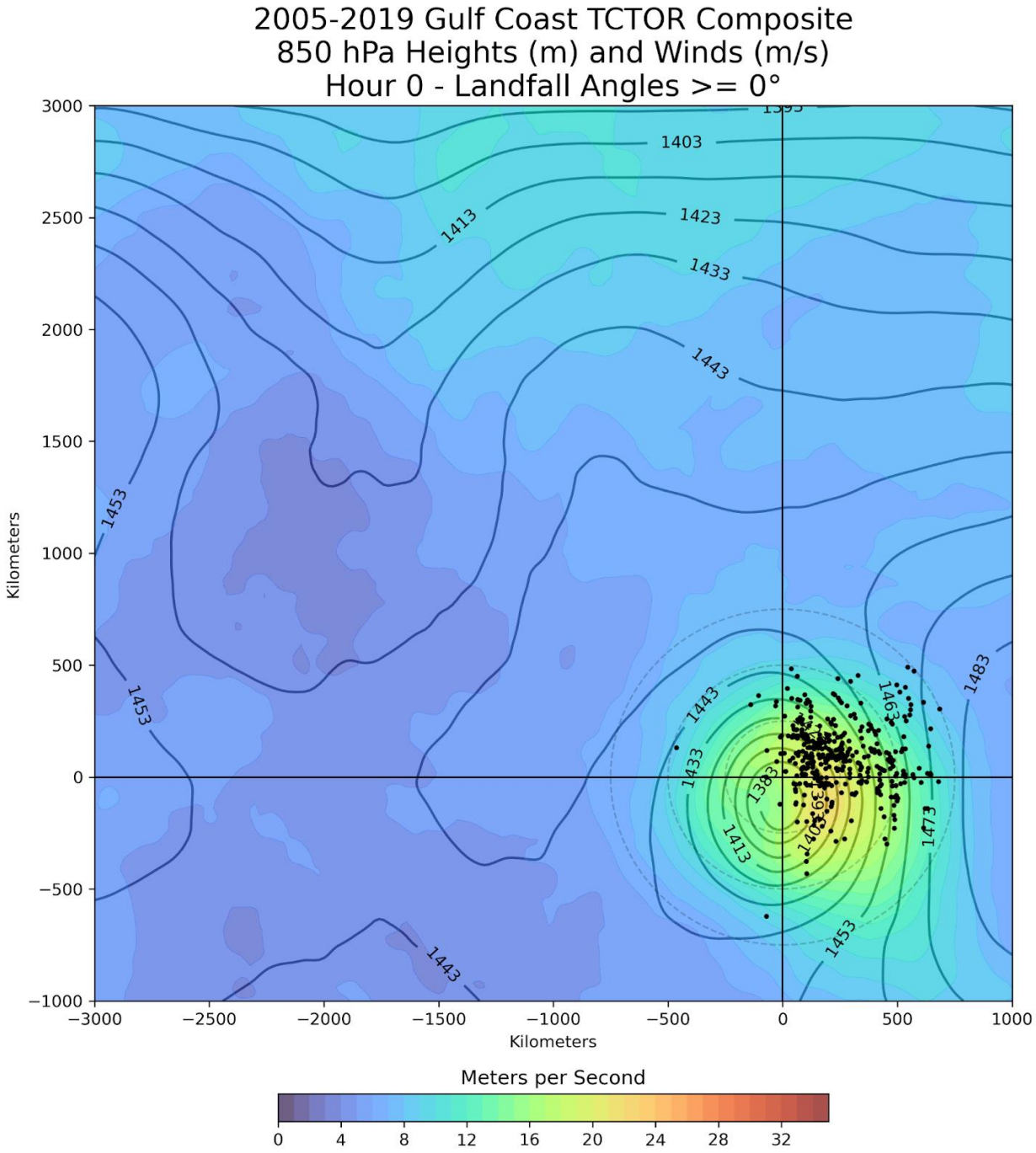

Figure 4.80: 2005-2019 Gulf Coast Composite 850-mb Heights (m) and Winds (m/s) at the time of TCTOR occurrence including TCs with a landfall angle >= 0°. Black dots indicate TCTOR locations. Crosshairs are approximate composite TC center. Light gray dashed circles are range rings at distances 250, 500, and 750 km from TC center.

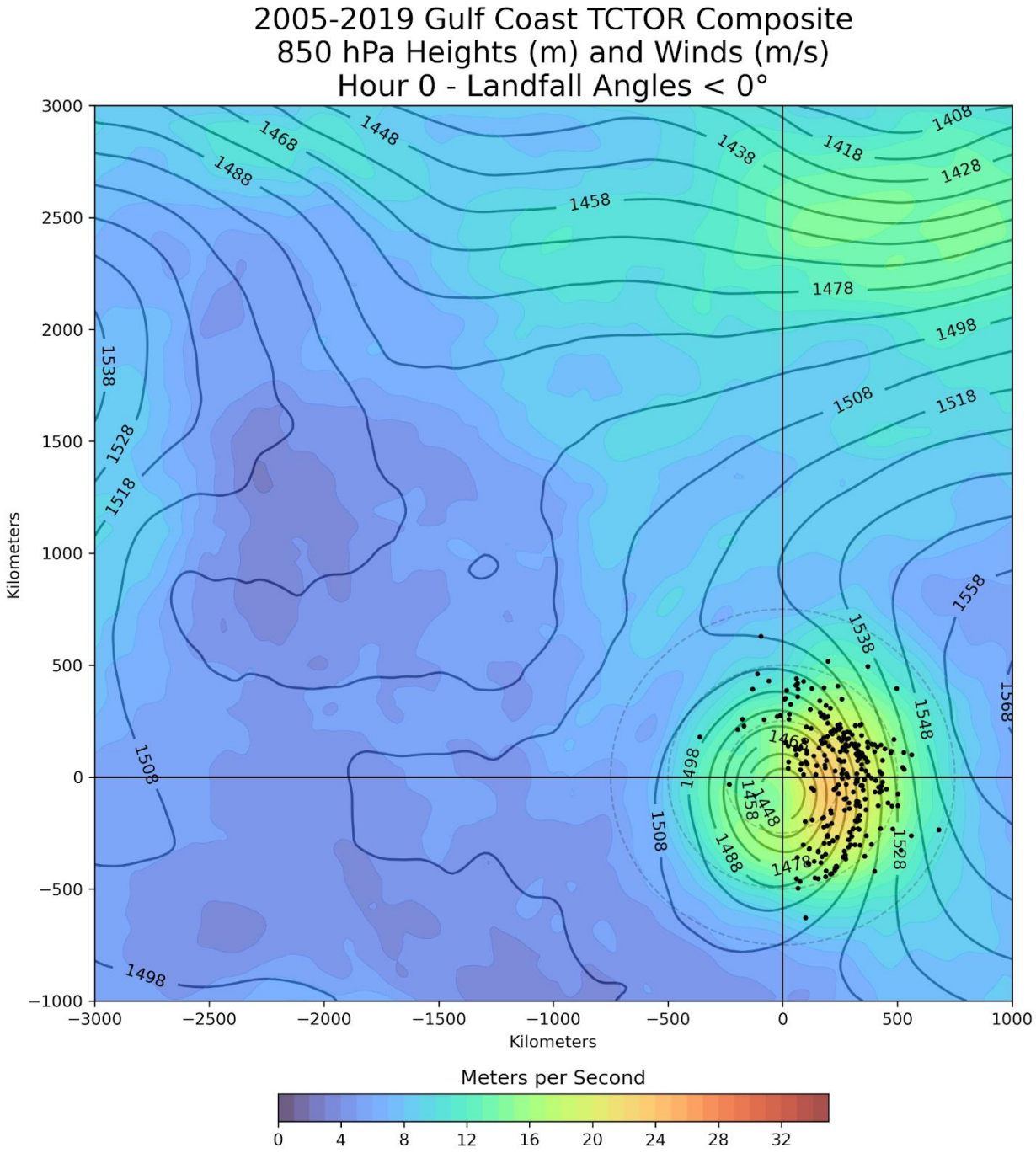

Figure 4.81: 2005-2019 Gulf Coast Composite 850-mb Heights (m) and Winds (m/s) at the time of TCTOR occurrence including TCs with a landfall angle < 0°. Black dots indicate TCTOR locations. Crosshairs are approximate composite TC center. Light gray dashed circles are range rings at distances 250, 500, and 750 km from TC center.

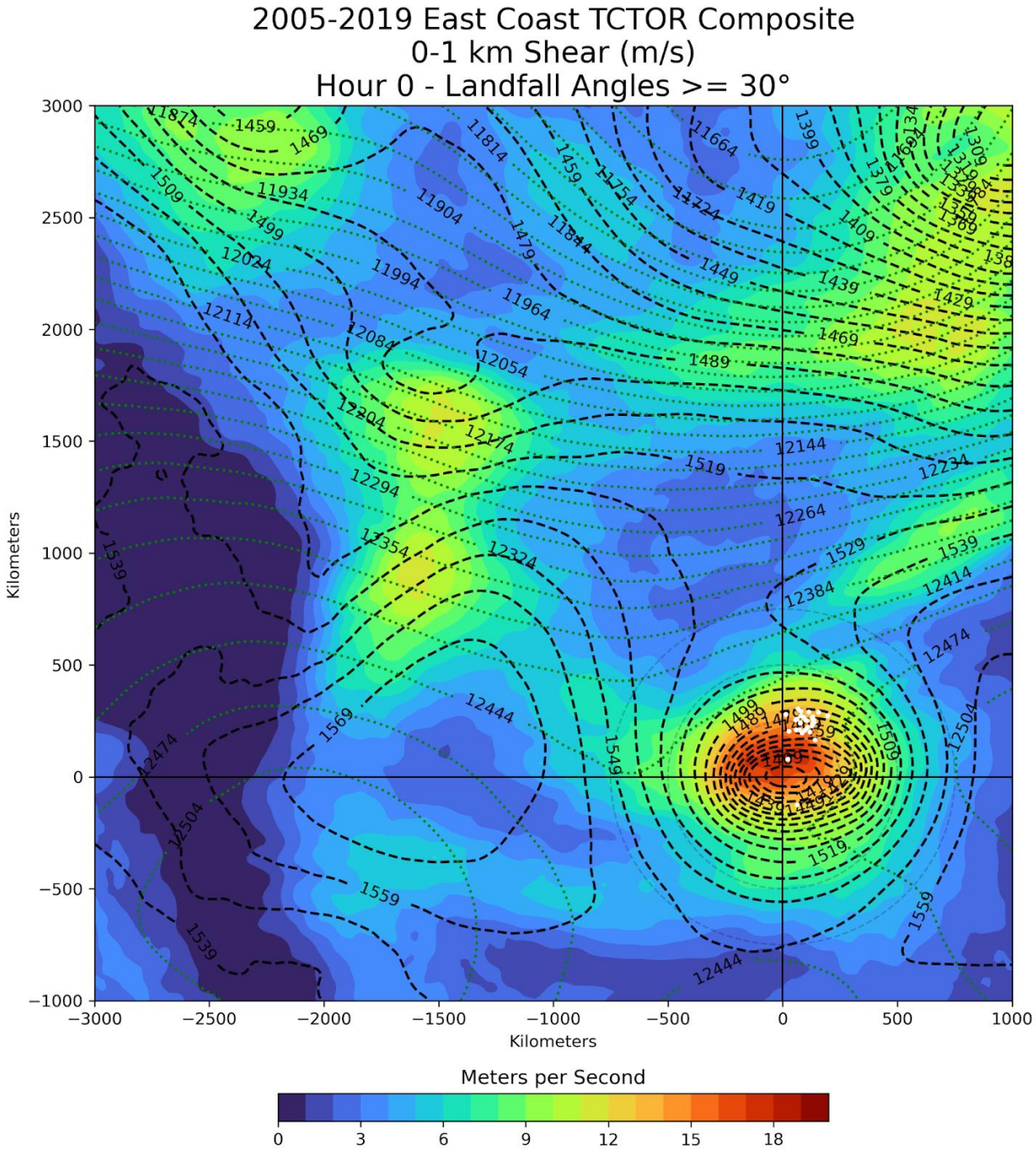

Figure 4.82: 2005-2019 East Coast Composite 0-1 km Bulk Shear (m/s) at the time of TCTOR occurrence including TCs with a landfall angle >= 30°. White dots indicate TCTOR locations. Crosshairs are approximate composite TC center. Light gray dashed circles are range rings at distances 250, 500, and 750 km from TC center. Black dashed lines are 850-mb heights (m), green dotted lines are 200-mb heights (m).

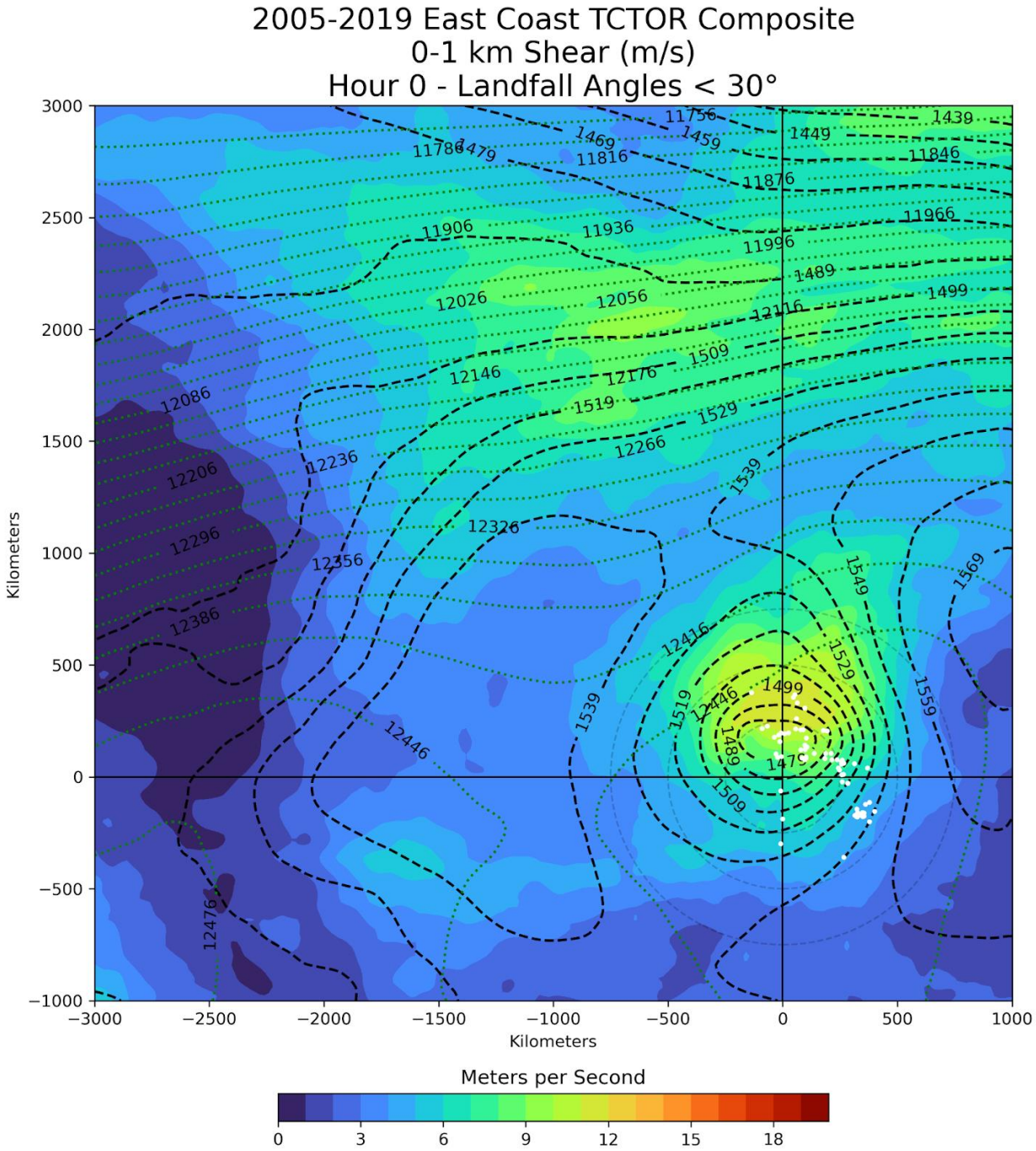

Figure 4.83: 2005-2019 East Coast Composite 0-1 km Bulk Shear (m/s) at the time of TCTOR occurrence including TCs with a landfall angle < 30°. White dots indicate TCTOR locations. Crosshairs are approximate composite TC center. Light gray dashed circles are range rings at distances 250, 500, and 750 km from TC center. Black dashed lines are 850-mb heights (m), green dotted lines are 200-mb heights (m).

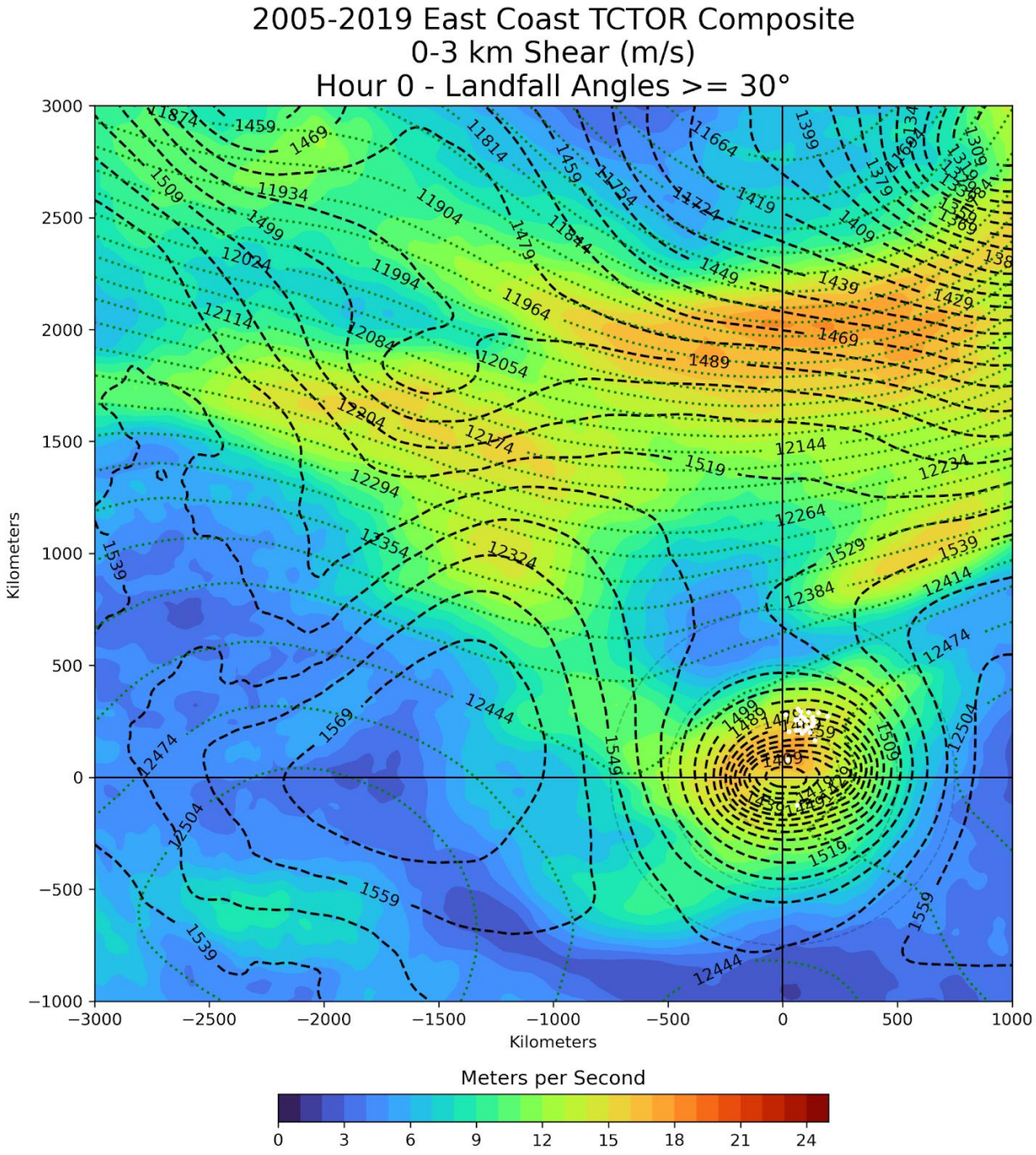

Figure 4.84: 2005-2019 East Coast Composite 0-3 km Bulk Shear (m/s) at the time of TCTOR occurrence including TCs with a landfall angle >= 30°. White dots indicate TCTOR locations. Crosshairs are approximate composite TC center. Light gray dashed circles are range rings at distances 250, 500, and 750 km from TC center. Black dashed lines are 850-mb heights (m), green dotted lines are 200-mb heights (m).

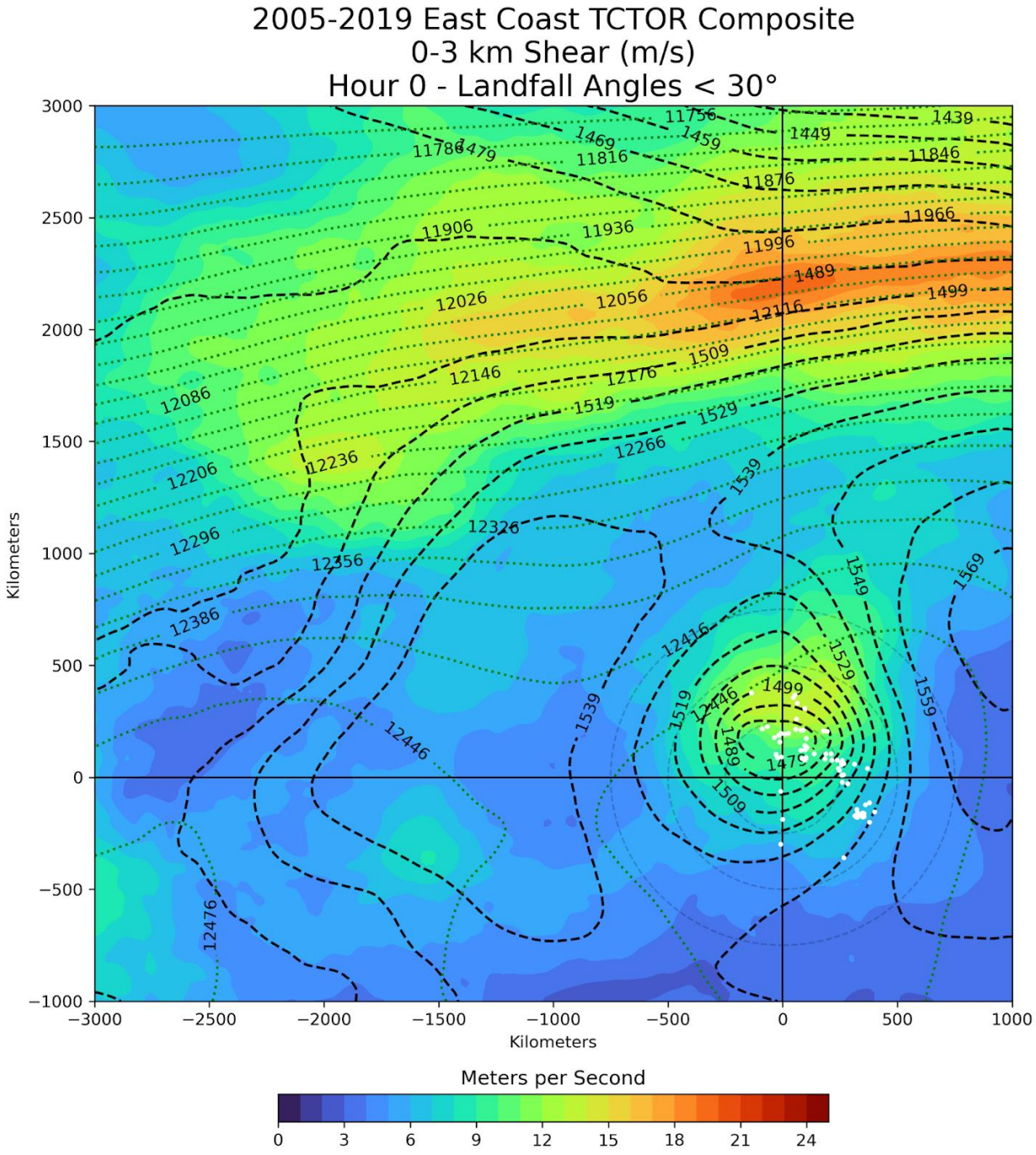

Figure 4.85: 2005-2019 East Coast Composite 0-3 km Bulk Shear (m/s) at the time of TCTOR occurrence including TCs with a landfall angle < 30°. White dots indicate TCTOR locations. Crosshairs are approximate composite TC center. Light gray dashed circles are range rings at distances 250, 500, and 750 km from TC center. Black dashed lines are 850-mb heights (m), green dotted lines are 200-mb heights (m).

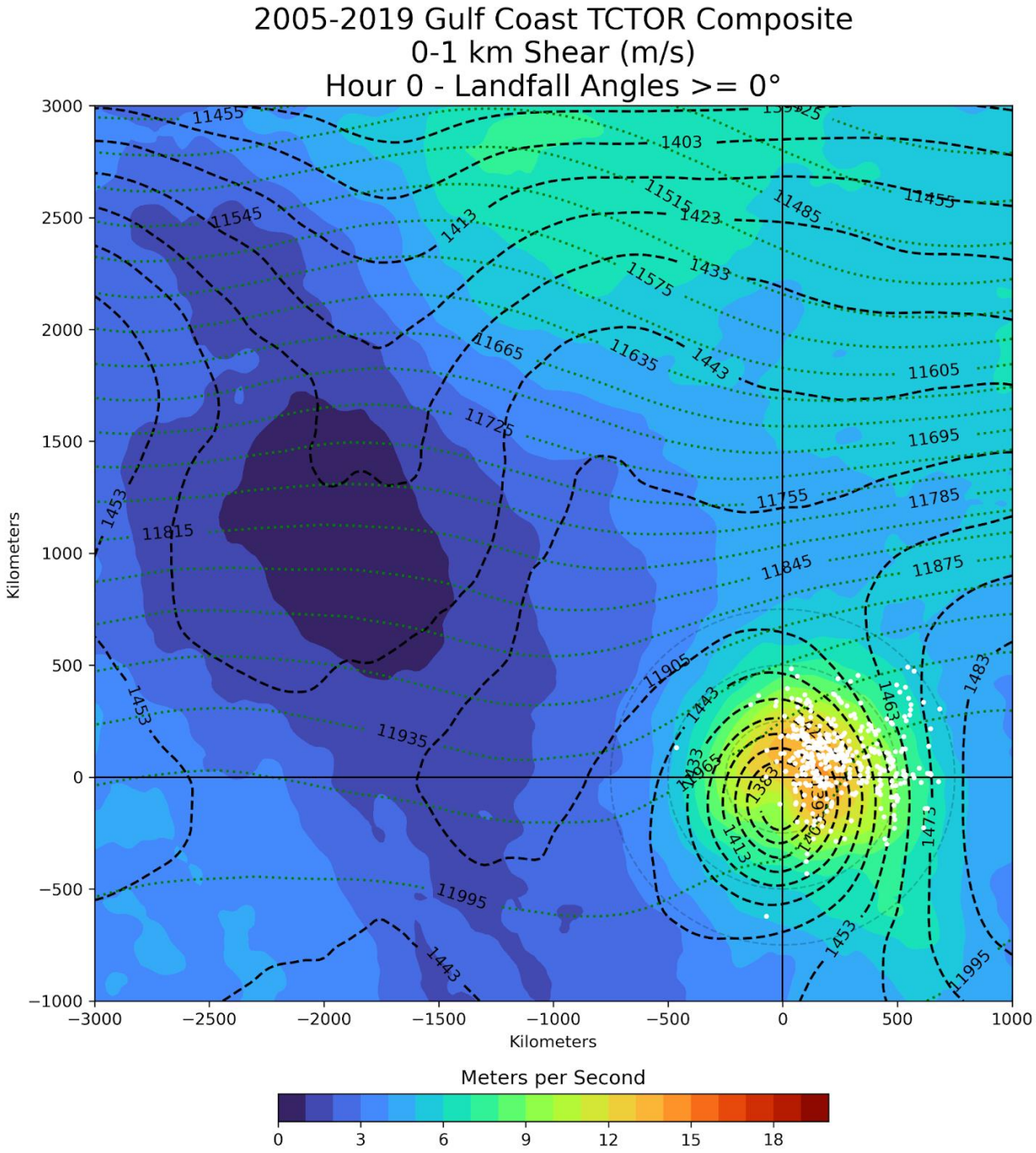

Figure 4.86: 2005-2019 Gulf Coast Composite 0-1 km Bulk Shear (m/s) at the time of TCTOR occurrence including TCs with a landfall angle >= 0°. White dots indicate TCTOR locations. Crosshairs are approximate composite TC center. Light gray dashed circles are range rings at distances 250, 500, and 750 km from TC center. Black dashed lines are 850-mb heights (m), green dotted lines are 200-mb heights (m).

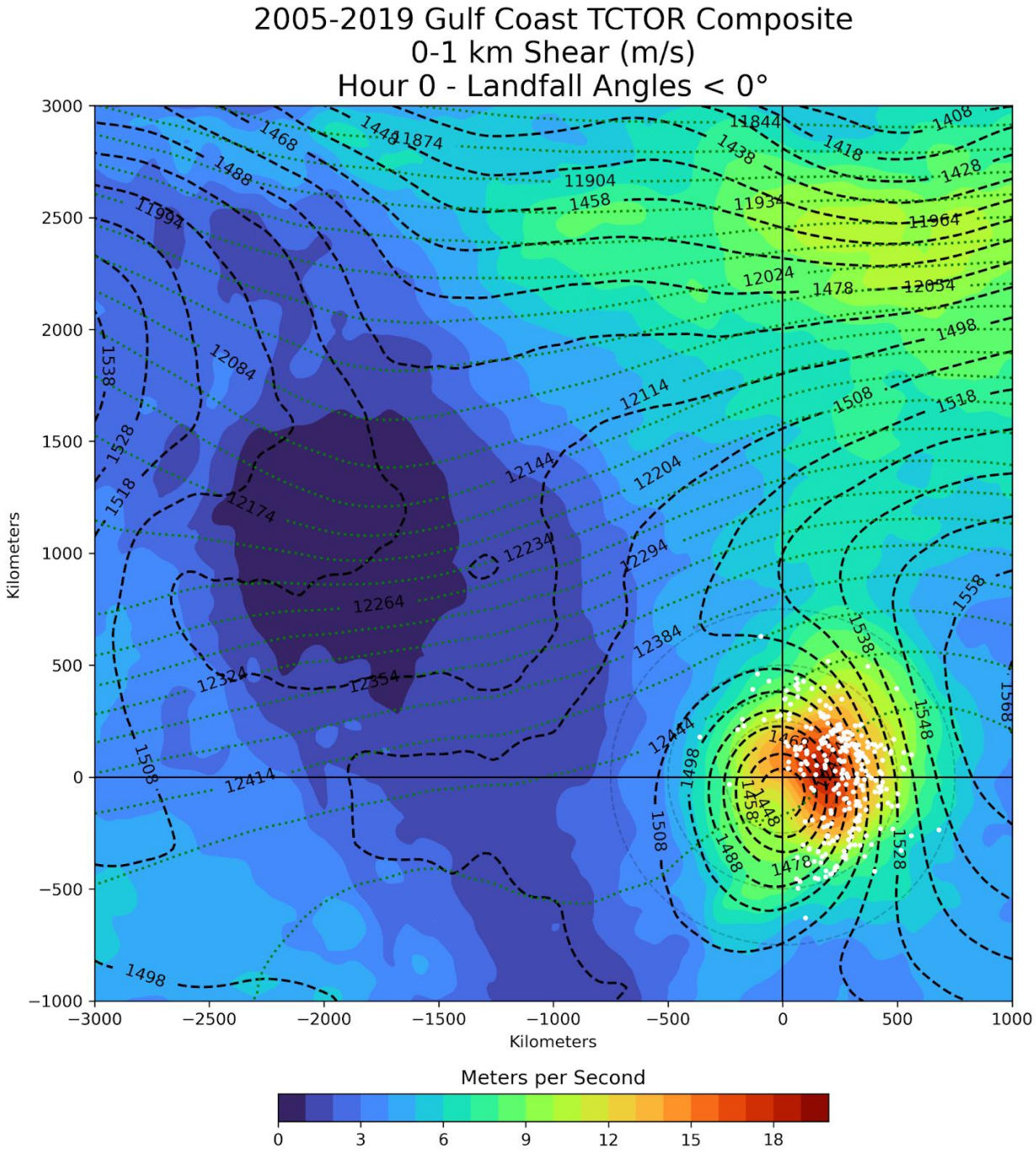

Figure 4.87: 2005-2019 Gulf Coast Composite 0-1 km Bulk Shear (m/s) at the time of TCTOR occurrence including TCs with a landfall angle < 0°. White dots indicate TCTOR locations. Crosshairs are approximate composite TC center. Light gray dashed circles are range rings at distances 250, 500, and 750 km from TC center. Black dashed lines are 850-mb heights (m), green dotted lines are 200-mb heights (m).

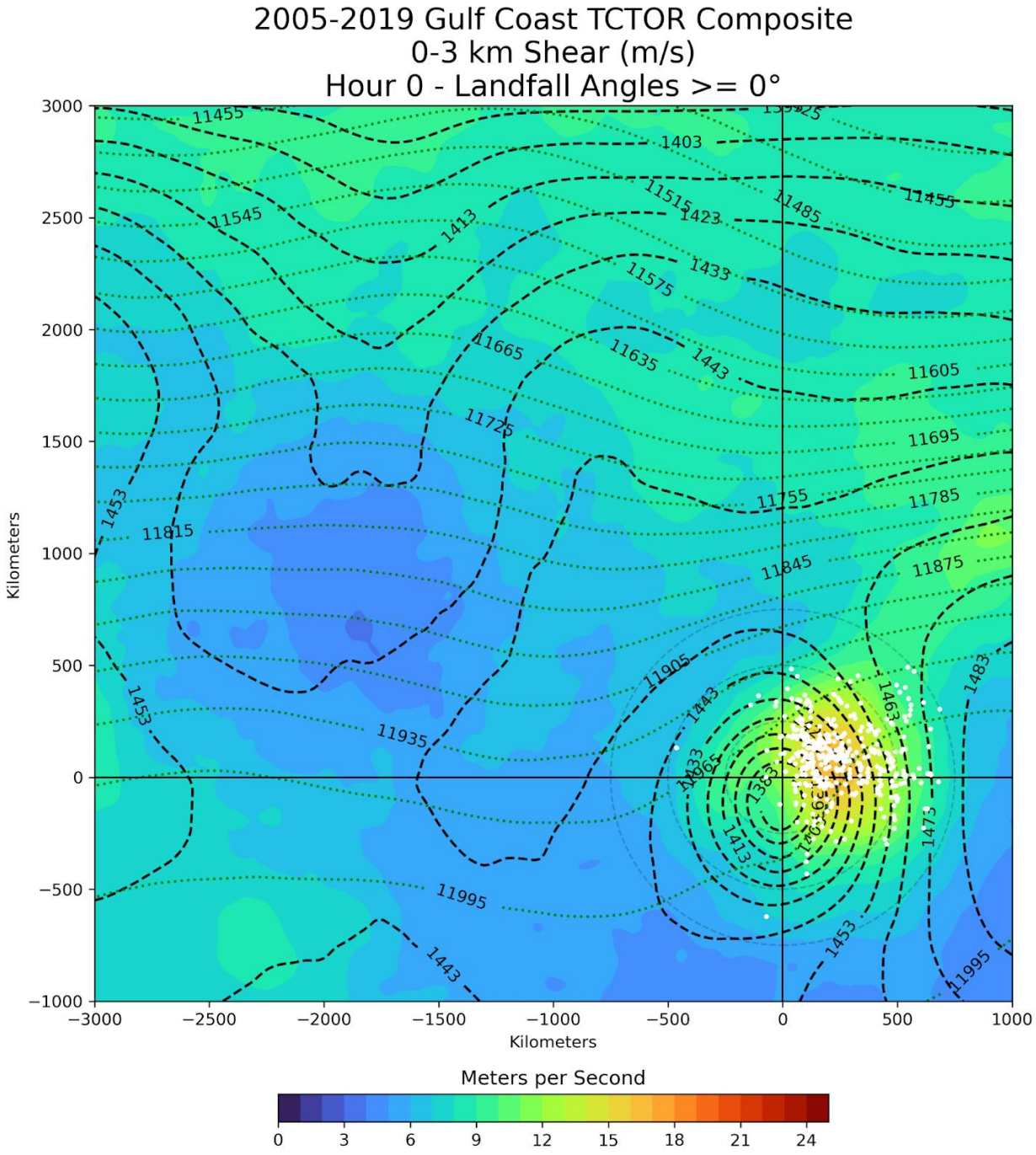

Figure 4.88: 2005-2019 Gulf Coast Composite 0-3 km Bulk Shear (m/s) at the time of TCTOR occurrence including TCs with a landfall angle >= 0°. White dots indicate TCTOR locations. Crosshairs are approximate composite TC center. Light gray dashed circles are range rings at distances 250, 500, and 750 km from TC center. Black dashed lines are 850-mb heights (m), green dotted lines are 200-mb heights (m).

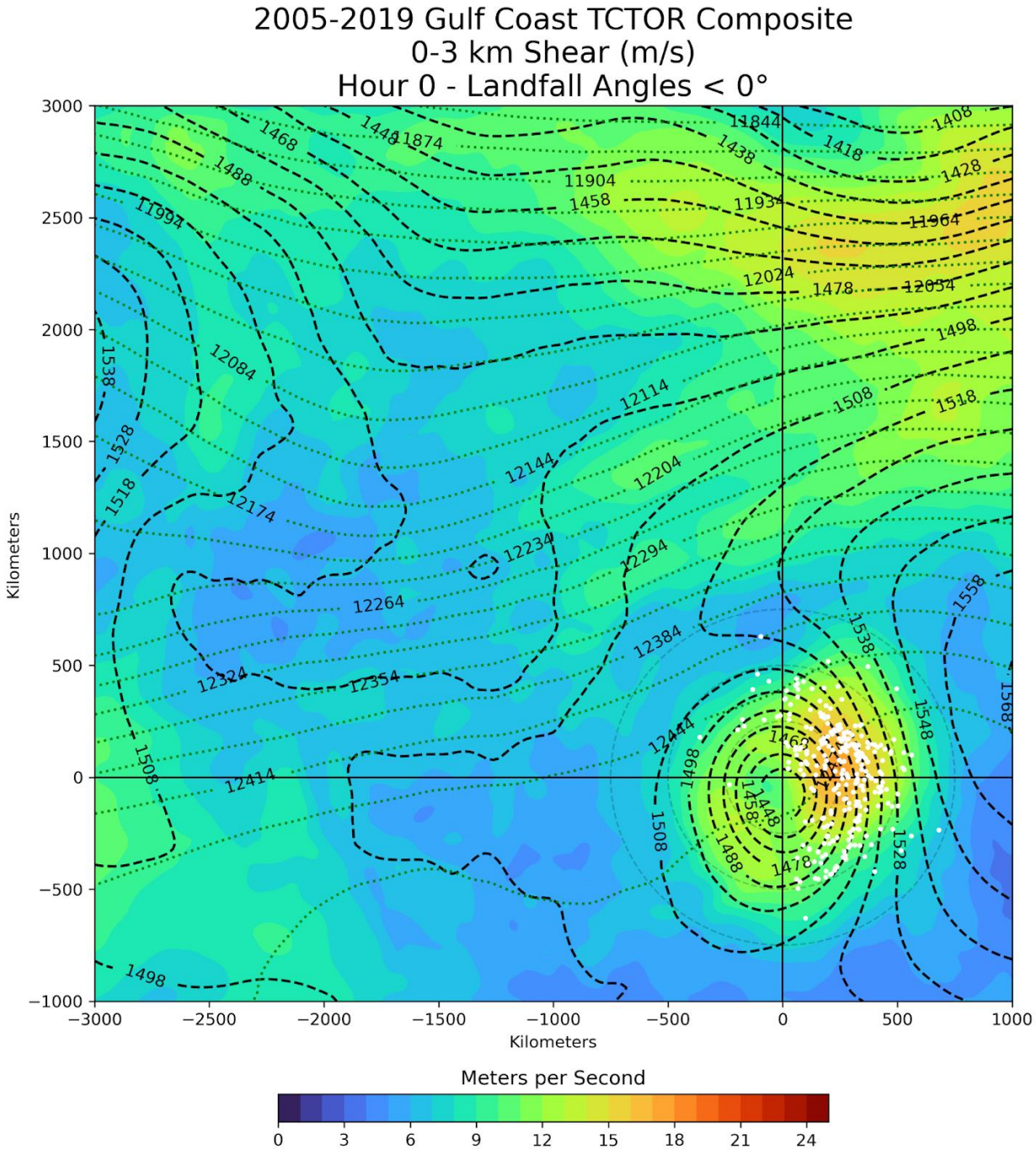

Figure 4.89: 2005-2019 Gulf Coast Composite 0-3 km Bulk Shear (m/s) at the time of TCTOR occurrence including TCs with a landfall angle < 0°. White dots indicate TCTOR locations. Crosshairs are approximate composite TC center. Light gray dashed circles are range rings at distances 250, 500, and 750 km from TC center. Black dashed lines are 850-mb heights (m), green dotted lines are 200-mb heights (m).

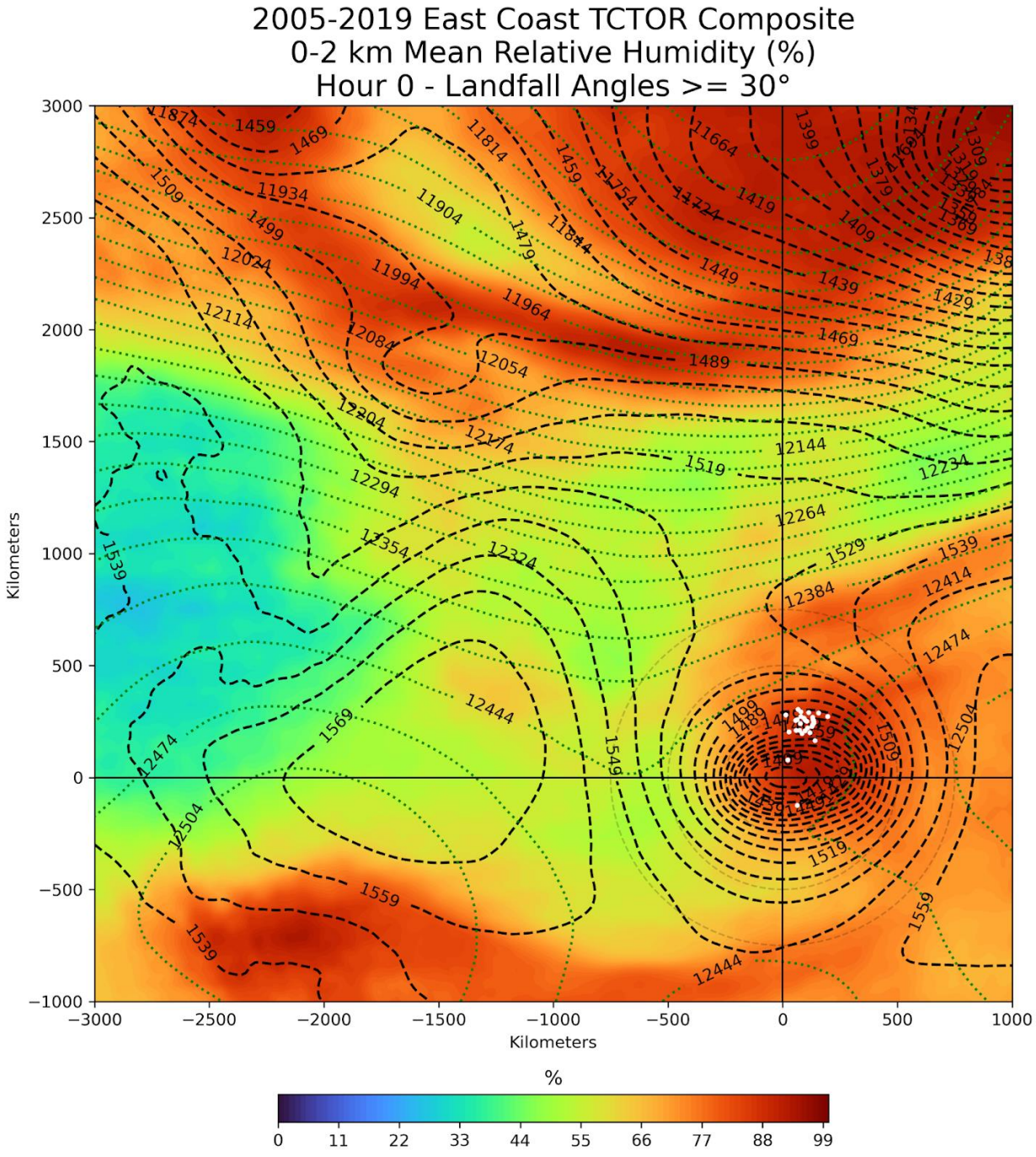

Figure 4.90: 2005-2019 East Coast Composite 0-2 km Mean Relative Humidity (%) at the time of TCTOR occurrence including TCs with a landfall angle >= 30°. White dots indicate TCTOR locations. Crosshairs are approximate composite TC center. Light gray dashed circles are range rings at distances 250, 500, and 750 km from TC center. Black dashed lines are 850-mb heights (m), green dotted lines are 200-mb heights (m).

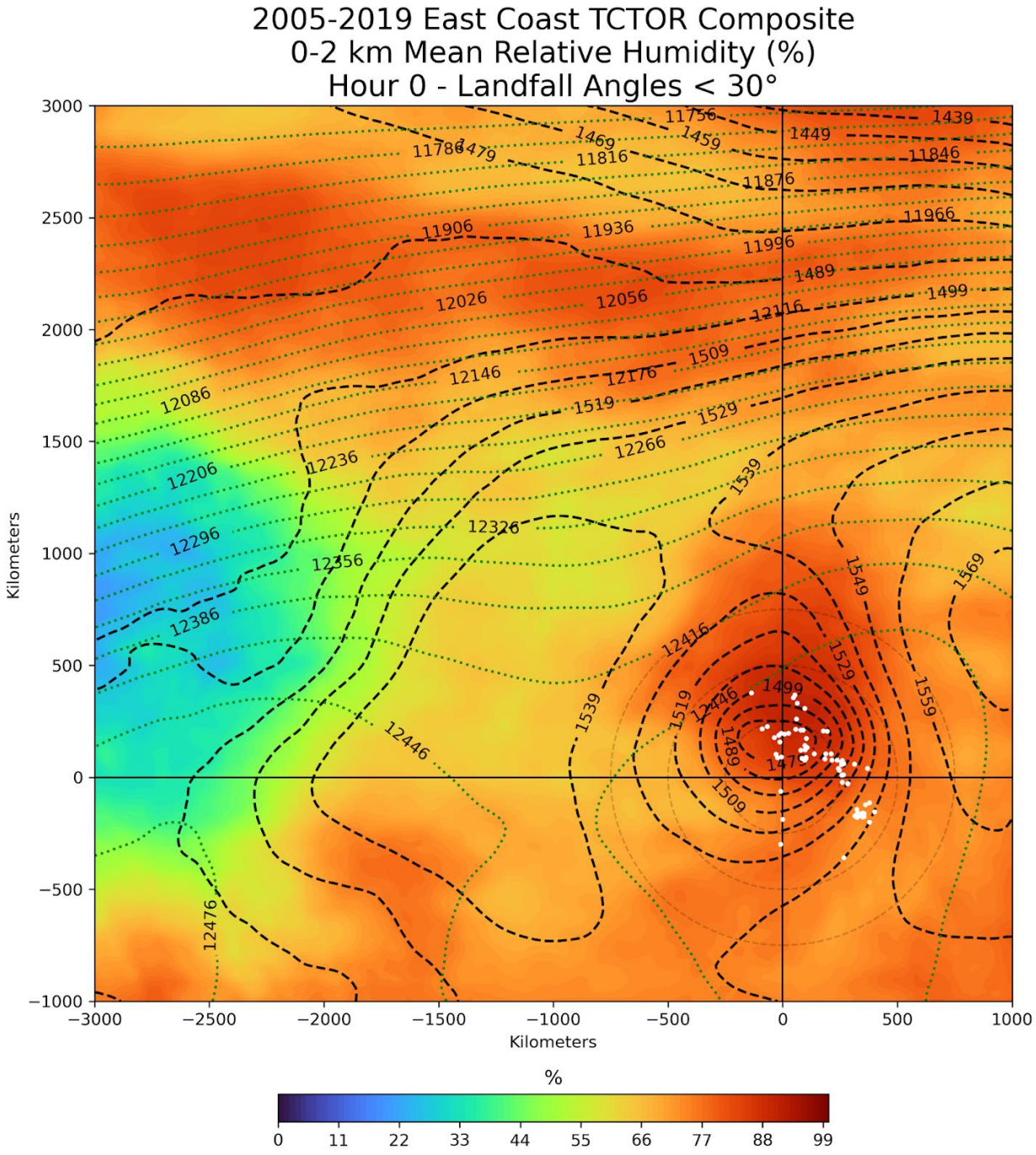

Figure 4.91: 2005-2019 East Coast Composite 0-2 km Mean Relative Humidity (%) at the time of TCTOR occurrence including TCs with a landfall angle < 30°. White dots indicate TCTOR locations. Crosshairs are approximate composite TC center. Light gray dashed circles are range rings at distances 250, 500, and 750 km from TC center. Black dashed lines are 850-mb heights (m), green dotted lines are 200-mb heights (m).

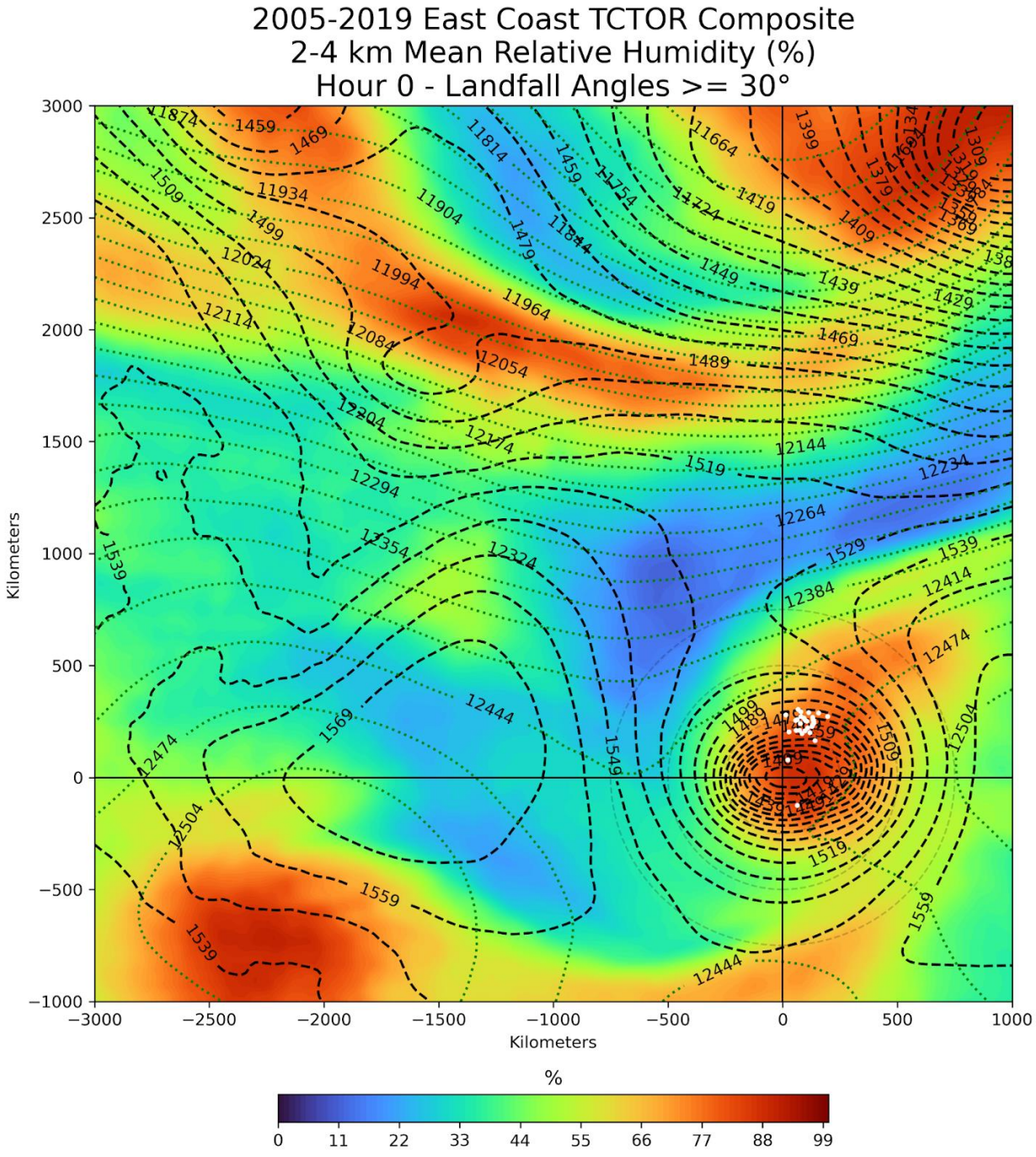

Figure 4.92: 2005-2019 East Coast Composite 2-4 km Mean Relative Humidity (%) at the time of TCTOR occurrence including TCs with a landfall angle >= 30°. White dots indicate TCTOR locations. Crosshairs are approximate composite TC center. Light gray dashed circles are range rings at distances 250, 500, and 750 km from TC center. Black dashed lines are 850-mb heights (m), green dotted lines are 200-mb heights (m).

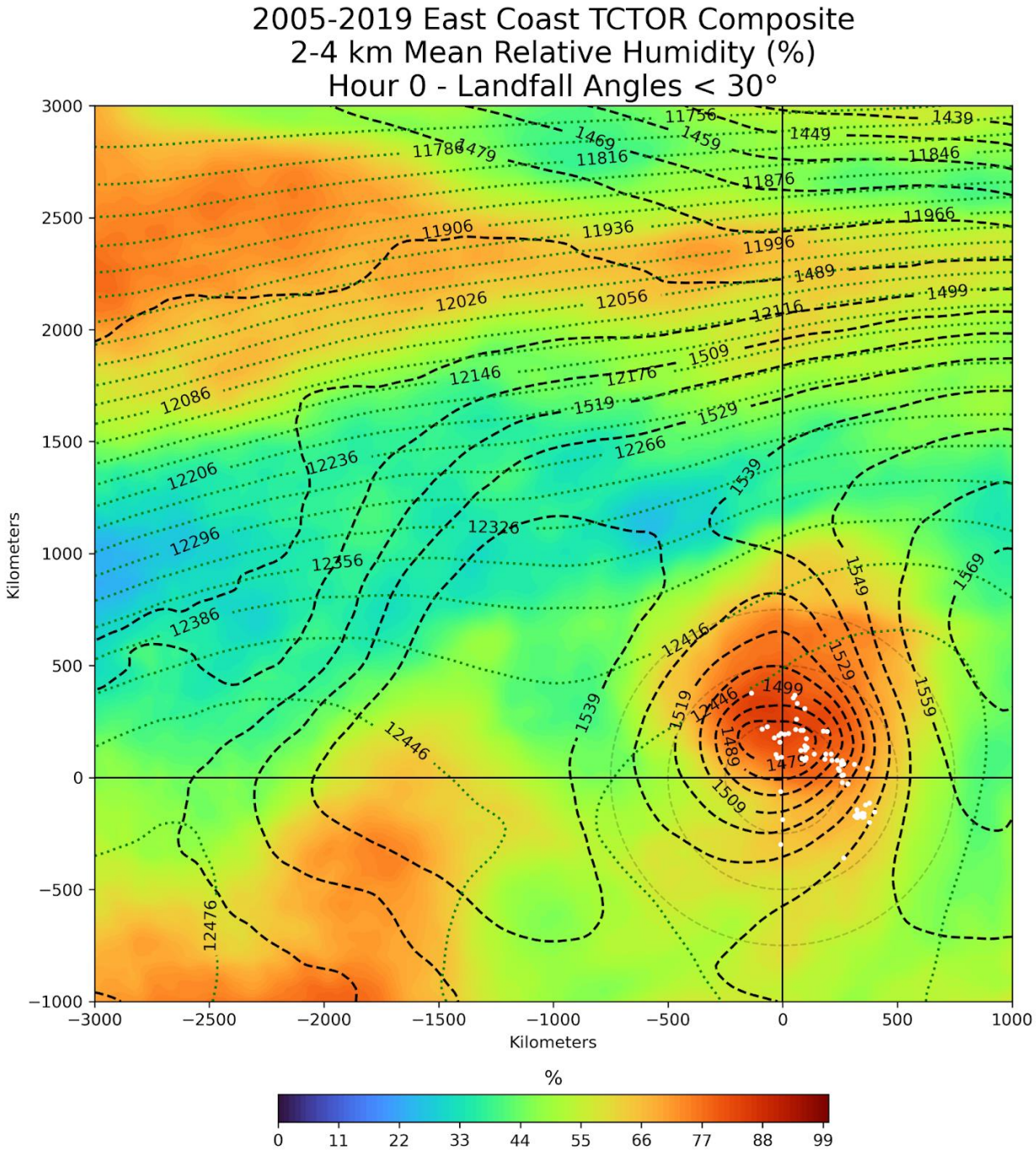

Figure 4.93: 2005-2019 East Coast Composite 2-4 km Mean Relative Humidity (%) at the time of TCTOR occurrence including TCs with a landfall angle < 30°. White dots indicate TCTOR locations. Crosshairs are approximate composite TC center. Light gray dashed circles are range rings at distances 250, 500, and 750 km from TC center. Black dashed lines are 850-mb heights (m), green dotted lines are 200-mb heights (m).

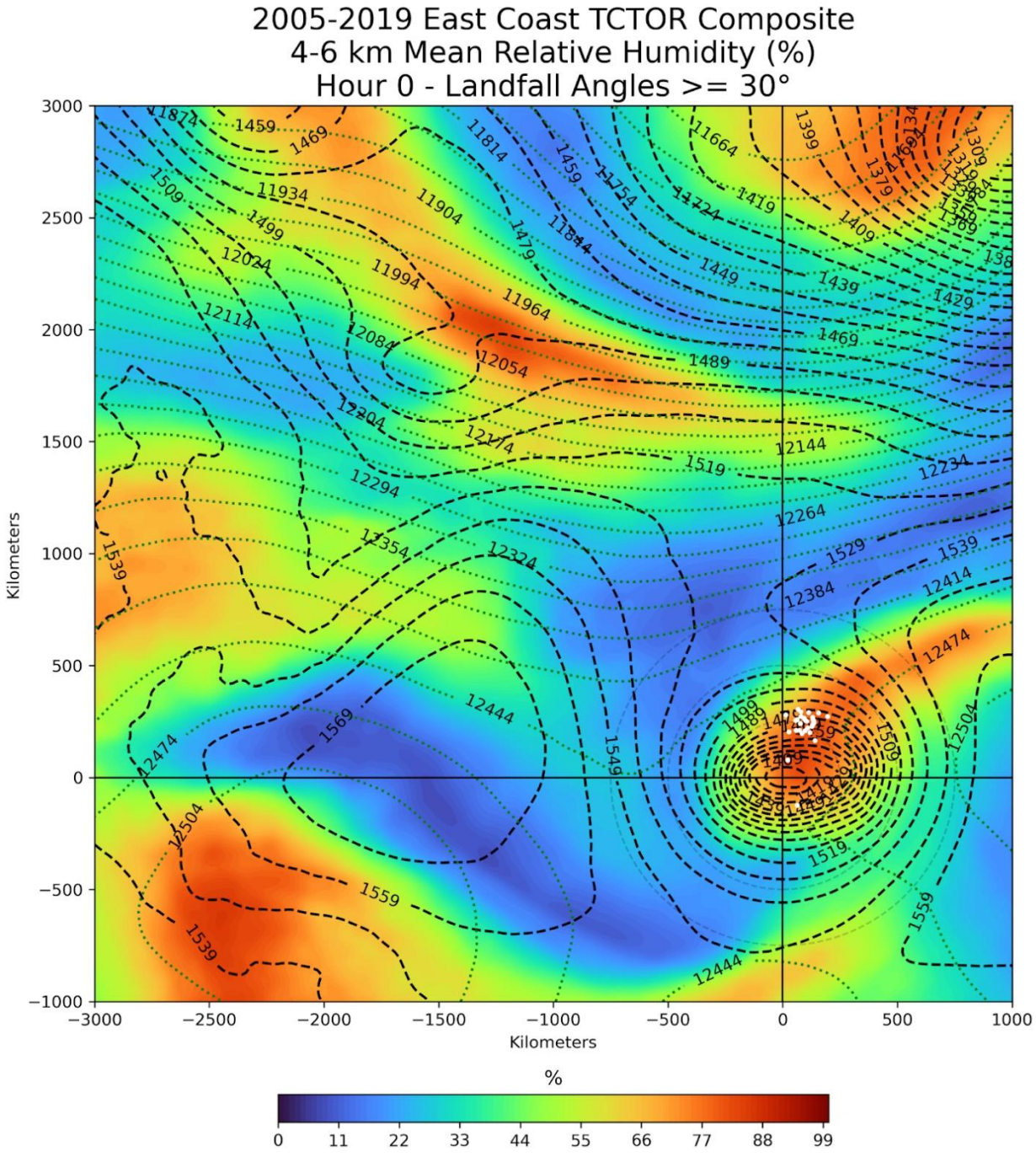

Figure 4.94: 2005-2019 East Coast Composite 4-6 km Mean Relative Humidity (%) at the time of TCTOR occurrence including TCs with a landfall angle >= 30°. White dots indicate TCTOR locations. Crosshairs are approximate composite TC center. Light gray dashed circles are range rings at distances 250, 500, and 750 km from TC center. Black dashed lines are 850-mb heights (m), green dotted lines are 200-mb heights (m).

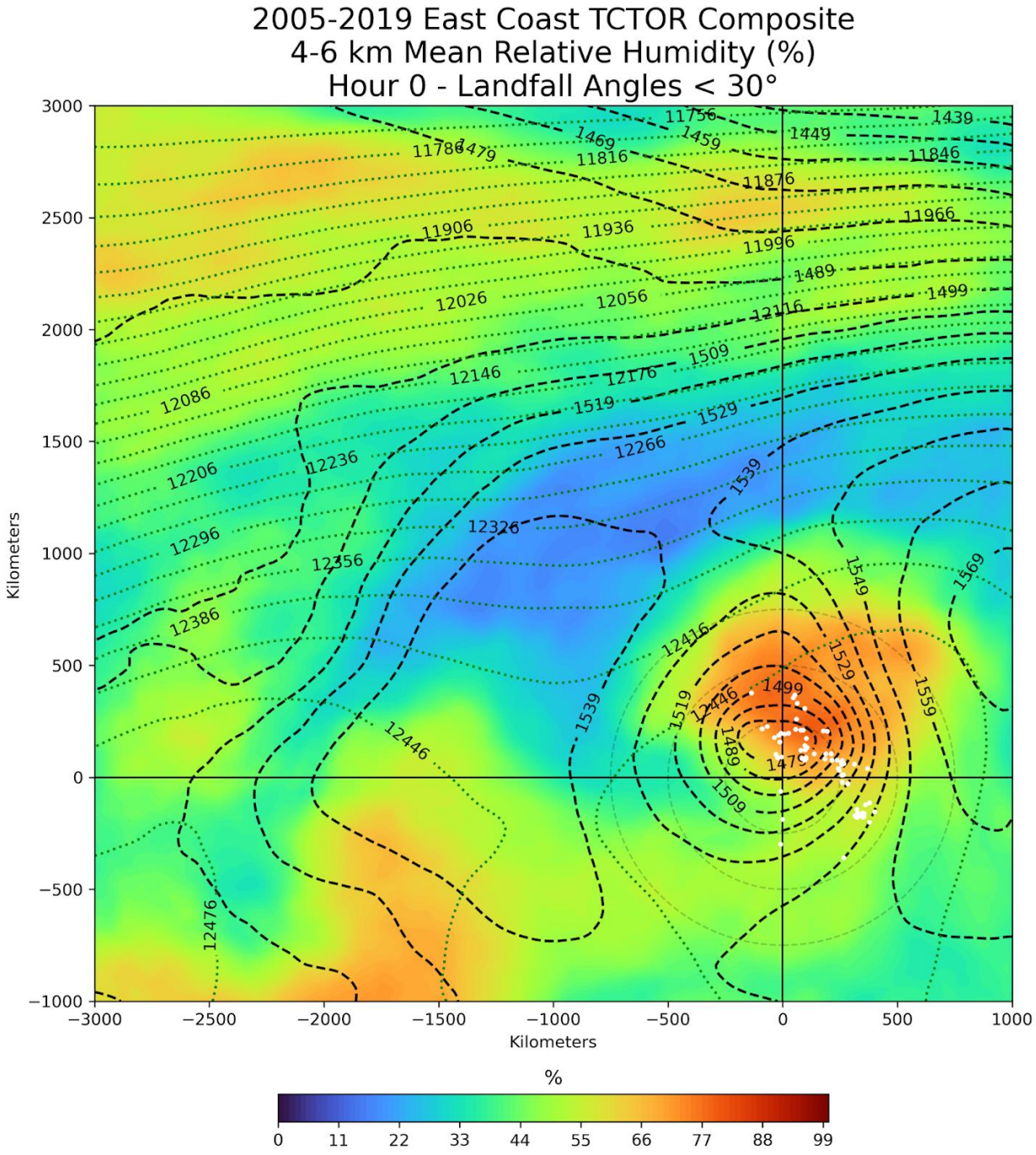

Figure 4.95: 2005-2019 East Coast Composite 4-6 km Mean Relative Humidity (%) at the time of TCTOR occurrence including TCs with a landfall angle < 30°. White dots indicate TCTOR locations. Crosshairs are approximate composite TC center. Light gray dashed circles are range rings at distances 250, 500, and 750 km from TC center. Black dashed lines are 850-mb heights (m), green dotted lines are 200-mb heights (m).

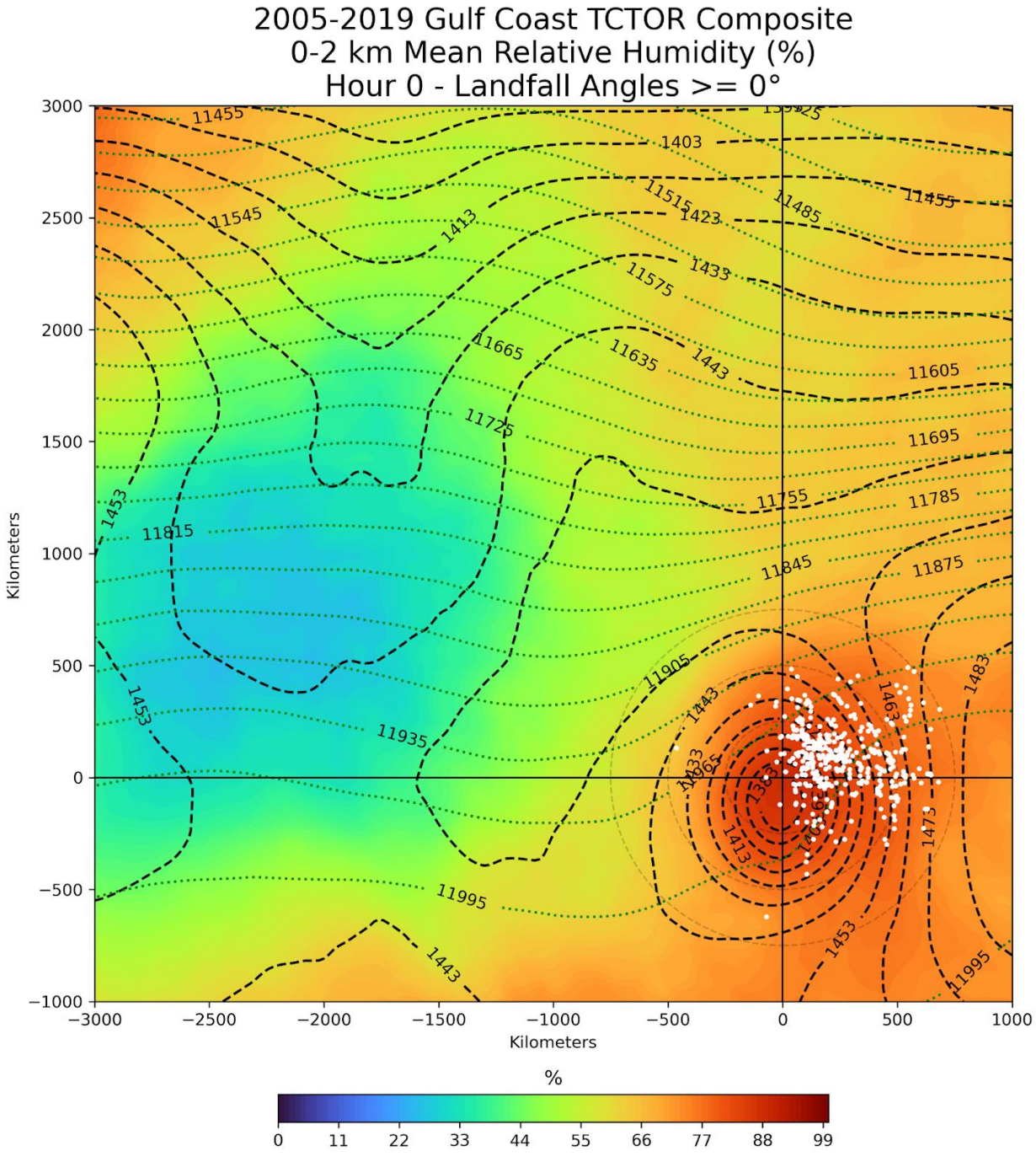

Figure 4.96: 2005-2019 Gulf Coast Composite 0-2 km Mean Relative Humidity (%) at the time of TCTOR occurrence including TCs with a landfall angle >= 0°. White dots indicate TCTOR locations. Crosshairs are approximate composite TC center. Light gray dashed circles are range rings at distances 250, 500, and 750 km from TC center. Black dashed lines are 850-mb heights (m), green dotted lines are 200-mb heights (m).

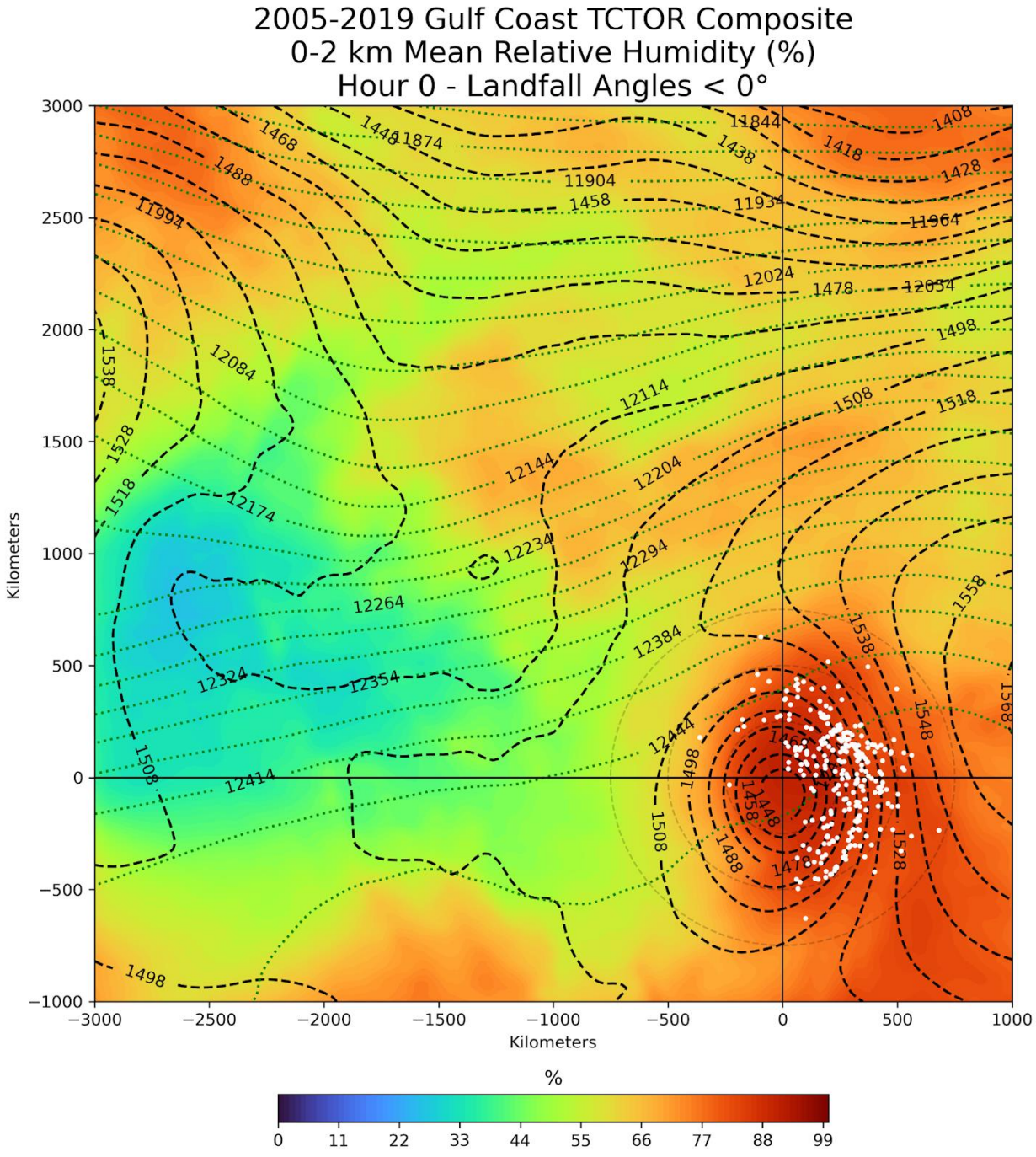

Figure 4.97: 2005-2019 Gulf Coast Composite 0-2 km Mean Relative Humidity (%) at the time of TCTOR occurrence including TCs with a landfall angle < 0°. White dots indicate TCTOR locations. Crosshairs are approximate composite TC center. Light gray dashed circles are range rings at distances 250, 500, and 750 km from TC center. Black dashed lines are 850-mb heights (m), green dotted lines are 200-mb heights (m).

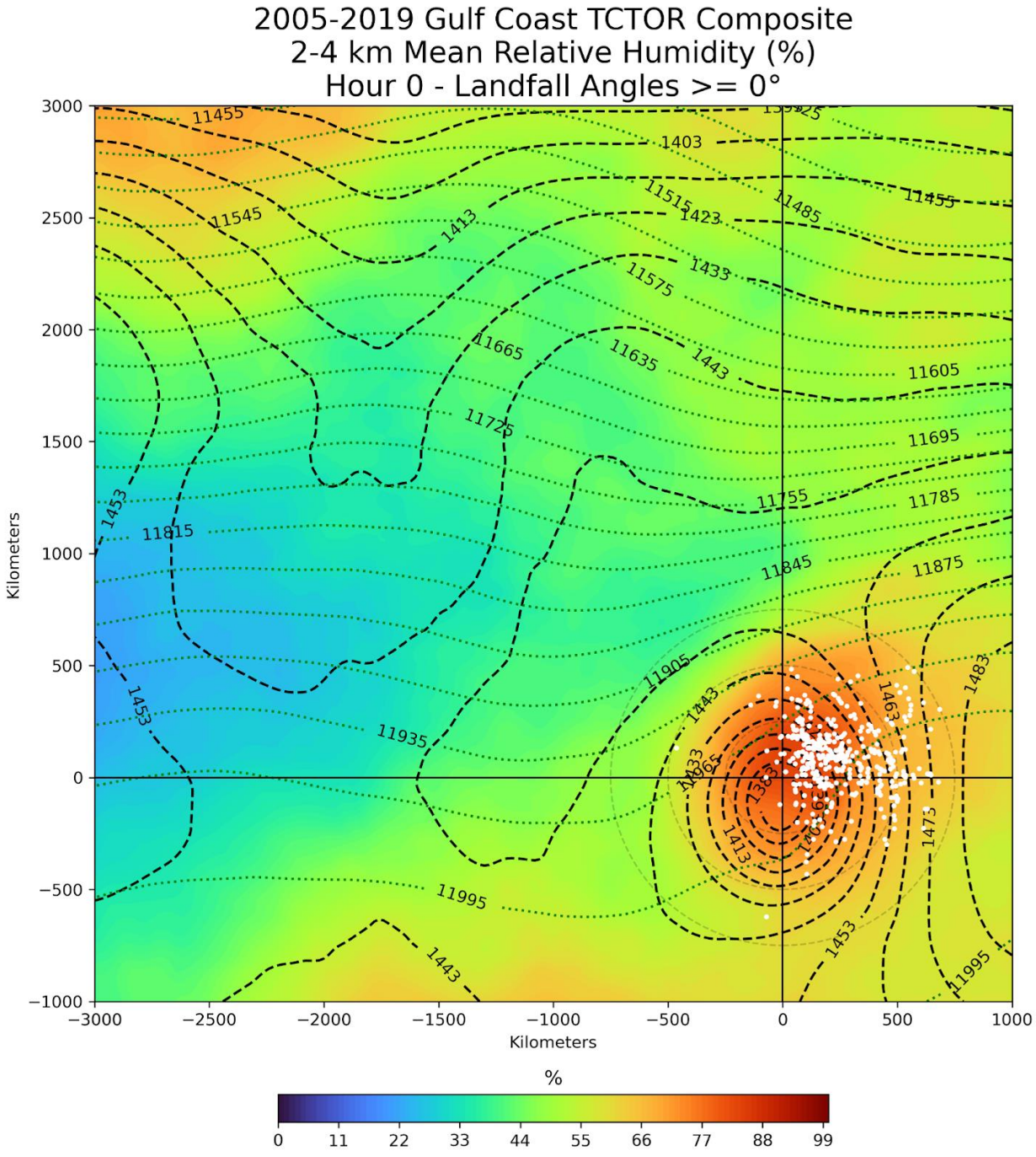

Figure 4.98: 2005-2019 Gulf Coast Composite 2-4 km Mean Relative Humidity (%) at the time of TCTOR occurrence including TCs with a landfall angle >= 0°. White dots indicate TCTOR locations. Crosshairs are approximate composite TC center. Light gray dashed circles are range rings at distances 250, 500, and 750 km from TC center. Black dashed lines are 850-mb heights (m), green dotted lines are 200-mb heights (m).

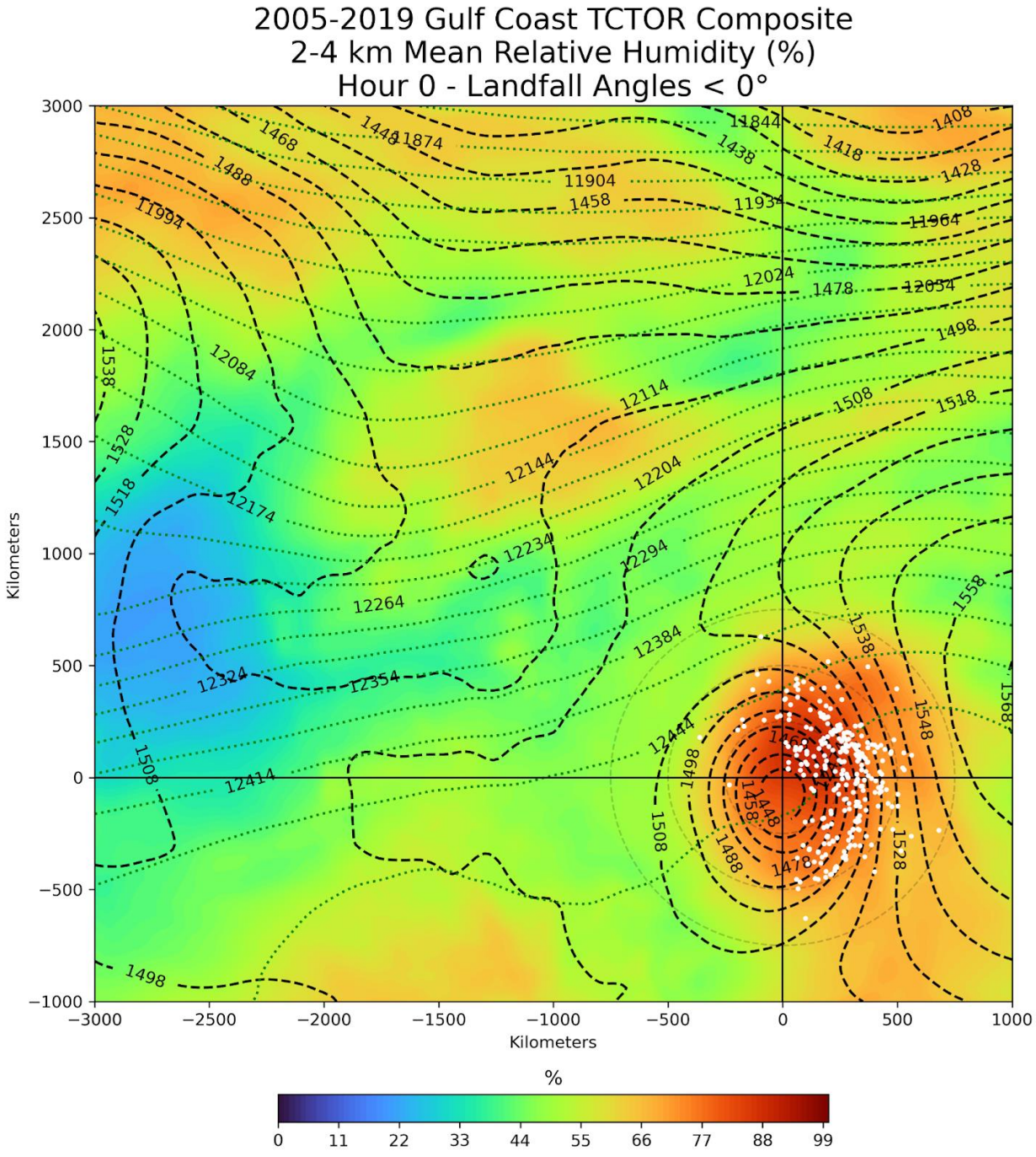

Figure 4.99: 2005-2019 Gulf Coast Composite 2-4 km Mean Relative Humidity (%) at the time of TCTOR occurrence including TCs with a landfall angle < 0°. White dots indicate TCTOR locations. Crosshairs are approximate composite TC center. Light gray dashed circles are range rings at distances 250, 500, and 750 km from TC center. Black dashed lines are 850-mb heights (m), green dotted lines are 200-mb heights (m).

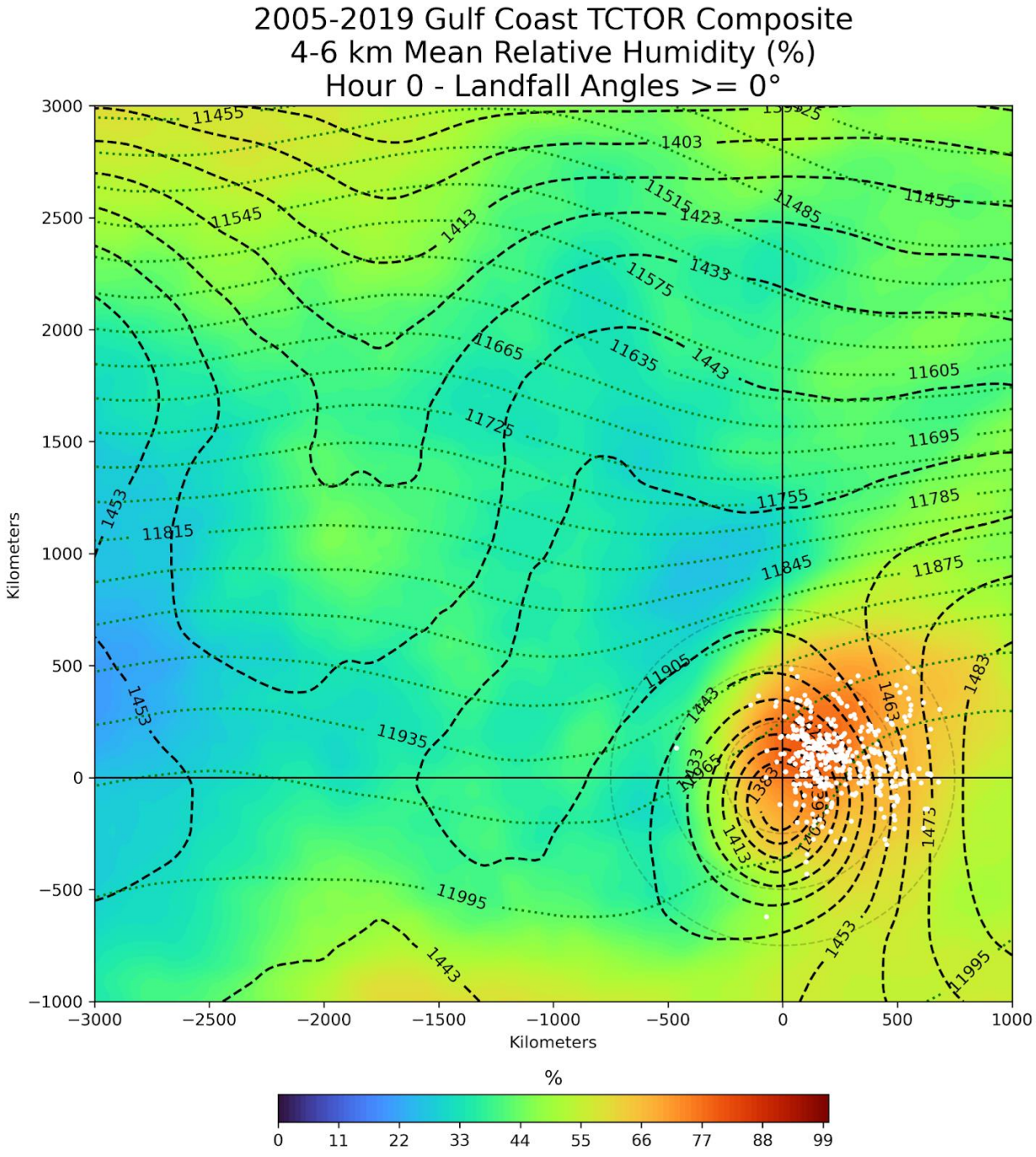

Figure 4.100: 2005-2019 Gulf Coast Composite 4-6 km Mean Relative Humidity (%) at the time of TCTOR occurrence including TCs with a landfall angle >= 0°. White dots indicate TCTOR locations. Crosshairs are approximate composite TC center. Light gray dashed circles are range rings at distances 250, 500, and 750 km from TC center. Black dashed lines are 850-mb heights (m), green dotted lines are 200-mb heights (m).

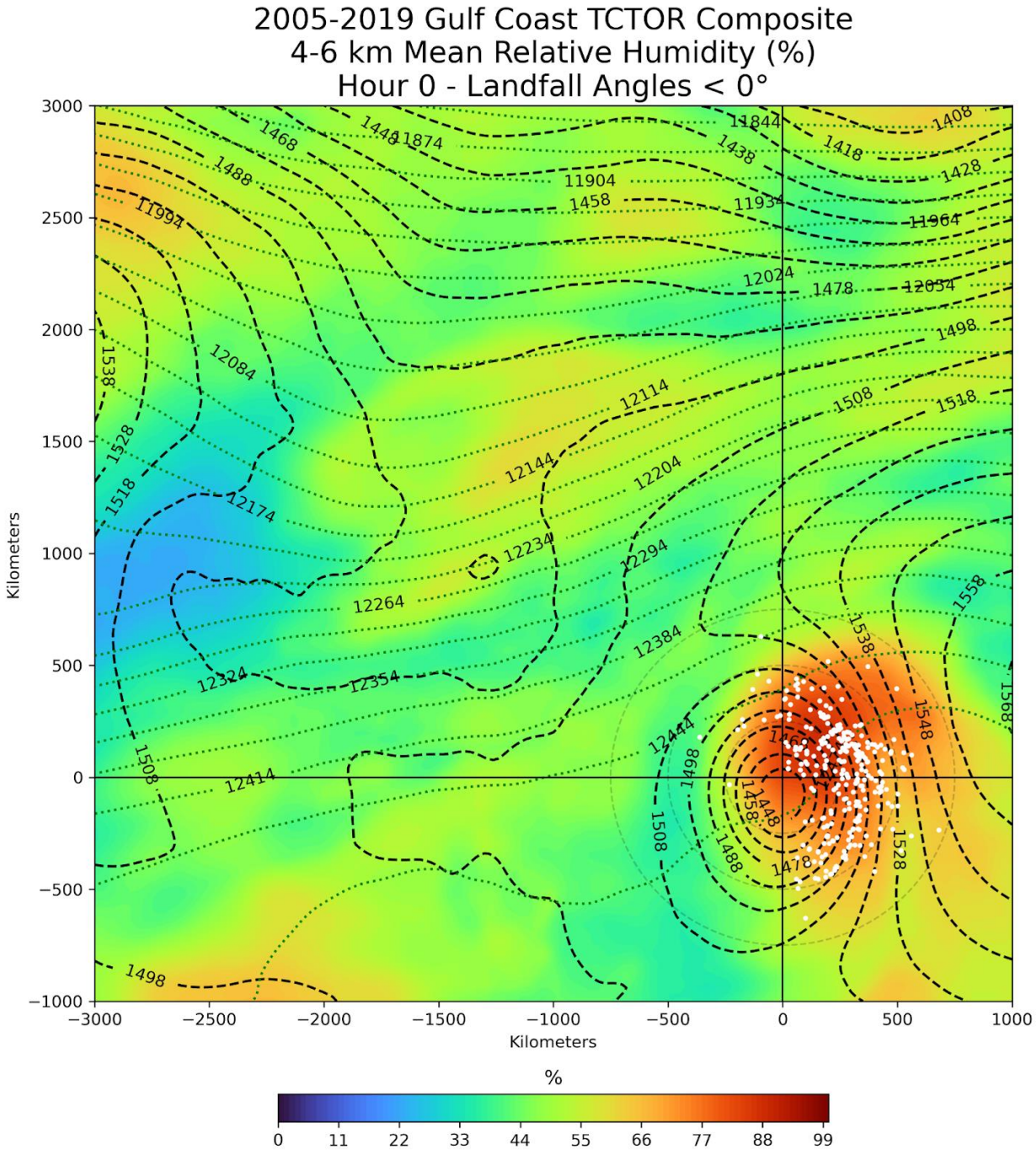

Figure 4.101: 2005-2019 Gulf Coast Composite 4-6 km Mean Relative Humidity (%) at the time of TCTOR occurrence including TCs with a landfall angle < 0°. White dots indicate TCTOR locations. Crosshairs are approximate composite TC center. Light gray dashed circles are range rings at distances 250, 500, and 750 km from TC center. Black dashed lines are 850-mb heights (m), green dotted lines are 200-mb heights (m).

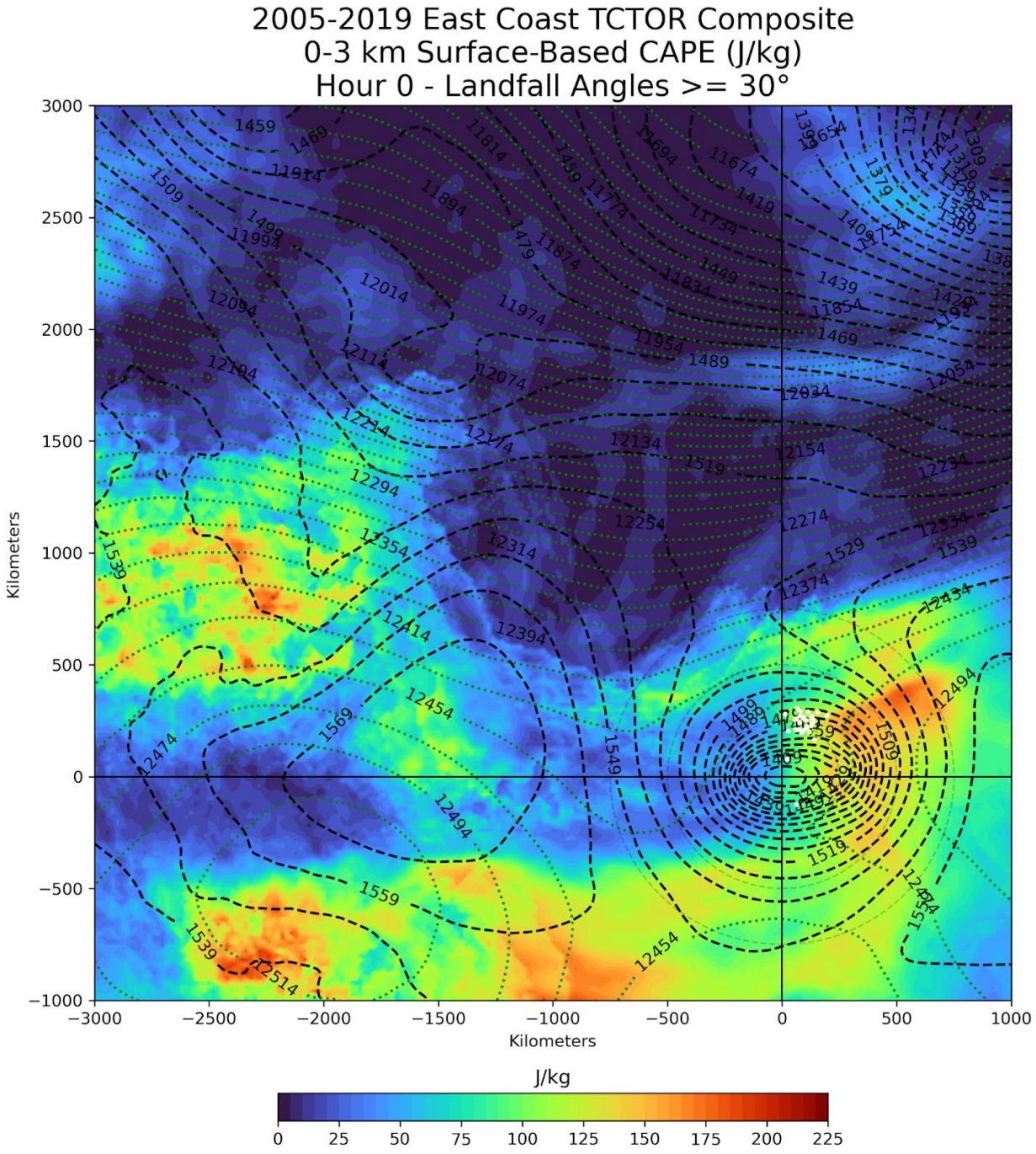

Figure 4.102: 2005-2019 East Coast Composite 0-3 km Surface-Based CAPE (J/kg) at the time of TCTOR occurrence including TCs with a landfall angle >= 30°. White dots indicate TCTOR locations. Crosshairs are approximate composite TC center. Light gray dashed circles are range rings at distances 250, 500, and 750 km from TC center. Black dashed lines are 850-mb heights (m), green dotted lines are 200-mb heights (m).

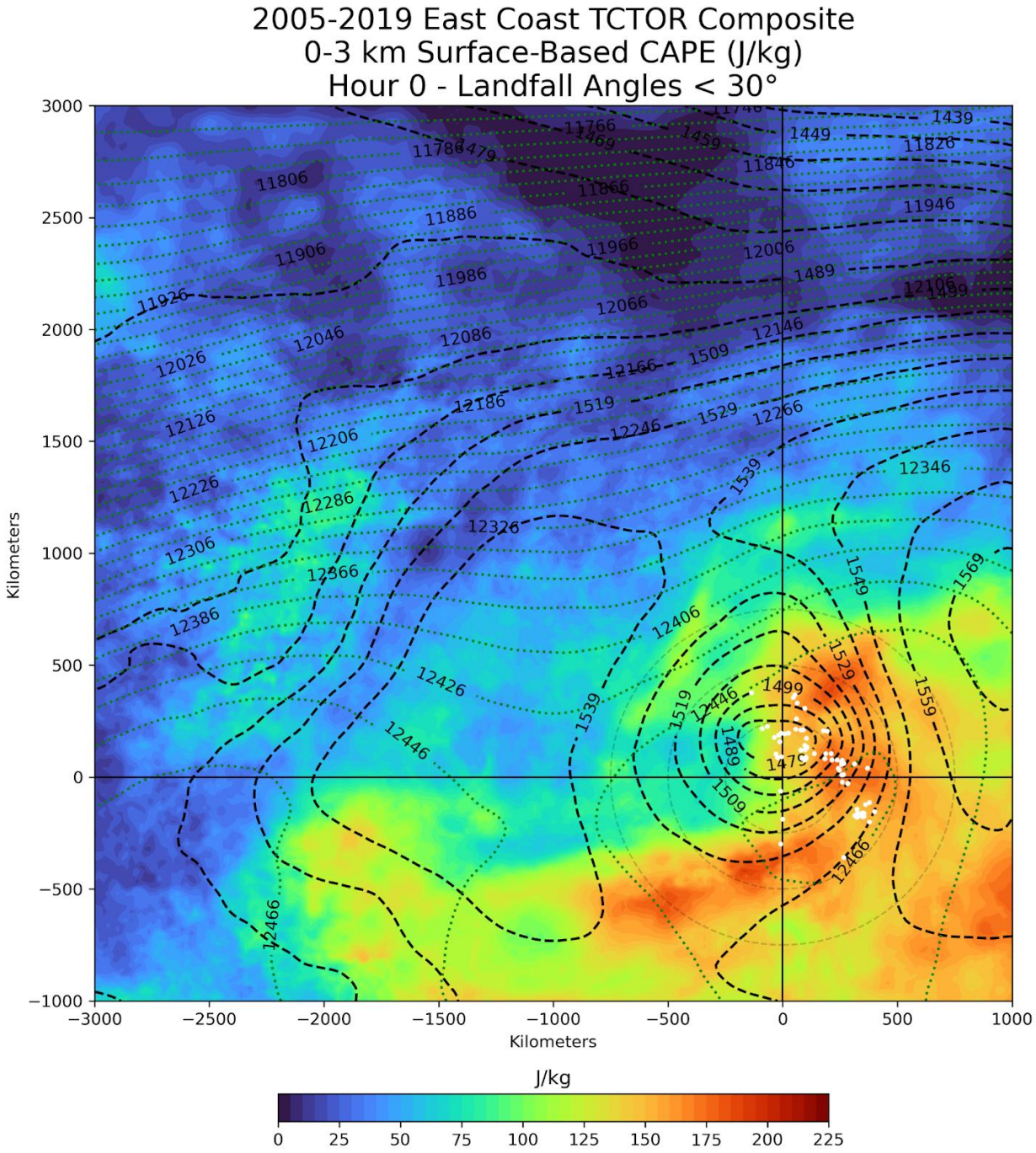

Figure 4.103: 2005-2019 East Coast Composite 0-3 km Surface-Based CAPE (J/kg) at the time of TCTOR occurrence including TCs with a landfall angle < 30°. White dots indicate TCTOR locations. Crosshairs are approximate composite TC center. Light gray dashed circles are range rings at distances 250, 500, and 750 km from TC center. Black dashed lines are 850-mb heights (m), green dotted lines are 200-mb heights (m).

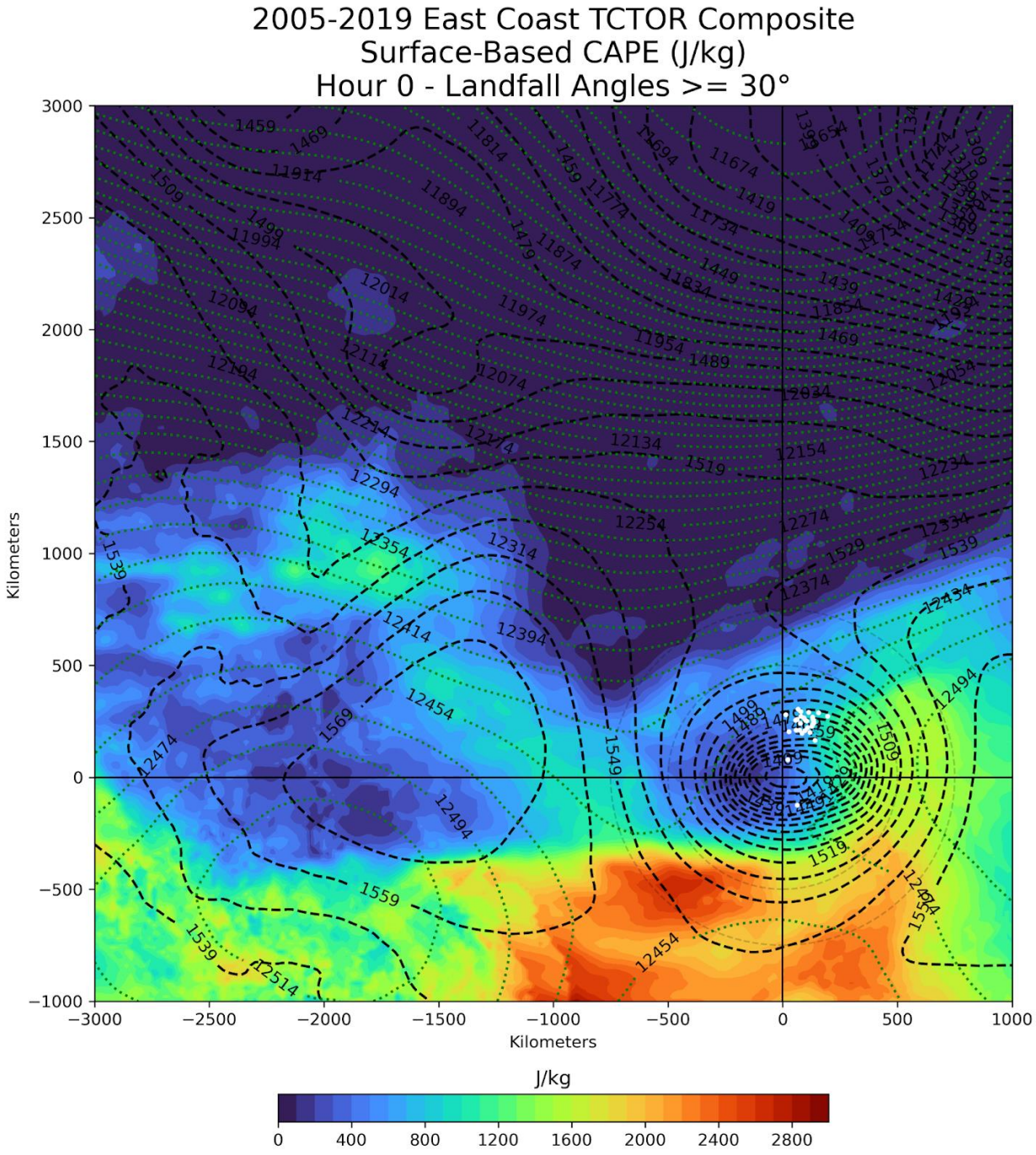

Figure 4.104: 2005-2019 East Coast Composite Surface-Based CAPE (J/kg) at the time of TCTOR occurrence including TCs with a landfall angle >= 30°. White dots indicate TCTOR locations. Crosshairs are approximate composite TC center. Light gray dashed circles are range rings at distances 250, 500, and 750 km from TC center. Black dashed lines are 850-mb heights (m), green dotted lines are 200-mb heights (m).

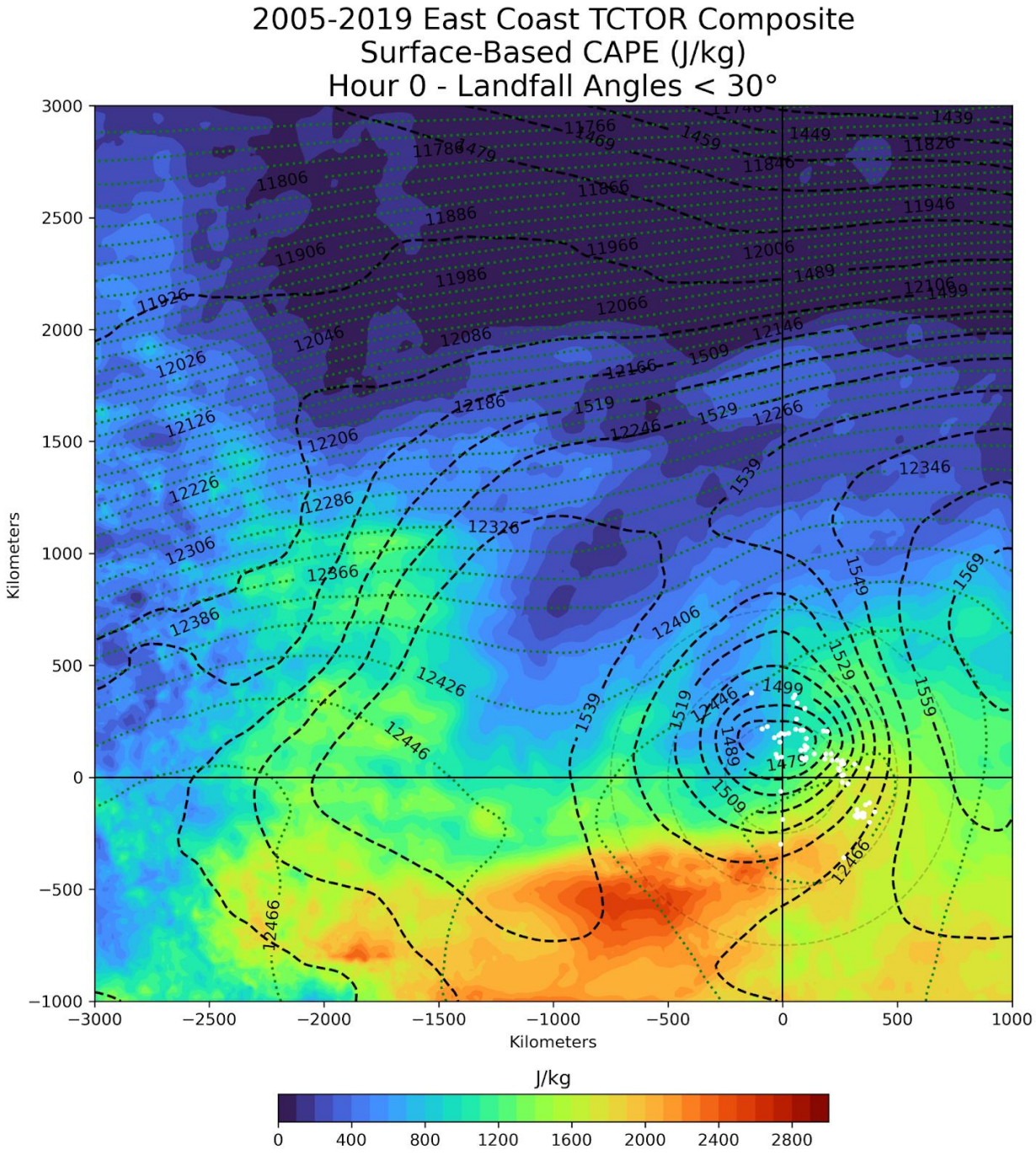

Figure 4.105: 2005-2019 East Coast Composite Surface-Based CAPE (J/kg) at the time of TCTOR occurrence including TCs with a landfall angle < 30°. White dots indicate TCTOR locations. Crosshairs are approximate composite TC center. Light gray dashed circles are range rings at distances 250, 500, and 750 km from TC center. Black dashed lines are 850-mb heights (m), green dotted lines are 200-mb heights (m).

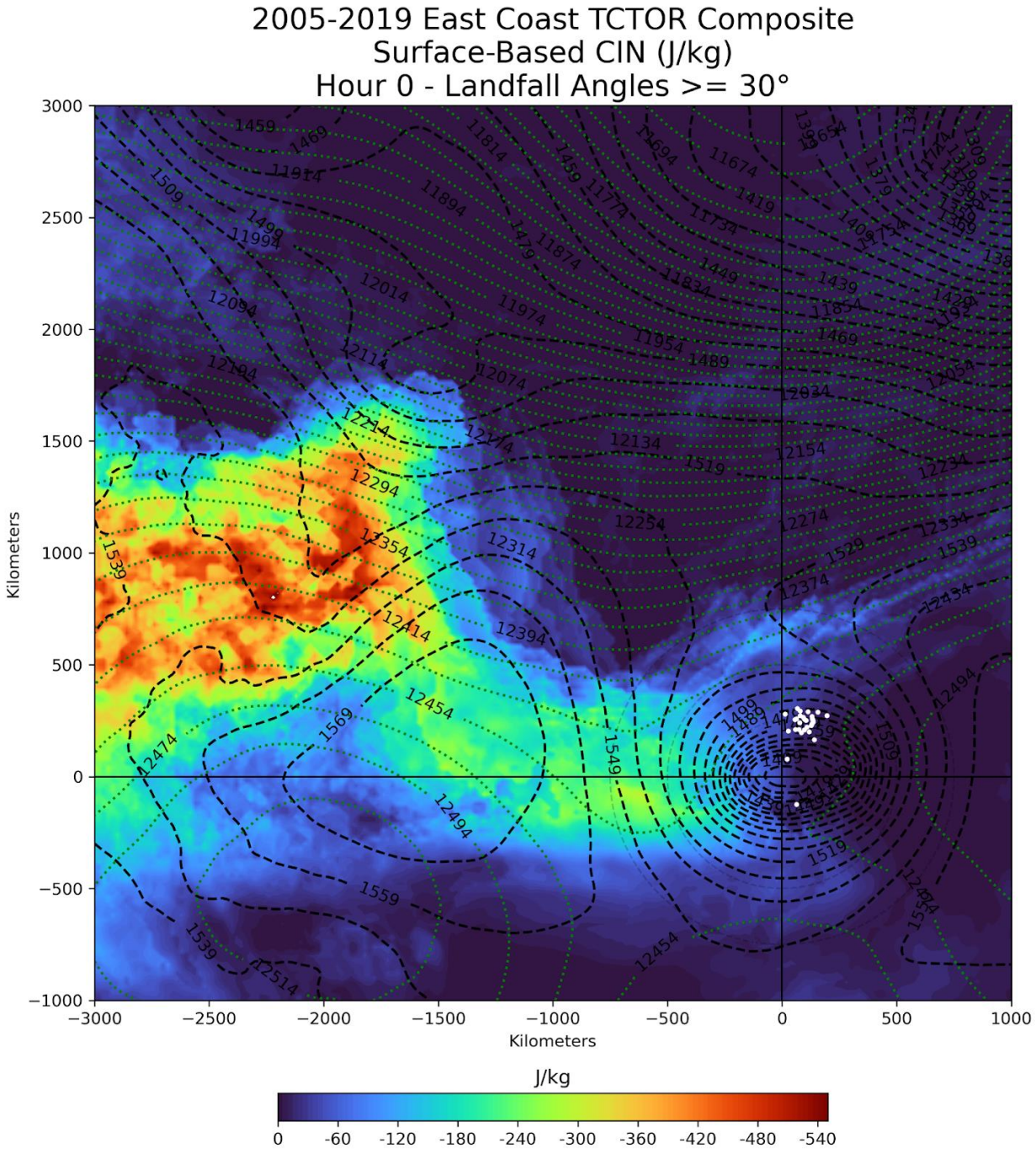

Figure 4.106: 2005-2019 East Coast Composite Surface-Based CIN (J/kg) at the time of TCTOR occurrence including TCs with a landfall angle >= 30°. White dots indicate TCTOR locations. Crosshairs are approximate composite TC center. Light gray dashed circles are range rings at distances 250, 500, and 750 km from TC center. Black dashed lines are 850-mb heights (m), green dotted lines are 200-mb heights (m).

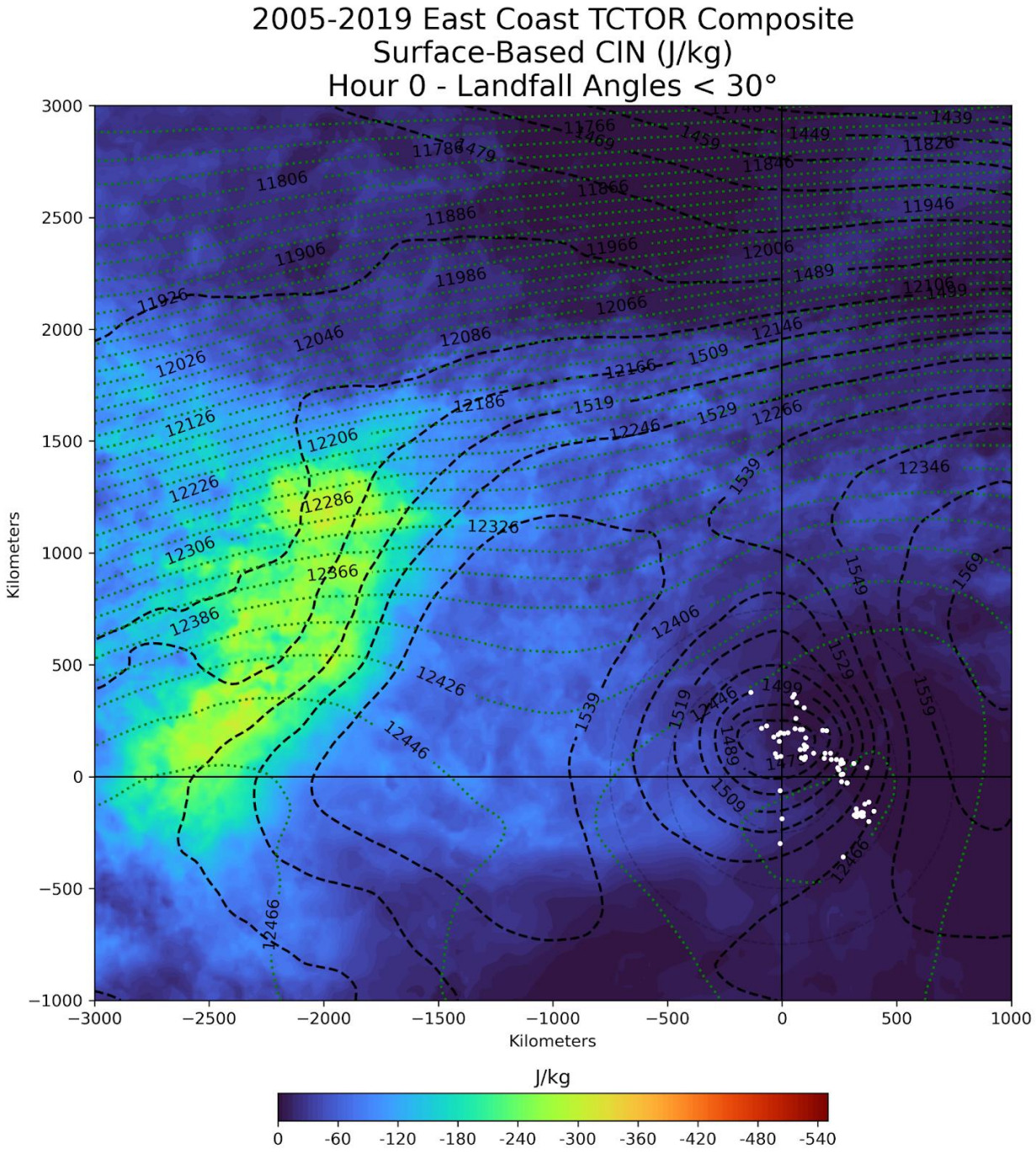

Figure 4.107: 2005-2019 East Coast Composite Surface-Based CIN (J/kg) at the time of TCTOR occurrence including TCs with a landfall angle < 30°. White dots indicate TCTOR locations. Crosshairs are approximate composite TC center. Light gray dashed circles are range rings at distances 250, 500, and 750 km from TC center. Black dashed lines are 850-mb heights (m), green dotted lines are 200-mb heights (m).

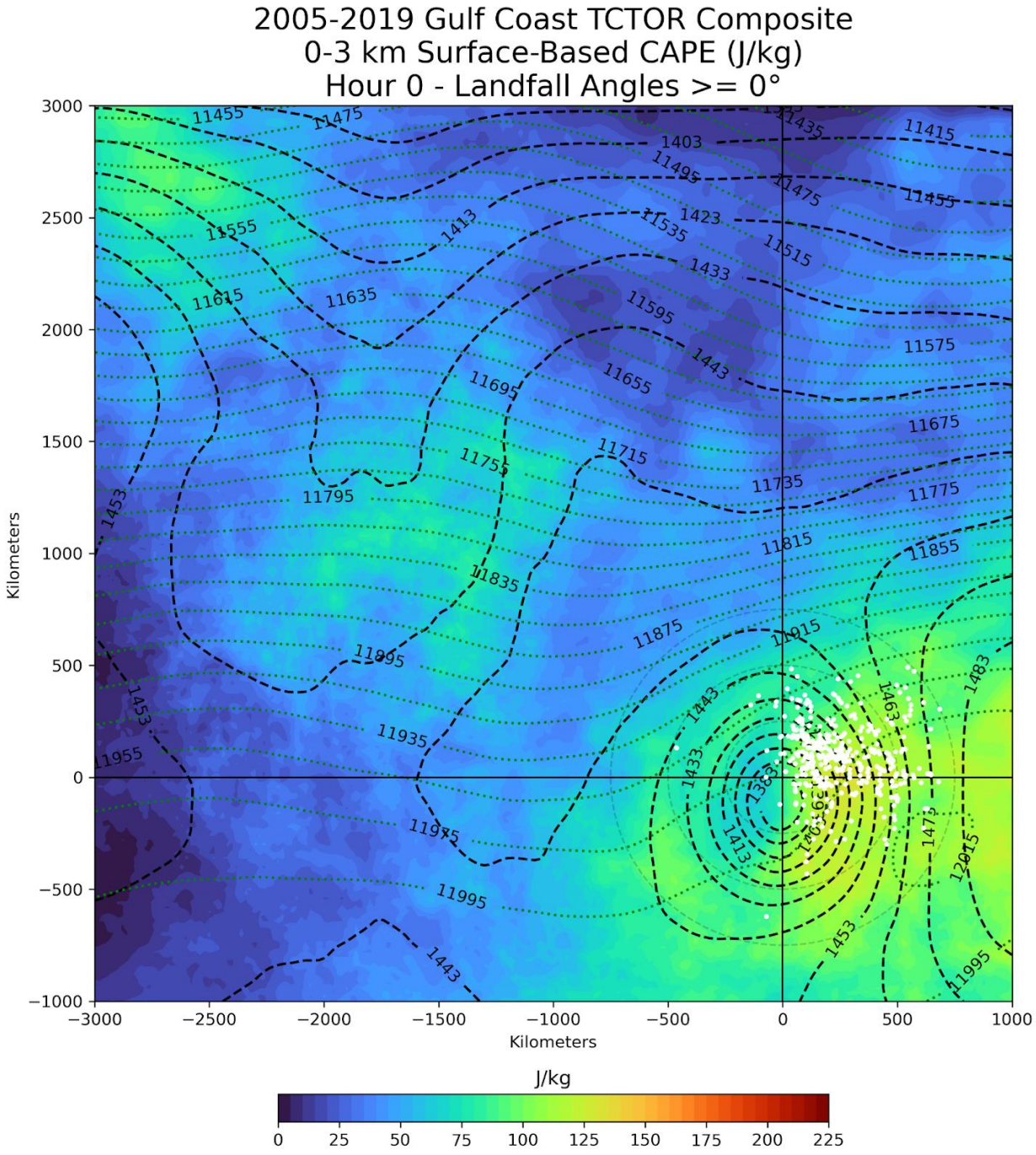

Figure 4.108: 2005-2019 Gulf Coast Composite 0-3 km Surface-Based CAPE (J/kg) at the time of TCTOR occurrence including TCs with a landfall angle >= 0°. White dots indicate TCTOR locations. Crosshairs are approximate composite TC center. Light gray dashed circles are range rings at distances 250, 500, and 750 km from TC center. Black dashed lines are 850-mb heights (m), green dotted lines are 200-mb heights (m).

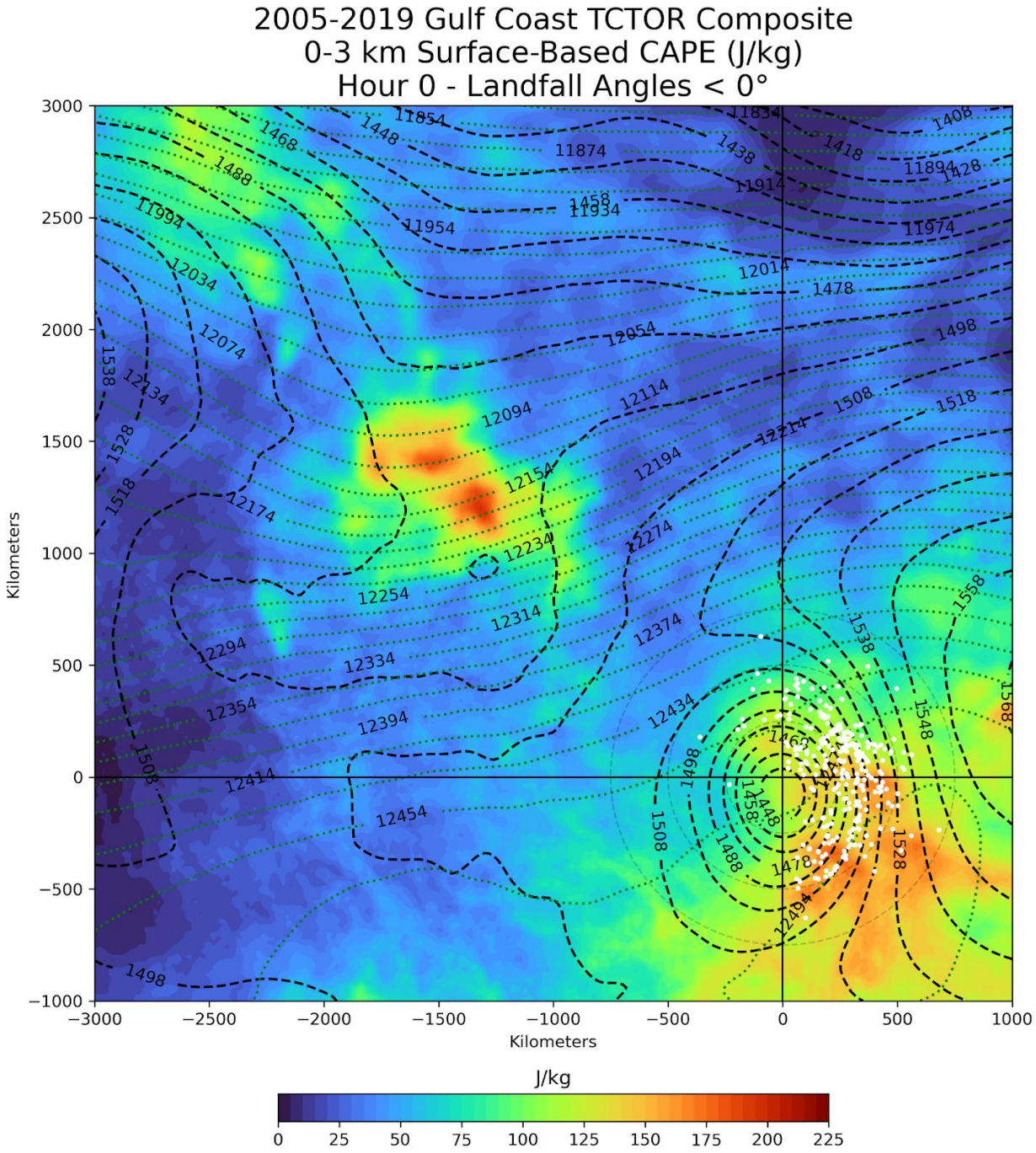

Figure 4.109: 2005-2019 Gulf Coast Composite 0-3 km Surface-Based CAPE (J/kg) at the time of TCTOR occurrence including TCs with a landfall angle < 0°. White dots indicate TCTOR locations. Crosshairs are approximate composite TC center. Light gray dashed circles are range rings at distances 250, 500, and 750 km from TC center. Black dashed lines are 850-mb heights (m), green dotted lines are 200-mb heights (m).

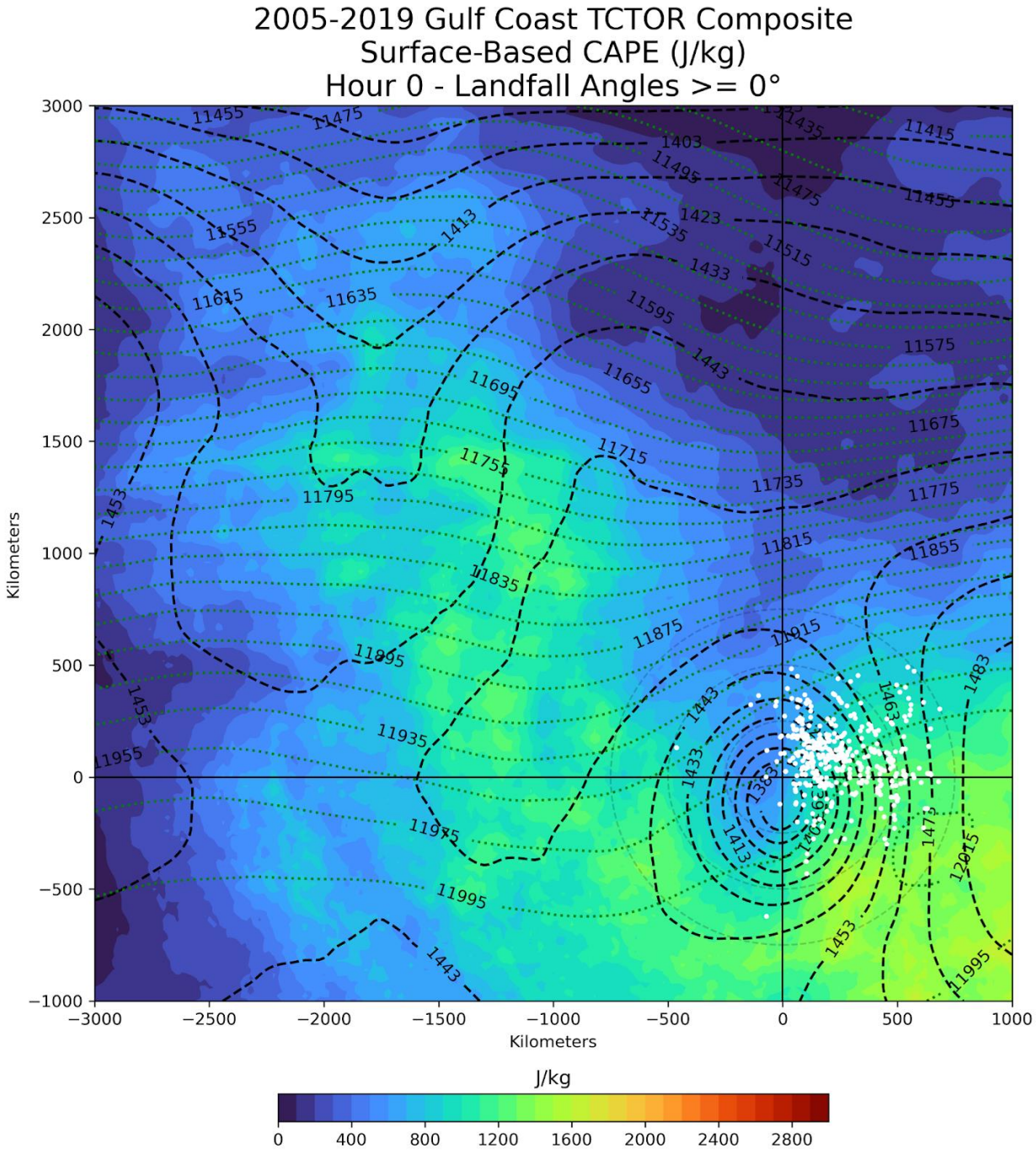

Figure 4.110: 2005-2019 Gulf Coast Composite Surface-Based CAPE (J/kg) at the time of TCTOR occurrence including TCs with a landfall angle >= 0°. White dots indicate TCTOR locations. Crosshairs are approximate composite TC center. Light gray dashed circles are range rings at distances 250, 500, and 750 km from TC center. Black dashed lines are 850-mb heights (m), green dotted lines are 200-mb heights (m).

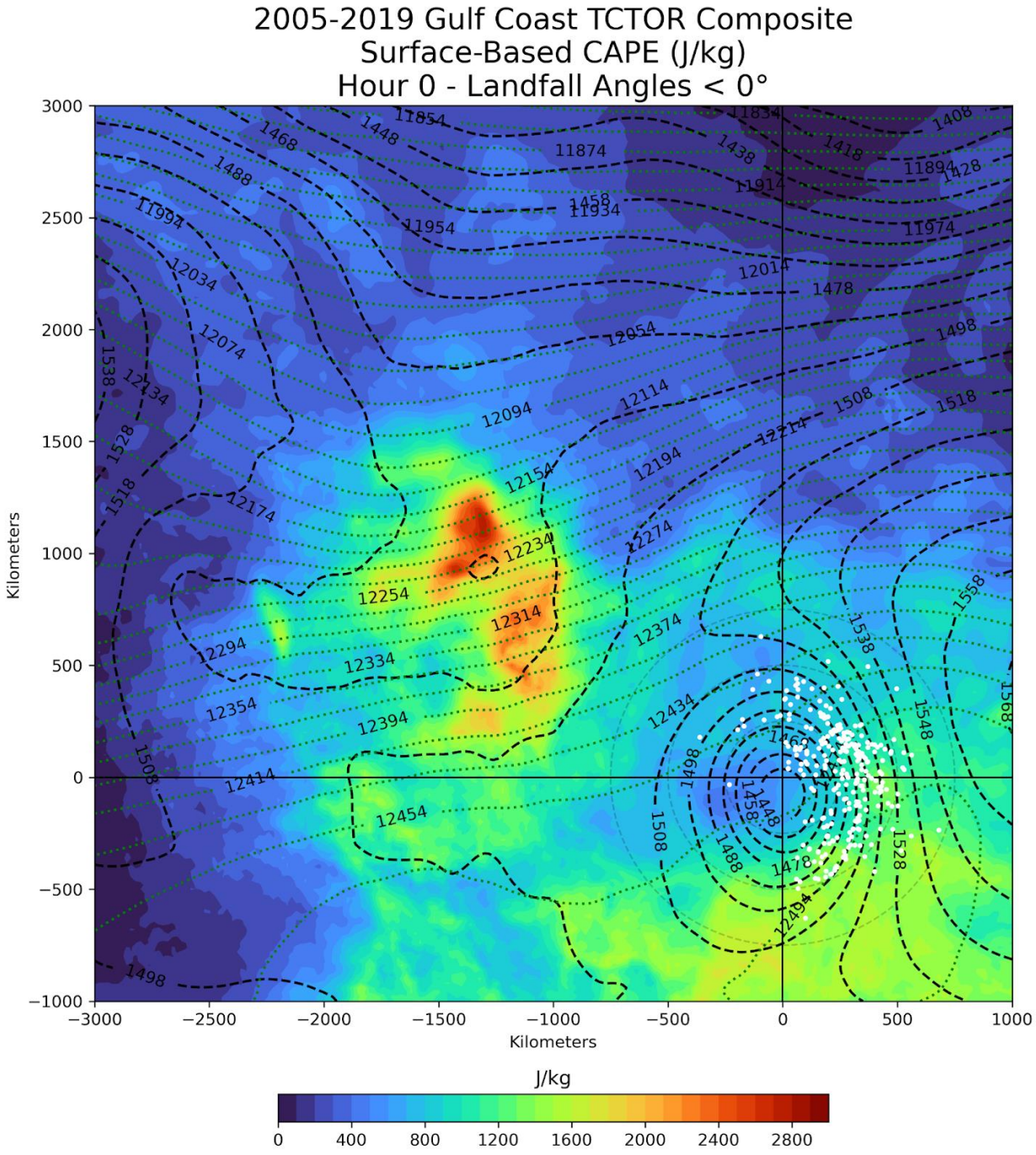

Figure 4.111: 2005-2019 Gulf Coast Composite Surface-Based CAPE (J/kg) at the time of TCTOR occurrence including TCs with a landfall angle < 0°. White dots indicate TCTOR locations. Crosshairs are approximate composite TC center. Light gray dashed circles are range rings at distances 250, 500, and 750 km from TC center. Black dashed lines are 850-mb heights (m), green dotted lines are 200-mb heights (m).

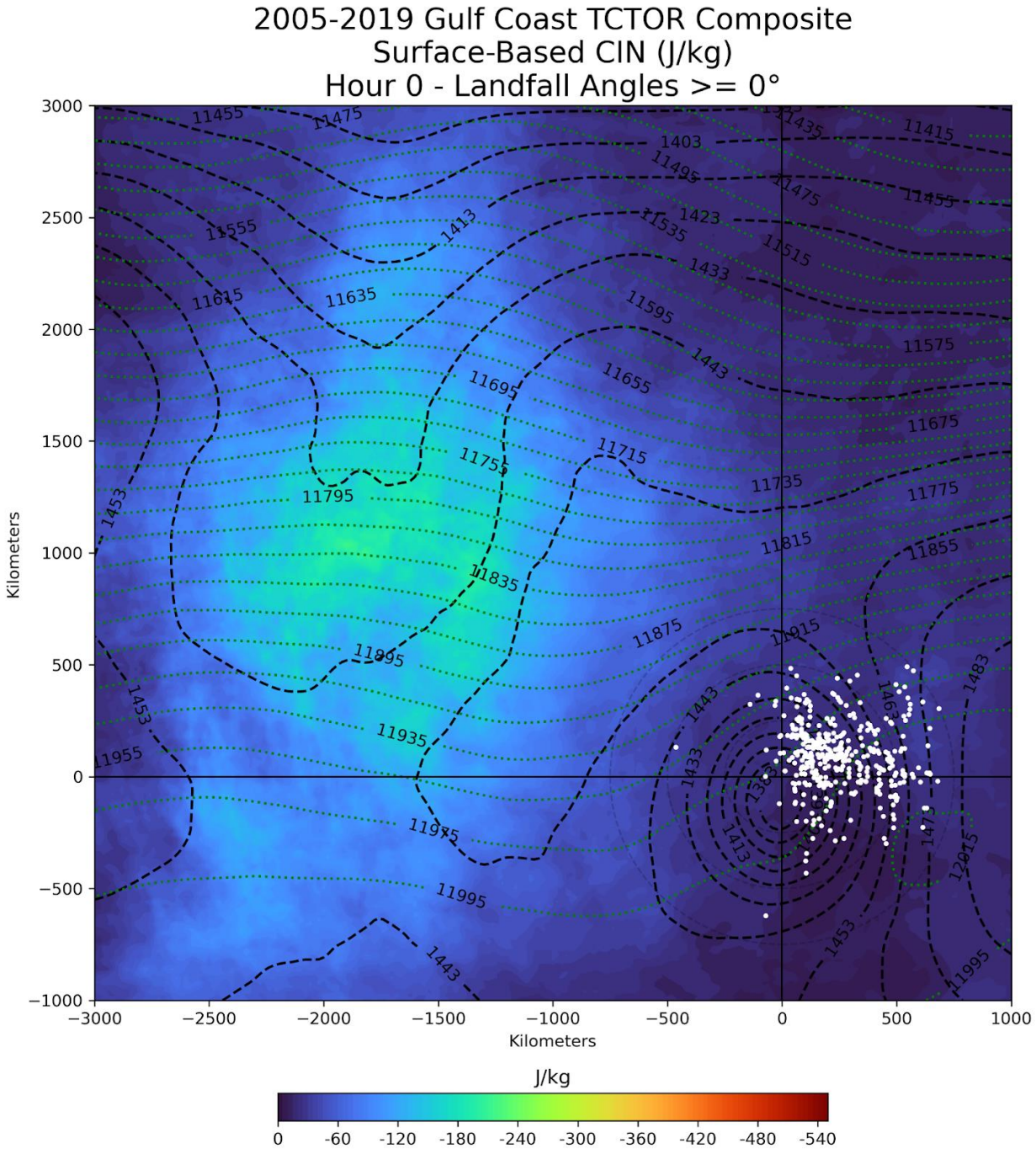

Figure 4.112: 2005-2019 Gulf Coast Composite Surface-Based CIN (J/kg) at the time of TCTOR occurrence including TCs with a landfall angle >= 0°. White dots indicate TCTOR locations. Crosshairs are approximate composite TC center. Light gray dashed circles are range rings at distances 250, 500, and 750 km from TC center. Black dashed lines are 850-mb heights (m), green dotted lines are 200-mb heights (m).

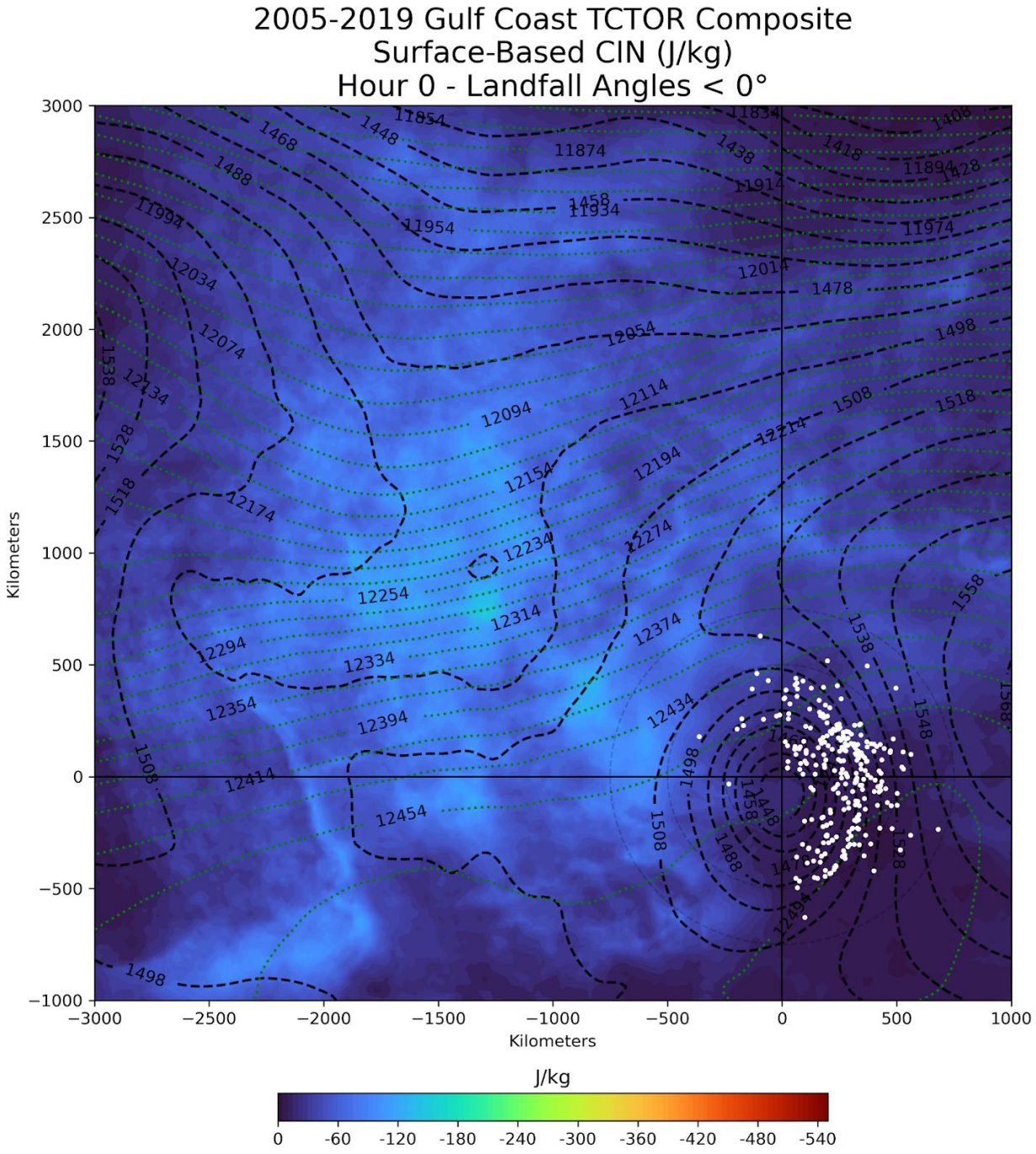

Figure 4.113: 2005-2019 Gulf Coast Composite Surface-Based CIN (J/kg) at the time of TCTOR occurrence including TCs with a landfall angle < 0°. White dots indicate TCTOR locations. Crosshairs are approximate composite TC center. Light gray dashed circles are range rings at distances 250, 500, and 750 km from TC center. Black dashed lines are 850-mb heights (m), green dotted lines are 200-mb heights (m).

Table 1: TCTOR Counts per East coast TC

STORM	YEAR	TCTOR COUNT
ABLE	1952	3
CONNIE	1955	4
DIANE	1955	1
CINDY	1959	6
GRACIE	1959	6
DONNA	1960	4
UNNAMED	1961	1
GINNY	1963	1
CLEO	1964	12
DORA	1964	3
BETSY	1965	2
INEZ	1966	2
ABBY	1968	5
DORIA	1971	1
BELLE	1976	1
DAVID	1979	34
DIANA	1984	1
ISIDORE	1984	1

STORM	YEAR	TCTOR COUNT
BOB	1985	4
GLORIA	1985	2
CHRIS	1988	5
HUGO	1989	2
BOB	1991	9
ERIN	1995	7
JERRY	1995	2
ARTHUR	1996	1
BERTHA	1996	15
FRAN	1996	4
BONNIE	1998	8
DENNIS	1999	1
FLOYD	1999	18
MICHELLE	2001	2
CRISTOBAL	2002	1
GUSTAV	2002	1
KYLE	2002	8
ISABEL	2003	1

STORM	YEAR	TCTOR COUNT
ALEX	2004	1
CHARLEY	2004	7
FRANCES	2004	12
GASTON	2004	18
HERMINE	2004	14
JEANNE	2004	42
KATRINA	2005	1
TAMMY	2005	1
ERNESTO	2006	5
HANNA	2008	1
IRENE	2011	9
BERYL	2012	4
ARTHUR	2014	6
ANA	2015	1
JULIA	2016	1
MATTHEW	2016	2
FLORENCE	2018	44
DORIAN	2019	25

Table 4.2: TCTOR Counts per Gulf coast TC

STORM	YEAR	TCTOR COUNT
BAKER	1950	2
ALICE	1953	2
HAZEL	1953	1
FLOSSY	1956	5
UNNAMED	1957	7
AUDREY	1957	20
BERTHA	1957	1
ESTHER	1957	1
ARLENE	1959	1
UNNAMED	1959	2
DEBRA	1959	2
JUDITH	1959	2
UNNAMED	1960	4
ETHEL	1960	5
FLORENCE	1960	1
CARLA	1961	19
UNNAMED	1964	3
ABBY	1964	1

STORM	YEAR	TCTOR COUNT
HILDA	1964	10
ISBELL	1964	9
UNNAMED	1965	2
BETSY	1965	4
ALMA	1966	4
BEULAH	1967	104
ABBY	1968	2
BRENDA	1968	1
CANDY	1968	23
GLADYS	1968	2
CAMILLE	1969	2
UNNAMED	1969	1
JENNY	1969	2
ALMA	1970	4
BECKY	1970	2
CELIA	1970	7
EDITH	1971	16
FERN	1971	5

STORM	YEAR	TCTOR COUNT
AGNES	1972	17
DELIA	1973	6
CARMEN	1974	6
CAROLINE	1975	1
ELOISE	1975	5
UNNAMED	1976	4
BABE	1977	14
AMELIA	1978	1
DEBRA	1978	3
BOB	1979	5
CLAUDETTE	1979	4
FREDERIC	1979	10
ALLEN	1980	29
DANIELLE	1980	5
ARLENE	1981	2
DENNIS	1981	2
ALBERTO	1982	3
UNNAMED	1982	10

STORM	YEAR	TCTOR COUNT
CHRIS	1982	6
ALICIA	1983	22
BOB	1985	1
DANNY	1985	39
ELENA	1985	10
JUAN	1985	11
BONNIE	1986	5
UNNAMED	1987	2
FLOYD	1987	1
FLORENCE	1988	4
GILBERT	1988	44
KEITH	1988	2
ALLISON	1989	10
CHANTAL	1989	5
JERRY	1989	6
MARCO	1990	4
ANDREW	1992	48
ARLENE	1993	1
ALBERTO	1994	1

STORM	YEAR	TCTOR COUNT
BERYL	1994	37
GORDON	1994	6
ALLISON	1995	6
DEAN	1995	5
ERIN	1995	6
OPAL	1995	33
DOLLY	1996	1
JOSEPHINE	1996	26
DANNY	1997	14
CHARLEY	1998	1
EARL	1998	15
FRANCES	1998	14
GEORGES	1998	48
HERMINE	1998	3
MITCH	1998	5
BRET	1999	6
HARVEY	1999	2
IRENE	1999	7
GORDON	2000	11

STORM	YEAR	TCTOR COUNT
HELENE	2000	16
ALLISON	2001	28
BARRY	2001	4
GABRIELLE	2001	18
FAY	2002	11
HANNA	2002	1
ISIDORE	2002	10
LILI	2002	25
BILL	2003	27
CLAUDETTE	2003	2
HENRI	2003	1
BONNIE	2004	18
CHARLEY	2004	15
FRANCES	2004	91
IVAN	2004	118
MATTHEW	2004	1
ARLENE	2005	4
CINDY	2005	48
DENNIS	2005	12

STORM	YEAR	TCTOR COUNT
EMILY	2005	11
KATRINA	2005	56
RITA	2005	97
WILMA	2005	8
ALBERTO	2006	17
BARRY	2007	2
ERIN	2007	7
HUMBERTO	2007	1
TEN	2007	1
DOLLY	2008	6
FAY	2008	50
GUSTAV	2008	49

STORM	YEAR	TCTOR COUNT
IKE	2008	33
CLAUDETTE	2009	1
ALEX	2010	10
HERMINE	2010	13
LEE	2011	25
DEBBY	2012	25
ISAAC	2012	17
ANDREA	2013	11
BILL	2015	19
COLIN	2016	1
HERMINE	2016	10
CINDY	2017	14

STORM	YEAR	TCTOR COUNT
EMILY	2017	1
HARVEY	2017	52
IRMA	2017	28
NATE	2017	22
ALBERTO	2018	4
GORDON	2018	2
MICHAEL	2018	16
BARRY	2019	2
IMELDA	2019	1
NESTOR	2019	6

Table 4.3: Convective metrics at each analyzed hour with associated t-statistic and p-value. Highlighted values are statistically significant at the 5% confidence level.

Convective Parameter	*Hour 0*		*Hour 1*		*Hour 2*	
	t-statistic	**p-value**	**t-statistic**	**p-value**	**t-statistic**	**p-value**
LCL	-6.042	0.0	-6.745	0.0	-7.489	0.0
LFC	-3.611	0.0	-4.643	0.0	-2.488	0.013
EL	2.177	0.03	2.108	0.035	2.137	0.033
SBCAPE	2.712	0.007	2.442	0.015	1.432	0.152
SBCIN	3.867	0.0	3.88	0.0	3.886	0.0
SBCAPE03	5.207	0.0	5.572	0.0	4.203	0.0
MLCAPE	3.946	0.0	3.502	0.0	2.392	0.017
MLCIN	2.987	0.003	2.963	0.003	2.949	0.003
MLCAPE03	7.86	0.0	7.171	0.0	6.119	0.0
MUCAPE	1.678	0.094	1.616	0.106	0.59	0.555
MUCIN	2.234	0.026	3.154	0.002	3.382	0.001
LR03	1.5	0.134	0.555	0.579	-0.537	0.591
LR700500	0.167	0.868	0.867	0.386	0.124	0.901
SBTHE	1.063	0.288	0.799	0.424	0.096	0.924
MLTHE	2.297	0.022	1.775	0.076	1.305	0.192
MLRH	6.722	0.0	7.682	0.0	7.752	0.0
RH02	4.849	0.0	5.235	0.0	4.581	0.0
RH24	-0.987	0.324	-1.398	0.163	-1.473	0.141
RH46	-0.623	0.528	-0.241	0.81	-0.222	0.824
DCAPE	-1.121	0.263	-1.146	0.252	-0.403	0.687
EFFBOT	-0.595	0.552	-0.6	0.549	-0.722	0.47
EFFTOP	-1.941	0.053	-2.517	0.012	-1.674	0.095

EFFDEP	-1.912	0.056	-2.455	0.014	-1.644	0.101
STMHLF	1.255	0.21	1.776	0.076	1.251	0.211
SHEAR01	-2.52	0.012	-2.716	0.007	-2.344	0.019
SHEAR03	-5.458	0.0	-6.039	0.0	-6.616	0.0
SHEAR06	-4.525	0.0	-4.704	0.0	-5.092	0.0
BRNSHEAR	-8.565	0.0	-8.902	0.0	-9.122	0.0
EFFSHEAR	-1.168	0.243	-2.369	0.018	-1.56	0.119
SRH05	-2.283	0.023	-2.326	0.02	-1.461	0.145
SRH01	-3.678	0.0	-3.557	0.0	-3.067	0.002
SRH03	-4.051	0.0	-4.281	0.0	-4.09	0.0
SRHEFF	-2.377	0.018	-3.226	0.001	-2.317	0.021
SCPFIX	-6.808	0.0	-7.199	0.0	-7.52	0.0
SCPEFF	-1.738	0.083	-2.864	0.004	-2.504	0.012
STPFIX	-0.163	0.871	0.341	0.733	-0.15	0.881
STPEFF	-1.398	0.162	-1.976	0.048	-1.857	0.064
SHERBS3	-5.103	0.0	-5.882	0.0	-7.252	0.0
SHERBE	-0.856	0.392	-2.189	0.029	-1.889	0.059

Table 4.4: Mean values of convective metrics at each analyzed hour. Highlighted values are statistically significant at the 5% confidence level.

Convective Parameter	*Hour 0*		*Hour 1*		*Hour 2*	
	East	**Gulf**	**East**	**Gulf**	**East**	**Gulf**
LCL	259.19	409.69	254.84	436.46	239.26	454.17
LFC	564.71	1186.63	506.92	1153.01	778.16	1198.04
EL	13245.96	12635.38	13246.73	12653.45	13121.91	12493.05
SBCAPE	1791.19	1517.75	1778.34	1531.66	1670.78	1518.68
SBCIN	-7.17	-20.47	-5.57	-22.09	-5.16	-19.62
SBCAPE03	195.33	148.11	196.78	147.48	185.03	146.18
MLCAPE	1113.85	851.09	1091.37	858.6	1022.58	856.72
MLCIN	-6.86	-19.46	-5.63	-23.9	-6.76	-21.34
MLCAPE03	126.75	79.21	123.41	79.35	114	77.44
MUCAPE	1836.58	1671.95	1826.69	1668.36	1719.32	1658.25
MUCIN	-4.25	-9.3	-2.83	-10.1	-2.03	-7.56
LR03	6.2	6.1	6.2	6.16	6.15	6.18
LR700500	5.55	5.54	5.58	5.53	5.57	5.56
SBTHE	357.16	356.6	357.01	356.56	356.42	356.33
MLTHE	354.05	352.9	353.78	352.88	353.31	352.59
MLRH	93.08	86.52	93.66	86.32	93.86	86.29
RH02	93.1	89.04	92.87	88.38	92.13	87.69
RH24	85.4	86.58	83.81	85.65	82.33	84.35
RH46	80.92	82.08	81.01	81.51	81.5	81.97
DCAPE	451.89	480.14	459.48	488.48	475	485.34
EFFBOT	0	2.74	0	5.63	0	2.79
EFFTOP	1604.64	1791.81	1515.57	1747.82	1502.14	1663.6

EFFDEP	1604.64	1789.07	1515.57	1742.18	1502.14	1660.81
STMHLF	6761.12	6541.59	6812.68	6522.79	6656.71	6509.21
SHEAR01	13.6	15.06	13.29	14.91	13.29	14.69
SHEAR03	15.69	18.85	15.38	18.83	14.85	18.48
SHEAR06	16.07	18.94	15.91	18.82	15.48	18.56
BRNSHEAR	8.04	30.58	7.74	30.13	7.17	28.8
EFFSHEAR	14.59	15.23	13.82	15.28	13.77	14.82
SRH05	116.36	138.32	113.06	135.76	114.51	128.56
SRH01	184.48	240.83	180.86	235.91	178.68	224.82
SRH03	253.51	333.67	242.99	326.04	233.88	309.11
SRHEFF	220.5	263.62	200.51	258.68	198.65	239.95
SCPFIX	0.97	3.65	0.82	3.48	0.67	3.09
SCPEFF	5.34	6.55	4.47	6.4	4.17	5.72
STPFIX	1.45	1.48	1.44	1.39	1.23	1.25
STPEFF	0.69	0.84	0.61	0.8	0.55	0.71
SHERBS3	0.7	0.83	0.69	0.83	0.66	0.83
SHERBE	0.63	0.65	0.6	0.66	0.59	0.64

Chapter 5: Future Research

5.1 Introduction

This chapter briefly summarizes the results of this project and describes the possibilities of future research. Section 5.2 discusses an overview of the most significant results of this project. Section 5.3 covers potential research that may stem from or build upon this project.

5.2 Summary

There are a number of differences between East and Gulf coast TCTOR climatologies and environments. Gulf coast TCs, on average, produced more TCTORs than East coast TCs, and had a distinct peak in June, early in the Atlantic hurricane season. There was also a notable difference in the spatial distribution of TCTOR events relative to the TC center with East coast TCTORS occurring more frequently in the northern regions of their respective TCs, on average, whereas Gulf coast TCTORs were more frequently produced in the northeastern quadrant. The mean landfall angles for East and Gulf coast TCs were also very different and provided a plausible explanation for the discrepancies in TCTOR counts as the location of the right-front quadrant with respect to land was an important factor in TCTOR development.

Regarding the local TCTOR environments, there were significant differences in a number of common convective metrics between the East and Gulf coasts. While several metrics were statistically significant, not all were pragmatic and may prove to be less than beneficial when assessing TCTOR risk in the event of a TC landfall. The metrics that may prove to be useful in forecasting include LCL, LFC, SBCAPE, MLCAPE, BRNSHEAR, SRH01, SRH03, SCPFIX, and SCPEFF. East coast LCLs and LFCs were lower than their Gulf coast counterparts by approximately 150 m and 600 m, respectively, which imply that a moister, conditionally unstable

environment is often present for East coast TCTOR development. The East coast SBCAPE and MLCAPE values were both greater than along the Gulf coast by ~270-280 J/kg, suggesting that the aforementioned moister boundary layer and conditionally unstable environment provided greater instability among East coast TCTOR environments. The BRNSHEAR values among East coast TCTOR environments were less than those among Gulf coast TCTOR environments by ~22 m^2/s^2. SRH01 and SRH03 values were also significantly less among East coast TCTOR environments when compared to their Gulf coast counterparts by approximately 60 and 80 m^2/s^2, respectively. The lesser values of BRNSHEAR, SRH01, and SRH03 among East coast TCTOR environments suggest that more sheared environments are present for Gulf coast TCTOR development. SCPFIX and SCPEFF values were also significantly less among East coast TCTOR environments by ~2.7 and 2, respectively, implying that the Gulf coast TCTOR environments are more conducive to supercell development due to the increased shear.

The synoptic environment in which TCTORs develop is also an important factor in TCTOR production. The presence of an upper-level jet with the right entrance region located in the vicinity of a TC's right-front quadrant may help provide additional lift while mid-level ridges could aid in producing regions of enhanced shear that collocate with the right-front region. Depending on the strength of the TCs, the synoptic pattern directs the TC motion which can impact the location of the right-front quadrant in relation to the land which directly impacts TCTOR production. The region of maximum shear was notably different between East and Gulf coast TCs with this region being located to the north of East coast TC centers and to the east of Gulf coast TC centers. East coast TCs also produced regions of shear that were lesser in magnitude than those produced by Gulf coast TCs. This discrepancy in maximum shear locations and magnitudes may help explain the large discrepancy in TCTOR production and

locations between the two coastlines. East coast TCs experienced environments that were much drier in the mid-levels than those of Gulf coast TCs, and experienced more mid-level dry air intrusions on average than Gulf coast TCs; however, the low-level environment was significantly more moist in the low-levels. Although synoptically the moisture environment differs significantly, the TCTORs developed in regions of high relative humidity. With respect to the synoptic pattern of SBCAPE, sharp gradients were present in the regions where TCTORs most frequently developed for both coastlines, suggesting that surface baroclinic boundaries may develop as a TC is making landfall which can help provide localized enhanced lift and shear to support TCTOR development.

5.3 Future Research

As with any research project, there remains more that can be done. This further research can either improve or expand upon the current project, or it can stem from the current project to present new findings. One improvement that can be made to the current project would be to perform an analysis of TCTORs as a function of distance from their respective coastline while also categorizing them based on TC intensity. The purpose of this would be to determine whether stronger TCs with a larger portion of the circulation onshore produce more TCTORs. With stronger TCs, there is increased vertical wind shear over a larger fraction of the right-front quadrant, and therefore, given sufficient surface-based CAPE, TCTOR development could be enhanced.

Another improvement would be to separate TCs into categories based on their TCTOR production. This would allow one to directly compare local environments that produced several TCTORs with those that did not. Approaching this could be somewhat subjective in how to

define a significant TCTOR-production event, but some previous studies have made these decisions and could provide insight into the best practices such as how many TCTORs are required to be defined as an outbreak (Verbout et al. 2007; Curtis 2004).

When considering how to expand upon this project, certain aspects can be investigated further. For one, the Goldilocks Zone can be analyzed at a much more detailed level through the use of already available RUC-RAP analyses data and through idealized numerical simulations. Drawing from the methodologies of Potvin et al. (2010), a similar approach to assessing the local TCTOR environment using the RUC-RAP analyses independent of the TC inflow to identify which ranges and timeframes would be most beneficial. To further expand and verify the observational study, idealized simulations could be initialized with high spatial and temporal resolution to allow for large profile samples to be analyzed. The aim would be to evaluate the evolution of environmental conditions within the right-front quadrant as it transitions onshore.

Further expansion of the current project could be through the development of a composite parameter to help simplify the assessment of TCTOR risk. This has been investigated in the past (Onderlinde and Fuelberg 2014), however, the dataset was limited to 9 years and evaluated fewer convective metrics than the current study. The results showed poorer skill in the 6-hour forecasts compared to the Storm Prediction Center's 24-hour forecasts. Through the advancements in observation capabilities and more expansive analyses data, a better understanding of the TCTOR environment is possible, and therefore, a more robust parameter could be constructed and tested against a larger sample of cases.

There is still much to be learned about TCTORs and their environments, and these suggestions are presented so that future research endeavors may be able to further aid forecasters

in predicting TCTORs and emergency managers to more adequately prepare for them during TC landfall events.

REFERENCES

Baker, A. K., M. D. Parker, and M. D. Eastin, 2009: Environmental Ingredients for Supercells and Tornadoes within Hurricane Ivan. *Wea. Forecasting*, **24**, 223-243, https://doi.org/10.1175/2008WAF2222146.1.

Blumberg, W. G., K. T. Halbert, T. A. Supinie, P. T. Marsh, R. L. Thompson, and J. A. Hart, 2017: SHARPpy: An Open-Source Sounding Analysis Toolkit for the Atmospheric Sciences. *Bull. Amer. Meteor. Soc.*, **98**, 1625-1636, https://doi.org/10.1175/BAMS-D-15-00309.1.

Bunkers, M. J., B. A. Klimowski, J. W. Zeitler, R. L. Thompson, and M. L. Weisman, 2000: Predicting Supercell Motion Using a New Hodograph Technique. *Wea. Forecasting*, **15**, 61-79, https://doi.org/10.1175/1520-0434(2000)015<0061:PSMUAN>2.0.CO;2.

Curtis, L. A., 2004: Midlevel Dry Intrusions as a Factor in Tornado Outbreaks Associated with Landfalling Tropical Cyclones from the Atlantic and Gulf of Mexico. *Wea. Forecasting*, **19**, 411-427, https://doi.org/10.1175/1520-0434(2004)019%3C0411:MDIAAF%3E2.0.CO;2.

Davies-Jones, R., 1984: Streamwise Vorticity: The Origin of Updraft Rotation in Supercell Storms. *Journal of the Atmospheric Sciences*, **41**, 2991-3006, https://doi.org/10.1175/1520-0469(1984)041<2991:SVTOOU>2.0.CO;2.

Doswell, C. A. III, and D.W. Burgess, 1988: On Some Issues of United States Tornado Climatology. *Mon. Wea. Rev.*, **116**, 495-501, https://doi.org/10.1175/1520-0493(1988)116%3C0495:OSIOUS%3E2.0.CO;2.

Doswell, C. A. III, and E. N. Rasmussen, 1994: The Effect of Neglecting Virtual Temperature Correction on CAPE Calculations. *Wea. Forecasting*, **9**, 4, 625-629, https://doi.org/10.1175/1520-0434(1994)009%3C0625:TEONTV%3E2.0.CO;2.

Eastin, M. D., and M. C. Link, 2009: Miniature Supercells in an Offshore Outer Rainband of Hurricane Ivan (2004). *Mon. Wea. Rev.*, **137**, 2081-2104, https://doi.org/10.1175/2009MWR2753.1.

Edwards, R., 2012: Tropical Cyclone Tornadoes: A Review of Knowledge in Research and Prediction. *Electronic J. Severe Storms Meteor.*, **7**, 6, 1-61.

Gentry, R. C., 1983: Genesis of Tornadoes Associated with Hurricanes. *Mon Wea. Rev.*, **111**, 1793-1805, https://doi.org/10.1175/1520-0493(1983)111%3C1793:GOTAWH%3E2.0.CO;2.

McCaul, E. W. Jr., 1991: Buoyancy and Shear Characteristics of Hurricane-Tornado Environments. *Mon. Wea. Rev.*, **119**, 8, 1954-1978, https://doi.org/10.1175/1520-0493(1991)119%3C1954:BASCOH%3E2.0.CO;2.

McCaul, E. W. Jr., 1993: Observations and Simulations of Hurricane-Spawned Tornadic Storms. *The Tornado: Its Structure, Dynamics, Prediction, and Hazards*, C. R. Church, Ed., Amer. Geophys. Union, 119-142.

McCaul, E. W. Jr., D. E. Buechler, S. J. Goodman, and M. Cammarta, 2004: Doppler Radar and Lightning Network Observations of a Severe Outbreak of Tropical Cyclone Tornadoes. *Mon. Wea. Rev.*, **132**, 1747-1763, https://doi.org/10.1175/1520-0493(2004)132%3C1747:DRALNO%3E2.0.CO;2.

Moore, T. W., and R. Dixon, 2011: Climatology of Tornadoes Associated with Gulf Coast-Landfalling Hurricanes. *Geog. Rev.*, **101**, 3, 371-395.

Novlan, D. J., and W. M. Gray, 1974: Hurricane-Spawned Tornadoes. *Mon Wea Rev.*, **102**, 476-488, https://doi.org/10.1175/1520-0493(1974)102%3C0476:HST%3E2.0.CO;2.

Onderlinde, M. J., and H. E. Fuelberg, 2014: A Parameter for Forecasting Tornadoes Associated with Landfalling Tropical Cyclones. *Wea. Forecasting*, **29**, 1238-1255, https://doi.org/10.1175/WAF-D-13-00086.1.

Paredes, M., B. A. Shenkel, R. Edwards, and M. Conigilo, 2021: Tropical cyclone Outer Size Impacts the Number and Location of Tornadoes. *Submitted to Geophysical Research Letters*.

Potvin, C. K., K. L. Elmore, and S. J. Weiss, 2010: Assessing the Impacts of Proximity Sounding Criteria on the Climatology of Significant Tornado Environments. *Wea. Forecasting*, **25**, 921-930, https://doi.org/10.1175/2010WAF2222368.1.

Powell, M. D., 1982: The Transition of the Hurricane Frederic Boundary-Layer Wind Field from the Open Gulf of Mexico to Landfall. *Mon. Wea. Rev.*, **110**, 1912-1932, https://doi.org/10.1175/1520-0493(1982)110%3C1912:TTOTHF%3E2.0.CO;2.

Rasmussen, E. N., 2003: Refined Supercell and Tornado Forecast Parameters. *Wea. Forecasting*, **18**, 3, 530-535, https://doi.org/10.1175/1520-0434(2003)18%3C530:RSATFP%3E2.0.CO;2.

Schenkel, B. A., R. Edwards, and M. Coniglio, 2020: A Climatological Analysis of Ambient Deep-Tropospheric Vertical Wind Shear Impacts upon Tornadoes in Tropical Cyclones. *Wea. Forecasting*. **35**, 2033-2059, https://doi.org/10.1175/WAF-D-19-0220.1.

Schenkel, B. A., M. Coniglio, and R. Edwards, 2021: How Does the Relationship between Ambient Deep-Tropospheric Vertical Wind Shear and Tropical Cyclone Tornadoes Change between Coastal and Inland Environments. *Wea. Forecasting*. **36**, 539-566, https://doi.org/10.1175/WAF-D-20-0127.1.

Schultz, L. A., and D. J. Cecil, 2009: Tropical Cyclone Tornadoes, 1950-2007. *Mon. Wea. Rev.*, **137**, 3471-3484, https://doi.org/10.1175/2009MWR2896.1.

Sherburn, K. D., and M. D. Parker, 2014: Climatology and Ingredients of Significant Severe Convection in High-Shear, Low-CAPE Environments. *Wea. Forecasting*, **29**, 4, 854-877, https://doi.org/10.1175/WAF-D-13-00041.1.

Thompson, R. L., C. M. Mead, and R. Edwards, 2007: Effective Storm-Relative Helicity and Bulk Shear in Supercell Thunderstorm Environments. *Wea. Forecasting*, **22**, 102–115, https://doi.org/10.1175/WAF969.1.

Verbout, S. M., D. M. Schultz, L. M. Leslie, H. E. Brooks, D. J. Karoly, and K. L. Elmore, 2007: Tornado Outbreaks Associated with Landfalling Hurricanes in the North Atlantic Basin: 1954-2004. *Meteor. Atmos. Phys.*, **97**, 255-271, https://doi.org/10.1007/S00703-006-0256-X.

Weiss S.J., 1987: Some Climatological Aspects of Forecasting Tornadoes Associated with Tropical Cyclones. *Preprints,* 17th Conf. Hurricanes and Tropical Meteor., Amer. Meteor. Soc., Miami, 160-163.

Weisman, M. L., and J. B. Klemp, 1982: The Dependence of Numerically Simulated Convective Storms on Vertical Wind Shear and Buoyancy. *Mon. Wea. Rev.*, **110**, 504–520, https://doi.org/10.1175/1520-0493(1982)110%3C0504:TDONSC%3E2.0.CO;2.